



Micro-simulation modelling of traffic loading on long-span bridges

Alessandro Lipari

The thesis is submitted to University College Dublin in fulfilment of the
requirements for the degree of Doctor of Philosophy

School of Civil, Structural and Environmental Engineering

Head of School: Dr Mark Richardson

Principal Supervisor: Prof Eugene OBrien

Doctoral Study Panel Members:

Dr Colin Caprani, Dr Paul Fanning, Dr Yaqian Zhao

March 2013

Table of contents

Abstract	ix
Statement of original authorship	x
Acknowledgements	xi
Chapter 1. Introduction	1
1.1 Background	1
1.2 Target and methodology	3
1.3 Outline and structure of the thesis	4
1.3.1 Chapter 2: Micro-simulation of single-lane traffic to identify critical loading conditions for long-span bridges	4
1.3.2 Chapter 3: Long-span bridge traffic loading using multi-lane traffic micro-simulation	5
1.3.3 Chapter 4: A methodology for computing traffic loading on long-span bridges based on micro-simulation and site-specific traffic data	5
1.3.4 Chapter 5: Accuracy of congested density estimates from point detectors	6
1.3.5 Chapter 6: The effect of controlling heavy vehicle gaps on long-span bridge loading	6
1.3.6 Appendices	6
Chapter 2. Micro-simulation of single-lane traffic to identify critical loading conditions for long-span bridges	8
2.1 Introduction	9
2.1.1 Data collection	9
2.1.2 Codes of practice and previous research on long-span bridge traffic loading	10
2.2 Micro-simulation model	13
2.2.1 The Intelligent Driver Model	13

2.2.2	Congested Traffic States	14
2.2.3	Multi-class simulations	17
2.3	Model and simulation parameters	18
2.3.1	Traffic stream	18
2.3.2	Road geometry and bottleneck strength	19
2.4	Traffic results	20
2.4.1	Spatio-temporal congestion plots	20
2.4.2	Effects of truck percentage	21
2.5	Loads on bridges	22
2.5.1	Introduction	22
2.5.2	Results for 200 m bridge	23
2.5.3	Results for 1000 m bridge	25
2.5.4	Discussion	27
2.6	Consideration of congestion frequency	27
2.6.1	Data on congestion	27
2.6.2	Combination of different congestion events	29
2.7	Conclusions	31
Chapter 3. Long-span bridge traffic loading based on multi-lane traffic micro-simulations		32
3.1	Introduction	33
3.1.1	Data	33
3.1.2	The lane-changing phenomenon	33
3.2	Micro-simulation	35
3.2.1	The Intelligent Driver Model	35
3.2.2	The MOBIL lane-changing model	36
3.2.3	Congested Traffic States	38
3.3	Model and Simulation Parameters	38
3.3.1	Traffic stream	38
3.3.2	Road geometry and bottleneck strength	39
3.3.3	Distribution of trucks between lanes	41
3.4	Traffic results	42

3.4.1	Spatio-temporal congestion patterns	42
3.4.2	Truck lane distribution	43
3.4.3	Lane-changing activity	44
3.4.4	Truck platoons	45
3.5	Loading results	46
3.5.1	Statistical extrapolation	46
3.5.2	200 m bridge	47
3.5.3	1000 m bridge	48
3.6	The effect of trucks in the fast lane	50
3.7	The effect of traffic composition	52
3.7.1	The effect of truck percentage	52
3.7.2	The effect of cars on loading	53
3.8	Conclusions	53
Chapter 4.	A methodology for computing traffic loading on long-span bridges based on micro-simulation and site-specific traffic data	55
4.1	Introduction	56
4.2	Non-recurrent congestion	57
4.2.1	Incidents	57
4.2.2	Capacity reduction	58
4.2.3	Other causes of non-recurrent congestion	60
4.2.4	Flow patterns and traffic composition	61
4.3	Methodology for computing the characteristic load	61
4.3.1	Data requirements	61
4.3.2	Analytical formulation	62
4.4	Micro-simulation	64
4.4.1	The Intelligent Driver Model	64
4.4.2	The MOBIL lane-changing model	64
4.4.3	Congested Traffic States	65
4.4.4	Traffic stream	65
4.4.5	Road geometry and capacity available	67
4.5	Simulation results	68

4.5.1	Traffic states	68
4.5.2	Consideration of only one incident and inflow	68
4.6	Application of the proposed methodology	70
4.6.1	Influence of the expected queue length	75
4.6.2	Influence of low flows with high truck percentage	76
4.6.3	Influence of full stop conditions	78
4.6.4	Influence of full stop conditions at low-flow	79
4.6.5	Dangerous site	79
4.7	Conclusions	81
Chapter 5.	Accuracy of congested density estimates from point detectors	82
5.1	Introduction	83
5.2	Traffic theory and data collection	83
5.2.1	The fundamental equation of traffic	83
5.2.2	The generalised fundamental equation of traffic	84
5.2.3	The fundamental equation of traffic and congestion	86
5.2.4	Loop detectors	87
5.2.5	Data collection for bridge traffic loading	88
5.3	Density estimation	89
5.3.1	Using one point detector	89
5.3.2	Using two point detectors	90
5.3.3	Using spatial detectors	91
5.4	Traffic micro-simulation	91
5.4.1	The Intelligent Driver Model	91
5.4.2	Congested traffic states	92
5.4.3	Model and simulation parameters	92
5.5	Assessment of density estimates	94
5.5.1	Estimation from the fundamental equation of traffic	94
5.5.2	Micro-estimation	96
5.5.3	Using two point detectors	99
5.5.4	Simulating real loop behaviour	99
5.6	Summary and conclusions	101

5.6.1	Summary	101
5.6.2	Conclusions	101
5.6.3	Implications for bridge traffic loading applications	102
Chapter 6. The effect of controlling heavy vehicle gaps on long-span bridge loading		104
6.1	Introduction	105
6.2	Micro-simulation	106
6.2.1	The Intelligent Driver Model	106
6.2.2	Congested Traffic States	107
6.2.3	Implementation of the control gap	107
6.3	Model and Simulation Parameters	109
6.3.1	Traffic stream	109
6.3.2	Road geometry and bottleneck strength	110
6.4	Traffic results	110
6.4.1	Spatio-temporal congestion patterns	110
6.4.2	Implementation of the control gap	111
6.5	Load results	112
6.5.1	Introduction	112
6.5.2	Results	113
6.5.3	Combination of congestions	114
6.6	Conclusions	115
Chapter 7. Conclusions		117
Appendix A. A comparative study of a bridge traffic load effect using micro-simulation and Eurocode load models		120
A.1	Introduction	121
A.2	The Eurocode load model	121
A.3	Model and simulation parameters	123
A.3.1	Traffic stream	123
A.3.2	Road capacity estimation	124
A.3.3	Road geometry and bottleneck strength	126
A.3.4	Congestion pattern	126

A.3.5	Sample bridges	127
A.4	Eurocode-based design	127
A.5	Microsimulation-based design	128
A.5.1	Introduction	128
A.5.2	Estimation	129
A.5.3	Statistical extrapolation	130
A.6	Comparison	131
A.7	Summary	132
Appendix B.	Multi-class traffic simulations	133
B.1	Introduction	133
B.2	Capacity of mixed traffic	133
B.2.1	Static capacity of single-class traffic	133
B.2.2	Multi-class traffic in the Highway Capacity Manual	136
B.2.3	Vehicle length and truck percentage	137
B.2.4	Generation of input files for SIMBA	137
B.2.5	Dynamic capacity for single-class traffic	138
B.2.6	Static and dynamic capacity for multi-class traffic	140
B.2.7	Heavy vehicle adjustment factors based on IDM simulations	142
B.2.8	Congested states	143
B.2.9	Extension to multi-lane simulations	146
B.2.10	Summary	146
B.3	Alternative means of computing the dynamic capacity	147
B.3.1	Open system	147
B.3.2	Ring road	150
B.3.3	Summary	153
B.4	Conclusions	153
Appendix C.	Micro-simulation modelling of congestion due to lane closures	155
C.1	Introduction	156
C.1.1	Previous research on merging manoeuvres and lane closures	156
C.2	Micro-simulation models	157
C.3	Traffic stream and model parameters	157

C.4	Results	160
C.5	Conclusions	162
Appendix D.	Refinement and calibration of the lane-changing model	163
D.1	Introduction	163
D.2	MOBIL formulation	164
D.3	Combination of IDM and MOBIL: cut-in manoeuvres	165
D.3.1	Data	166
D.3.2	IDM modifications	167
D.3.3	Microscopic results	170
D.3.4	Macroscopic results	171
D.3.5	Summary	173
D.4	Combination of IDM and MOBIL: platoon modification	173
D.5	Calibration of the lane-changing model	176
D.5.1	Free Traffic	180
D.5.2	Congestion	184
D.5.3	Injection of trucks in the fast lane - Free traffic	188
D.5.4	Injection of trucks in the fast lane - Congestion	189
D.5.5	Summary	191
D.6	Safe braking calibration	192
D.6.1	Summary	195
D.7	Lane distribution	195
D.7.1	Flow distribution between lanes - Free traffic	195
D.7.2	Flow distribution between lanes - Congestion	196
D.7.3	Load distribution between lanes	197
D.8	Conclusions	202
Appendix E.	Traffic data collection for bridge loading applications	203
E.1	Introduction	203
E.2	Calculation of load effects from point measurements	204
E.2.1	Proposed approach based on individual speeds	206
E.2.2	Consideration of different congestion patterns	207
E.2.3	Methods of headway estimations from individual speeds	212

E.3	Comparison with actual load effects	214
E.3.1	Influence of detector position	214
E.3.2	Comparison with actual spacing	218
E.3.3	Summary	219
E.4	The development of a camera system for bridge loading applications	220
E.4.1	Background and requirements	220
E.4.2	Definitions	221
E.4.3	Image processing	222
E.4.4	Fundamentals of geometrical optics	243
E.4.5	Site setup	248
E.4.6	Recommendations and conclusions	252
Appendix F. SIMBA overview		254
F.1	Introduction	254
F.2	Upgrades and releases	255
F.3	Model formulations	255
F.4	Generation of input files	256
F.5	Program settings	256
F.6	Generation of inhomogeneities	258
References		261

Abstract

Traffic loading on long-span bridges is governed by congestions. Most previous research uses simplified traffic models, typically consisting of a queue of vehicles at minimum bumper-to-bumper distances, in fact neglecting lighter and more frequently observed forms of congestions. Moreover, the available load models assume conservative frequencies of occurrence of congestion.

In this research, micro-simulation is used to reproduce several observed congestion patterns. Different combinations of traffic streams and congestion strengths are simulated, thus allowing the analysis of several traffic features and their effects to long-span bridge loading.

It is found that the queue of vehicles at a standstill, widely used in previous research, is not always the most critical congested state for long-span bridge loading. In fact, also slow-moving traffic can be critical. It is also found that the load does not significantly depend on the inflow, as long as congestion is triggered, implying that critical loading events may also happen out of rush hours.

A new methodology is proposed to compute the characteristic load based on site-specific traffic data, such as incident patterns and hourly flow distributions. This methodology is applied to traffic data available from the literature. It is found that flows with high truck percentage, typically occurring at night-time in combination with low flows, largely contribute to the characteristic load, even though congestion in such conditions is quite rare.

Finally, some issues related to traffic data collection for bridge loading are dealt with and a promising application for bridge loading control is proposed.

Statement of original authorship

I hereby certify that the submitted work is my own work, was completed while registered as a candidate for the degree stated on the Title Page, and I have not obtained a degree elsewhere on the basis of the research presented in this submitted work.

The research activity for this thesis was undertaken by the author, under the supervision of Prof Eugene OBrien. Dr Colin Caprani from Dublin Institute of Technology co-supervised the research and provided and programmed the micro-simulation tool used.

Acknowledgements

Firstly, I would like to thank my supervisors and the funding agency (the European Commission under the 7th Framework Programme) for the important opportunity I was given. Colin, I think 573 emails say a lot about the work done... Then, thanks to Ciaran, Mark and Andrew for sorting out the unavoidable and essential administration. Finally, thanks to all the colleagues of room G68 in the last 3 years and to the proof-readers. Last but not least, a big thank you to those who helped me in any way in the last three years, whether faraway or close. They know who they are.

Dublin, 28 March 2013

Chapter 1

Introduction

*The safety factor is an ignorance factor
(attributed to E. Giangreco)*

1.1 Background

Bridges are an essential part of any ground transportation network. As everything else, they deteriorate and their resistance decreases over time, especially as they approach the end of their lifespan. Authorities have to increasingly cope with the maintenance of the ageing infrastructure network, that in some cases may become unsafe.

Road bridges have the main objective of carrying traffic and traffic loading is a primary source of stress on the structure. However, traffic conditions are rather variable, as they depend on many factors, ranging from the macro scale (for instance, economic development) to the micro scale (such as individual driver behaviour).

Not surprisingly, of particular interest in bridge loading is the weight of vehicles. In this regard, trucks are far more important than cars. Maximum truck weights are regulated by national governments and the truck weight allowance has constantly increased over the last few decades. Not only have the single truck weights increased, but also the number of trucks in the road has grown. Therefore, on the one hand the road infrastructure is deteriorating (i.e., it is losing resistance), and on the other the load to which it is exposed is increasing. The safety conditions of existing bridges need then to be carefully reassessed.

Considerable research has been devoted to the study of the resistance of bridges, whereas less attention has been paid to the load to which a bridge is actually exposed. Given the large variability of vehicle weights and traffic conditions, codes of practice prescribe rather conservative traffic models for the design of the new bridges (European Committee for

Standardization, 2003; American Association of State Highway and Transportation Officials, 2010). Few codes are available for the assessment of existing bridges (AASHTO, 2011; The Highways Agency, 2001). Furthermore, the vast majority of codes is limited to short and medium-span bridges.

Most bridges are likely not to experience the high level of load prescribed in the design codes, with the consequence that the load models may be disproportionate to the traffic the bridge actually carries. This conservatism is generally acceptable for new bridges, where an increase in load typically requires a less than proportionate increase in construction costs, whereas in the case of existing bridges, it may play a decisive role in planning expensive maintenance operations. This may result in the bridge being replaced unnecessarily or prematurely.

Therefore, if an existing bridge could be assessed by considering its site-specific traffic features, the maintenance operations could be tailored on the actual traffic to which it is exposed, thus allowing significant savings, both in economic and environmental terms (e.g., saved maintenance costs and pollution and avoided congestion due to the traffic disruption).

In recent years, research has been mainly conducted on studies of traffic loading on short-span bridges. In this case, the governing traffic case is made up of one or two big vehicles, which dynamically interact with the bridge. No cars are involved in the governing case. On the other hand, long-span bridges are governed by congestion. Of particular interest is the interaction between vehicles, resulting in a large variability of inter-vehicle gaps. In long spans, cars cannot be neglected and play an important "indirect" role, as they keep heavy vehicles apart. However, congestion patterns are still under debate among the traffic engineering community, mainly due to a shortage of data during congestion and to site-specific differences. This is reflected in the fact that traffic loading on long-span bridges is often based on conservative assumptions.

In this thesis, a long-span bridge is defined as a bridge whose governing traffic case is congestion, as opposed to a short-span bridge, which is governed by one or two trucks dynamically interacting with the bridge. The threshold between the two cases is not clear-cut, but it typically lies between 30 and 50 m. In this regard, a long-span bridge has a shorter span than what may be commonly understood.

1.2 Target and methodology

The aim of this research is to understand the implications of different traffic conditions and features on the loading of long-span bridges. Indeed, to calculate the required load carrying capacity of a bridge, it is necessary to understand the nature of the traffic it carries.

Most previous research in traffic loading for long-span bridges considers a simplified traffic model, based on a queue of vehicles at minimum bumper-to-bumper distances (Ivy et al., 1954; Buckland et al., 1980; Harman et al., 1984; Flint and Neill Partnership, 1986; Ditlevsen and Madsen, 1994; Prat, 2001; Nowak et al., 2010). However, research in traffic engineering and experience suggest that many congestion patterns can occur and that in most cases speeds are likely to vary significantly, like in the so-called ‘stop-and-go waves’. Finally, the frequencies of congestion in these studies were based on little or no data.

Nowadays, increased computer performance enables sophisticated analyses to be carried out. *Micro-simulation* simulates vehicles individually, as opposed to *macro-simulation* which treats traffic in terms of aggregated quantities, such as flow or density. Micro-simulation is a powerful tool to generate realistic traffic congestions based on the widely available free traffic measurements, and it allows the study of the interaction between vehicles. Micro-simulation is used throughout this thesis and is implemented in the in-house software, "SIMBA" (*Simulation for Bridge Assessment*).

Micro-simulation models divide into car-following (single-lane) and lane-changing models (multi-lane). The car-following model used throughout this thesis is the *Intelligent Driver Model* (IDM), which has been found to successfully replicate observed congested states on several motorways (Treiber et al., 2000). Heavy vehicles are explicitly introduced in the IDM, as they are the main source of bridge loading. The IDM is then combined with the lane-changing model *MOBIL* (Kesting et al., 2007). Both models have relatively few parameters and therefore are a good compromise between computational speed and accuracy. They are calibrated against data available in the literature.

Congestion can be generated with a local variation of the model parameters. Resulting congested states can be broadly divided into oscillatory (stop-and-go waves) and

homogeneous states, where all vehicles drive at approximately the same speed (Treiber et al., 2000; Schönhof and Helbing, 2007).

Finally, statistical analyses of extreme values are carried out to find the characteristic maximum load corresponding to given return periods (from 1 to 1000 years).

1.3 Outline and structure of the thesis

The main body of this thesis comprises five papers submitted or ready for submission to international journals, one for each of Chapters 2-6. The material presented in each chapter is the work of the author, with the support of his supervisors. Minor modifications are made in the text to fit them into the context of this thesis and to minimise duplication. While Chapters 2-4 were or are going to be submitted to structural engineering journals, Chapters 5 and 6 were or are going to be submitted to transportation journals.

1.3.1 Chapter 2: Micro-simulation of single-lane traffic to identify critical loading conditions for long-span bridges

The main question addressed in Chapter 2 is whether there is a particular traffic congestion pattern which is more critical for bridge loading than other types. It also presents a literature review of available studies and models on long-span bridge traffic loading. Single-lane micro-simulations are carried out to simulate different congestion patterns and the loading on two long spans is computed. Surprisingly enough, in this study, it is found that the full stop condition (queue of vehicles at minimum bumper-to-bumper distances) frequently considered in most previous research is not always the governing case. Slow-moving traffic may be critical as well, especially for relatively shorter spans. This is due to the fact that full stop queues involve only one realisation of vehicles per congestion event, which actually reduces the probability of finding an extreme loading scenario. On the other hand, oscillatory states are found less critical, although they occur more frequently. In this study, the frequencies of occurrence of different congestion patterns are taken into account and a method is proposed for combining them. It is found that considering only the worst traffic condition (for loading) over-estimates the load by up to 10%, depending on the truck percentage and the span length.

1.3.2 Chapter 3: Long-span bridge traffic loading using multi-lane traffic micro-simulation

Chapter 3 extends the car-following IDM model with the lane-changing model MOBIL. While car-following models are relatively more established, lane-changing models suffer from a greater lack of data, as it is quite problematic to track the movements of the many vehicles involved in a single lane-changing manoeuvre. Here, the lane-changing model is calibrated with available data in literature. The introduction of the lane changes allows the consideration of the changes in car-truck mix due to the overtaking manoeuvres, which would not be possible with a car-following model. In fact, car drivers do not feel comfortable driving closely in between trucks and in these conditions they tend to move to the fast lane, thus increasing the frequency of long truck-only platoons in the slow lane.

Multi-lane micro-simulations are then carried out to simulate congestions with a variety of traffic compositions. This study confirms that slow-moving traffic may be as critical as full stop conditions. Most importantly, it points out that critical loading events may occur out of rush hours: indeed, the inflow does not significantly affect the bridge loading, provided that congestion breaks down. Finally, the effects of truck platoons, truck lane distribution and truck percentage, as well as the influence of cars, are analysed and quantified.

1.3.3 Chapter 4: A methodology for computing traffic loading on long-span bridges based on micro-simulation and site-specific traffic data

Chapter 4 analyses the frequency of congestion, and thus of critical loading events, to which a bridge is expected to be exposed. Indeed, some rural highway bridges are hardly ever affected by congestion. For sites with low traffic demand, congestion is caused by unpredictable events, such as incidents. A new methodology is proposed to compute the characteristic load based on traffic micro-simulation and site-specific traffic data, such as incident patterns and hourly flow distributions. The methodology is then applied to traffic data available from the literature. It is found that flows with high truck percentage, typically occurring at night-time in combination with low flows, largely contribute to the characteristic load, even though congestion in such conditions is quite rare.

1.3.4 Chapter 5: Accuracy of congested density estimates from point detectors

Chapter 5 deals with the estimation of traffic density, defined as the number of vehicles per unit length of road. In fact, traffic data is largely collected at single points in space (e.g., by induction loop detectors), thus returning information only at cross-sections. Density is often inferred from such point measurements, following an assumption of constant speed. Most previous studies in bridge loading use a similar approach, where vehicle data comes from point measurements and then vehicles are placed over a bridge following a typical assumption of constant speed. While such an assumption is acceptable for free traffic, it does not always hold during congestion, as conditions are very changeable over space and speeds are likely to vary, like during stop-and-go waves. For bridge loading, if the number of vehicles over a bridge is significantly wrong, so will be the loading.

It is found that the maximum density estimated from point detectors, necessary for identifying critical loading events, may be significantly inaccurate in oscillatory traffic, while homogeneous congested states are less affected. On the other hand, average values of density are fairly well estimated.

1.3.5 Chapter 6: The effect of controlling heavy vehicle gaps on long-span bridge loading

Chapter 6 outlines a promising application of micro-simulation to bridge loading control. Traditionally, the way to limit the load on a bridge is to restrict the heavy vehicle weights. Here, an alternative way of limiting the load on long-span bridges by keeping the trucks apart, is put forward. The effects of a system capable of warning truck drivers when their gap to the front vehicle falls below a certain threshold are investigated by means of single-lane micro-simulations. It is found that significant reductions in bridge loading can be attained, while disrupting the traffic only marginally.

1.3.6 Appendices

The appendices comprise of synopses of two published papers (Appendix A and C) and four further appendices reporting supplementary information and analyses. The description of the appendix contents is reported in Table 1.1.

Table 1.1 - Appendix contents.

Appendix	Description
A 'A comparative study of a bridge traffic load effect using micro-simulation and Eurocode load models'	Real traffic data is used to derive design load effects from single-lane micro-simulations. Results are compared to the Eurocode load model. It is shown that the micro-simulation-based design load effects are about 25% less than the one prescribed in the Eurocode, while keeping the required safety level. It is related to the work presented in Chapter 2.
B 'Multi-class traffic simulations'	Trucks need to be introduced in the micro-simulation model, but they significantly affect the traffic. Details on how to consider trucks in the micro-simulation model are provided. It is related to the work presented in Chapter 2, but the procedures proposed here are applied also in Chapters 3, 4 and 6.
C 'Micro-simulation modelling of congestion due to lane closures'	The modelling of merging manoeuvres in proximity of a lane closure requires a different lane-changing parameter calibration. This more precise modelling is compared to the equivalent local variation of parameters used elsewhere in the thesis. It is related to the work of Chapter 3.
D 'Refinement and calibration of the lane-changing model'	The refinement and the calibration process needed for the lane-changing model used in Chapter 3 and 4 is described in detail.
E 'Traffic data collection for bridge load applications'	This appendix extends the work of Chapter 5, highlighting the implication of the traffic data collection method on bridge loading. A camera system for congested data collection is outlined and recommendations are made for further development.
F 'SIMBA overview'	This appendix gives an overview of the micro-simulation tool used throughout this work.

Chapter 2

Micro-simulation of single-lane traffic to identify critical loading conditions for long-span bridges

Authors:

Eugene J. OBrien

Alessandro Lipari

Colin C. Caprani

Paper Status:

Submitted for publication to *Engineering Structures*. Minor modifications are done to fit into the context of this thesis.

Note to the Reader:

The work in this chapter is entirely the work of the author under the supervision of Prof OBrien and Dr Caprani.

2.1 Introduction

It has been long acknowledged that long-span road bridges are governed by congested traffic rather than free-flowing conditions (Ivy et al., 1954). In free flowing traffic, vehicles have large gaps between them, while congestion implies long queues of closely spaced vehicles. In congested conditions, vehicle-bridge dynamic interaction is not significant, since critical events occur at slow speeds (Buckland et al., 1980). The bridge length threshold between the two cases depends on many factors but it is thought to lie between 30 and 50 m (Bruls et al., 1996b; O'Connor and O'Brien, 2005; Caprani, 2012c).

Traffic loading for long-span bridges is not taken into account in most codes of practice. The use of short-span bridge load models for longer spans is rather conservative, as the average intensity of loading tends to reduce with increasing span (Buckland et al., 1980; Flint and Neill Partnership, 1986; Nowak et al., 2010). In the case of existing bridges, excessive conservatism is a greater problem as it may lead to expensive and unnecessary interventions.

Real-world observations show that congestion can take up different forms. Nevertheless, most previous studies on bridge traffic loading consider only a queue of vehicles at minimum bumper-to-bumper distances (Ivy et al., 1954; Buckland et al., 1980; Harman et al., 1984; Flint and Neill Partnership, 1986; Vrouwenvelder and Waarts, 1993; Ditlevsen and Madsen, 1994; Bailey and Bez, 1999; Prat, 2001; Nowak et al., 2010). Micro-simulation simulates the behaviour of individual vehicles and allows the generation of observed congested patterns, thus providing a valuable tool to study the effects of different congestion patterns and traffic compositions on long-span bridge loading.

2.1.1 Data collection

Traffic weight data is based on either truck surveys, or, more recently, weigh-in-motion (WIM) measurements. However, many WIM devices deployed on highways can weigh vehicles only at high speeds. Furthermore, traffic data, such as vehicle counts or speeds, is typically collected by means of induction loops (sometimes combined with WIM devices), which may not be reliable at very low speeds (Klein et al., 2006). As a consequence, data is generally collected during free-flowing traffic conditions, which also occur much more frequently than congestion.

Free flowing traffic measurements are suitable for the analysis of traffic loading on short-span bridges, whose critical loading is made up of one or two big vehicles (see for instance Buckland et al. (1980)). In such cases, the inter-vehicle gaps (or headways) can be taken directly from the WIM database, or from an assumed headway model (OBrien and Caprani, 2005). However, in long-span bridges, congestion governs and the gaps in such situations are mostly unknown.

Not only is the data collection problematic during congestion, but also the analysis of the traffic data can pose some issues (Banks, 2002; Ni, 2007). Traffic data is generally collected only at point locations and vehicle positions can then only be estimated from such point measurements. However, bridge load effects, such as bending moments and shear forces, are strongly influenced by the spatial distribution of the vehicles. The estimation of the maximum number of vehicles present on a stretch of road during congestion may result in a significant loss of accuracy, as shown in Chapter 5. The use of spatial detectors (such as cameras) over a stretch of road allows the collection of the vehicle positions during congestion, without resorting to estimation. Although cameras are the best solution from a theoretical point of view, they are not often used for practical reasons and because of sensitivity to weather and lighting conditions (Klein et al., 2006). They have however been deployed for research purposes (Treiterer and Myers, 1974; Coifman et al., 1998; Hoogendoorn et al., 2003; Federal Highway Administration, 2005) and are becoming more popular. Recommendations for the development of a camera system for bridge loading applications are made in Section E.4.

In bridge loading studies, only Buckland et al. (1980) and Nowak et al. (2010) state that they have used video recordings. Ricketts and Page (1997) use videos at various UK sites for manual vehicle classification during congestion. OBrien et al. (2012) manually analyse videos for a micro-simulation model calibration. Zaurin and Catbas (2010) propose a procedure for automatically tracking vehicles in the context of bridge health monitoring.

2.1.2 Codes of practice and previous research on long-span bridge traffic loading

Research on traffic loading for bridges is often related to studies for developing codes and standards. Existing load models for long-span bridges account for the variability of truck weights, but they often assume a simplified traffic model, typically represented by a mix of

cars and heavy vehicles at minimum bumper-to-bumper distances (Ivy et al., 1954; Buckland et al., 1980; Harman et al., 1984; Flint and Neill Partnership, 1986; Vrouwenvelder and Waarts, 1993; Ditlevsen and Madsen, 1994; Bailey and Bez, 1999; Prat, 2001; Nowak et al., 2010).

The normal load model in Eurocode 1 (European Committee for Standardization, 2003) is based on traffic data collected at Auxerre (France), considering 100% trucks in the slow lane for jammed situations (Bruls et al., 1996a) and later confirmed with a more extensive database (O'Connor et al., 2001). Its application is valid only for the design of bridges up to 200 m. Details of the current Eurocode load model are reported in Section A.2. Other national codes, for example the British and Italian ones, suggest loading curves for longer spans (British Standard, 2006; Consiglio Superiore dei Lavori Pubblici, 2008). The Highways Agency (2001) prescribes a reduction factor for the design load model for long-span bridge assessment in the United Kingdom.

The American code (AASHTO, 2010) may be considered to apply to “ordinary bridges” with spans up to 152 m (Buckland, 1991; AASHTO, 2002), although in the calibration of its current traffic load model, the maximum span considered is 60 m (Nowak, 1995). Lutomirska (2009) shows that the AASHTO load model can be used for most spans up to 1500 m. Previously, the American Society of Civil Engineers (Committee on Loads and Forces on Bridges of the Committee on Bridges of the Structural Division, 1981) recommended a load model for the design of spans up to 1951 m, based on the work of Buckland et al. (1980). For assessment, the AASHTO (2011) prescribes a “legal” vehicle for the rating of existing bridges longer than 60 m.

Besides codes and standards, Ivy et al. (1954) record 5629 heavy vehicles on a long-span bridge in San Francisco; the trucks are all placed at an average distance recorded in the field. Harman et al. (1984) develop a procedure for predicting live-load effects by using traffic surveys. The Flint and Neill Partnership (1986) uses truck surveys and (free flow) data to build up queues of heavy vehicles and cars; the results are extrapolated to find a characteristic loading curve. Vrouwenvelder and Waarts (1993) develop a load model based on data from the Netherlands, differentiating between free, congested and full stop traffic. Ditlevsen and Madsen (1994) develop a theoretical framework for building up queues based on a cell

discretisation of the bridge. Bailey and Bez (1999) develop a methodology to derive probability distributions of extreme traffic actions based on site-specific data; they differentiate traffic in free, congested and at-rest, and assign a probability distribution to gaps. Nowak et al. (2010) use WIM data and videos of congested traffic to develop a design load model made up of an average heavy vehicle queue on the slow lane.

Table 2.1 lists the assumed congested gaps in selected models. Note that vehicles are generally moved along the bridge: the first vehicle is removed, the queue is then moved forward and a vehicle is added at the other end of the bridge. All of these methods exclude the observed variability of congested patterns, perhaps with the exception of Vrouwenvelder and Waarts (1993) and Bailey and Bez (1999), whose traffic models were quite simple, though, with all the vehicles moving at the same constant speed. Moreover, congestion frequencies of occurrence are assumed or based on little data.

Table 2.1 - Congested gaps and maximum span length application for selected existing load models.

Models	Congested gaps (m)	Span Length (m)
Ivy et al. (1954)	2.4	> 120
ASCE (Buckland et al., 1980)	1.5	15 – 1951
Flint and Neill Partnership (1986)	0.9 - 1.8	75 – 1600
Vrouwenvelder and Waarts (1993)	1 - 10	2 – 200
Eurocode studies (Prat, 2001)	5*	5 – 200
Nowak et al. (2010)	4.5	180 – 1500

* between subsequent axles.

Recently, traffic micro-simulation has been used to achieve a more accurate traffic modelling, with the notable advantage that widely-available free-flowing traffic measurements can be used to generate congested traffic scenarios. OBrien et al. (2012) study a long-span bridge in the Netherlands and calibrate a commercial micro-simulation tool using WIM data, videos and strain gauge measurements. Chen and Wu (2011) use the cellular automaton approach (initially proposed by Nagel and Schreckenberg (1992)), in which the bridge is divided into 7.5 m long cells. However, the cellular structure does not allow for the variability of vehicle lengths and gaps between vehicles and this is critically important in bridge loading. Caprani (2012b) uses micro-simulation to calibrate a simple congested load model for short- to medium-length bridges.

2.2 Micro-simulation model

Micro-simulation is widely used in traffic engineering with many models having been developed in the past decades (Brackstone and McDonald, 1999; Hoogendoorn and Bovy, 2001; Orosz et al., 2010). Micro-simulation takes account of the interaction between vehicles, thus introducing driver behaviour into the model. Free traffic measurement can be used to generate initial traffic conditions but congested data is still required for calibration and validation (Hidas and Wagner, 2004).

Micro-simulation models divide into car-following (single-lane) and lane-changing (multi-lane) models. Throughout this thesis, a car-following model is used which has been found to replicate several kinds of observed congestion on several motorways (Treiber et al., 2000). The micro-simulation model is implemented in an in-house program known as SIMBA (*SIMulation for Bridge Assessment*). An overview of SIMBA is given in Appendix F.

Single-lane micro-simulations are carried out considering a high inflow rate, representative of peak hour traffic. Different kinds of congestion are generated and the total load is studied on two long spans (200 and 1000 m). The focus here is to identify congestion states which may be critical for long-span bridge loading.

Lane change activity is known to be low during congestion (Sparmann, 1979), thus making the present single-lane approach relevant to multi-lane roadways as well. The consideration of a high truck percentage can represent the slow lane of a multi-lane roadway, where the majority of trucks is typically concentrated.

2.2.1 *The Intelligent Driver Model*

The *Intelligent Driver Model* (IDM) is a car-following model, which, in spite of having few parameters and using identical vehicles with constant parameters, has been shown to provide a good match with real congested traffic on some German *multi-lane* motorways (Treiber et al., 2000). It has also been calibrated with trajectory data (Kesting and Treiber, 2008; Chen et al., 2010; Hoogendoorn and Hoogendoorn, 2010) and compared to other calibrated car-following models, returning results comparable to more complex models (Brockfeld et al., 2004; Punzo and Simonelli, 2005). Therefore, it appears as an optimal compromise between

accuracy and computational speed. The IDM simulates driver behaviour in time through an acceleration function:

$$\frac{dv(t)}{dt} = a \left[1 - \left(\frac{v(t)}{v_0} \right)^4 - \left(\frac{s^*(t)}{s(t)} \right)^2 \right] \quad (2.1)$$

where a is the maximum acceleration, v_0 the desired speed, $v(t)$ the current speed, $s(t)$ the current gap to the front vehicle, and $s^*(t)$ the desired minimum gap, given by:

$$s^*(t) = s_0 + Tv(t) + \frac{v(t)\Delta v(t)}{2\sqrt{ab}} \quad (2.2)$$

in which, s_0 is the minimum jam distance, T the safe time headway, $\Delta v(t)$ the speed difference between the current vehicle and the vehicle in front, and b the comfortable deceleration. The motion results from the interaction of a deceleration and an acceleration strategy. The term $dv(t)/dt = -a(s^*(t)/s(t))^2$ represents the tendency to brake when a vehicle gets too close to the leader, whereas the term $dv(t)/dt = a[1 - (v(t)/v_0)^4]$ represents the tendency to accelerate to the desired speed v_0 on a free road. Equations (2.1) and (2.2) are discretised here into 250 ms steps.

There are five parameters in this model to capture driver behaviour, which are relatively easy to measure. For simulation purposes, the length of the vehicles must also be known.

2.2.2 Congested Traffic States

Treiber et al. (2000) show that congestion can be effectively generated by either locally decreasing the desired speed v_0 or increasing the safe time headway T (*flow-conserving inhomogeneity*). Such local parameter variations slow the traffic in a similar way to on-ramp bottlenecks or lane-closures. Throughout this thesis, inhomogeneity is generated by increasing the safe time headway T downstream, say T' , which Treiber et al. (2000) state to be more effective than decreasing v_0 .

The bottleneck strength, ΔQ , can be defined as the difference between the outflow Q_{out} with the original parameter set and the outflow Q'_{out} with the modified safe time headway T' :

$$\Delta Q(T') = Q_{\text{out}}(T) - Q'_{\text{out}}(T') \quad (2.3)$$

The outflow here is the *dynamic capacity*, that is, the outflow from a congested state. It is well established that, after traffic flow breaks down, the maximum outflow drops from the *static capacity* Q_{max} to a value related to the discharge rate of the queue (Kerner and Rehborn, 1996; Cassidy and Bertini, 1999; Transportation Research Board, 2010), which is the *dynamic capacity* Q_{out} . The bottleneck strength can be also computed as an equivalent on-ramp inflow (Schönhof and Helbing, 2007). For practical applications, the velocity at the detector nearest to the bottleneck can also be used as a proxy for the bottleneck strength (Treiber and Kesting, 2012).

Depending on the inflow Q_{in} and the bottleneck strength ΔQ , and for a given traffic history, the traffic can take up any of the traffic states explained in Table 2.2 (Treiber et al., 2000; Schönhof and Helbing, 2007). A combination of these congested states may also occur. In general, increasing bottleneck strength has the effect of moving down the table to a higher intensity of congestion. Congested states that occupy a significantly long stretch of road (the so-called *extended* states), such as SGW, OCT and HCT, are of significance for long-span bridge loading applications.

Table 2.2 - Congested traffic states.

Acronym	Explanation of traffic state
FT	Free traffic
MLC	Moving localized cluster
PLC	Pinned localized cluster
SGW	Stop and go waves
OCT	Oscillating congested traffic
HCT	Homogeneous congested traffic

A trajectory plot is a graph showing the position of vehicles through time. The slope of each vehicle trajectory curve is proportional to its speed. An example of typical trajectory data for traffic made up of identical vehicles is given for two bottleneck strengths in Figure 2.1 (for the parameters, see the car set in Table 2.3). Figure 2.1a shows a typical SGW state. Each vehicle goes through cycles of slower and faster travel (low slope and steep slope). The congestion waves propagate backwards at about 10 km/h, which is in the lower range of observed wave propagation speeds. However, there is no typical wavelength or period

(Schönhof and Helbing, 2007; Zielke et al., 2008). In between the waves, drivers recover speed up to 60 km/h before meeting another wave. Figure 2.1b shows an OCT state in which waves exist but are less pronounced. The waves keep their characteristic propagation speed, but they are closer and the speed amplitude is less, as vehicles rarely exceed 40 km/h in between the waves. The downstream speed amplitude is even smaller, getting close to a HCT state, which shows no oscillation at all.

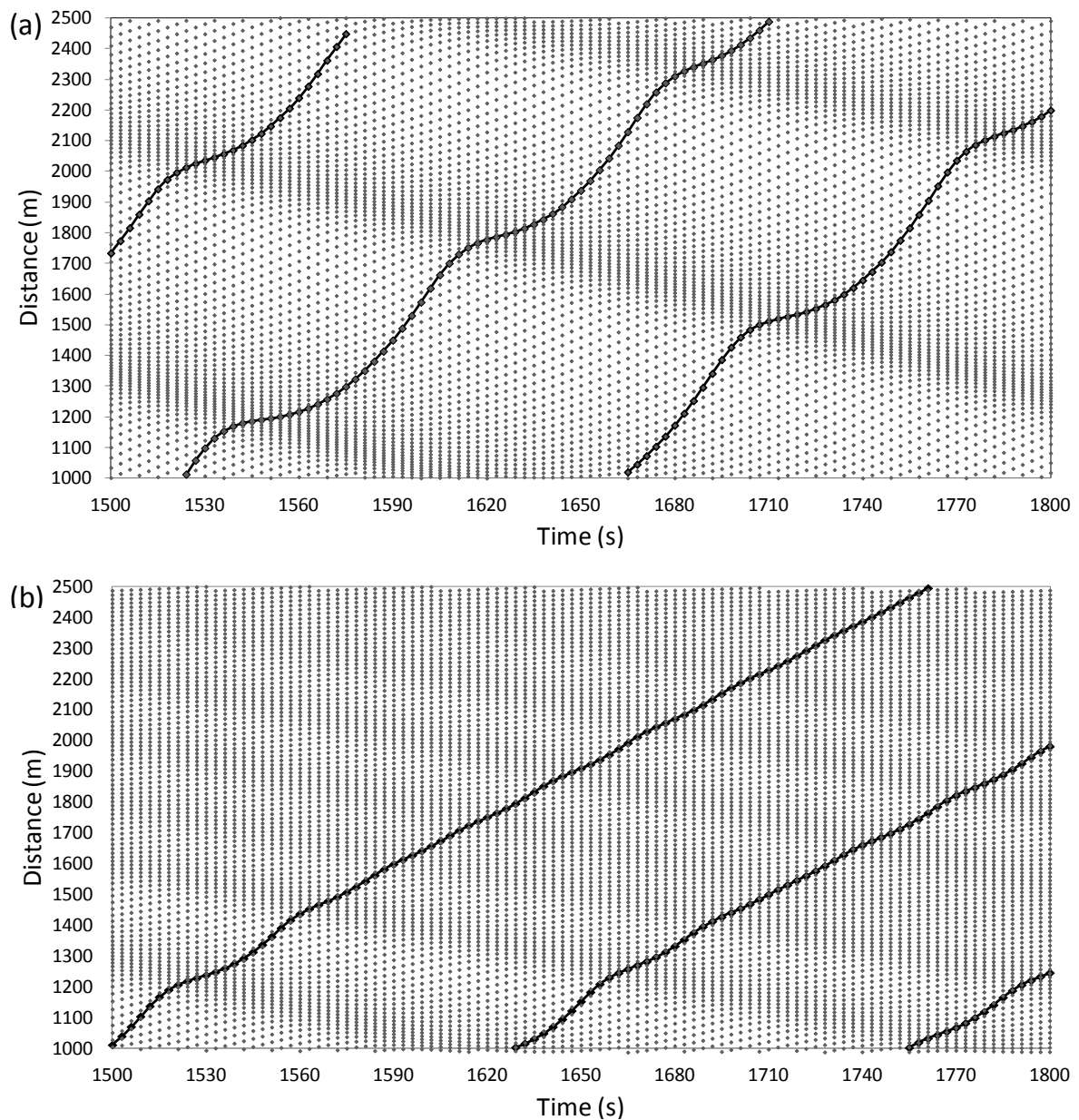


Figure 2.1. Example of trajectory data for (a) SGW and (b) OCT. Trajectories of vehicle Nos. 650, 700 and 750 are highlighted.

Table 2.3 - Model parameters.

Parameter	Car	Truck
Desired speed, v_0	120 km/h	80 km/h
Safe time headway, T	1.6 s	1.6 s
Maximum acceleration, a	0.73 m/s ²	0.73 m/s ²
Comfortable deceleration, b	1.67 m/s ²	1.67 m/s ²
Minimum jam distance, s_0	2 m	2 m
Vehicle length, l	4 m	12 m
Gross Vehicle Weight, GVW	20 kN	432 kN*

* Normally distributed with CoV = 0.1.

2.2.3 Multi-class simulations

The work of Treiber et al. (2000) is based on identical vehicles. However, in this research trucks need to be introduced, as they are the largest source of load. It is well known that the truck presence reduces the capacity of a road (Transportation Research Board, 2010). Therefore, traffic streams with different truck percentages have different dynamic capacities Q_{out} , which affect the bottleneck strength ΔQ through Equation (2.3), and subsequently the expected congested state. In order to make a meaningful comparison between congestion states with different truck percentages, it is important that the effects on traffic be equivalent, that is, pairs of $Q_{in}/\Delta Q$ that return the same congestion must be found. The Highway Capacity Manual (Transportation Research Board, 2010) suggests *heavy-vehicle adjustment factors* f_{hv} in order to scale the capacity of mixed traffic to an equivalent base flow made up of passenger cars only. A similar equivalence is set out here in terms of the dynamic capacity Q_{out} .

In order to compute the dynamic capacity Q_{out} , it is necessary to induce congestion without modifying the original parameter set (Table 2.3), thus inhomogeneities cannot be introduced. The outflow is then worked out by creating an overflow, i.e., by injecting a number of vehicles higher than the road capacity Q_{max} . Doing this leads to the formation of localized vehicle clusters, whose outflow is deemed to be the dynamic capacity Q_{out} . Further details on the computation process of the static and dynamic capacity are given in Appendix B.

Truck proportions of 20% and 50% are randomly injected between cars. The lesser percentage is adopted as a common truck percentage on a busy commercial route, while the greater percentage accounts for multi-lane carriageways, which typically have a greater truck percentage in the slow lane (see Section 3.4.2). Note also that such a high percentage is

possible when flow is low, typically at night or in the early morning (Flint and Neill Partnership, 1986; Ricketts and Page, 1997; Hallenbeck et al., 1997; Caprani et al., 2012a).

Table 2.4 gives the dynamic capacity Q_{out} for the mixed traffic conditions, as well as the static capacity Q_{max} , which can be attained only in free traffic. The reference condition of 0% trucks and the condition of 100% trucks are included for comparison. For the parameter set chosen (Table 2.3), Q_{out} and Q_{max} are quite close, whereas in real traffic the difference may be higher (Kerner and Rehborn, 1996; Cassidy and Bertini, 1999). Moreover, the static capacities are smaller than typical observed values (Knoop et al., 2008; Transportation Research Board, 2010). However, the IDM has been calibrated to reproduce observed congested states, which are critical for long-span bridge loading.

Table 2.4 - Capacity of multi-class traffic.

Truck percentage	Q_{out} (veh/h)	f_{hv}	Q_{max} (veh/h)	Q_{out}/Q_{max}
0%	1686	1.00	1790	0.94
20%	1590	0.94	1630	0.98
50%	1462	0.87	1489	0.98
100%	1291	0.77	1311	0.98

2.3 Model and simulation parameters

2.3.1 Traffic stream

In order to minimize the number of variables whilst retaining the essential features of the problem, the vehicle stream is taken as being made up of two classes: cars and trucks. Each vehicle of the same class is given the same set of parameters, shown in Table 2.3. The car parameter set is based on that used by Treiber et al. (2000), while the truck parameters are chosen by judgement, acknowledging that they are slower, longer, and heavier.

A standard truck configuration is adopted with mean GVW arbitrarily taken as the minimum European legal limit of 44 t (The Council of the European Union, 1996) and normally distributed with a Coefficient of Variation (CoV, standard deviation divided by mean) of 0.1. The distribution of weight between axles (Figure 2.2) is representative of this vehicle class in the Auxerre traffic data on which the Eurocode load model is based (Grave et al., 2000). Front

and back overhangs of 0.9 m are assumed. The assumed truck distribution is rather heavy and does not represent actual traffic. These simplifications are deliberate – they seek to keep the underlying assumptions about the traffic stream as simple as possible, in order to identify the effects of different congestion patterns on loading.

Distributions of GVW collected from real traffic are likely to be not as heavy as the one assumed here. An application of single-lane micro-simulation based on GVW data collected from WIM stations is reported in Appendix A. It shows that, for that data, the microsimulation-based design leads to a 25% reduction in the characteristic design load compared to the current European code (European Committee for Standardization, 2003), while keeping the required safety level.

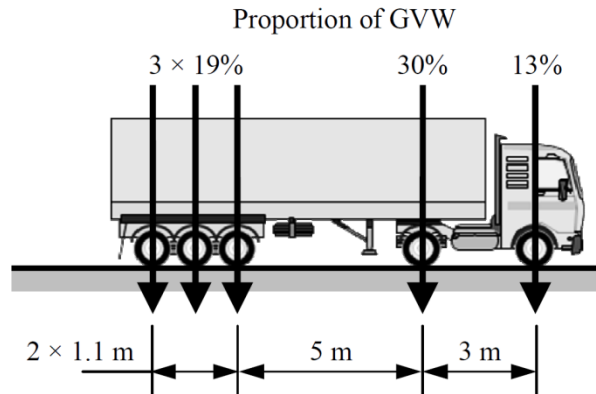


Figure 2.2 - Assumed truck configuration and axle weight proportions of GVW.

2.3.2 Road geometry and bottleneck strength

A single-lane 5000 m long road is used in this work. The safe time headway is given the value T for locations in the range from 0 to 2700 m (see Table 2.3). Then it increases gradually to the value T' at 3300 m. A range of values for T' (and consequently bottleneck strengths, ΔQ) are considered: 1.9, 2.2, 2.8, 4.0 and 6.4 s. The inflows Q_{in} are set equal to the dynamic capacity Q_{out} , corresponding to the relevant truck percentage (Table 2.4).

Figure 2.3 shows the relationship between the applied inhomogeneity, $\Delta T = T - T'$, and the resulting equivalent bottleneck strength, ΔQ_{eq} . It can be seen that the same inhomogeneities return similar equivalent bottleneck strengths, regardless of the percentage of trucks. More details on the derivation of the equivalent bottleneck strengths are given in Section B.2.8.

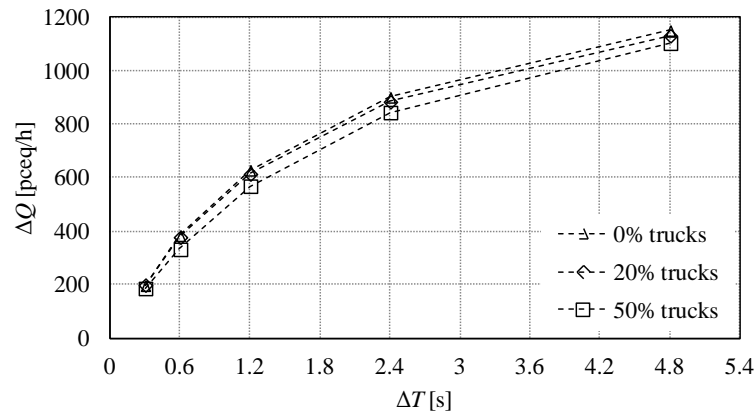


Figure 2.3 - Equivalent bottleneck strength.

For comparison with the common traffic loading assumption, the full stop condition (FS) is also simulated. This corresponds to $\Delta T = \infty$ or $Q'_{\text{out}} = 0$ veh/h. Then the equivalent bottleneck strength ΔQ_{eq} is 1686 passenger-car equivalents per hour (pceq/h), according to Equation (2.3). Note that in most previous load models, the queue of vehicles at a minimum bumper-to-bumper distance is often moved across the bridge, so that the traffic state could actually resemble a HCT state, rather than a full stop condition, but with shorter gaps.

Finally, it is assumed that the road is recurrently affected by one hour of congestion each working day of a 250-day year. Two years of congested traffic are simulated for each bottleneck strength and truck percentage, giving a total of 6000 hours of congestion analysed.

2.4 Traffic results

2.4.1 Spatio-temporal congestion plots

Spatio-temporal plots are useful for visualizing congested patterns. It is convenient to draw a comparison in terms of mean speed, since flow or density may vary significantly depending on the truck percentage. The speed axis is depicted upside down, so that peaks represent congestion. Here, the *space mean speed* is used, computed as the harmonic mean of the individual vehicle speeds collected at one point (Wardrop, 1952). The space mean speed is collected at four virtual point detectors placed between 1000 and 2500 m and is aggregated in 60 s intervals. Figure 2.4a shows a SGW state, where the waves are clearly visible as peaks (see also Figure 2.1a). Figure 2.4b shows a combined HCT/OCT state, where the upstream

small oscillations typical of the OCT state fade away into a HCT state downstream, where there are no significant oscillations.

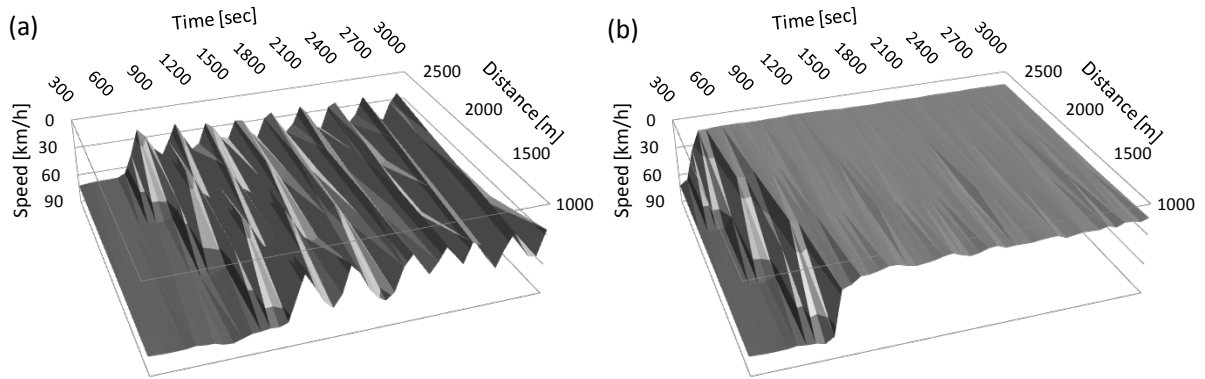


Figure 2.4. Spatio-temporal speed plots of (a) SGW and (b) HCT/OCT with 20% trucks.

2.4.2 Effect of truck percentage

After determining the heavy-vehicle adjustment factors f_{hv} for the different traffic compositions analysed (Table 2.4), it is useful to see how the congested states change in response to the varying truck percentage. Figure 2.5a shows that the generated congested states are actually quite similar in terms of average speed over the congested area 1000-2500 m. Note that two HCT states are generated, which differ only in the average speed and are labelled HCT(1) and HCT(2), with the latter representing a very heavy state of congestion, where speeds are of the order of 5 km/h and vehicles are spaced at about 4.5 m

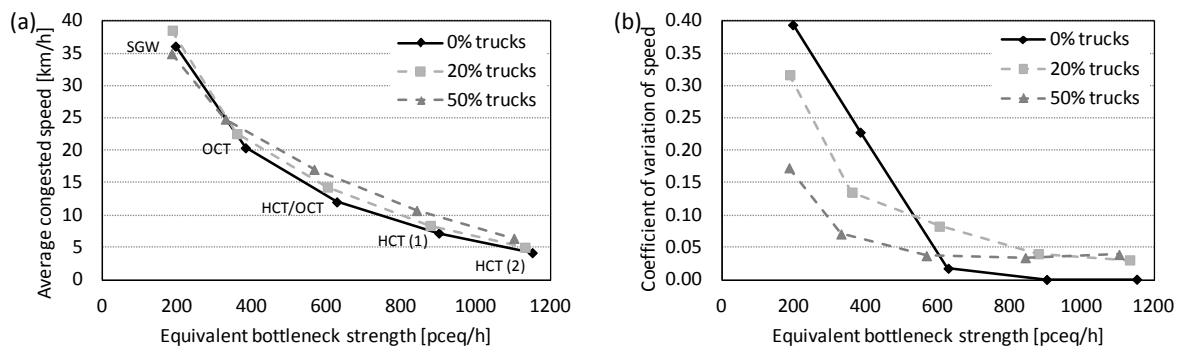


Figure 2.5. Distribution of speed in the congested area: (a) average, (b) coefficient of variation.

It is also interesting to consider the traffic oscillation properties, which show a greater sensitivity to the truck percentage (Figure 2.5b). A greater coefficient of variation of the speed

indicates prominent oscillatory behaviour. Indeed the lightest bottleneck strengths show a high coefficient of variation, which reduces as the bottleneck strength increases. The truck presence actually dampens the speed oscillations at the lightest bottlenecks, probably due to their slower desired speed. On the other hand, their different properties introduce a small disturbance in the homogenous congested states which, in the absence of trucks, show no oscillations.

2.5 Loads on bridges

2.5.1 Introduction

In this section, the total load on two long spans (200 and 1000 m) is computed. The bridges are placed upstream of the inhomogeneity and centred at 2000 m in the 5000 m length of roadway modelled. As common in traffic loading studies, a probabilistic approach is used for determining the load, z , which has a given probability of non-exceedance, $F(z)$, usually expressed in terms of *return period*, T (Coles, 2001). The two variables are linked through the relation:

$$T(z) = \frac{1}{1 - F(z)} \quad (2.4)$$

The maximum total load for each one-hour congestion event is captured. Assuming one hour of congestion per day, the hourly/daily maximum values of the total load are extrapolated to determine 5-year characteristic values. Doing so assumes that only one type of congestion occurs during the 5-year reference period. The issue of mixing different congestion types is addressed in Section 2.6.

The Generalised Extreme Value (GEV) distribution is fitted to the simulated daily maximum total loads. The probability F that a load level, z , is not exceeded is (Coles, 2001):

$$F(z) = \exp \left\{ - \left[1 + \xi \left(\frac{z - \mu}{\sigma} \right) \right]^{\frac{1}{\xi}} \right\} \quad (2.5)$$

where μ is the location, σ the scale and ξ the shape parameter. Equation (2.5) is defined for any value z for which $1 + \xi\left(\frac{z - \mu}{\sigma}\right) > 0$. The GEV parameters are inferred through maximum likelihood estimation, whose procedure is outlined in Section A.5.2. When $\xi = 0$, the GEV distribution reduces to the Gumbel distribution:

$$F(z) = \exp\left\{-\exp\left[-\left(\frac{z - \mu}{\sigma}\right)\right]\right\} \quad (2.6)$$

Gumbel probability paper is used to illustrate the extrapolation procedure (Ang and Tang, 2007). On this scale, data from a Gumbel distribution appears as a straight line. The y-axis ordinate, or Standard Extremal Variate (SEV), is given by $-\log\left[-\log\left(F(z)\right)\right]$. For the 5-year return period and with 250 working days per year, the target probability of non-exceedance for maximum-per-day data $F(z^*)$ is 0.9992 and the target SEV is $-\log\left[-\log\left(1 - 1/(5 \times 250)\right)\right] = 7.13$.

2.5.2 Results for 200 m bridge

The probability paper plots for the 200 m span are shown in Figure 2.6, as well as the 5-year characteristic hourly/daily maximum values z^* . The hourly maximum values for free flowing traffic are shown for reference and can be seen on the left-hand side of the plot, to be quite separate from the congested ones. The distribution for the combination of congestion types is also plotted and it is addressed in Section 2.6.

It can be seen that the different congestion types are separate from each other and that greater bottleneck strength implies greater load, with the exception of the FS. Figure 2.6a gives results for the more common case of 20% trucks. Most trends curve upwards, suggesting compliance with the Weibull distribution ($\xi < 0$). The Weibull distribution indicates data for which there is an upper bound which is not exceeded as the cumulative probability approaches unity. This is reasonable given that traffic cannot be infinitely heavy. The two full HCTs are the most critical congestion states. FS tends to be low because it is the maximum of just one realisation of truck weights. FS conditions have a greater scale parameter σ ,

indicating more scattering across the load range, and smaller shape parameter ξ , indicating higher curvature upwards or more bounded behaviour (Table 2.5).

The high truck percentage (Figure 2.6b) has the effect of reducing the variability of truck concentrations, so that the load values for each congestion type are concentrated in a smaller range (as a smaller scale parameter σ shows, Table 2.5). Several maxima for the full stop condition are relatively low (see also Figure 2.7) but the slope of the maximum likelihood fit is also low with the result that the characteristic value exceeds all others.

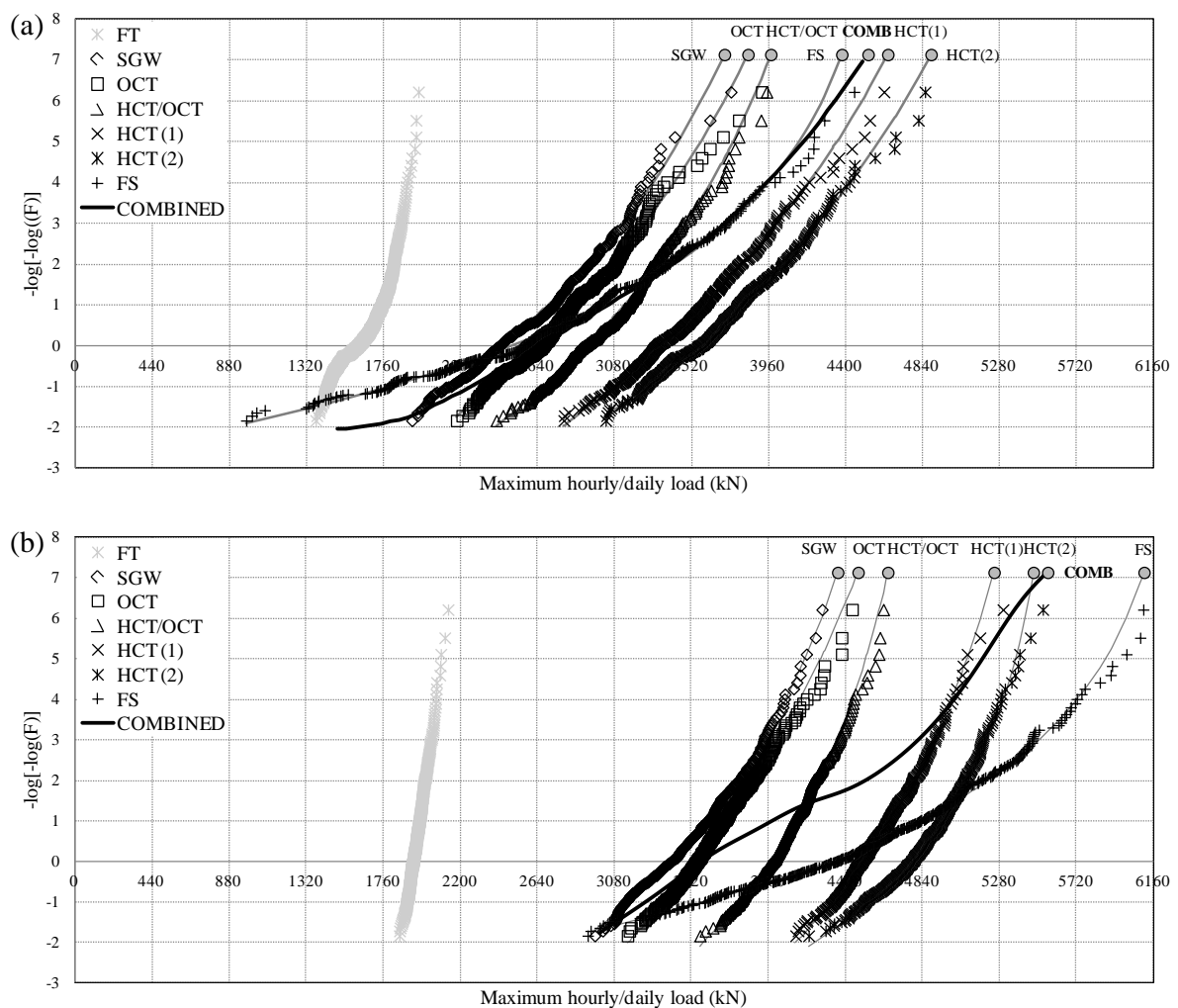


Figure 2.6. Probability paper plot of total load on 200 m span with (a) 20% and (b) 50% trucks; each vertical gridline approximately represents the weight of one average truck.

The average hourly/daily maxima are illustrated in Figure 2.7. The general trend is one of linearly increasing total load with increasing bottleneck strength, with the exception of the

average FS condition for the reasons discussed above. The GEV parameters for the maximum likelihood fits are given in Table 2.5 for all cases, together with the characteristic maximum total loads.

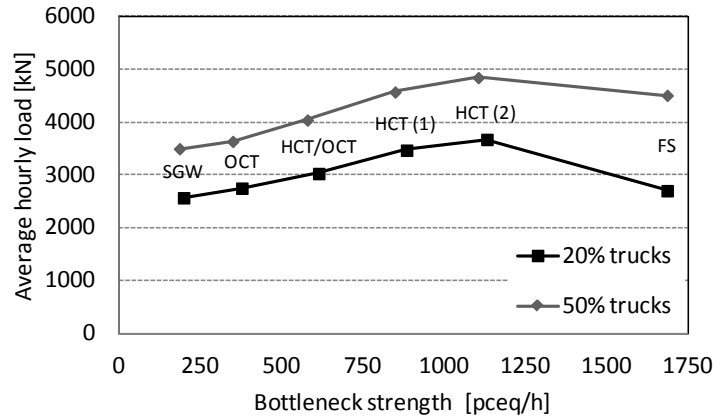


Figure 2.7 - Average maximum load for an hour of congestion on the 200 m span.

Table 2.5 - Parameters and extrapolated values of the GEV distribution (200 m span).

Congestion type	20% trucks				50% trucks			
	μ	σ	ζ	z^*	μ	σ	ζ	z^*
SGW	2441	279.8	-0.139	3708	3399	221.7	-0.154	4358
OCT	2635	240.5	-0.105	3842	3550	177.5	-0.093	4474
HCT/OCT	2923	230.9	-0.137	3973	3973	160.8	-0.166	4644
HCT (1)	3346	257.4	-0.104	4641	4498	164.7	-0.135	5251
HCT (2)	3544	272.4	-0.110	4889	4767	210.0	-0.245	5475
FS	2490	608.0	-0.277	4379	4301	606.0	-0.294	6108

2.5.3 Results for 1000 m bridge

Results of simulations for the 1000 m span are given in Figure 2.8 and Table 2.6. For this longer span, the full stop condition governs regardless of the percentage of trucks. However, it is important to note that this finding is only valid if all congestion types are equally probable. Moreover, the separation between different congested states becomes clearer, as the congested states are now spread over a wider range. For 50% trucks, the full stop condition is the most critical condition for any return period. Again, the high truck percentage shows a smaller scale parameter σ (Table 2.6), indicating less scattering. Finally, FS conditions have again a greater scale parameter σ and smaller shape parameter ζ .

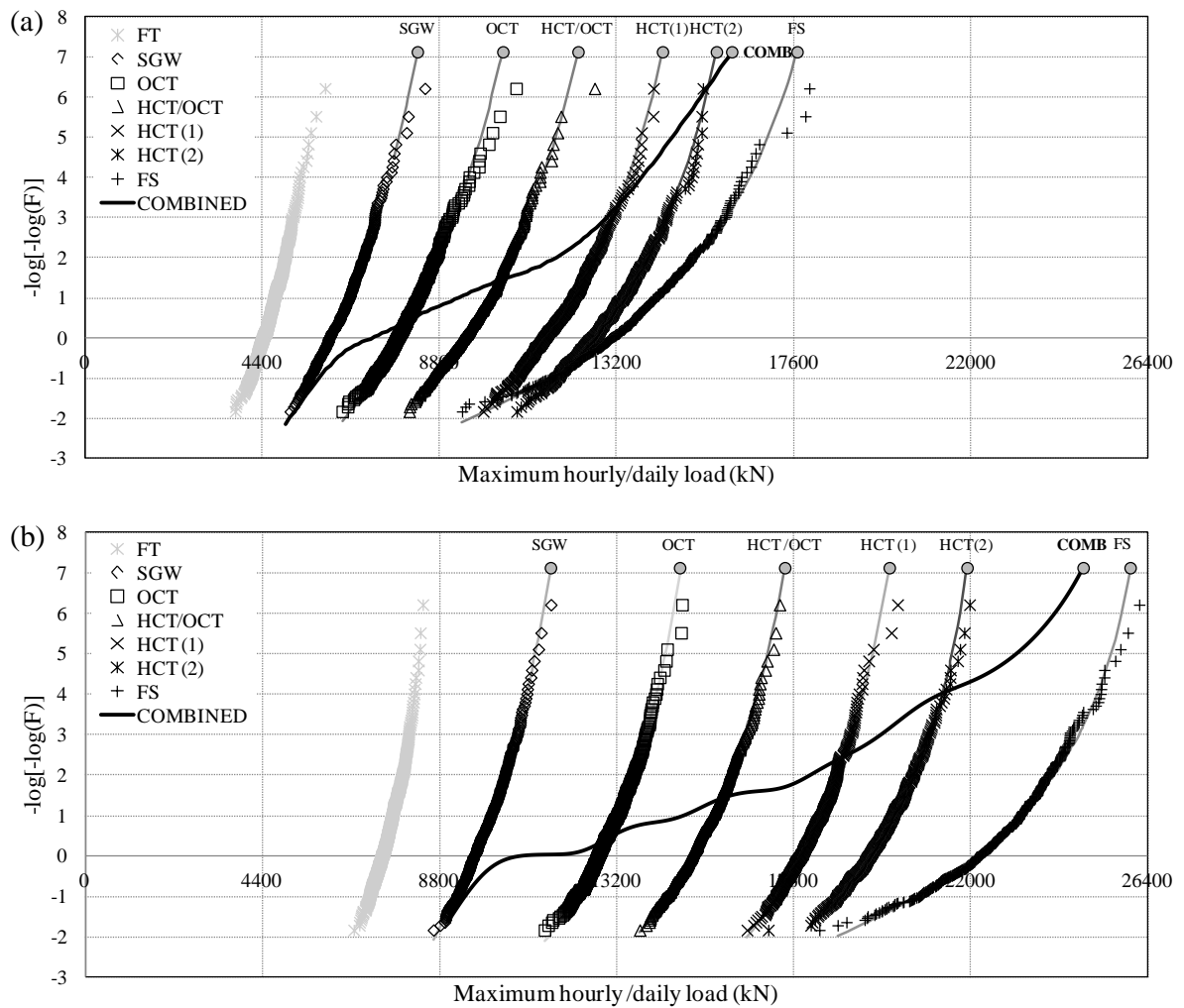


Figure 2.8 - Probability paper plot of total load on 1000 m span with (a) 20% and (b) 50% trucks; each vertical gridline approximately represents ten trucks of load.

Table 2.6 - Parameters of the GEV distribution (1000 m span).

Congestion type	20% trucks				50% trucks			
	μ	σ	ξ	z^*	μ	σ	ξ	z^*
SGW	6092	472.0	-0.134	8262	9670	426.6	-0.147	11554
OCT	7756	567.7	-0.131	10384	12747	516.0	-0.190	14763
HCT/OCT	9385	675.8	-0.161	12251	15046	569.0	-0.174	17373
HCT (1)	11448	717.0	-0.177	14349	17755	544.0	-0.175	19970
HCT (2)	12604	825.0	-0.206	15688	19459	706.0	-0.235	21902
FS	13029	1352.0	-0.236	17691	22125	1283.0	-0.294	25954

2.5.4 Discussion

It should be noted that smaller inflows need stronger bottlenecks to generate congestion. This causes the traffic to go straight to the heavy HCT/OCT and HCT states, in fact skipping the oscillatory congested states SGW and OCT (Treiber et al., 2000; Schönhof and Helbing, 2007). This is unfortunate, because smaller inflows do not allow the formation of oscillatory congested traffic, which gives less critical loading events for the bridge. Note that the full stop condition does not depend on the inflow, unlike the other congested states which are determined by a combination of inflow (demand) and outflow (capacity). The analysis of the traffic loading due to a range of inflows is addressed in Chapters 3 and 4.

2.6 Consideration of congestion frequency

2.6.1 Data on congestion

Real world observations have shown that many types of congestion can occur. As discussed in Section 2.1.2, most research on bridge traffic loading assumes only a queue at a minimum bumper-to-bumper distance (Ivy et al., 1954; Buckland et al., 1980; Harman et al., 1984; Flint and Neill Partnership, 1986; Ditlevsen and Madsen, 1994; Prat, 2001; Nowak et al., 2010). Intuitively, light forms of congestion are more frequent than strong ones. Schönhof and Helbing (2007) categorise more than 240 traffic breakdowns occurred on the busy A5 motorway in Germany. The most frequent extended congestion states were SGW and OCT, whereas HCT states were typical of congestion resulting from serious accidents. In that study, the FS condition was not observed. The full stop condition is generally caused by an exceptionally serious incident, where all the lanes needs to be closed.

Data about *accident* frequency is relatively abundant in the literature. However, for bridge loading applications, it is important to know the consequences for the traffic and the road layout, rather than the severity or the cause. On the other hand, available data about *incident* frequency and lane closure is modest, but it is becoming more common. For the single-lane application considered in this chapter, it is assumed that any incident blocking at least two lanes will generate a full stop condition, since in most highways there is a shoulder where traffic would be diverted if the driving lane were obstructed.

Where an explicit incident rate is not available, Equation (2.7) is used to compute the full stop rate, FSr :

$$FSr = FS\% \times Ir = FS\% \times \frac{N \times 10^6}{ADT \times L \times T} \quad (2.7)$$

where $FS\%$ is the percentage of incidents blocking two or more lanes; Ir is the incident rate (number of incidents per million vehicle kilometres travelled, I/MVkmT); N is the total number of incidents; ADT is the average daily traffic (veh/day); L is the length of road observed (km) and T is the duration of observation (days).

Tasnim et al. (2008) analyse 17 796 incidents in Portland, USA, in 2005. By means of Equation (2.7), it is possible to calculate a rate of about 5 I/MVkmT, with 5% of these blocking two or more lanes; it is then straightforward to deduce a full-stop rate of 0.25 FS/MVkmT. Giuliano (1989) suggests a rate of about 6 I/MVkmT from a smaller database of 652 incidents, with only 2% of those reported as blocking two or more lanes. Skabardonis et al. (1997) report greater rates, but the site was known to be especially prone to incidents. Skabardonis et al. (1999) report similar rates. Rodgers et al. (2006) reported a lower rate of 2.32 I/MVkmT on the M25 motorway in the United Kingdom over four weeks, with 7.6% blocking two or more lanes. These results are summarised in Table 2.7.

Table 2.7 - Incident rates and full-stop rates from the literature.

Authors	Incident rate (I/MVkmT)	Incidents blocking ≥ 2 lanes (%)	Full stop rate (FS/MVkmT)
Giuliano (1989)	≈ 6	2	0.12
Skabardonis et al. (1997)	64.6	0.6	0.39
Skabardonis et al. (1999)	57.7	0.45	0.26
Rodgers et al. (2006)	2.32	7.6	0.18
Tasnim et al. (2008)	≈ 5	5	0.25

The Highway Capacity Manual (Transportation Research Board, 2000) suggests that the peak hour typically carries around 10% of the average daily traffic. From the previous assumption of a peak hour traffic of 1590 veh/h, an ADT of 16 000 veh/day is implied, of which 20% are assumed to be trucks.

Obviously, only congestion forming downstream of the bridge will affect the bridge itself. It is assumed here that incidents occurring up to 5 km downstream of the bridge will affect it. Therefore there are 80 000 km travelled each day on the 5 km stretch, equating to 20 MVkmT per 250-day year. Then, using the more highly sampled rate deduced from Tasnim et al. (2008), 5 full stop events are to be expected each year. Following the previous assumption of 250 congested events per year, the full stop frequency is 2%. These values need to be adjusted for particular site-specific traffic conditions. In order to test the sensitivity of results to these assumptions, a double full stop frequency is considered as well.

The full stop frequency is used to infer a distribution of congestion frequencies for the selected bottleneck strengths (Figure 2.9). The relative frequencies sum up to 1. The curve is taken to be exponential, consistent with proportions shown by Schönhof and Helbing (2007).

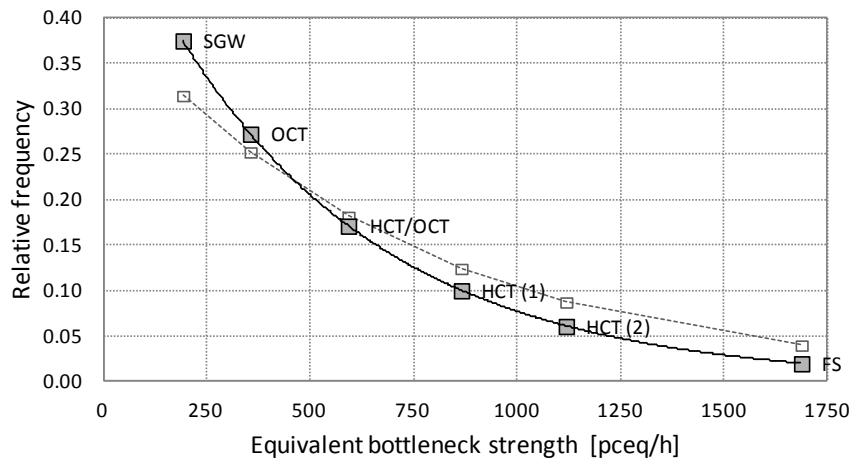


Figure 2.9 - Frequency of occurrence of congestion for 2% (solid) and 4% (dotted) full stop frequencies.

2.6.2 Combination of different congestion events

Once the congestion frequencies are assigned, it is necessary to statistically combine the six different congestion types, all of which can occur with the assigned probabilities of Figure 2.9. This is done by applying the law of total probability. The probability P that the maximum load does not exceed z is:

$$P(z) = \sum_{j=1}^6 F_j(z) \cdot f_j \quad (2.8)$$

where F_j is the cumulative distribution function of the maximum load for the j^{th} congestion type (Equation 2.5; see also Table 2.5 and Table 2.6) and f_j is the probability of occurrence for that type according to Figure 2.9. Equating $P(z)$ to the target probability of 0.9992 (Section 2.5.1) gives the characteristic combined load level, z^* .

The combined probability distribution function $P(z)$ curves are shown in the probability paper plots of Figure 2.6 and Figure 2.8. It can be seen that the 5-year characteristic values are in the range of the strongest congestion HCT and FS, although they are rarer. In fact, the load z^* corresponding to the target probability $P(z^*) = 0.9992$ is impossible to attain in the lightest congestion states, however frequent they are, as the tails are bounded at lower values of load. On the other hand, at lower return periods, the combined load gets closer to the light congestion.

Figure 2.10 shows the characteristic values per unit of length (EUDL, Equivalent Uniformly Distributed Load), when considering that all the congested events are of the most severe congested states (either HCT(2) or FS), and as described above. For the 200 m span (Figure 2.10a) and 20% truck percentage, the characteristic load for the FS condition is similar to the combined load. However, in this case it is the HCT state that is the most critical (see Figure 2.6a), giving a load higher by 7.9% than the combined value. As the truck percentage increases, the error in considering only the most severe congested state (FS) increases to 9.9%. For the 1000 m span (Figure 2.10b) and 20% trucks, the error due to the consideration of only one congestion type is 10.1%, whereas with the 50% truck percentage it drops to 4.7%. Figure 2.10 also confirms previous findings that the EUDL decreases as the span length increases (Buckland et al., 1980). The reduction is more pronounced for lower truck percentages. On the other hand, the increase in truck percentage has a sharper effect on the load for the longer span: +23% for the 200 m span and +56% for the 1000 m span.

The application of the congestion frequencies based on the 4% (doubled) full stop frequency (Figure 2.9) increases the characteristic combined load by between 1.1% (200 m, 20% trucks) and 2.7% (200 m, 50% trucks), suggesting that the total load is not largely sensitive to the congestion frequencies.

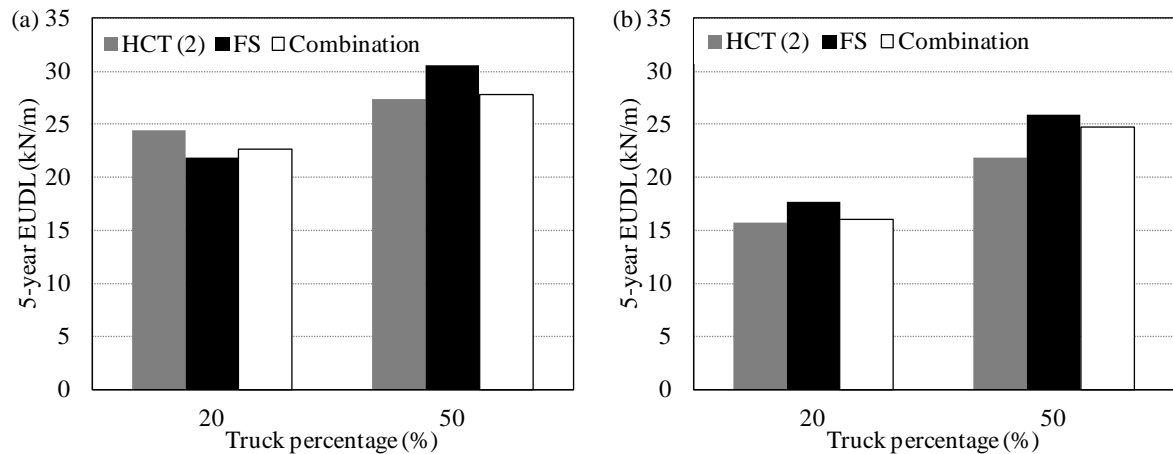


Figure 2.10 - Comparison of characteristic EUDL for (a) 200 m and (b) 1000 m bridge.

2.7 Conclusions

This chapter investigates the effects of different observed congestion patterns on the total load of two long-span bridges (200 and 1000 m long) by means of traffic micro-simulation. Most previous research neglects the existence of different congestion patterns, assuming a queue of vehicles at a minimum bumper-to-bumper distance. The single-lane micro-simulation model used here is able to reproduce observed congested patterns and it is extended in order to include different truck percentages.

Results show that the bumper-to-bumper queue is not always the most critical loading event for the 200 m span. In fact, slow-moving traffic states can be critical as well. This is due to the fact that full stop queues consider only one realisation of vehicles on the bridge which reduces the probability of finding an extreme scenario. It is also found that oscillatory congested traffic (SGW and OCT) is less critical for bridge loading than other stronger forms of congestion.

A number of different congestion types will affect the bridge during its lifetime, rather than a single congestion pattern. Each congestion type is assigned a frequency of occurrence, based on available literature data. For 20% trucks, it is found that the consideration of only the most critical congestion type leads to an increase in the total load by 7.9% (200 m) and 10.1% (1000 m). However, when considering a high truck percentage (representative of slow lanes in multi-lane highways) and a 1000 m span, the error drops to about 5%.

Chapter 3

Long-span bridge traffic loading based on multi-lane traffic micro-simulations

Authors:

Colin C. Caprani

Eugene J. OBrien

Alessandro Lipari

Paper Status:

Submitted for publication to *Structure and Infrastructure Engineering*. Minor modifications are done in the text in order to minimise repetitions and to fit into the context of the thesis.

Note to the Reader:

The work in this chapter is entirely the work of the author under the supervision of Prof OBrien and Dr Caprani.

3.1 Introduction

As seen in Chapter 2, micro-simulation is a suitable tool to generate observed congestion patterns and analyse their effects on long-span bridge loading. This chapter extends the work of Chapter 2 with the modelling of multi-lane roadways. Different traffic compositions and congestion patterns are analysed in relation to their traffic features (with a special focus on lane change activity) and effects on long-span bridge loading.

3.1.1 Data

As mentioned in Section 2.1.1, there is a shortage of data about congestion. Data collection is even more problematic when studying lane changes, and not only during congestion, because several vehicles are involved in a single lane-changing manoeuvre and they need to be tracked over space and time. As a consequence, lane-changing models are less established than car-following models.

Consideration of multi-lane layouts involves an important feature for bridge loading applications not present in single-lane roads: when overtaking is allowed, the car-truck mix for congestion is expected to be different to that for free traffic, since car drivers do not feel comfortable following trucks and tend to overtake them (Peeta et al., 2005). This typically results in longer truck-only convoys in congested traffic than in free-flowing conditions. The introduction of a lane-changing model allows the consideration of the formation of such truck platoons.

3.1.2 The lane-changing phenomenon

Lane-changing manoeuvres are traditionally divided into *discretionary* and *mandatory*. Mandatory lane changes are performed in order to follow a specific path, for instance in presence of on- or off-ramps, while discretionary lane changes are performed because of a (perceived) advantage in the target lane (Kesting et al., 2007). In this chapter, the focus is on discretionary lane changes, whereas mandatory lane changes are modelled in Appendix C.

Sparmann (1979) observes and computes lane-changing frequencies over a 1 km stretch of road on the A5 Autobahn near Karlsruhe (Germany). He finds that, with increasing flow, the

lane change rate increases up to about 600 lane changes per kilometre per hour (LC/km/h) at about 2000 veh/h. Then the rate decreases to approximately 400 LC/km/h at 3000 veh/h. There is also some limited data about lane changes during congestion. In this case, lane change rates are substantially less than in free traffic. He states that there is a very slight decreasing relation between the lane change rate and the proportion of trucks, but no details are given.

Yousif and Hunt (1995) observes lane changes and lane utilisation on a motorway and two dual-carriageways in the United Kingdom. They find that the lane change rate has a peak of 600 LC/km/h at about 2000 veh/h and then decreases to about 300 LC/km/h at 3000 veh/h. The average percentage of truck traffic is 20%, but no analysis of truck influence is performed. They also analyse a 3-lane section of the M4 motorway and find a similar lane change rate trend with a peak of about 1100 LC/km/h at 3000 veh/h.

McDonald et al. (1994) analyse the lane usage and lane changes on several 3-lane motorways in the United Kingdom. They find quite a constant lane change rate, unlike the studies of Sparmann (1979) and Yousif and Hunt (1995). However, their flow range is limited compared to the other two studies and roughly centres on the expected peak at 3000 veh/h. They also state that lane change rates appear to be independent of the heavy vehicle percentage (which is at most 24%).

More recently, Knoop et al. (2010) analyse data from the 3-lane M42 motorway (UK). They find a similar trend in the lane change rate with a peak of 1300 LC/km/h. Interestingly, they use other parameters to quantify lane changes instead of the usual lane change rate per km and per hour. They find that one lane change occurs for every kilometre of road travelled (LC/veh-km) in very light traffic conditions to 0.5 LC/veh-km, as traffic approaches capacity. In a further paper, Knoop et al. (2012) analyse video data from a 2-lane motorway in the Netherlands. In this case, they find that 0.4-0.5 lane changes occur for every km travelled. The difference from the M42 dataset is stated to be due to differences in road layout, which leads to mandatory lane changes.

The Federal Highway Administration (2005) has made available about 90 minutes of trajectory data of congested traffic from two freeways in the United States. The lane change

rates that can be deduced are rather high (Cambridge Systematics Inc., 2005a; Cambridge Systematics Inc., 2005b). However, they suffer from a complex multi-lane layout with on- and off-ramps, as well as from detection issues (Thiemann et al., 2008; Jin, 2010). One of the available dataset is used to refine the lane-changing model used here. Details are given in Section D.3.

In all the above papers, there is no data about lane change rates in congested conditions, except for a few points by Sparmann (1979). Moreover, there is no analysis of the lane changes performed by trucks. Moridpour et al. (2010) show that there are differences between the lane-changing behaviour of heavy vehicles and passenger cars under congestion. However, the dataset is taken from the Federal Highway Administration (2005), which is too small to establish general conclusions. No study of truck lane change rates is performed, but it can be deduced that, on average, a truck performs 0.21 lane changes for every km travelled.

In the bridge loading field, Hayrapetova (2006) analyses the lane changes occurring in one day over a 3-lane motorway bridge in the Netherlands. She observes a trend similar to other studies and indicates that about 10% of the lane changes are performed by trucks. However, no analysis of either car or truck lane change rates is reported.

3.2 Micro-simulation

As done elsewhere in this thesis, the car-following *Intelligent Driver Model* is used (Treiber et al., 2000). Here, it is extended with the lane-changing model MOBIL (Kesting et al., 2007). The focus is to relate critical events for long-span bridge loading to multi-lane traffic features, such as traffic flow, lane change rates, truck percentage and truck distribution between lanes.

3.2.1 The Intelligent Driver Model

The *Intelligent Driver Model* (IDM) has been presented in Section 2.2.1. The main equations of the model are repeated here for convenience:

$$\frac{dv(t)}{dt} = a \left[1 - \left(\frac{v(t)}{v_0} \right)^4 - \left(\frac{s^*(t)}{s(t)} \right)^2 \right] \quad (3.1)$$

$$s^*(t) = s_0 + Tv(t) + \frac{v(t)\Delta v(t)}{2\sqrt{ab}} \quad (3.2)$$

It must be noted that, when the front vehicle is faster, the desired minimum gap s^* in Equation (3.2) can turn negative, generating an inconsistent driver behaviour. Therefore, the desired minimum gap s^* is limited to be greater than or equal to the minimum jam distance s_0 . Further details can be found in Section D.3.

3.2.2 The MOBIL lane-changing model

The MOBIL lane-changing model has been proposed in Kesting et al. (2007). MOBIL can be adapted to symmetric and asymmetric passing rules. With the symmetric passing rule, vehicles can overtake from any side (e.g., in the United States), whereas with the asymmetric rules, vehicles must use only the designated lane(s) for overtaking (e.g., European Union). Here, asymmetric rules are used.

The topology of a lane change event is illustrated in Figure 3.1, where the subscript c refers to the lane-changing vehicle, o refers to the old follower (in the current lane) and n to the new one (in the target lane). The tilde identifies the situation after the lane change. The front vehicles play an important passive role, representing a “constraint” which affects the acceleration of the lane-changing vehicle. All the accelerations, current and proposed, are calculated according to the car-following model given in Equations (3.1) and (3.2).

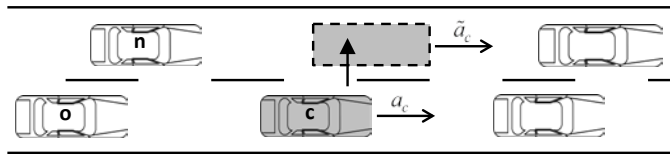


Figure 3.1 - Vehicles involved in a lane-changing manoeuvre (adapted from Kesting et al. (2007)).

A lane change occurs if both the *incentive* and the *safety criteria* are fulfilled. For a slow-to-fast lane change, the incentive criterion is expressed as follows:

$$\tilde{a}_c(t) - a_c(t) > \Delta a_{th} + \Delta a_{bias} + p(a_n(t) - \tilde{a}_n(t)) \quad (3.3)$$

This means that the lane-changing acceleration advantage $\tilde{a}_c - a_c$ must be greater than the sum of: the *acceleration threshold* Δa_{th} , which prevents overtaking with a marginal advantage; the *bias acceleration* Δa_{bias} , which acts as an incentive to keep the slow lane; and the imposed disadvantage to the new follower in the fast lane $a_n - \tilde{a}_n$, weighted through a *politeness factor* p , which adjusts the driver aggressiveness. On the other hand, the incentive criterion for a fast-to-slow lane change is:

$$\tilde{a}_c(t) - a_c(t) > \Delta a_{th} - \Delta a_{bias} + p[(a_n(t) - \tilde{a}_n(t)) + (a_o(t) - \tilde{a}_o(t))] \quad (3.4)$$

In this case, the acceleration advantage must be greater than the sum of the acceleration threshold Δa_{th} , minus the bias acceleration Δa_{bias} (which acts as incentive to move back to the slow lane), plus the disadvantage imposed to both the new follower n in the slow lane and to the current follower o in the fast lane, weighted through the politeness factor p . Equation (3.4) is based on the work of Treiber (2011) and is preferred to the formulation in Kesting et al. (2007), which does not include the disadvantage to the new target follower $a_n - \tilde{a}_n$. Further details about the formulation of the incentive criterion are given in Section D.2.

The *safety criterion* limits the imposed deceleration to the follower n in the target lane to the *safe braking* value b_{safe} :

$$\tilde{a}_n(t) \geq -b_{safe} \quad (3.5)$$

Provided that the politeness factor is not excessively low, the safety criterion (3.5) applies only to high flows. In this situation, a vehicle may have a larger acceleration advantage to gain in performing a lane change and therefore the incentive criteria (3.3) and (3.4) can be met at the expense of a big imposed deceleration to the follower $a_n - \tilde{a}_n$. See Section D.6 for the details about the conditions for the application of safety criterion.

From the strategy of Equations (3.3) and (3.4) the MOBIL acronym (Minimizing Overall Braking Induced by Lane changes) arises. For this work, Equations (3.1-5) are discretized into 250 ms steps.

3.2.3 Congested Traffic States

As seen in Section 2.2.2, flow-conserving inhomogeneities are a convenient way to generate congestion. It is not necessary to explicitly model the cause of congestion (e.g., an on-ramp or a lane closure), but a simpler modification of the safe time headway T , or the desired speed v_0 , can return similar effects on the traffic congestion pattern (Treiber et al., 2000). An analysis of the differences between the explicit modelling of a lane closure and the application of an equivalent flow-conserving inhomogeneity is reported in Appendix C. The results confirm that the flow-conserving inhomogeneity effectively reproduces a similar traffic pattern to the one resulting from the explicit modelling of a lane closure. However, details of traffic features in the close proximity of the lane closure may be different.

An important parameter in determining the congested states is the bottleneck strength ΔQ , as defined in Section 2.2.2 by:

$$\Delta Q(T') = Q_{\text{out}}(T) - Q'_{\text{out}}(T') \quad (3.6)$$

The resulting congested states are listed again in Table 3.1 for the reader's convenience.

Table 3.1 - Definitions of traffic states.

Acronym	Explanation of traffic state
FT	Free Traffic
MLC	Moving Localized Cluster
PLC	Pinned Localized Cluster
SGW	Stop and Go Waves
OCT	Oscillating Congested Traffic
HCT	Homogeneous Congested Traffic

3.3 Model and Simulation Parameters

3.3.1 Traffic stream

As assumed in Chapter 2, a simplified vehicle stream made up of two classes of vehicle, cars and trucks, is used. Each vehicle of a class is given the same set of parameters, shown in Table 3.2. The Gross Vehicle Weights and the IDM parameters are the same described in

Section 2.3.1, but with the desired velocities of both classes of vehicle uniformly distributed, as assumed by Kesting et al. (2007).

Several tests have been performed to calibrate the lane change parameters. A constraint was to find a parameter set that could match the observed lane change rates for 2-lane motorways (Sparmann, 1979; Yousif and Hunt, 1995). The calibration process is described in detail in Appendix D.

Note that the modelling of a road layout different from the stretch of road considered in this chapter may require a different calibration of the MOBIL parameter set. Appendix C proposes a different MOBIL set to correctly simulate the mandatory merging manoeuvres occurring in proximity of a lane closure.

Table 3.2 - Model parameters.

	Cars	Trucks
Desired speed, v_0	120 km/h ($\pm 20\%$)	80 km/h ($\pm 10\%$)
Safe time headway, T	1.6 s	1.6 s
Maximum acceleration, a	0.73 m/s ²	0.73 m/s ²
Comfortable deceleration, b	1.67 m/s ²	1.67 m/s ²
Minimum jam distance, s_0	2 m	2 m
Vehicle length, l	4 m	12 m
Politeness factor, p	0.1	0.1
Changing threshold, Δa_{th}	0.2 m/s ²	0.2 m/s ²
Bias for the slow lane, Δa_{bias}	0.2 m/s ²	0.2 m/s ²
Maximum safe deceleration, b_{safe}	6 m/s ²	6 m/s ²
Gross Vehicle Weight	20 kN	432 kN*

* Coefficient of Variation 0.1.

3.3.2 Road geometry and bottleneck strength

A two-lane 8000 m long road is used in this work. The safe time headway is $T = 1.6$ s from 0 to 5700 m (see Table 3.2), then increases gradually to the value T' at 6300 m. A range of values for T' (and consequently bottleneck strengths, ΔQ) are considered: 1.9, 2.2, 2.8, 4.0 and 6.4 s, which are the same used in Chapter 2. Trucks comprise 20% of the traffic and are

injected in the slow lane, which is where they are expected to stay, being characterised by a slower desired speed v_0 . The issue of a different split between lanes is addressed later.

The dynamic capacity $Q_{out}(T)$ for the traffic with 20% trucks, calculated by means of simulation as detailed in Section B.2, is 3070 veh/h. Figure 3.2 shows the relation between the applied inhomogeneity, $\Delta T = T' - T$, and the resulting bottleneck strength, ΔQ .

The inflows Q_{in} are set equal to 1250, 2000 and 3000 veh/h. A flow of 3000 veh/h is close to capacity; 2000 veh/h is the flow at which most lane changes are expected to occur and 1250 veh/h represents a moderately light traffic.

For the inflow of 1250 veh/h, the truck percentage is increased to 48%, in order to represent night-time traffic which typically has a high percentage of trucks (Flint and Neill Partnership, 1986; Hallenbeck et al., 1997; Caprani et al., 2012a). Such a traffic percentage means 600 trucks per hour (just like the case of 3000 veh/h and 20% trucks), which also allows the study of the effect of cars on loading. These cases are discussed later in Sections 3.7.

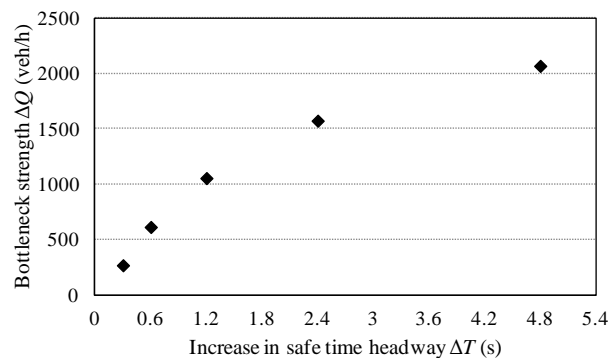


Figure 3.2 - Bottleneck strength.

In total, five traffic cases are studied. For comparison with the common traffic loading assumption, the full stop condition (FS) is also simulated. This corresponds to infinite ΔT or $Q'_{out} = 0$ veh/h, then the bottleneck strength ΔQ is 3070 veh/h, according to Equation (3.6).

Finally, it is assumed that the road is subject to one hour of congestion each day of a 250-day working year, as in Section 2.5. One year of congested traffic is simulated for each bottleneck strength and traffic case considered, for a total of 7500 hours of congestion analysed.

3.3.3 *Distribution of trucks between lanes*

For the inflow of 3000 veh/h, 25% of the total trucks are injected in the fast lane. This takes into account different road layouts that may exist on a motorway, such as the effects of previous junctions, or the presence of frequent and busy on- and off-ramps that some trucks might avoid. At lower inflows, the vast majority of trucks tends to stay in the slow lane (Fwa and Li, 1995).

Limited data is available in the literature about the distribution of trucks between lanes, and it is mostly related to pavement engineering codes. In the field of bridge loading, OBrien and Enright (2011) analyse an extensive WIM database of two European motorways and find about 7% of the trucks recorded to be in the fast lane. Vrouwenvelder and Waarts (1993) assume that 10% of the trucks are in the fast lane. In the field of pavement engineering, the AASHTO (1993) specifies a percentage of between 80 and 100% of the load in the design (slow) lane of pavement structures for 2-lane motorways, while the Portland Cement Association (1984) suggests 70 to 100%, depending on the Average Daily Traffic (ADT). The Highways Agency (2006) prescribes the percentage of trucks in the heaviest loaded lane as a function of the daily flow of commercial vehicles.

In light of the data reported above, 25% does appear to be a reasonable upper limit for the lane split. Note that such a lane distribution may well also represent traffic on a 3-lane motorway, where trucks are prohibited from travelling in the fastest lane. In pavement engineering, Fwa and Li (1995) observe on several 3-lane expressways in Singapore that, as flow increases, so does the percentage of the total truck traffic in the middle lane, leading to an average of 25%. Hayrapetova (2006) indicates that for a Dutch bridge, the percentage of the total truck traffic in the middle lane is 35% in free traffic (density less than 20 veh/km/lane) and 28% in "congested" traffic (density greater than 20 veh/km/lane).

3.4 Traffic results

3.4.1 Spatio-temporal congestion patterns

As seen in Section 2.4.1, spatio-temporal speed plots are useful for visualizing congested patterns. Here, the lane-averaged space mean speed is collected at five virtual point detectors placed between 3500 and 5500 m and aggregated in 60 s intervals. Figure 3.3a shows a SGW state, where congestion peaks can be easily recognised. Figure 3.3b shows a combined HCT/OCT state, where the small oscillations upstream that are typical of the OCT state (e.g., at a distance of 3500 m), fade away into a HCT state downstream, where there are essentially no oscillations (e.g., at a distance of 5500 m).

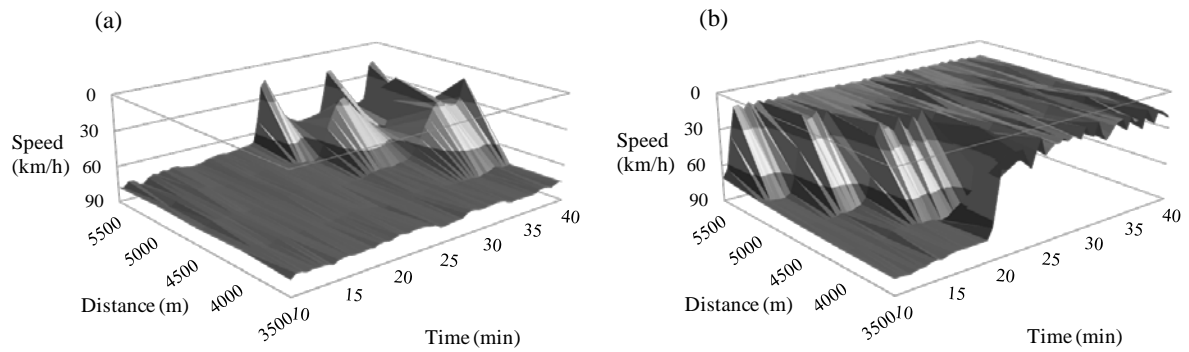


Figure 3.3 - Spatio-temporal speed plots: (a) SGW traffic (b) HCT/OCT traffic (refer to Table 3.1 for abbreviations).

Figure 3.4a shows the average speed in the area close to the inhomogeneity. It can be seen that, for the 3000 veh/h inflow, speeds decrease, as expected, with higher bottleneck strength ΔQ . Two HCT states are generated, which differ only in the average speed and are labelled HCT(1) and HCT(2), where HCT(1) has average speed 8.7 km/h and HCT(2) has 5.0 km/h. The trend and congested states are similar to the one shown in Figure 2.5a.

Importantly, at lower inflows, low bottleneck strengths do not cause any congestion, as the vehicles can rearrange themselves to drive through the inhomogeneity. However, when the bottleneck strength is high enough to trigger congestion for a lower inflow, the congested states are very much the same, regardless of the inflow. In the rest of the chapter, only the free traffic conditions with the highest bottleneck strength are considered, as all the smaller

bottleneck strengths would have similar traffic features and are not relevant to long-span bridge loading.

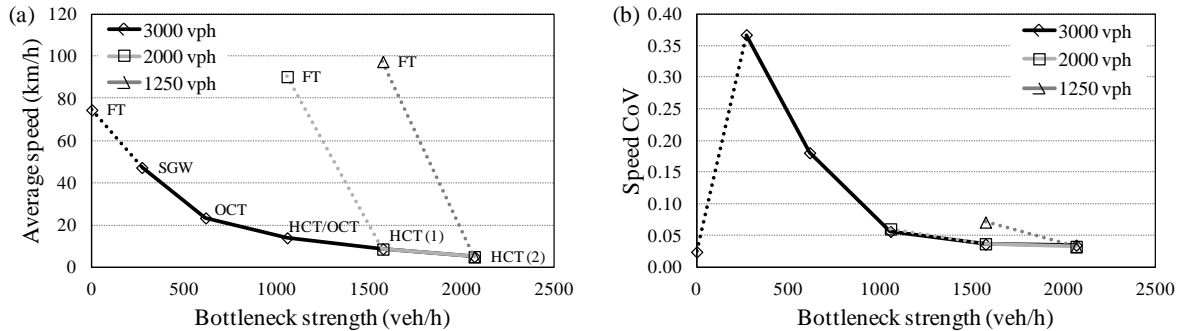


Figure 3.4 - Speed near the congestion-inducing inhomogeneity:
(a) Average and (b) Coefficient of variation.

The coefficient of variation of speed (Figure 3.4b) shows that in free traffic the variation of speed is small (less than 5%). However, as soon as traffic gets congested, the coefficient of variation rises significantly, indicating stop-and-go wave states (SGW). Afterwards, the coefficient of variation decreases to values similar to those of free traffic, indicating homogeneous congested traffic (HCT). This trend is similar to the one shown in Figure 2.5b.

3.4.2 Truck lane distribution

Figure 3.5 shows the percentage of the total truck traffic in the fast lane. It can be seen that there is no clear pattern with bottleneck strength. However, there are more trucks in the fast lane when the inflow is high (average 11.6%), rather than when the inflow is lower, which accords with the observations of Fwa and Li (1995).

When considering the traffic in the sole slow lane, the percentage of trucks is 38% on average. Such a percentage does not vary largely with inflow and congestion state. Further information is given in Section D.7.2.

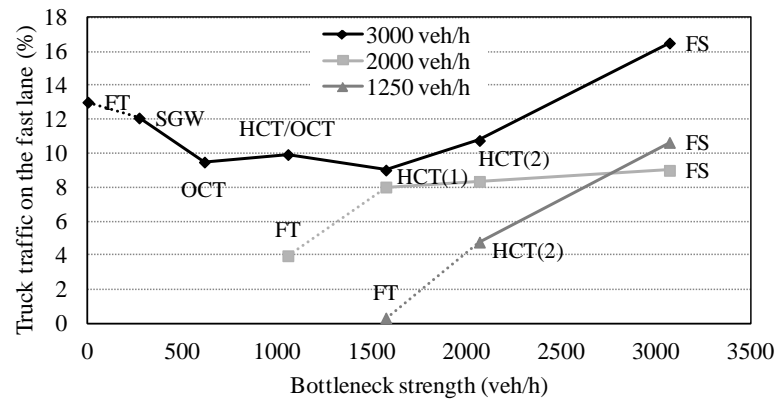


Figure 3.5 - Percentage of truck traffic in the fast lane.

3.4.3 Lane-changing activity

Figure 3.6a shows the lane change rates for the different bottleneck strengths. As detailed in Appendix D, the available data for lane change rates in free traffic (Sparmann, 1979; Yousif and Hunt, 1995) has been used to calibrate the lane-changing model. Note that during congestion events the lane change rates may be quite different, depending on the location on the road. They are likely to be relatively high when approaching the queue front and rather low inside the queue (Caprani et al., 2012a).

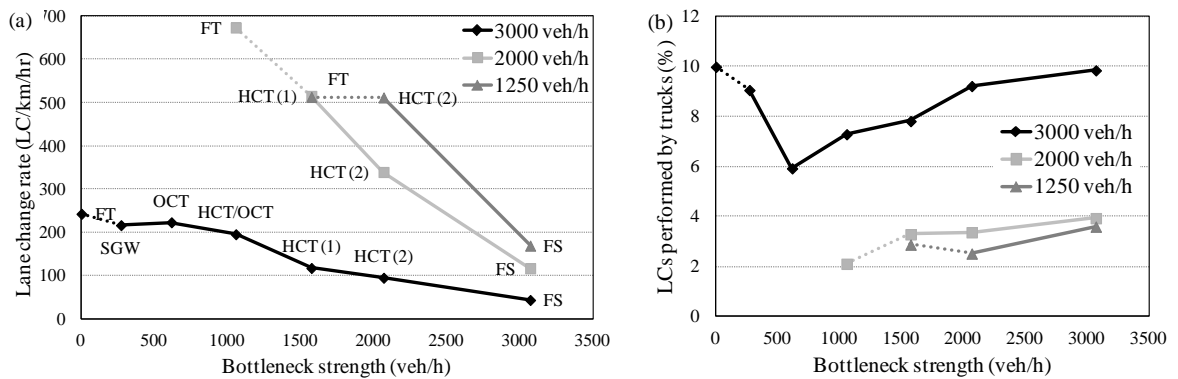


Figure 3.6 - Lane changes: (a) Lane change rate and (b) Percentage of lane changes performed by trucks.

Figure 3.6b shows how many lane changes are performed by trucks. It can be seen that there is not a large variation among the congested states. At 3000 veh/h an average of 8.5% of the lane changes are performed by trucks, close to the observations of Hayrapetova (2006), whereas this figure drops to about 3% at lower inflows. This may be due to the fact that, at

busier flows, more truck drivers change lanes because the other lane appears less congested than the current one. At lower inflows, the current lane is not so busy and trucks tend to remain in the slow lane (Figure 3.5).

3.4.4 *Truck platoons*

Research and experience suggest that car drivers do not feel comfortable driving closely between trucks (Peeta et al., 2005), and generally wish to drive faster than trucks. Therefore, cars tend to move out from between trucks. Figure 3.7 shows the cumulative frequencies of truck platoon size (i.e. number of consecutive trucks in the same lane) for different inflows, as they cross a virtual point detector placed at 5000 m. For comparison, the curve for the case in which no lane changes are allowed is depicted as well. It can be seen that there is little platooning at 3000 veh/h (Figure 3.7a), since there are few gaps available in the traffic flow and most cars caught between trucks remain there. In general, there is little difference between congested states, except for the OCT state, which results in more platooning. In all cases, quite long platoons are possible (up to 24 for the OCT and up to 16 for the other states).

The highest platooning occurs at 2000 veh/h, as shown in Figure 3.7b by a greater separation of the congested frequencies from the no lane change case. This is expected because at this inflow the lane-changing activity is at its peak (Sparmann, 1979; Yousif and Hunt, 1995). However, although the proportion of long platoons is greater than for the case of 3000 veh/h, the largest platoon lengths are similar to the case of 3000 veh/h.

For lower inflows, platooning decreases, possibly because there are fewer vehicles in the flow and thus fewer chances to have very long truck platoons (Figure 3.7c). In the fast lane (not depicted in the figure) the platoon size hardly ever exceeds 5 at any inflow, as there are far fewer trucks there (Figure 3.5).

Finally, Figure 3.7d compares the platoon formation for the same bottleneck strength at different inflows. It confirms that the platoons are more likely to form at 2000 veh/h, although very long platoons may occur also at 3000 veh/h.

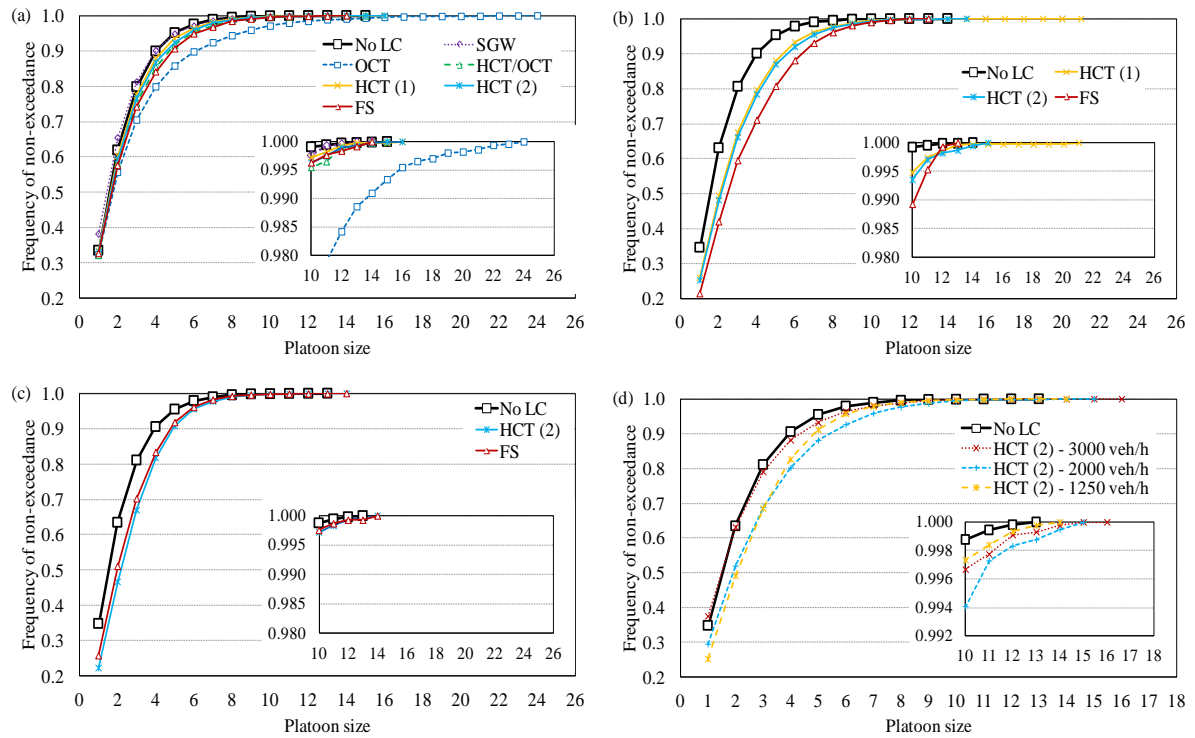


Figure 3.7 - Cumulative frequencies for truck platoons in the slow lane at (a) 3000 veh/h, (b) 2000 veh/h, (c) 1250 veh/h, (d) $\Delta Q = 2067$ veh/h (HCT (2)).

3.5 Loading results

3.5.1 Statistical extrapolation

In this section, the total load on two long spans (200 and 1000 m) for the different traffic scenarios is reported. The bridges are placed before the bottleneck, centred at 5000 m in the 8000 m length of roadway modelled. As done in Section 2.5, the maximum total load for each one-hour congestion event is captured. Assuming one congestion event per working day, the hourly/daily maximum values of the total load are extrapolated to determine 5-year characteristic values for each type of congestion. The Generalized Extreme Value (GEV) distribution is fitted to the simulated daily maximum total loads and Gumbel probability papers are used to illustrate results. For the 5-year return period and with 250 working days per year, the target Standard Extremal Variate is 7.13. The procedure is described in greater detail in Section 2.5.1.

3.5.2 200 m bridge

An example probability paper plot for the 200 m span and inflow of 3000 veh/h is shown in Figure 3.8. The data for each type of congestion, as well as the 5-year characteristic maximum values z^* , are given. The hourly maximum values for free flowing traffic are also shown for reference and are expectedly lower than the congested ones.

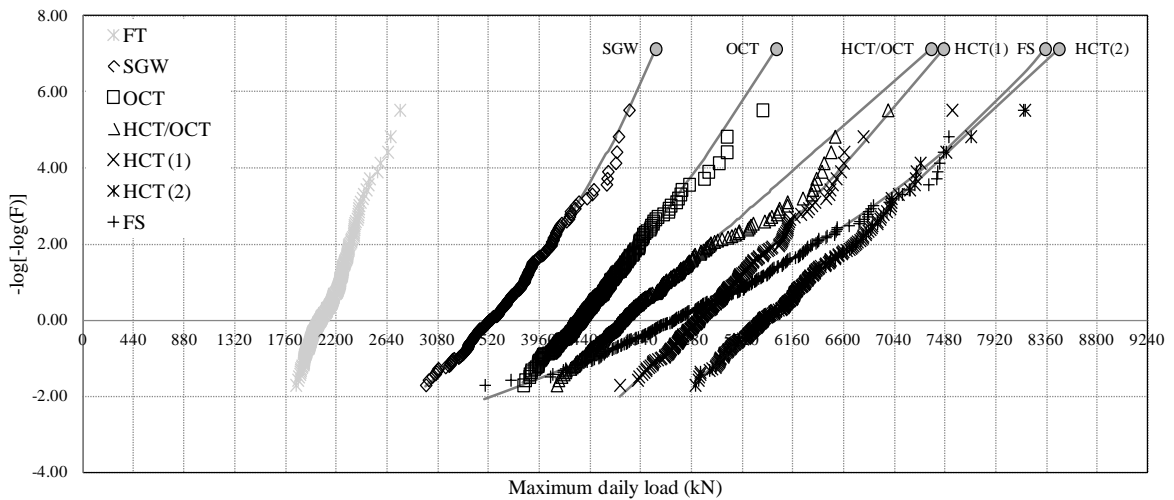


Figure 3.8 - Total load results for 200 m bridge length and $Q_{in} = 3000$ veh/h (space between each vertical gridline represents the weight of one average truck).

Similarly to the probability paper plot derived for single-lane simulations (Figure 2.5a), the different congestion types are separate from each other, indicating that stronger bottleneck strengths imply greater load, with the exception of the full stop situation (FS), whose maxima cover a wide range. Most trends curve upwards, suggesting compliance with the Weibull distribution ($\zeta < 0$). The HCT(2) state is found to be the most critical congestion state for the inflows of 3000 and 2000 veh/h (Table 3.3). At the lowest inflow, it is the FS condition that governs. Table 3.3 shows also that FS conditions tend to have a greater scale parameter σ (indicating more scatter across the load range) and a smaller shape parameter ζ (indicating higher curvature upwards), as found in Section 2.5.2. Information about the load distribution between lanes is given in Section D.7.3.

Table 3.3 - Parameters and extrapolated values of the GEV distribution (200 m span).

Parameter	Inflow Congestion type	3000 veh/h		2000 veh/h		1250 veh/h	
		HCT(2)	FS	HCT(2)	FS	HCT(2)	FS
location, μ		5908	5140	5788	5305	4962	5445
scale, σ		366.4	694.5	382.6	825.9	588.3	760.1
shape, ζ		-0.006	-0.132	-0.099	-0.332	-0.269	-0.286
5-year char. max., z^*		8467	8347	7744	7557	6829	7755

Figure 3.9 shows the characteristic values, z^* , for the three inflows considered, expressed as an equivalent uniformly distributed load (EUDL, total load divided by bridge length). In general, the loads resulting from different inflows with the same bottleneck strength are quite similar (within a range $\pm 11\%$), as long as the bottleneck is strong enough to trigger congestion. This suggests that the effect of the inflow on loading is not as strong as that of bottleneck strength and implies that critical loading events may occur also out of rush hours, if congestion happens to be triggered.

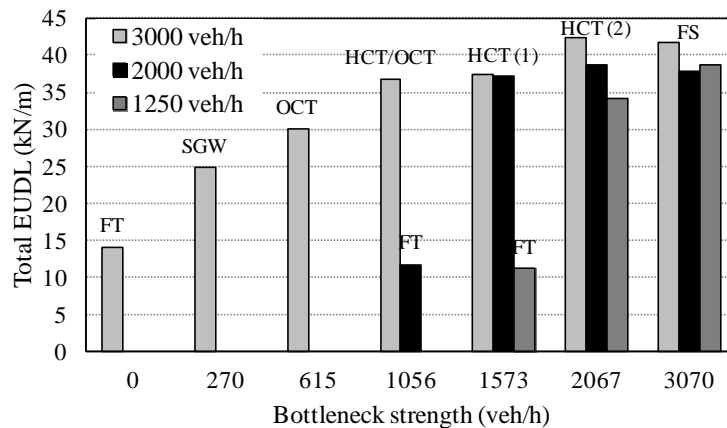


Figure 3.9 - 5-year total EUDL for a 2-lane 200 m span bridge.

3.5.3 1000 m bridge

The probability plot for the 1000 m span and 3000 veh/h is given in Figure 3.10. For this longer span, the full stop condition governs, regardless of the inflow. There are greater differences between the loads caused by different congested states (compared to the 200 m results), spread over a wider range, similarly to what found for single-lane simulations in Section 2.5.3. FS conditions are again more variable with greater scale parameter σ and smaller shape parameter ζ (Table 3.4).

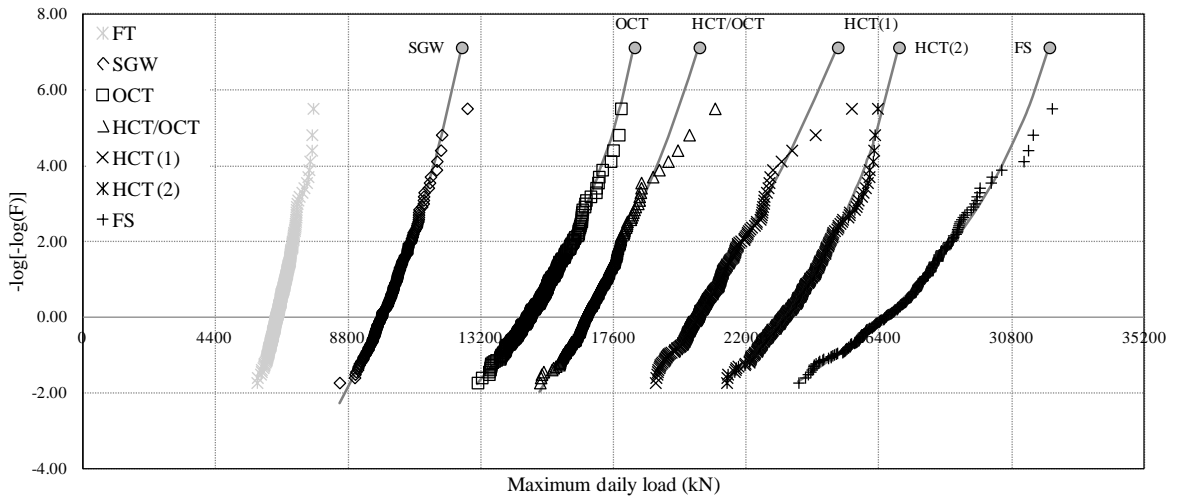


Figure 3.10 - Total load results for 1000 m bridge length and $Q_{in} = 3000$ veh/h (space between each vertical gridline represents the weight of ten average trucks).

Table 3.4. Parameters and extrapolated values of the GEV distribution (1000 m span).

	Inflow Congestion type	3000 veh/h		2000 veh/h		1250 veh/h	
		HCT(2)	FS	HCT(2)	FS	HCT(2)	FS
Parameter	location, μ	23212	26519	22478	26686	13863	26986
	scale, σ	954.0	1415.3	1036.4	1755.0	1178.7	1730.7
	shape, ζ	-0.179	-0.190	-0.141	-0.275	-0.184	-0.253
	5-year char. max., z^*	27056	32041	27137	32168	18548	32705

Figure 3.11 shows the characteristic EUDL values for the three inflows considered. Again, the different inflows return similar load values, with the exception of the HCT(2) state at 1250 veh/h. This is due to the slower congestion growth occurring at lower flows, which takes somewhat less than an hour to fill the bridge up, thus giving fewer realizations of critical events.

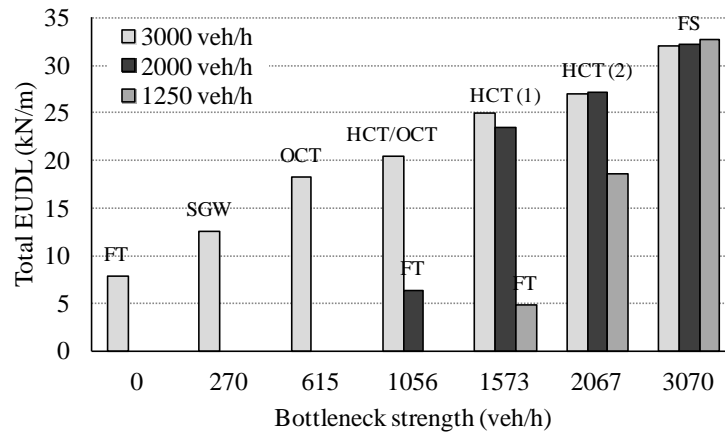


Figure 3.11 - 5-year total EUDL for a 2-lane 1000 m span bridge.

3.6 The effect of trucks in the fast lane

In this section, the effects of injecting 25% trucks in the fast lane (i.e., slow/fast lane split of 75-25) are compared to the previous case of trucks injected only in the slow lane (split of 100-0) at the inflow of 3000 veh/h. The injection of trucks in the fast lane is not found to have a large global effect on traffic. No significant differences appear in speed patterns. The most important change is, unsurprisingly, in the truck distribution between lanes: there is now an average 32.5% of the total truck traffic in the fast lane. The lane change rates with the 75-25 split are about 20% less than with the 100-0 split (Figure 3.12a), whereas the average percentage of lane changes performed by trucks is about 3% higher (Figure 3.12). All these variables follow a similar trend, compared to when injection is only in the slow lane. Finally, the platoons are shorter (they do not exceed 11), but now some platoons form also on the fast lane (Figure 3.13) and they may coincide with long platoons in the slow lane.

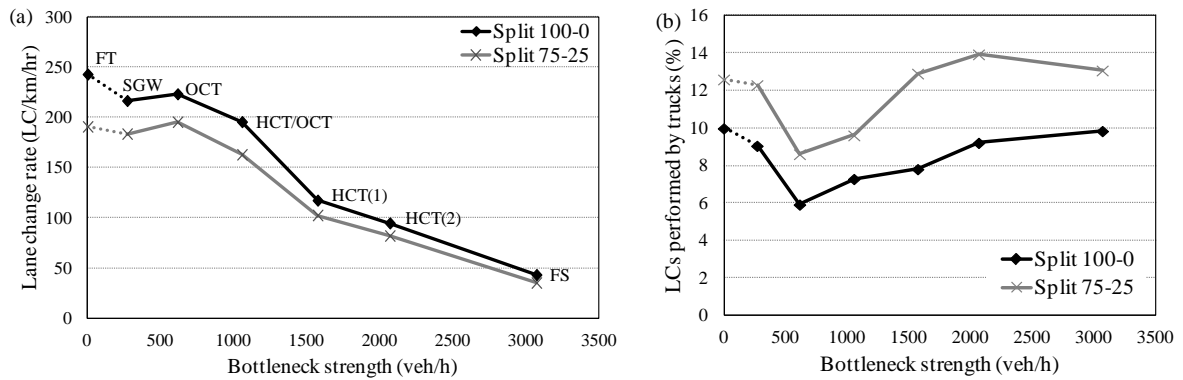


Figure 3.12 - Lane changes: (a) lane change rate and (b) percentage of lane changes performed by trucks.

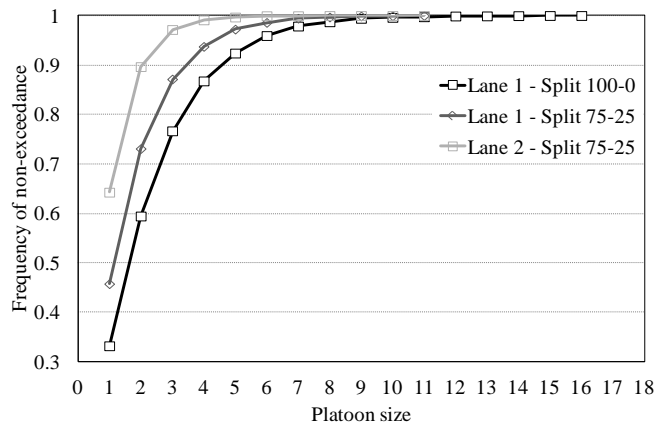


Figure 3.13 - Cumulative frequency of truck platoons or two truck distributions between lanes with $\Delta Q = 2067$ veh/h (HCT(2)). Lane 1 = slow lane; Lane 2 = fast lane.

Figure 3.14 shows the 5-year characteristic values for the inflow of 3000 veh/h. For the 200 m span, it can be seen that the values are similar in magnitude – within the range $\pm 9\%$. They are higher for free traffic and lighter bottleneck strengths, where oscillations occur, suggesting that the effect of coincidence of heavy vehicles between lanes compensate for the shorter platoons. On the other hand, at higher bottleneck strengths (HCT), the effect of the longer truck platoons dominate, as the load is higher when trucks are all injected in the slow lane. In the 1000 m span, the 75-25 split is consistently higher but never by more than 10%. The 5-year characteristic loads separately for the slow and the fast lane are given in Section D.7.3.

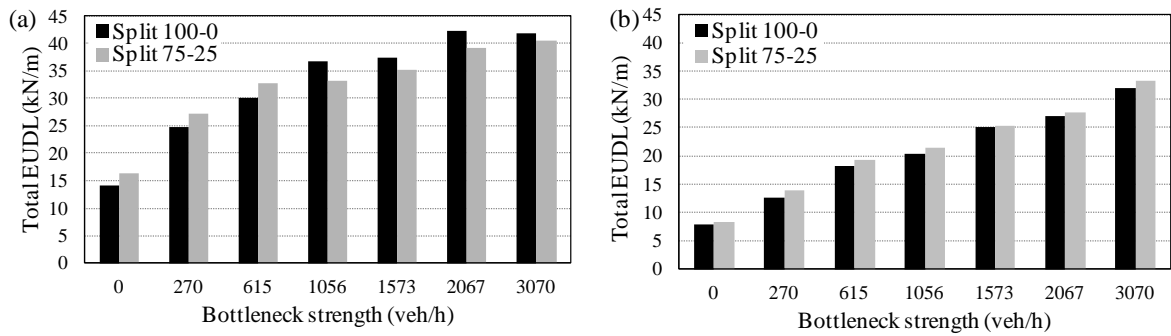


Figure 3.14 - 5-year EUDL for (a) 200 m and (b) 1000 m spans with different truck lane splits at injection for a flow of 3000 veh/h.

3.7 The effect of traffic composition

3.7.1 The effect of truck percentage

In this section, the effect of an increased percentage of trucks is considered. The percentage of trucks is increased to 48% for the inflow of 1250 veh/h. Firstly, a greater truck percentage has a significant impact on the traffic flow, as it reduces the road capacity (Transportation Research Board, 2010). Therefore, the dynamic capacities Q_{out} and Q'_{out} in Equation (3.6) are both less (see also Table 2.4), globally resulting in a lower bottleneck strength ΔQ , which implies that the same inflow Q_{in} , but with a greater truck percentage, would return a lighter congested state. Therefore, the inhomogeneity applied to generate the HCT(2) state ΔT is increased from 4.8 to 6.0 s, in order to return the same congestion features in terms of average speed and allow for a meaningful comparison between traffic with different truck percentages.

For the same inflow, increasing the truck percentage significantly reduces the lane change rate (Table 3.5), as cars tend not to move to the slow lane, which is increasingly occupied by trucks. Indeed, very long platoons of trucks form there. Table 3.5 shows that, as a result of the greater number of trucks, the percentage of lane changes performed by trucks increases significantly to up to 29%. The load is also higher, with the increase being more significant in the 1000 m span, as noted in Section 2.6.2 for single-lane simulations.

Table 3.5. Lane change activity and EUDL with different truck percentages and congestion states.

Truck percentage	Lane change rate (LC/km/h)		Lane changes performed by trucks (%)		EUDL 200 m (kN/m)		EUDL 1000 m (kN/m)	
	20%	48%	20%	48%	20%	48%	20%	48%
FT ($\Delta Q = 1727$ veh/h)	513	167	2.88	16.66	11.18	10.37	4.85	6.10
HCT(2) ($\Delta Q = 2067$ veh/h)	512	141	2.52	26.41	34.15	46.49	18.55	37.81
FS ($\Delta Q = 3070$ veh/h)	169	49	3.60	29.13	38.77	49.45	32.71	45.87

3.7.2 The effect of cars on loading

A comparison between the case of 3000 veh/h and 20% trucks against the case of 1250 veh/h and 48% cars, which share the same truck flow of 600 trucks/hour, is particularly interesting, as many current weigh-in-motion systems do not store information about cars. As a consequence, at these stations much data is available for trucks, whereas little is available for cars. Figure 3.15 shows that, as expected, cars have a beneficial effect on loading at high bottleneck strengths, reducing the load by about 12% (200 m span) and 29% (1000 m). On the other hand, at lower bottleneck strengths, cars cause congestion since the total flow is higher, thus resulting in critical loading events for long-span bridges.

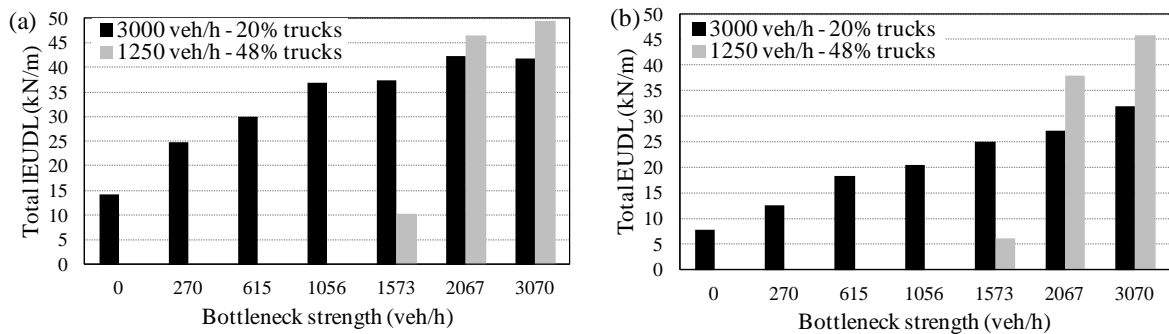


Figure 3.15 - 5-year EUDL for (a) 200 m and (b) 1000 m spans with 600 truck/hour and different car proportions.

3.8 Conclusions

This chapter investigates the effects of different observed congestion patterns and traffic compositions on the total load of two sample long-span bridges (200 and 1000 m long) by

means of multi-lane traffic micro-simulation. Most previous research neglects the influence of different congestion patterns, assuming a queue of vehicles at a minimum bumper-to-bumper distance. They also do not consider driver behaviour and lane-changing activity, which tend to form truck concentrations. The multi-lane model has been calibrated with available data from the literature. Five different combinations of inflow and traffic composition are considered and both traffic and loading features are analysed.

Firstly, results confirm the findings of Chapter 2 for single-lane simulations, that is the bumper-to-bumper queue is not always the most critical loading event. In fact, homogeneous slow-moving traffic states may be critical as well for the shorter span considered here (200 m).

A new finding is that it is the bottleneck strength that governs the loading, rather than the inflow. At lower inflows, a greater bottleneck strength is needed to break the traffic down, but once this happens, the resulting load does not vary significantly from the load generated with the same bottleneck strength and higher inflow. This implies that congestion arising outside of peak hours can be critical for bridge loading.

Other findings are that the truck distribution between lanes has a limited effect on the total load; long truck platoons forms with a moderate flow of about 2000 veh/h, although very long platoons may form also a higher flows; and the effect of cars is important in reducing the total load at the critical high bottleneck strengths. All these effects become more pronounced for the longer span considered (1000 m).

Chapter 4

A methodology for computing traffic loading on long-span bridges based on micro-simulation and site-specific traffic data

Authors:

Alessandro Lipari

Colin C. Caprani

Eugene J. OBrien

Paper Status:

Ready for submission to *Structural Safety*. Minor modifications are done in the text in order to minimise repetition and to fit into the context of the thesis.

Note to the Reader:

The work in this chapter is entirely the work of the author under the supervision of Prof OBrien and Dr Caprani.

4.1 Introduction

As seen in Section 2.1, traffic loading for long-span bridges is not addressed in most codes of practice and available traffic load models often assume simplified and conservative traffic models. Recently, traffic micro-simulation has been used to achieve a more accurate traffic modelling, with the notable advantage that widely-available free-flowing traffic measurements can be used to generate congested traffic scenarios.

A probabilistic approach to long-span bridge loading requires the expected number of congestions over a reference period. Ricketts and Page (1997) acknowledge the importance of congestion frequencies. They also state that only standstill traffic is critical for bridge loading, and that this happens only on 2% of the congested time. Buckland et al. (1980) assume 800 standstill traffic events per year, with 15% of them involving two or more lanes. The Flint and Neill Partnership (1986) assumes one jam with a queue at minimum bumper-to-bumper distances every 80 000 km travelled (or equivalently 12.5 jams every million vehicle km travelled) and does not report a large sensitivity of the load to the jam frequency. Ditlevsen and Madsen (1994) consider a queue occurrence of 1.27 queues per km and per year, based on data from a German motorway. Section 2.6 has introduced frequencies of occurrence of congestion for sites exposed to congestions on a daily basis (a form of *recurrent congestion*, as will be explained in Section 4.2).

However, many highway bridges, especially in rural areas, do not experience congestion frequently, if ever. Indeed, bridges carrying low or moderate traffic are less exposed to extreme scenarios than bridges over busy roads and this aspect should be considered in developing a traffic load model for such bridges.

Therefore, it is clear that a modelling framework that takes into account different congestion states and their frequency of occurrence is needed to compute a site-specific traffic loading. This important aspect has not been comprehensively considered in the previous research. In recent times, data about traffic disruptions is becoming increasingly available, especially about traffic incidents, and therefore this information can be beneficially introduced in traffic loading studies.

In this chapter, a methodology is proposed to compute characteristic load effects from the consideration of different congestion states and their frequency of occurrence based on site-specific traffic features. Micro-simulation is used to model traffic congestions. This methodology addresses long-span bridges that do not suffer from recurrent congestions, but only from occasional congestions due to unpredictable events (*non-recurrent congestions*), such as incidents. The methodology is applied to study three long-span bridges on a two-lane same-direction road.

4.2 Non-recurrent congestion

Congestions are typically divided into *non-recurrent* and *recurrent*. Oddly, this classification is not made on their frequency of occurrence, but rather on the cause. Non-recurrent congestion is caused by incidents, work zones, special events or inclement weather (Dowling et al., 2004). Among those causes, incidents have the biggest impact (Kwon et al., 2006; Cambridge Systematics Inc., 2005c). They are typically unpredictable and infrequent. Recurrent congestion is caused by anything else (the main example being insufficient road capacity). In this case, the jam location is typically easy to predict (for instance in proximity of an on-ramp at peak hours) and congestion often happens on a daily basis.

4.2.1 Incidents

Whereas data about *accident* frequency is abundant in the literature, available data about *incident* frequency is more limited, although it is becoming increasingly available. Incident rates, I_r , are usually given in number of incidents per million vehicle kilometre travelled (I/MVkmT). The total number of incidents N over a stretch of road L (km) and a certain period T (day) with average daily traffic ADT (veh/day) is:

$$N = \frac{I_r \cdot ADT \cdot L \cdot T}{10^6} \quad (4.1)$$

Incident rates vary greatly. Many factors can affect the measured incident rate: inclusion of very small incidents, different incident detection techniques (e.g., cameras, patrols, tow trucks, statistics, loop detectors), different definitions of what is considered to be an incident, site-specific differences in alignment and layout (e.g., curves, absence of shoulder lane), etc.

Incidents may be classified by their cause (collision, breakdown, debris, etc.), severity (injuries, property damage, etc.), location (shoulder, driving lane), or number of lanes blocked. This latter parameter is relevant to bridge loading as it affects the road layout, thus reducing the road capacity and being a potential source of congestion.

The majority of incidents do not block driving lanes. The proportion of incidents causing the closure of one driving lane can be up to one third (Tasnim et al., 2008). Unsurprisingly, smaller proportions are found for closures of two or more lanes. Incidents causing the closure of two or more lanes are here considered to fully block the road, so the corresponding rate is named *full-stop rate* FSr (FS/MVkmT), similarly to the definition of Section 2.6.1.

Some studies on incidents have been presented in Section 2.6.1. The incident rates and the proportions of lane-blocking incidents that can be deduced from those studies are summarised in Table 4.1. Remarkably, while the incident rates are spread over a wide range, the full stop rates cover a much smaller range. This may be due to the fact that many small incidents can be unnoticed, while it is unlikely for a large incident causing lane closures to go unrecorded. Note that the full stop rates in Table 4.1 are much lower than the one used by the Flint and Neill Partnership (1986). Only the most complete and relevant studies for bridge loading applications are reported in Table 4.1. Several other studies about incidents are available (Pal et al., 1998; Roberts et al., 1994; Dowling et al., 2004; Potter et al., 2007; Bertini et al., 2005; Petrov et al., 2002; Kopf et al., 2005).

Table 4.1 - Incident rates and lane-blocking incidents from selected literature.

Authors	Incident rate (I/MVkmT)	Incidents blocking 1 lane (%)	Incidents blocking ≥ 2 lanes (%)	Full stop rate (FS/MVkmT)
Giuliano (1989)	≈ 6	6.5	2	0.12
Skabardonis et al. (1997)	64.6	3.1	0.6	0.39
Skabardonis et al. (1999)	57.7	9.15	0.45	0.26
Rodgers et al. (2006)	2.32	23.8	7.6	0.18
Tasnim et al. (2008)	≈ 5	33	5	0.25

4.2.2 Capacity reduction

Once an incident occurs, the road capacity, Q_{\max} , will be reduced. The capacity Q_{\max} , can be defined as "the maximum number of vehicles than can pass a given point during a specific

period under prevailing roadway, traffic, and control conditions" (Transportation Research Board, 2010). Quite obviously, a full road blockage leaves no capacity available, whereas a lane closure disproportionately affects the traffic in that the proportion of capacity available is smaller than the proportion of lanes closed. The Highway Capacity Manual (Transportation Research Board, 2000; Transportation Research Board, 2010) suggests that the capacity available drops to 35% when one lane out of two is blocked. A shoulder accident drops the capacity to 81%.

Knoop et al. (2009) find a 28% reduction in the queue discharge rate, Q_{out} , from 20 shoulder lane closures on a 3-lane motorway in the Netherlands. As mentioned in Section 2.2.2, the queue discharge rate, or dynamic capacity, Q_{out} , is smaller than the capacity, or static capacity, Q_{max} , referred to in the Highway Capacity Manual.

Roberts et al. (1994) suggest an average 1-min flow of 1670 passenger cars per hour per lane (pc/h/lane) due to an obstruction. In this case, they compute a 24.2% reduction compared to the theoretical per-lane capacity, or an available capacity of 38%.

It is not clear if such available capacities stated in the HCM (Transportation Research Board, 2000; Transportation Research Board, 2010) & Roberts et al. (1994) refer to the reduced capacity, Q'_{max} , or to the reduced queue discharge rate due to the incident, Q'_{out} . HCM refers to capacity, without mentioning any queue discharge rate. However, to measure the reduced capacity, Q'_{max} , the traffic should be uncongested. Otherwise, the reported values are the queue discharge rates due to the incident, Q'_{out} .

To clarify, Knoop et al. (2009) state that "*there has been no research to the maximum possible flow in free flow around an incident location*". Therefore, all the values in previous research should be intended as a queue discharge rate due to an incident Q'_{out} and not as a reduced capacity Q'_{max} . Accordingly, it seems more correct to consider the values from the HCM and Roberts et al. (1994) as the ratio of the queue discharge rate due to an incident Q'_{out} to the road capacity Q_{max} , and this is what it is intended for capacity available i in the remaining of the chapter:

$$i = \frac{Q'_{out}}{Q_{max}} \tag{4.2}$$

The *capacity reduction* is the complement of the capacity available.

4.2.3 Other causes of non-recurrent congestion

Work zones are included among the causes of non-recurrent congestion, but they are usually planned by the road agency, thus they are easier to predict. The HCM (Transportation Research Board, 2010) suggests that the capacity at a *short-term work zone* is 1600 pc/h/lane, regardless of the lane closure configuration. Sarasua et al. (2004) propose 1460 pc/h/lane. These values have to be adjusted for a *heavy vehicle adjustment factor* f_{hv} , as the presence of trucks reduces the capacity (Transportation Research Board, 2010). An application of the HCM heavy vehicle adjustment factors is given in Section B.2.2.

Inclement weather is another cause of non-recurrent congestion. Probability of occurrence should be assigned based on site-specific expected weather conditions. The HCM (Transportation Research Board, 2010) suggests little differences in capacity for light rain, light snow, temperature and wind, and an average 14% reduction for heavy rain and 22% for heavy snowfall. However, Kwon et al. (2006) and Medina Soto (2010) suggest that weather accounts only for a minimal proportion of the total delay due to congestions based on their American and Dutch sites, respectively.

There is no extensive literature available about *special events*, as they clearly depend on the activities in the area served by the road. Therefore, site-specific assumptions need to be made. Kwon et al. (2006) find that special events occurred in 45 out of 110 observed weekdays, on the I-880 in the USA. Kopf et al. (2005) find 32 special events over two months of observations over 3 sites near Seattle.

Finally, a special cause of non-recurring congestion is *rubbernecking*, which occurs when drivers are distracted by an accident or some other incident in the adjacent carriageway or surrounding area. In such cases, the capacity reduction is due to a change in driver behaviour, rather than a physical obstruction. The HCM (Transportation Research Board, 2010) suggests a capacity reduction from 5 to 25%, "*based on experience*". Giuliano (1989) quotes previous work quantifying the reduction due to rubbernecking as 25%. Roberts et al. (1994) observe two incidents reducing the flow in the opposite direction by 13 and 38%. Knoop et al. (2008) suggest as little as 50% capacity available as a consequence of two large accidents in the

Netherlands. It is clearly stated that they intend the capacity available as $Q'_{\text{out}}/Q_{\text{max}}$, as defined in Equation (4.2). Knoop et al. (2009) suggest a 69% capacity available intended as $Q'_{\text{out}}/Q_{\text{out}}$, for 29 rubbernecking events on a 3-lane motorway.

4.2.4 Flow patterns and traffic composition

As shown in Equation (4.1), the total number of incidents depends on the flow. Flow is strongly site-specific, but information about flow is quite easy to obtain, typically by *induction loop* detectors. In general, the night-time flow is much lower than the day-time, as traffic is typically related to business hours. During the day, some sites are characterised by one or two sharp peaks (peak hour), while others do not show sharp peaks. Importantly, the low night-time flow may be characterised by a high truck percentage, while during the day those percentages are smaller (Flint and Neill Partnership, 1986; Hallenbeck et al., 1997; Caprani et al., 2012a). The range between night- and day-time flows is typically large for car traffic, while it is more limited for truck traffic. Truck traffic has typically no peaks, indicating that peak hours are characterised only by an increase in cars.

4.3 Methodology for computing the characteristic load

In this section, a methodology for computing the characteristic load (or a load effect), z^* , corresponding to an assigned return period, T , based on traffic micro-simulation and site-specific flow and incident data is proposed.

4.3.1 Data requirements

For the first step, a typical flow pattern over the day is required. Typically, flow patterns are given in hourly distributions and are repeatable over the same group of days, e.g. weekdays/weekends (Transportation Research Board, 2010). Note that weekend traffic usually has small truck proportions, so weekdays are of interest for bridge loading. A frequency of occurrence f_q can be then assigned to chosen flow values q . This information is site-specific and widely available, as discussed above. Then, an incident rate, I_r , has to be assigned. This information is site-specific and less commonly available, but can be estimated based on available data (Table 4.1).

To find out the total number of incidents N , a length of the road L must be set, as indicated in Equation (4.1). This length must be longer than the bridge itself, as incidents originating after the bridge may cause congestion that propagates back to the bridge. The growth of the congestion depends on the inflow and the capacity reduction. The higher the inflow and the capacity reduction, the faster the congestion growth. The length of the queue depends also on the incident duration. Moreover, after the incident removal, congestion will remain for some time before complete dissipation. These complex aspects of congestion growth and dissipation are not taken into account here and an expected queue length may be used. Depending on the road layout, L may be also related to the distance to the next junction. This might be appropriate, for example, when congestion occurring after the junction does not propagate further backwards, provided that incoming vehicles are free to exit. Either way, with the expected queue length L known, the total number of incidents can be then found from Equation (4.1). The influence of the expected queue length is further analysed later.

An incident causes a reduction of the capacity. The frequency of occurrence of capacity available due to an incident f_i can be assigned to any value of capacity available chosen i , as defined in Equation (4.2). This information is again site-specific, but not so common. If not available, such frequencies may be assigned based on available literature data.

4.3.2 Analytical formulation

The law of total probability can be used to determine the joint frequencies $f_{i,q}$ of having an incident characterised by a capacity available i at a certain flow q , provided that an incident has occurred. It must be noted that higher flow rates have higher probability of having an incident, as per Equation (4.1). Therefore, the joint frequencies $f_{i,q}$ are:

$$f_{i,q} = f_i \cdot f_q \cdot \frac{24 \cdot q}{ADT} \quad (4.3)$$

where f_i is the frequency of occurrence of an incident causing a capacity available i ; f_q is the frequency of occurrence of a flow q ; and ADT is the average daily traffic. The joint frequencies sum up to 1. The distribution of the number of incidents causing a capacity available i at a certain flow q , and over a reference *return period*, T , is:

$$N_{i,q} = f_{i,q} \cdot N \quad (4.4)$$

where is computed from Equation (4.1). Other forms of congestion, such as a work zone characterised by a capacity available i at the flow q , may be introduced in Equation (4.4), by increasing the relevant value of $N_{i,q}$ and rescaling the joint frequencies $f_{i,q}$:

$$f_{i,q} = \frac{N_{i,q}}{\sum_{i,q} N_{i,q}} \quad (4.5)$$

Then, for each combination of inflow q and capacity available i , a number of incident events of fixed duration D are simulated. They can be simulated by means of traffic micro-simulation, as shown in the previous chapters. The maximum total load of each incident event $z_{i,q}$ is then captured. Note that not all the incidents generate congestion. For instance, minor incidents (high i) do not cause congestion unless the flow q is high.

Similarly to the previous chapters, the Generalized Extreme Value (GEV) distribution is fitted to the simulated maximum total loads for each inflow q and capacity available i :

$$F_{i,q}(z_{i,q}) = \exp \left\{ - \left[1 + \xi_{i,q} \left(\frac{z_{i,q} - \mu_{i,q}}{\sigma_{i,q}} \right) \right]^{\frac{1}{\xi_{i,q}}} \right\} \quad (4.6)$$

where $\mu_{i,q}$ is the location, $\sigma_{i,q}$ the scale and $\xi_{i,q}$ the shape parameter of the GEV distribution. The GEV parameters are inferred through maximum likelihood estimation.

The probability P that the maximum load due to incidents does not exceed z is:

$$P(z) = \sum_i \sum_q F_{i,q}(z) \cdot f_{i,q} \quad (4.7)$$

where $F_{i,q}$ is the cumulative distribution function of the maximum load for the i^{th} value of capacity available and the q^{th} flow (Equation 4.6), and $f_{i,q}$ is the joint probability as defined in Equation (4.3). The target probability $P(z^*)$ corresponding to the return period T should be assigned in order to find the characteristic load z^* . The total number of incidents N in the return period T is given by Equation (4.1). The total duration of incidents over the return

period T is $N \cdot D$. Then, the target probability of non-exceedance for maximum-per-incident data is:

$$P(z^*) = 1 - \frac{1}{T(z^*)} = 1 - \frac{1}{N \cdot D} \quad (4.8)$$

4.4 Micro-simulation

In order to apply the proposed methodology, multi-lane micro-simulation is used to reproduce the effects of incidents on the traffic stream. As in Chapter 3, the *Intelligent Driver Model* (Treiber et al., 2000) is extended with the MOBIL lane-changing model (Kesting et al., 2007).

4.4.1 The Intelligent Driver Model

The *Intelligent Driver Model* (IDM) has been presented in Section 2.2.1. The main equations of the model are repeated here for convenience:

$$\frac{dv(t)}{dt} = a \left[1 - \left(\frac{v(t)}{v_0} \right)^4 - \left(\frac{s^*(t)}{s(t)} \right)^2 \right] \quad (4.9)$$

$$s^*(t) = s_0 + Tv(t) + \frac{v(t)\Delta v(t)}{2\sqrt{ab}} \quad (4.10)$$

In Equation (4.10), the desired minimum gap s^* is limited to be greater than or equal to the minimum jam distance s_0 (see Section D.3 for further details).

4.4.2 The MOBIL lane-changing model

The MOBIL lane-changing model has been presented in Section 3.2.2. The main equations of the model for asymmetric rules are repeated here for convenience. The *incentive criteria* for a slow-to-fast lane change and for a fast-to-slow lane change are:

$$\tilde{a}_c(t) - a_c(t) > \Delta a_{th} + \Delta a_{bias} + p(a_n(t) - \tilde{a}_n(t)) \quad (4.11)$$

$$\tilde{a}_c(t) - a_c(t) > \Delta a_{th} - \Delta a_{bias} + p[(a_n(t) - \tilde{a}_n(t)) + (a_o(t) - \tilde{a}_o(t))] \quad (4.12)$$

The *safety criterion* is:

$$\tilde{a}_n(t) \geq -b_{safe} \quad (4.13)$$

For this work, Equations (4.9-13) are discretized into 250 ms steps.

4.4.3 Congested Traffic States

As seen in Section 2.2.2, flow-conserving inhomogeneities are a convenient way to generate congestion. It is not necessary to explicitly model the effects of an incident event (e.g., a lane closure), but a simpler modification of the safe time headway T can return similar effects on the traffic congestion pattern. Inhomogeneity is generated by increasing the safe time headway T downstream, to T' . The resulting congested states are reported again in Table 4.2 for the reader's convenience.

Table 4.2 - Definitions of traffic states.

Acronym	Explanation of traffic state
FT	Free Traffic
MLC	Moving Localized Cluster
PLC	Pinned Localized Cluster
SGW	Stop and Go Waves
OCT	Oscillating Congested Traffic
HCT	Homogeneous Congested Traffic

4.4.4 Traffic stream

As done in the previous chapters, a simplified vehicle stream made of two classes of vehicle, cars and trucks, is used. The parameters are the same used in Chapter and are reported in Table 4.3 for the reader's convenience.

Table 4.3 - Model parameters.

	Cars	Trucks
Desired speed, v_0	120 km/h ($\pm 20\%$)	80 km/h ($\pm 10\%$)
Safe time headway, T	1.6 s	1.6 s
Maximum acceleration, a	0.73 m/s ²	0.73 m/s ²
Comfortable deceleration, b	1.67 m/s ²	1.67 m/s ²
Minimum jam distance, s_0	2 m	2 m
Vehicle length, l	4 m	12 m
Politeness factor, p	0.1	0.1
Changing threshold, Δa_{th}	0.2 m/s ²	0.2 m/s ²
Bias for the slow lane, Δa_{bias}	0.2 m/s ²	0.2 m/s ²
Maximum safe deceleration, b_{safe}	6 m/s ²	6 m/s ²
Gross Vehicle Weight	20 kN	432 kN*

* Coefficient of Variation 0.1.

Seven inflows are considered: 3000, 2500, 2000, 1500, 1000, 500, and 250 veh/h. Such inflows are characterised with a different truck percentage, in order to acknowledge that low flows may have high truck percentages. Figure 4.1 shows data from Caprani et al. (2012a) and from typical hourly flow patterns combined with typical hourly truck percentages (Hallenbeck et al., 1997; Transportation Research Board, 2000). A logarithmic envelope is built and this is taken into account for simulations.

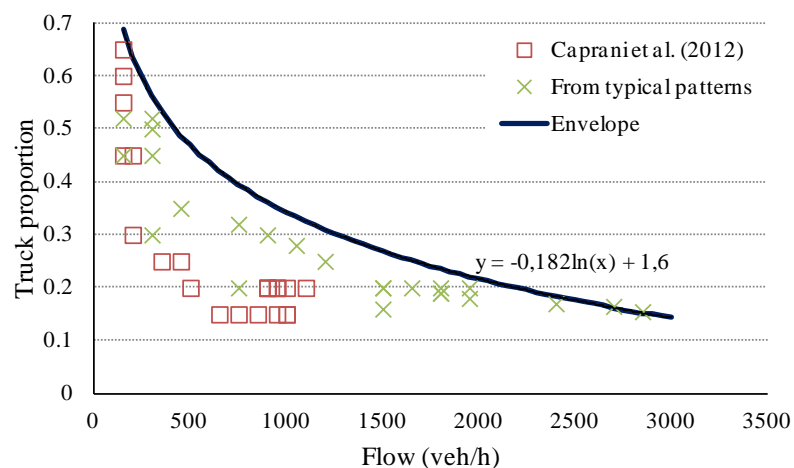


Figure 4.1 - Truck percentage values.

Each of this inflow has its own values of capacity Q_{\max} and queue discharge rate Q_{out} , since the truck presence negatively affects the road capacity (Transportation Research Board, 2010). The capacity and the queue discharge rate are calculated by means of simulations, as described in Section B.2, and are reported in Table 4.4. Trucks are injected in the slow lane, which is where they are expected to stay, being characterised by a slower desired speed v_0 .

Table 4.4 – Capacity and queue discharge rate of inflows considered.

Inflow q (veh/h)	Truck percentage	Truck flow (truck/h)	Capacity Q_{\max} (veh/h)	Queue discharge rate Q_{out} (veh/h)
3000	15	450	3282	3092
2500	18	450	3248	3078
2000	22.5	450	3189	3055
1500	28	420	3124	3016
1000	35	350	3056	2966
500	48	240	2949	2876
250	60	150	2841	2785

4.4.5 Road geometry and capacity available

A two-lane 8000 m long road is used in this work. Eight different levels of capacity available i are considered: 0, 0.3, 0.4, 0.5, 0.6, 0.7, 0.8, and 0.9. The capacity available $i = 0$ represents full road blockage.

The reduced queue discharge rates Q'_{out} can then be found from the capacities Q_{\max} in Table 4.4 through Equation (4.2). The reduced queue discharge rates are different for every inflow and capacity available.

Flow-conserving inhomogeneities $\Delta T = T' - T$ are then applied in order to return the required queue discharge rates Q'_{out} . The safe time headway is $T = 1.6$ s from 0 to 5700 m (see Table 4.3), then increases gradually to the appropriate value of T' at 6300 m, to generate the required queue discharge rate Q'_{out} .

In total, 56 traffic cases are simulated. For each case, 250 incident events are simulated, each of which is one-hour long. This value is close to the average incident duration recorded by Rodgers et al. (2006), but in most cases incidents are shorter (Giuliano, 1989; Tasnim et al., 2008).

The total load on three long spans (200, 600 and 1000 m) for the different inflows and capacity available is computed. The bridges are placed before the bottleneck, centred at 5000 m in the 8000 m length of roadway modelled.

4.5 Simulation results

4.5.1 Traffic states

Figure 4.2 shows the average speeds due to incidents. The resulting traffic states are also marked, according to Table 4.2. It can be seen that incidents with no driving lane closure ($i > 0.5$) cause congestion only at high flows. When this occurs and $i > 0.7$, the congestion is oscillatory, which is not the most critical case for bridge loading, as discussed in Section 2.5. A one-lane closure ($i = 0.3-0.4$) does not cause any congestion if the flow is lower than 1000 veh/h. However, when the inflow is higher, the resulting congestion type is the critical HCT state.

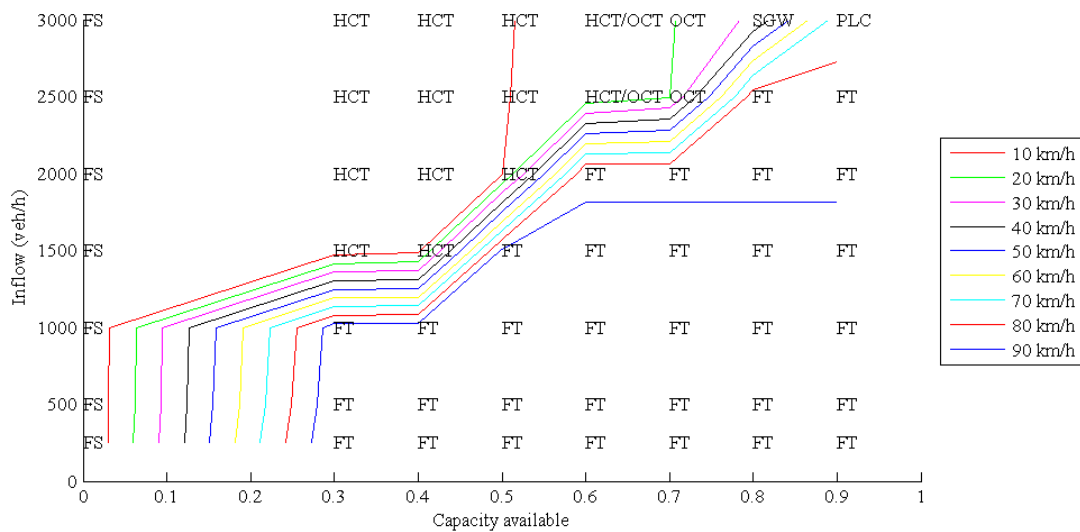


Figure 4.2 – Average speeds due to incidents.

4.5.2 Consideration of only one incident and inflow

In order to identify possible combinations of capacity and inflow particularly critical for bridge loading, it is initially assumed that a single combination of capacity available i and inflow q occurs during the return period T , i.e. $f_{i,q} = 1$. The maximum total load following

each one-hour incident event, $z_{i,q}$, is captured and is fitted with the GEV distribution (Equation 4.6). Assuming that an incident occurs every day of a 250 working day year, 5-year characteristic values are determined for each pair of capacity available i and inflow q . The target probability is then $P(z^*) = 1 - 1/1250 = 0.9992$.

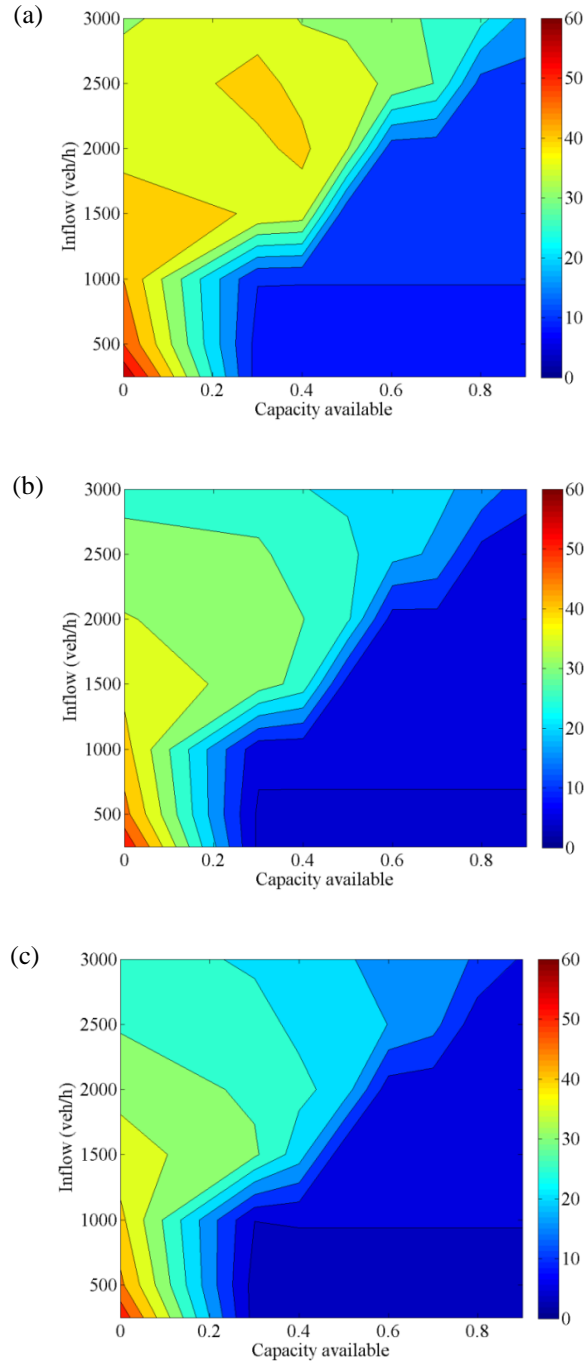


Figure 4.3 – 5-year characteristic EUDL for different bridge spans (values in kN/m): (a) 200 m, (b) 600 m, (c) 1000 m.

The results are shown in Figure 4.3, where the Equivalent Uniformly Distributed Load (EUDL) is plotted, for ease of comparison between different spans. Figure 4.3a shows the 5-year EUDL for the span of 200 m. For inflows greater than 2000 veh/h, the full stop condition ($i = 0$) is not the most critical case, whereas for longer spans (Figure 4.3b,c) the full stop is always the most critical case, regardless of the inflow. This confirms the findings described in Sections 2.5 and 3.5.

It can also be seen that several combinations of capacity available and inflow do not cause critical loading events, as the traffic is free. Importantly, for any span the most critical case occurs with low inflow of 250 veh/h, which is characterised by a high truck percentage (Figure 4.1).

4.6 Application of the proposed methodology

The incident rate and proportions are initially taken from Tasnim et al. (2008). The 33% one-lane closures are equally assigned to the capacities available $i = 0.3$ and $i = 0.4$, since HCM (Transportation Research Board, 2010) suggests a capacity available of 0.35, as mentioned earlier. Modest information is available for distributing the cases involving no driving lane closure. Frequencies are then distributed by acknowledging that smaller i of the order of 0.5 and 0.6 are not reported in literature as a consequence of incidents (Section 4.2.2). As it will be shown later, this assumption has a negligible impact on the final result. In order to compute the total number of incidents (Equation 4.1), an expected queue length L of 5 km is used.

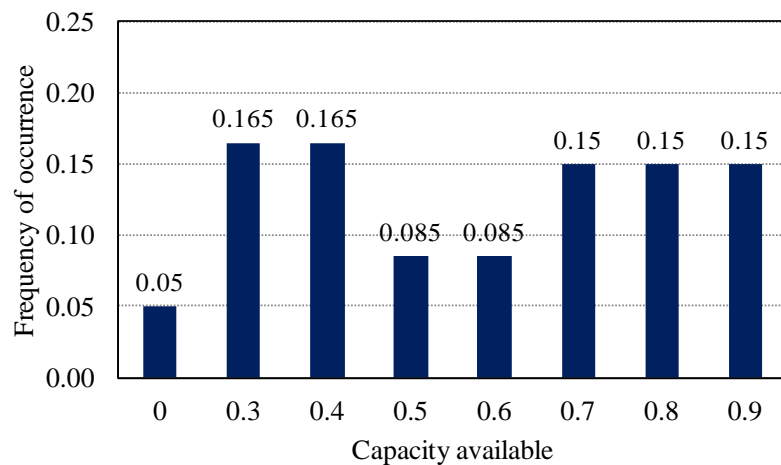


Figure 4.4 – Distribution of capacity available derived from Tasnim et al. (2008).

Two values of daily flow ADT are considered: 50 000 and 25 000 veh/day. The hourly flow distributions are based on data from German motorways (Geistefeldt and Hohmann, 2013). The road is assumed to satisfy the traffic demand ($q < Q_{\max}$), and therefore not to be affected by recurrent congestions. A daily flow of 50 000 veh/day implies that the road is quite busy over the day-time, and with no peaks. Except for transition periods, the flow is made up of a day-time flow of 3000 veh/h and a night-time flow of 500 veh/h.

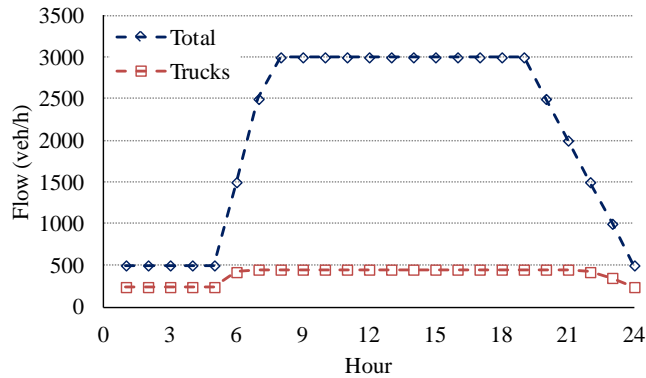


Figure 4.5 – Hourly flow distribution (ADT = 50 000 veh/day).

For the smaller flow of 25 000 veh/day, peaks are possible. Here it is assumed that there is a very strong morning peak (case 1, Figure 4.6a). The flat pattern, like the one in Figure 4.5, is also considered (case 2, Figure 4.6b).

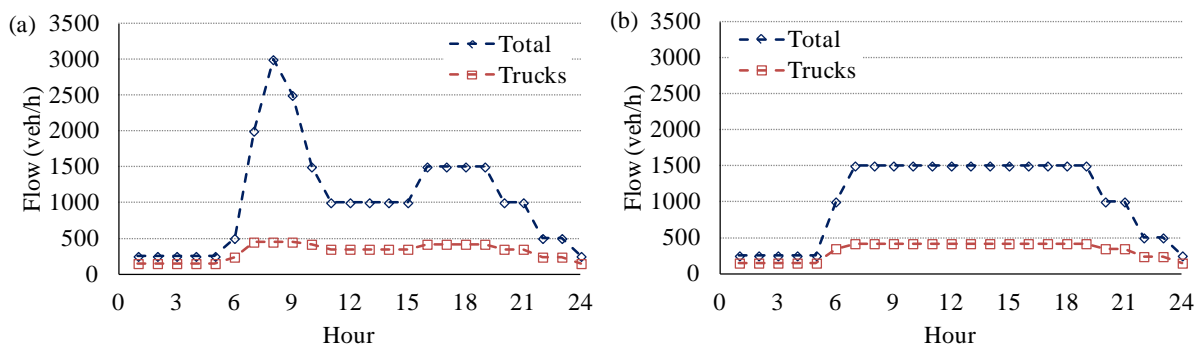


Figure 4.6 – Hourly flow distribution (ADT = 25 000 veh/day) for (a) peaked and (b) flat pattern.

Table 4.5 shows the number of incidents expected over one year. Incidents with ADT 50 000 veh/day causes a high number of congestions, and then possible critical events for the bridge, due to the frequent high flow of 3000 veh/h. The smaller inflow causes much less congestions. Note that the number of full stops is much lower than the one assumed in

Buckland et al. (1980) and Flint and Neill Partnership (1986). On the other hand, they are higher than the 6.35 full stops per year than can be deduced from Ditlevsen and Madsen (1994) for a road of length $L = 5$ km.

Table 4.5 – Number of incidents.

	Daily flow (veh/day)	Number of incidents per year ¹
Total	50 000	312.50
	25 000 (1)	156.25
	25 000 (2)	156.25
Causing congestion	50 000	261.06 (83.7%)
	25 000 (1)	56.44 (36.1%)
	25 000 (2)	48.03 (30.7%)
One lane closure causing congestion	50 000	94.88 (30.4%)
	25 000 (1)	30.94 (19.8%)
	25 000 (2)	40.22 (25.7%)
Causing full stop	50 000	15.63 (5.0%)
	25 000 (1)	7.81 (5.0%)
	25 000 (2)	7.81 (5.0%)

¹ In parenthesis the ratio to the total number of incidents.

As done in previous chapters, the probability functions $P(z)$ are plotted on Gumbel probability papers. On this scale, the y-axis ordinate, or Standard Extremal Variate (SEV), is given by $-\log[-\log(P(z))]$. The y-axis values are directly related to the hours of incidents, or simply to the number of incidents N , following the assumption of one-hour incidents. In contrast, and contrary to the usual case for Gumbel paper, the return periods T are not directly related to the y-axis values, since the total number of incidents vary with the daily flow (Table 4.5).

Figure 4.7 illustrates the combined curves of probability of the total load for the flow cases considered. The values corresponding to $T = 5$ years and $T = 1$ year are highlighted. The curves have similar shape and features, regardless of the span length. For high return periods, the curves tend asymptotically to the most critical condition, although infrequent, which is the full stop at night-time. This explains the fact that, for $T = 5$ years, the daily flow of 50 000 veh/day returns a smaller load than the daily flow of 25 000 veh/day (Table 4.6), even though there are twice as much incidents, and then congestion events (Table 4.5). In fact, with 50 000 veh/day, the night-time flow is 500 veh/h with 48% of trucks (see Figure 4.5 and Table 4.4), which does not return the most critical load (Figure 4.3). Indeed, the most critical flow is the

250 veh/h, which has a higher truck percentage than the 500 veh/h flow, although a smaller truck flow (Table 4.4). The 250 veh/h flow occurs in both cases of daily flow 25 000 veh/day. Finally, it can be seen that the hourly pattern is not important for high return periods.

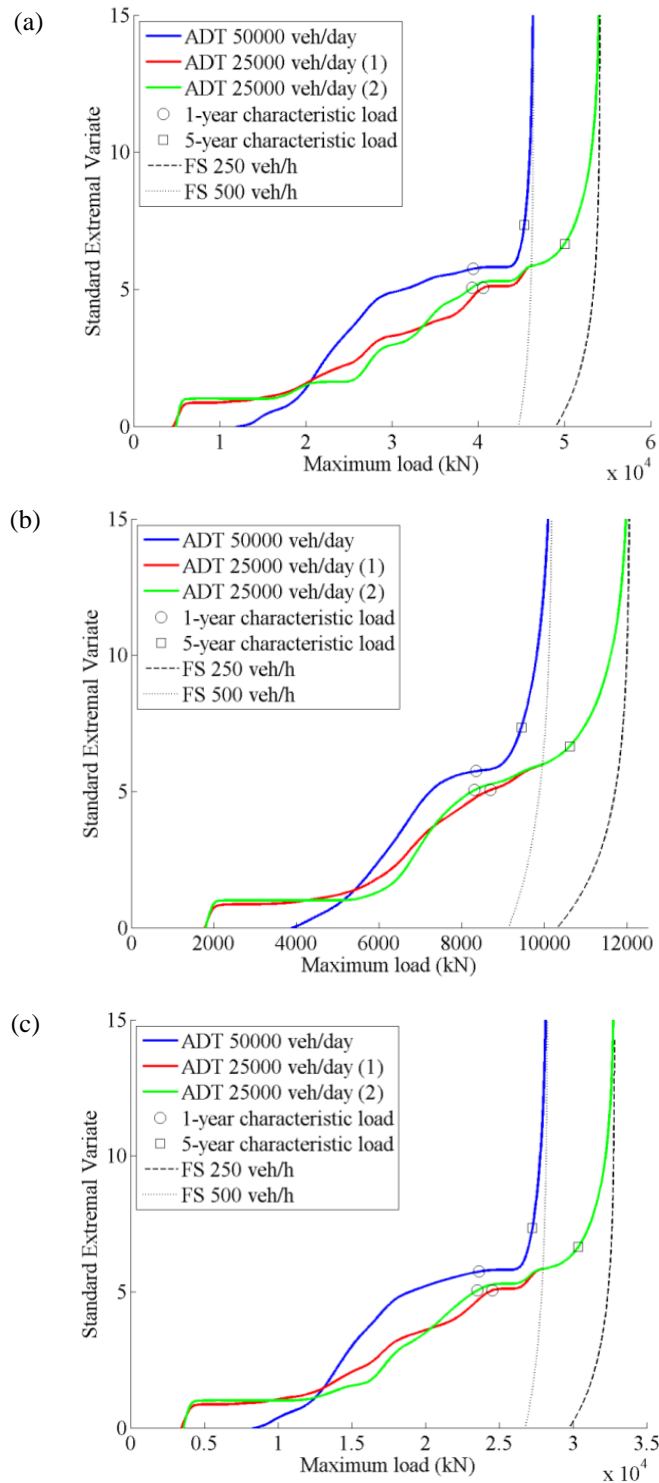


Figure 4.7 – Combined probability of total load for bridge span: (a) 200 m, (b) 600 m, (c) 1000 m.

Table 4.6 – Characteristic load.

Span (m)	Return period (years)	Daily flow (veh/day)	Characteristic load (kN)
200	1	50 000	8341
		25 000 (1)	8694
		25 000 (2)	8309
	5	50 000	9441
		25 000 (1)	10 611
		25 000 (2)	10 611
600	1	50 000	23 618
		25 000 (1)	24 527
		25 000 (2)	23 512
	5	50 000	27 250
		25 000 (1)	30 372
		25 000 (2)	30 372
1000	1	50 000	39 400
		25 000 (1)	40 561
		25 000 (2)	39 256
	5	50 000	45 348
		25 000 (1)	50 026
		25 000 (2)	50 026

Before tending to the asymptote, all the curves are much flatter, suggesting sensitivity to the return period. This is the region corresponding to return periods of the order of one year. In this region, the characteristic values lie in a small range (Figure 4.7). The hourly flow distribution makes a small difference in the one-year characteristic load, with peaky pattern slightly greater.

Many congestion events contribute to generate the shape of this area. Figure 4.8a shows the frequencies of incidents $f_{i,q}$ for ADT = 50 000 veh/day. Since 3000 veh/h is the most likely flow, incidents at that flow have a higher probability of occurrence. The most frequent congested states are highlighted in Figure 4.8b. The heaviest and most frequent HCT states ($i = 0.3$ and 0.4) seem to lead the slope of the probability curve before the flat part.

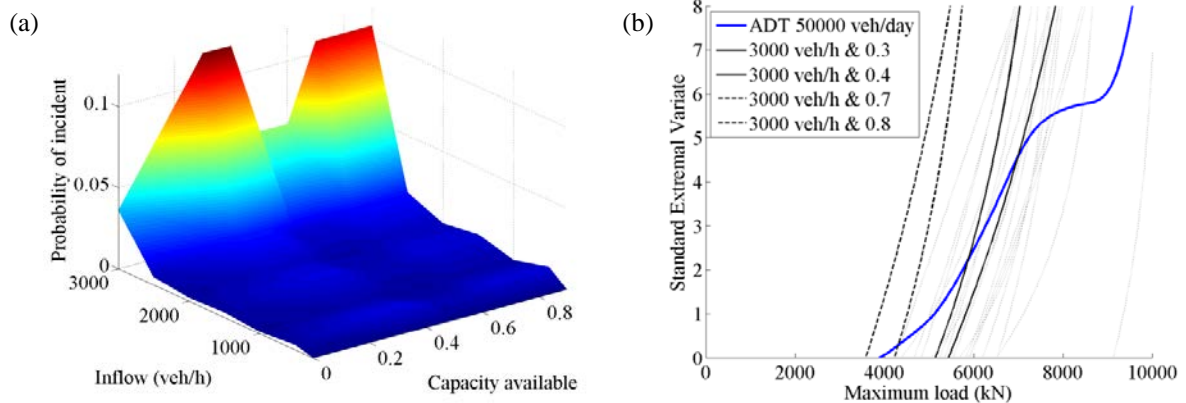


Figure 4.8 – (a) Incident frequency and (b) contributions to the combined probability of total load.

In conclusion, the results suggest that the truck percentage plays a crucial role in bridge loading, while daily flow, truck traffic, and hourly flow distribution are not as important, at least for the relatively high return periods typical in bridge applications. In addition, Section 3.5 has also shown that the total (hourly) flow is not important either for the total load, provided that congestion arises.

4.6.1 Influence of the expected queue length

An increase in the expected queue length L acts as an increase in the incident rate Ir (Equation 4.1). To examine its influence, a tenfold increase in the expected queue length is applied, while the incident frequencies $f_{i,q}$ remain unchanged. Therefore, the combined probability function is the same, but the characteristic value for a given return period T is different. Table 4.7 shows that the increase in the 5-year load is modest for any span and daily flow, while it is more pronounced for the 1-year load. Note that a tenfold increase in the incident rate would not be realistic, as the resulting full stop rate would be excessively high.

Table 4.7 – Characteristic load due to an expected queue length $L = 50$ km.

Span (m)	Return period (years)	ADT (veh/h)	Characteristic load (kN)	Variation on $L = 5$ km (%)
200	1	50 000	9569	14.72
		25 000 (1)	10 956	26.02
		25 000 (2)	10 956	31.86
	5	50 000	9780	3.59
		25 000 (1)	11 424	7.66
		25 000 (2)	11 424	7.66
600	1	50 000	27 438	16.17
		25 000 (1)	31 049	26.59
		25 000 (2)	31 049	32.06
	5	50 000	27 741	1.80
		25 000 (1)	31 905	5.05
		25 000 (2)	31 905	5.05
1000	1	50 000	45 590	15.71
		25 000 (1)	51 164	26.14
		25 000 (2)	51 164	30.33
	5	50 000	45 945	1.32
		25 000 (1)	52 599	5.14
		25 000 (2)	52 599	5.14

4.6.2 Influence of low flows with high truck percentage

It has been shown that the combined probability curves tend to the night-time full stop condition. The two hourly flow distributions considered for ADT = 25 000 veh/day share the same number of low-flow hours (Figure 4.6). It is then interesting to see what the effect is for sites characterised by longer periods of low flows with a high truck percentage. Figure 4.9a shows the hourly flow distribution when the low-flow is increased from 6 to 10 hours, and then to the ideal case of 24 hours. Figure 4.9b shows the combined probability of load for the 200 m span. Although the total daily traffic and the number of incidents decrease as the number of low-flow hours increases, the curves tend quicker to the full stop condition. Table 4.8 shows that sensitivity to the low-flow hours is rather small for the 5-year return period, even for the extreme case of 24-hour low-flow. As in Figure 4.7, the curves are quite flat around the return period corresponding to 1 year, and therefore sensitive to changes in the number of low-flow hours.

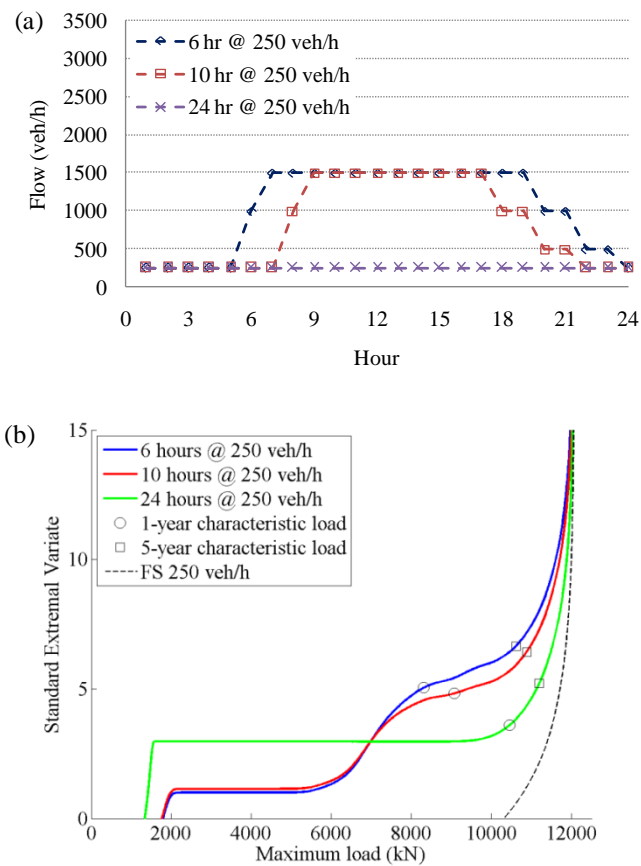


Figure 4.9 – (a) Low-flow hourly distributions and (b) resulting combined probability of load.

Table 4.8 – Characteristic load for different durations of low flow periods with high truck percentage.

Span (m)	Return period (years)	Low-flow period (hours)	Characteristic load (kN)	Variation on the 6-hour low flow (%)
200	1	10	9065	9.1
		24	10 457	25.9
	5	10	10 879	2.5
		24	11 195	5.5
600	1	10	26 687	13.5
		24	30 056	27.8
	5	10	30 901	1.7
		24	31 497	3.7
1000	1	10	44 543	13.5
		24	49 496	26.1
	5	10	50 915	1.8
		24	51 916	3.8

4.6.3 Influence of full stop conditions

Since the combined probability of load tends to the night-time full-stop condition, it is interesting to analyse the difference in the characteristic load when considering only the full stop condition. Figure 4.10a shows the combined curve when neglecting all the congestion types, except full stop for the 200 m span. The full stop rate is unchanged to 0.25 FS/MVkmT. In spite of the drastic reduction in the total number of incidents (they are now only 5% of the actual values), there are no differences in the characteristic load. Figure 4.10b shows the combined curves when full stop conditions are neglected. The characteristic loads are significantly lower by 20-29%.

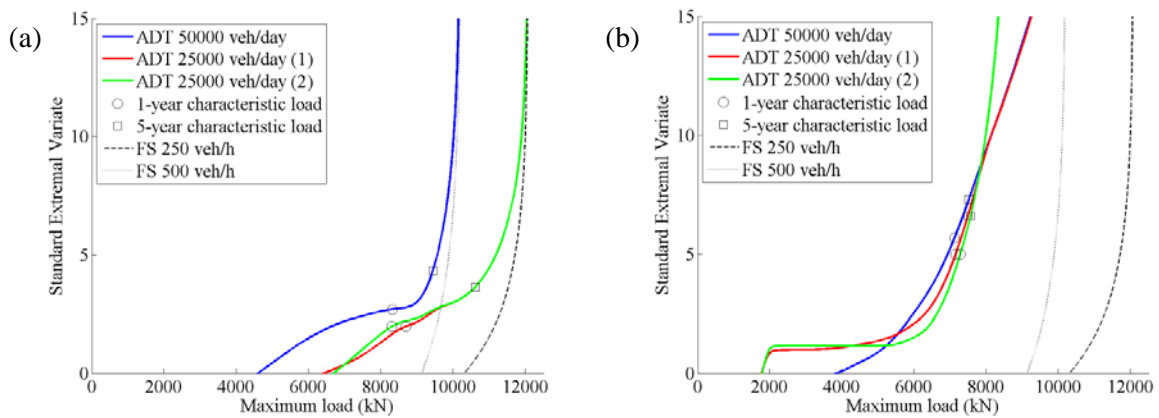


Figure 4.10 – Combined probability of total load (200 m span): (a) only full stop and (b) no full stop.

Also for the other spans, the error in considering only the full stop is none for the return periods considered. This is an important finding, as it suggests that the knowledge of non-full stop events is not necessary for an accurate computation of the characteristic load. Indeed, to achieve an accurate characteristic load, it is important to assume correct full stop rates, which are relatively limited (Table 4.1), and a correct proportion of flows with high percentage.

Moreover, full stop events come from incidents, as planned work zones typically maintain a minimum road operation level. Special events also do not cause full road blockage, nor do inclement weather. Therefore, information about other forms of non-recurring congestion is not needed to compute the characteristic load.

4.6.4 *Influence of full stop conditions at low-flow*

A further simplification can be made when considering only the full-stop conditions at night-time, that is only the dotted curves in Figure 4.7 and Figure 4.10. In this case, the number of incidents N per year drastically drops to 0.94 (ADT 50 000 veh/day) and 0.47 (ADT 25 000 veh/day). There are no variations in the 5-year characteristic values for all the spans considered.

4.6.5 *Dangerous site*

Skabardonis et al. (1997) report higher incident and full stop rates (Table 4.1) for an incident-prone site than for the ones considered in Figure 4.4 from Tasnim et al. (2008). The assigned frequencies of capacity available are shown in Figure 4.11. For the high ADT 50 000 veh/day there are as many as 807.5 inc/year, of which 4.8 are full stops. Table 4.9 shows that, in spite of the higher number of incidents, the increase compared to the incident data from Tasnim et al. (2008) is rather small for the 5-year return period and more significant for the one-year return period.

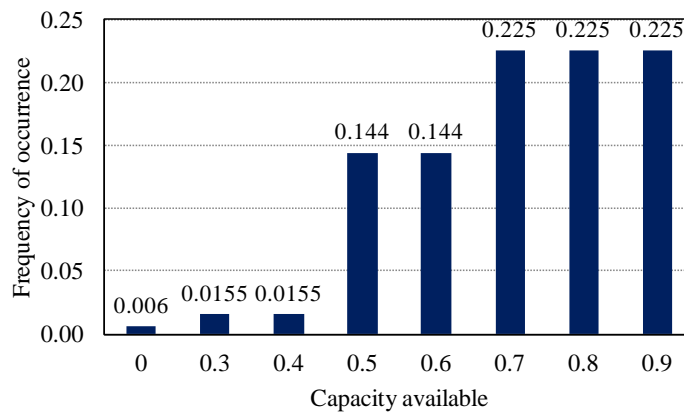


Figure 4.11 – Distribution of capacity available derived from Skabardonis et al. (1997).

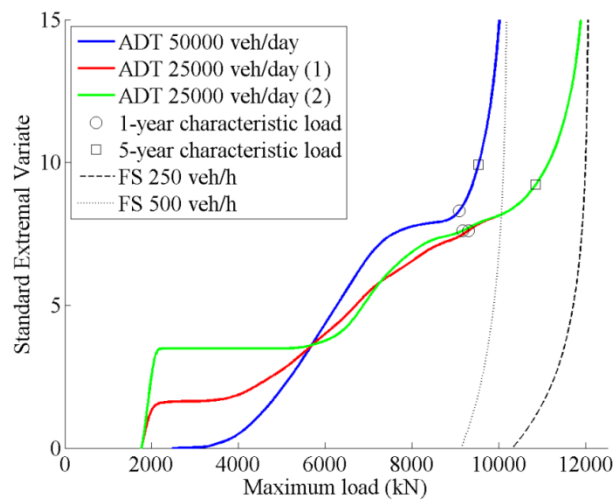


Figure 4.12 – Combined probability of total load with incident data from Skabardonis et al. (1997) (span 200 m).

Table 4.9 – Characteristic load with incident data according to Skabardonis et al. (1997).

Span (m)	Return period (years)	Daily flow (veh/day)	Characteristic load (kN)	Variation on Tasnim et al. (2008) (%)
200	1	50 000	9083	8.90
		25 000 (1)	9293	6.89
		25 000 (2)	9163	10.28
	5	50 000	9526	0.90
		25 000 (1)	10 846	2.21
		25 000 (2)	10 846	2.21
600	1	50 000	26 708	13.08
		25 000 (1)	27 039	10.24
		25 000 (2)	26 839	14.15
	5	50 000	27 375	0.46
		25 000 (1)	30 387	0.05
		25 000 (2)	30 387	0.05
1000	1	50 000	44 592	13.18
		25 000 (1)	45 054	11.08
		25 000 (2)	47 770	21.69
	5	50 000	45 510	0.36
		25 000 (1)	50 808	1.56
		25 000 (2)	50 808	1.56

4.7 Conclusions

Frequently in bridge traffic loading studies, different type of congestions have been neglected and conservative frequencies of occurrence of congestions have been assumed. An original methodology is presented for computing the characteristic load from micro-simulation and site-specific traffic flow and incident data. While flow data is usually widely available, incident data is more limited, but is becoming increasingly available. Micro-simulation is a suitable tool to model the traffic due to incidents.

Data available from the literature is used to apply the proposed methodology. It is found that full stop conditions are crucial for determining the total load. Information about other lighter congestion events does not largely affect the characteristic load for return periods higher than one year. The rates of full stop found in the literature lie in a relatively small range and are much lower than the ones used in previous bridge loading studies.

Then, as the return period increases, the characteristic load tends to the most critical, although rarest case. This is given by flows with high truck percentage, which typically occur at night-time in combination with low flows. Therefore, it is necessary to accurately model such low flows, as this is the condition that affects the load most. In comparison, other features, such as truck flow, total daily flow and hourly flow distribution are not as important, at least for return periods of the order of 5 years and longer.

Chapter 5

Accuracy of congested density estimates from point detectors

Authors:

Alessandro Lipari

Colin C. Caprani

Eugene J. OBrien

Paper Status:

Submitted for publication to *Proceeding of the ICE - Transport*. Minor modifications are done in the text in order to minimise repetitions and to fit into the context of the thesis.

Note to the Reader:

The work in this chapter is entirely the work of the author under the supervision of Prof OBrien and Dr Caprani.

5.1 Introduction

An accurate knowledge of the traffic stream characteristics is a necessary basis for any traffic-related application. The most common traffic characteristics are the *flow* (sometimes named *flux* or *volume*), the *density* (sometimes called *concentration*), and the mean speed. Flow is inherently a temporal quantity (number of vehicles per unit of time, veh/h), density is a spatial one (number of vehicles per unit of length, veh/km), and the mean speed (km/h) can be either, depending on whether it is averaged over time or space.

In practice, flow is easier to measure than density, by means of point detectors, such as induction loops. Therefore, researchers have devoted much attention to analysing traffic flow data, while this is not the case for density data. Often, density is estimated from flow measurements, sometimes at the cost of accuracy, especially during periods of congested traffic. However, accurate density measurements are important not only for traffic applications (for example, Intelligent Transport Systems and more specifically ramp metering), but also for infrastructure management (for instance, traffic loading on bridges and tunnel surveillance). In particular, in the case of bridge traffic loading, density is directly related to the load on a bridge, and any inaccuracy in density is likely to significantly affect the load.

As seen in Chapter 2, traffic micro-simulation offers a means to generate realistic congested traffic scenarios. In this work, different congestion strengths are generated. Density estimates from virtual point detectors are compared to the actual values collected with virtual cameras. Different detector layouts are considered, and a method for increasing the accuracy of density estimation during congestion is proposed. The behaviour of real induction loops is also simulated.

5.2 Traffic theory and data collection

5.2.1 *The fundamental equation of traffic*

Density, k , is related to flow, q , and space mean speed, v_S , through the well-known fundamental equation of traffic (Wardrop, 1952):

$$q = k \cdot v_s \quad (5.1)$$

These are all *macroscopic* quantities and are intended as averages. Equation (5.1) implicitly assumes that each vehicle maintains a constant speed, although individual speeds may be different. The ‘natural’ way to collect flow data is by using point detectors, while the natural way to collect density is by using spatial detectors. On the other hand, there is more than one way to compute the space mean speed (Hall, 1994; Treiber and Kesting, 2013).

Point detectors return traffic information at a certain location over time. Examples are induction loops, microwave radars and laser sensors, among others. In practice, a point detector occupies a short section of road, but, with reasonable approximation, it can be considered to give a point measurement. Point measurements are by far the most common way of collecting traffic data and are now an essential part of a highway management system. On the other hand, spatial detectors return information at a certain point in time over space. However, they are rarely used in real-world applications, as it will be discussed later. As a consequence, density is often computed from point measurements, by means of the fundamental equation of traffic (5.1).

5.2.2 The generalised fundamental equation of traffic

A vehicle’s motion can be identified through both time and space by tracking its trajectory. A trajectory gives the most complete information about the traffic stream. Figure 5.1 gives an example of a trajectory dataset taken from the literature.

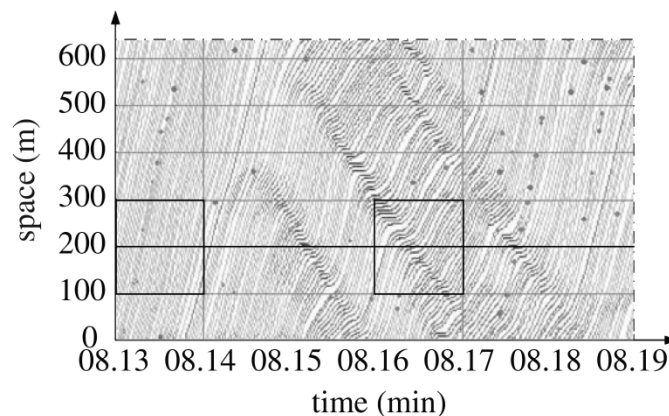


Figure 5.1 - Example of vehicle trajectories collected on the US-101 highway near Los Angeles (after Orosz et al. (2010)). The horizontal line indicates how a point detector would collect data.

The fundamental equation of traffic (5.1) can be generalised for any region in the space-time domain (Edie, 1974). Space-time domains can be generated with a rapid sequence of aerial photographs or a video (Treiterer and Myers, 1974; Hoogendoorn et al., 2003), or else with a dense installation of loop detectors or other point sensors (Wilson, 2011). In fact, both options are often not practicable in traffic management. Nevertheless, the generalised fundamental equation of traffic helps to have a better understanding of the implications of the collection method on the accuracy of the data. The three traffic stream characteristics are defined as:

$$\left\{ \begin{array}{l} q = \frac{\sum_i x_{A,i}}{|A|} \\ k = \frac{\sum_i t_{A,i}}{|A|} \\ v_s = \frac{\sum_i x_{A,i}}{\sum_i t_{A,i}} \end{array} \right. \quad (5.2)$$

where $|A|$ is the size of the region in the space-time domain, $x_{A,i}$ is the distance travelled by vehicle i in A and $t_{A,i}$ is the time travelled by i in A . Again, the values of flow and density have to be understood as averages over the space-time domain A . Equations (5.2) can be rewritten for the case of a point detector, that is, $|A| = T dx$:

$$\left\{ \begin{array}{l} q = \frac{\sum_i x_{A,i}}{|A|} = \frac{N \cdot dx}{T \cdot dx} = \frac{N}{T} \\ k = \frac{\sum_i t_{A,i}}{|A|} = \frac{dx \cdot \sum_i \frac{1}{v_i}}{T \cdot dx} = \frac{\sum_i \frac{1}{v_i}}{T} \\ v_s = \frac{\sum_i x_{A,i}}{\sum_i t_{A,i}} = \frac{N}{\sum_i \frac{1}{v_i}} \end{array} \right. \quad (5.3)$$

in which N is the total number of vehicles in A , i.e., the number of vehicles crossing the detector.

Equations (5.3) show that density and space-mean speed can be calculated from a single *point* measurement, even though they are inherently *spatial* quantities. They also make clear that the space-mean speed is the *harmonic* mean of the individual speeds recorded at one point, as also Wardrop (1952) pointed out. The use of the arithmetic mean (referred to as *time mean speed*) for inferring density from point measurements is incorrect. A similar argument shows that the space mean speed v_s collected over a stretch of road $|A| = L dt$ is the *arithmetic* mean of the observed speeds.

5.2.3 The fundamental equation of traffic and congestion

Traditionally, empirical data has been described by means of the diagrams q - k , k - v and q - v , which relate the three quantities present in the fundamental equation (5.1). Flow, q , and speed, v , come from field measurements, while k is estimated. A typical example is given in Figure 5.2a. A model is then fitted to the empirical data, for instance Greenshields (1935) or Transportation Research Board (2010). Observations have shown that there is an actual proportionality between speed and density (equal to the free flow speed), but only at low densities (uncongested flow). In fact, a wide scattering can be noticed at higher densities, typical of congested flow. It can also be seen that flow itself is not a good indicator of the state of traffic, as for a fixed flow value, there may be either free traffic or congestion.

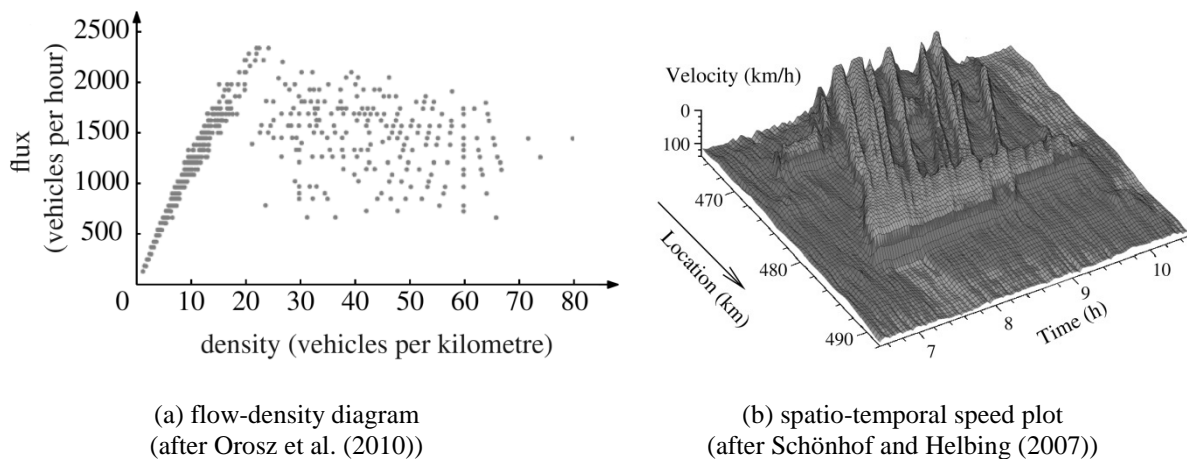


Figure 5.2 – Empirical data from A5 motorway near Frankfurt.

During congestion, a vehicle's speed is likely not to be constant, as a result of stop-and-go waves and similar fluctuations (Figure 5.2b). Therefore, the underlying assumption of each

vehicle keeping its speed in Equation (5.1), which allows the link between temporal and spatial quantities, does not hold and results in the characteristic scattering at high density.

In other words, if information is available for a small location dx , it is not generally possible to infer from this for a larger region ΔX , unless speeds do not change over ΔX . For instance, in the space-time plot of Figure 5.1, the density estimation from a point detector placed at 200 m would be accurate for the first framed region, but in the second one would probably not.

5.2.4 Loop detectors

Nowadays, induction loop detectors are the most common traffic sensors. They are relatively inexpensive and can count vehicles accurately, if properly installed and maintained (Coifman, 2006). Loop detectors are made up of an in-roadway wire loop linked to an electronic unit. They are able to detect either the presence or passage of metallic objects overhead (Klein et al., 2006).

A single loop detector returns the count of vehicles, n , and the time the loop remains on, t_{on} , usually aggregated over a time interval T , varying from 20 s to 5 min, with a typical value of 60 s. Occupancy, ρ , is defined as the fraction of time in which a vehicle i is over the detector, and this depends on the length l_i and speed v_i of the vehicle, as well as on the physical length of the detector d (typically equal to about 2 m). The aggregated occupancy over a time interval T is thus:

$$\rho = \frac{\sum_i t_{on,i}}{T} = \frac{1}{T} \sum_i \frac{l_i + d}{v_i} \quad (5.4)$$

Assuming that the vehicles have uniform lengths $l_i = L$ and Equation (5.1) holds, it is possible to find a linear relationship between density and occupancy:

$$\rho = (L + d) \cdot \frac{1}{T} \cdot \sum_i \frac{1}{v_i} = (L + d) \cdot \frac{q}{N} \cdot \sum_i \frac{1}{v_i} = (L + d) \cdot \frac{q}{v_s} = (L + d) \cdot k \quad (5.5)$$

The space mean speed v_s can be then obtained from Equation (5.5) as:

$$v_s = \frac{q \cdot (L + d)}{\rho} \quad (5.6)$$

However, this equation is correct only if vehicle lengths are uniform. Assuming constant speeds and variable lengths also leads to the same expression. Although neither assumption is met in practice, Equations (5.5) and (5.6) are widely used by assuming an average vehicle length (Hall, 1994).

A double loop detector consists of two paired wire loops, typically spaced 1.5 m apart. Such an installation allows the computation of individual speeds v_i , based on the difference in time at which the two loops are activated $t_{12,i}$:

$$v_i = \frac{d_{12}}{t_{12,i}} \quad (5.7)$$

where d_{12} is the distance between equivalent points of the two loops. It is also possible to identify the vehicle length l_i from the time a loop remains on $t_{on,i}$:

$$l_i = v_i \cdot t_{on,i} - d \quad (5.8)$$

In general, spatial quantities, such as the vehicle lengths, are exact only if the speed is constant during the measurement (Treiber and Kesting, 2013).

5.2.5 Data collection for bridge traffic loading

Traffic data for bridge loading typically comes from two sources, very often paired: weigh-in-motion (WIM) stations and double loop detectors (Figure 5.3). Both of them are point detectors. WIM stations are able to weigh axles at high speeds and time gaps between axles can be output. Double loop detectors, such as the ones described above, are used for supplementing information regarding speed (Equation 5.7) and then calculating the vehicle configuration (distance between axles). An assumption of constant speed of the vehicle crossing the detector is implicitly made.



Figure 5.3 – Typical WIM station coupled with double loop detectors (taken from wim.zag.si).

Data from paired WIM and loop stations has been widely used. Very often unaggregated vehicle-by-vehicle data is available, although sometimes it may be available only for heavy vehicles. The data recorded is directly used for load calculations, or else it is used for generating artificial traffic with Monte Carlo simulations based on the recorded traffic (OBrien and Caprani, 2005; Enright and OBrien, 2012).

For bridge loading calculations, a constant speed is typically assumed within the traffic stream (Eymard and Jacob, 1989; Bailey and Bez, 1999), although the recorded speeds were different. This means that vehicles keep the same time headways as were recorded, but not the space headways, which depend on the assumed speed. The average speed of the original traffic appears a sensible choice for setting such a constant speed. This is acceptable in free traffic, when the speed variation is not large and the actual speed is close to the average. However, when load effects are calculated with such a method during congestion, significant errors may occur, due to the large variations in speed. Assuming the same speeds as recorded may cause overlapping of vehicles in the simulation, as a faster vehicle may catch up with a slower leader. This aspect is particularly significant for longer spans, where the length to be inferred is greater. Details are given in Appendix E, where several issues related to traffic data collection for bridge loading are dealt with extensively.

5.3 Density estimation

5.3.1 Using one point detector

When using loop detectors, common practice widely uses Equation (5.1). If the flow is quite uniform, then the density calculated through (5.1) is reliable. This happens in free traffic, and

sometimes in congestion, but only when the speed is approximately constant, as will be shown later. In all other cases, the accuracy of density estimation should be checked. This includes the frequent case of stop-and-go waves, such as those depicted in Figure 5.1 and Figure 5.2b.

Some networks are programmed to output only the arithmetic mean of individual speeds, i.e. the time mean speed. The incorrect use of the time mean speed in Equation (5.1) would lead to an under-estimation of density, since the space mean speed is less than or equal to the time mean speed (Wardrop, 1952). However, a method to work out the space mean speed from time mean speed measurements has been recently found (Rakha and Zhang, 2005; Soriguera and Robusté, 2011).

5.3.2 Using two point detectors

An average density can be computed by using two loop detectors at the beginning and end of the road section of interest of length L and counting the number of vehicles crossing the upstream detector, N_u , and the downstream one, N_d , at the same time interval. The relation follows from the conservation of vehicles and therefore it is exact and works under any traffic condition:

$$k(t+1) - k(t) = \frac{N_u(t) - N_d(t)}{L} \quad (5.9)$$

This equation gives the change in density on a section of road between two consecutive time steps t and $t+1$. It therefore needs to be initialised, for instance at night, in order to have $k(0) = 0$. Moreover, any uncompensated counting error will accumulate.

Several researchers have used Equation (5.9), often combined with a Kalman filtering technique based on other available traffic information, in order to correct measurement errors and other possible assumptions. For instance, Gazis and Knapp (1971) use speed data available at the detectors; Nahi (1973) assumes flow homogeneity; Kurkjian et al. (1980) use occupancy data. Other authors combine loop data with other sources of information. For instance, Qiu et al. (2010) use data from vehicles equipped with GPS, in order to have local variations of density as well.

Another method is the so-called $n-t$ method, which is based on plots of cumulative vehicle counts n and time t , built over two loop detectors. Since the time travelled by each vehicle is available, density can be accurately calculated by definition (Equation 5.2). However, similarly to the previous approach, the vehicle counting must be initialised and is sensitive to uncompensated miscounting (Ni, 2007).

The above methods do not consider lane-changing. However, they can be easily extended to multi-lane traffic flows, when treating the flow as a whole. If lane data is required, additional information is needed. For instance, Coifman (2003) uses data from two loop detectors, combined with a vehicle re-identification algorithm.

5.3.3 Using spatial detectors

When density accuracy is a primary requirement, spatial detectors, such as cameras, are the optimal solution from the theoretical point of view. This is equivalent to making $t \rightarrow 0$ in the space-time domain $|A|$ in Figure 5.1. Images should be then post-processed, in order to recognise and count vehicles. At the present stage, this is rarely done in common practice, mainly because of the large amount of data and the intensive computation required for image post-processing (Klein et al., 2006; Treiber and Kesting, 2013). However, there are applications for research purposes (Treiterer and Myers, 1974; Hoogendoorn et al., 2003; Federal Highway Administration, 2005). The development of a camera system for bridge loading applications is described in Section E.4.

5.4 Traffic micro-simulation

5.4.1 The Intelligent Driver Model

The Intelligent Driver Model (IDM) has been presented in Section 2.2.1. The main equations are retained here for the reader's convenience:

$$\frac{dv(t)}{dt} = a \left[1 - \left(\frac{v(t)}{v_0} \right)^4 - \left(\frac{s^*(t)}{s(t)} \right)^2 \right] \quad (5.10)$$

$$s^*(t) = s_0 + Tv(t) + \frac{v(t)\Delta v(t)}{2\sqrt{ab}} \quad (5.11)$$

For this work, Equations (5.10) and (5.11) are discretised in 100 ms steps.

5.4.2 Congested traffic states

As seen in Section 2.2.2, flow-conserving inhomogeneities are a convenient way to generate congestion. Here, inhomogeneity is induced by increasing the safe time headway, T , downstream to T' .

An important parameter in determining the congested states is the bottleneck strength ΔQ , as defined in Section 2.2.2 by:

$$\Delta Q(T') = Q_{out}(T) - Q'_{out}(T') \quad (5.12)$$

The resulting congested states are listed again in Table 5.1 for the reader's convenience.

Table 5.1 - Traffic states definitions

Acronym	Explanation of traffic state
FT	Free traffic
MLC	Moving localized cluster
PLC	Pinned localized cluster
SGW	Stop and go waves
OCT	Oscillating congested traffic
HCT	Homogeneous congested traffic

5.4.3 Model and simulation parameters

For this study, the vehicle stream is taken as being homogenous. Each vehicle is given the same set of parameters, shown in Table 5.2. The parameters are taken from Treiber et al. (2000).

A single-lane 5000 m long road is used here. For the parameters chosen, the static capacity Q_{max} is 1743 veh/h, while the dynamic capacity Q_{out} is 1689 veh/h (Treiber et al., 2000).

The safe time headway is $T = 1.6$ s from 0 to 2700 m (see Table 5.2), then increases linearly to 3300 m where it reaches the value T' . Five different values of T' (1.9, 2.2, 2.8, 4 and 6.4 s, as in Section 2.3.2) with a high inflow $Q_{in} = 1680$ veh/h, are considered for the simulations, each of which is 60-minute long. These values are chosen in order to generate a wide range of congestion types.

Table 5.2 - Model parameters of the IDM.

Parameter	Value
Desired velocity, v_0	120 km/h
Safe time headway, T	1.6 s
Maximum acceleration, a	0.73 m/s ²
Comfortable deceleration, b	1.67 m/s ²
Minimum jam distance, s_0	2 m
Vehicle length, l	5 m

For the values of T' considered, the bottleneck strengths ΔQ are plotted in Figure 5.4 against the increase in safe time headway $\Delta T = T' - T$. Four different kinds of congestion are found: stop-and-go waves (SGW); oscillating congested traffic (OCT); a combined state with homogenous congested traffic near the inhomogeneity and oscillating congestion further upstream (HCT/OCT), and a full homogeneous congested traffic state.

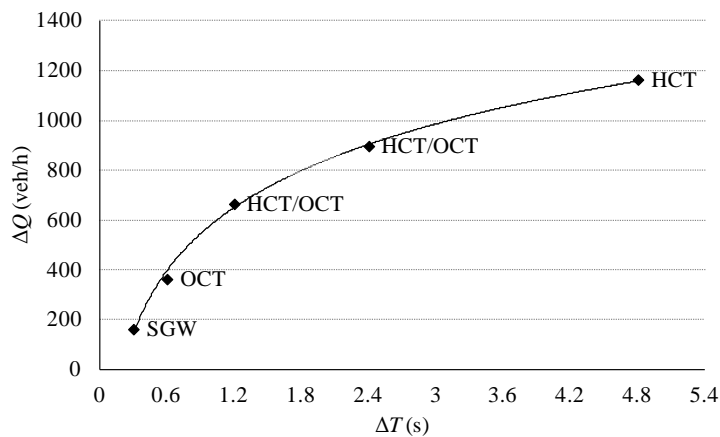


Figure 5.4 - Variation of bottleneck strength with safe time headway increase. Note that the bottleneck strength increases not linearly with the safe time headway.

The propagation wave speed in the SGW state is about -10 km/h, since the wavelength is about 1.2 km and its period is about 7 min. Typically, there is a bunch of 5 to 8 vehicles going

at a very low speed (below 15 km/h). Traffic is free between the waves with speeds higher than 70 km/h, unlike the OCT state, where speeds never exceed 50 km/h. Then, oscillations reduce and the congested speed is nearly constant, down to 4 km/h for the highest bottleneck strength, $\Delta Q = 1164$ veh/h. Such a state represents very heavy congestion, typically non-recurring and due to serious accidents (Schönhof and Helbing, 2007).

5.5 Assessment of density estimates

5.5.1 Estimation from the fundamental equation of traffic

A virtual point detector is placed at 2000 m. The detector returns flow, time and space mean speed, as well as time headways and individual speeds, i.e. it works like a double loop detector. Data is aggregated over 60 s and density is calculated according to Equation (5.1). In the following, this procedure will be referred to as a *macroscopic* means of estimation.

A virtual camera takes snapshots over 100, 200, 500 and 1000 m centred on the virtual detector and returns the actual density, where a vehicle is accounted for only if fully contained in the relevant road section. Note that the results coming from a point measurement do not refer to a specific length, since the underlying assumption is flow homogeneity. Such results are compared to the relevant snapshots, in order to understand the extent of the density accuracy that can be inferred from a point measurement.

Figure 5.5 shows an example of a SGW state. The actual density values over 100 and 1000 m length of road are displayed, as well as the point estimates. It can be seen that oscillations are averaged out for the longest stretch, while the point measurements are not able to fully catch the density peaks occurring over 100 m.

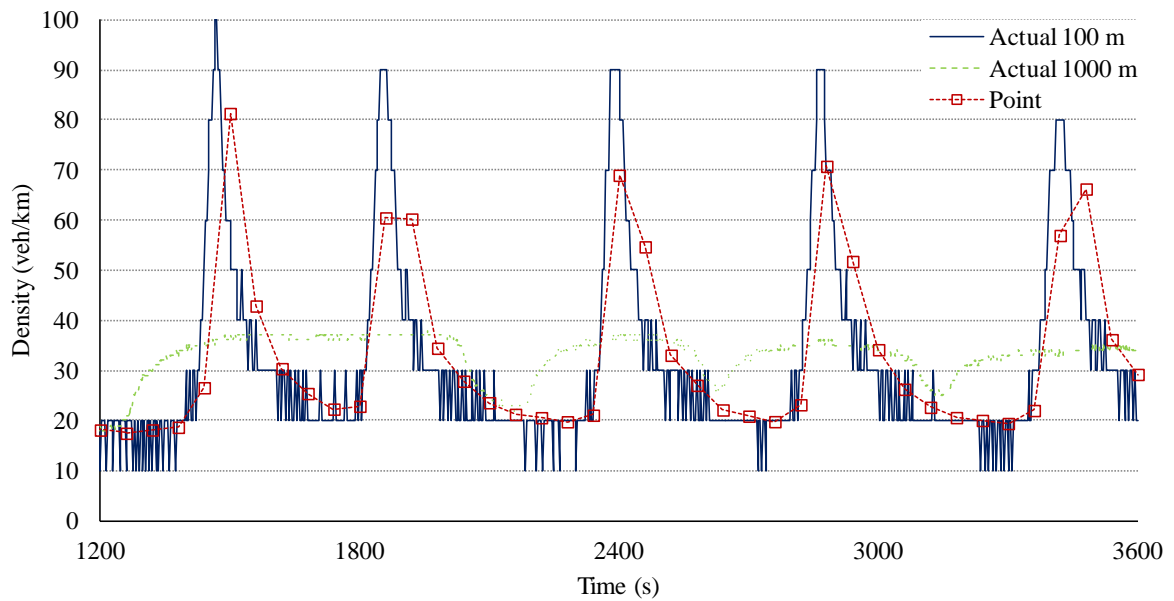


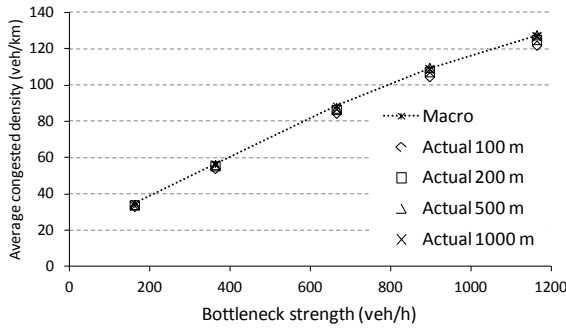
Figure 5.5 – Example of point-measured and actual density (SGW state).

Figure 5.6a shows the actual and estimated average densities over the 60 minute period of simulation. It can be seen that the single point detector slightly over-estimates the average congested density over any stretch of road up to 1000 m (by at most 5.1%), regardless of the congestion type. Congestion is considered after the first time the actual density exceeds 30 veh/km on the 100 m length.

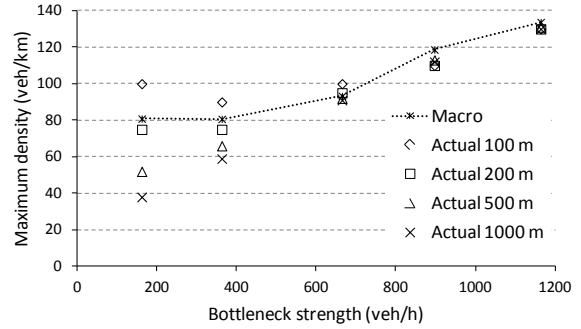
The analysis of the maximum values, however, show a different result (Figure 5.6b). The maxima can be accurately inferred only for the three highest bottleneck strengths, where traffic oscillations die out, with a relative error within $\pm 8\%$. For lighter bottleneck strengths, where oscillations are present, the point maxima are close to the 200 m values. The maximum density for the 100 m length is under-estimated, whereas it is significantly over-estimated for the 500 and 1000 m lengths (see also Figure 5.5). Note also that the maxima for the longer stretches of road are very close to the average values in Figure 5.6a.

The coefficient of variation ($\text{CoV} = \text{standard deviation} / \text{mean}$) of the actual and estimated densities is determined and shown in Figure 5.6c. The CoV is a measure of how much the density is oscillating during the measurement period. It can be seen from Figure 5.6c that the estimated density varies more than the actual one for longer lengths of road.

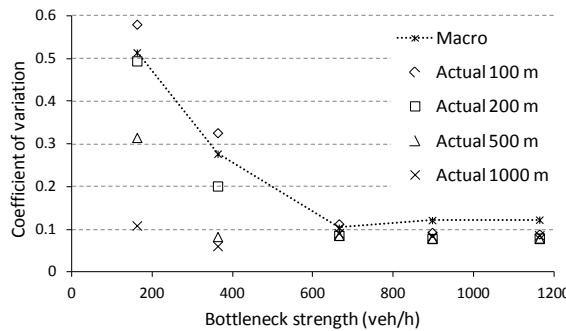
The *cross-correlation coefficient* is commonly used in statistics and offers a measure of how alike two time series are (van Etten, 2005). Two signals exactly the same have a cross-correlation coefficient of 1.0 at zero lag (i.e. *auto-correlation*). The cross-correlations of the estimated density time-series against the true density time-series are shown in Figure 5.6d. It is clear that the point estimate of density is close to the actual only for high bottleneck strengths.



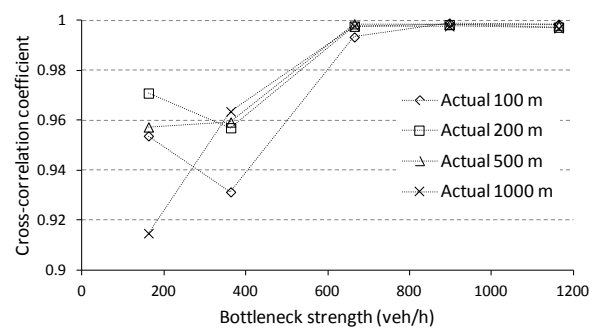
(a) Average density



(b) Maximum density



(c) Coefficient of variation



(d) Cross-correlation coefficient

Figure 5.6 – Actual and macro-estimated density estimate statistics from single-point measurements.

While average values are well estimated in all cases (a), only high bottleneck strengths are for the other statistics (b, c, d).

5.5.2 Micro-estimation

In the following a method named *micro-estimation* is proposed, since it is based on the estimation of individual space headways h_i from time headways $t_i - t_{i-1}$:

$$h_i = v_{i-1} \cdot (t_i - t_{i-1}) \quad (5.13)$$

For each vehicle i passing over the detector, the space headways between the current vehicle i and as many $i + j$ vehicles as fit on the relevant section of length L are found. The density estimate k_i at the time t_i comes from the count of vehicles from the most downstream vehicle, n_{i-d} , to the most upstream vehicle, n_{i+u} , estimated to be in the observed length L :

$$k_i(t_i) = \frac{\sum_{j=-d}^u n_{i+j}}{L} \quad (5.14)$$

The indices d and u are found by imposing the conditions:

$$\begin{aligned} \sum_{j=0}^d h_{i-j} &\leq \frac{L}{2} \\ \sum_{j=1}^u h_{i+j} &\leq \frac{L}{2} \end{aligned} \quad (5.15)$$

It requires unaggregated data from double loop detectors as input. It implicitly assumes that the leading vehicle $i - 1$ does not change its speed. Since the space headways h_i are kept constant over the observed length as they were computed when the vehicles crossed the detector, the vehicle clusters are moved across the road and local density variations are accounted for. This method can be also used for calculating individual gaps. A comparison between actual and estimated gaps is shown in OBrien et al. (2011).

Tables 5.3 and 5.4 summarize the results of both macro- and micro-estimation approaches. It can be seen that the micro-estimation regularly leads to better maximum estimates (see also Figure 5.7), at the cost of slightly under-estimated averages. Moreover, the improvement on the error in the cross-correlation coefficients suggests a better match with the actual values.

Table 5.3 - Relative error of macro- and micro-estimation from a single point measurement ($\Delta Q = 162$ veh/h).

Observed length (m)	Relative error (%)							
	100		200		500		1000	
Estimation	Macro	Micro	Macro	Micro	Macro	Micro	Macro	Micro
Average	5.1	-6.6	2.4	-8.5	1.6	-10.1	3.6	-10.2
Maximum	-19.1	-10.0	7.8	6.7	55.5	23.1	113	36.8
Coefficient of variation	-11.4	-5.5	4.0	1.3	63.2	35.3	372	222
Cross-correlation*	4.62	3.91	2.91	1.54	4.27	2.40	8.52	3.98

* Relative error defined as 1 (perfect cross-correlation) minus the actual cross-correlation expressed as percentage.

Table 5.4 - Relative error of macro- and micro-estimation from a single point measurement ($\Delta Q = 363$ veh/h).

Observed length (m)	Relative error (%)							
	100		200		500		1000	
Estimation	Macro	Micro	Macro	Micro	Macro	Micro	Macro	Micro
Average	4.8	-8.9	2.0	-8.9	0.8	-11.5	0.9	-14.9
Maximum	-10.2	0.0	7.8	6.7	22.5	-6.1	37.0	-13.6
Coefficient of variation	-15.0	23.2	37.7	59.9	234	149	355	69.9
Cross-correlation*	6.87	2.25	4.3	1.65	4.07	2.92	3.64	0.40

* Relative error defined as 1 (perfect cross-correlation) minus the actual cross-correlation expressed as percentage

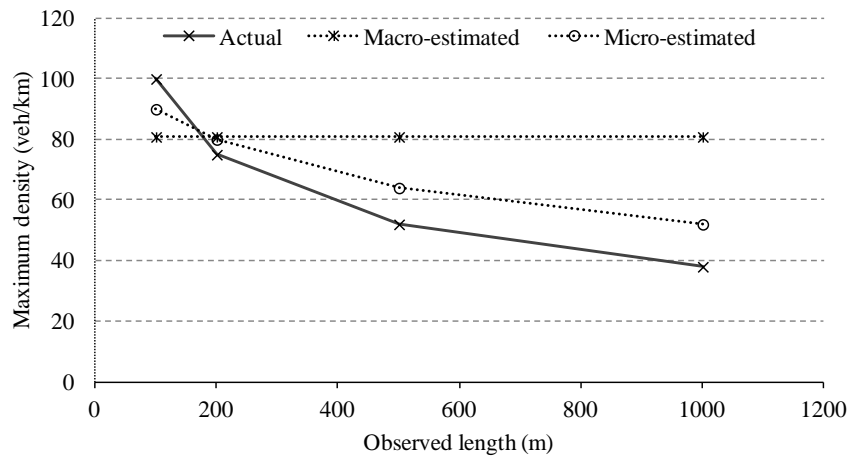


Figure 5.7 - Actual, macro- and micro-estimated maximum densities ($\Delta Q = 162$ veh/h). The macro-estimated maxima follow the actual density trend.

5.5.3 Using two point detectors

In this section, the combined use of two detectors spaced 100 and 500 m apart is examined, as this arrangement may achieve a better density estimate over 200 and 1000 m, respectively, for the critical lowest bottleneck strengths. The density is averaged between the two point measurements and then compared to the actual value. It can be seen from Tables 5.5 and 5.6, that there is an improvement in the maximum estimates, while the other statistics do not generally lose accuracy.

Table 5.5 - Relative errors (%) on 1- and 2-point macro-estimated density (200 m observed length).

Bottleneck strength (veh/h)	Relative error (%)			
	162		363	
Number of detectors	1	2	1	2
Average	2.4	2.5	0.5	0.9
Maximum	8.5	-5.7	7.2	-4.5
Coefficient of variation	3.8	-4.6	46.0	-3.8
Cross-correlation*	2.91	3.27	4.30	2.57

* Relative error defined as 1 (perfect cross-correlation) minus the actual cross-correlation expressed as percentage

Table 5.6 - Relative errors (%) on 1- and 2-point macro-estimated density (1000 m observed length).

Bottleneck strength (veh/h)	Relative error (%)			
	162		363	
Number of detectors	1	2	1	2
Average	3.6	0.9	-0.6	-0.2
Maximum	114	39.9	36.3	3.7
Coefficient of variation	371	165	382	116
Cross-correlation*	8.52	2.78	3.64	0.67

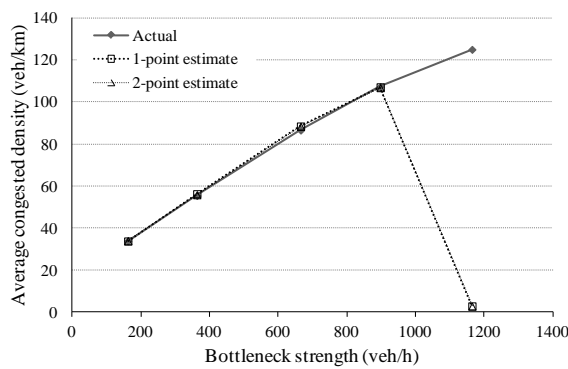
* Relative error defined as 1 (perfect cross-correlation) minus the actual cross-correlation expressed as percentage

5.5.4 Simulating real loop behaviour

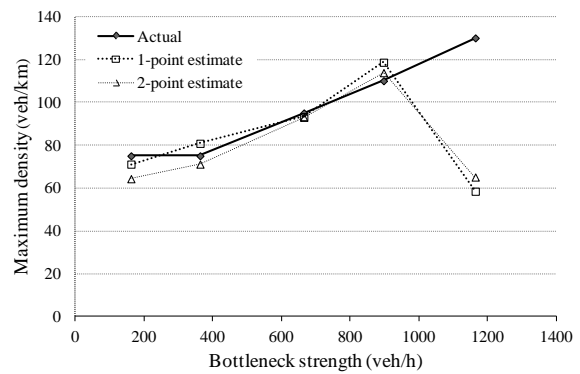
Actual loop detectors lose accuracy at very low speeds. In fact, loop detectors can be designed for detecting either the presence or the passage of vehicles. The speed threshold between the two modes can be taken as 5 km/h (Klein et al., 2006). Therefore, all the vehicle data with speed lower than 5 km/h is filtered out. The results are shown for the 200 and 1000 m observed length, both using a single point detector and two detectors. Note that WIM stations are not generally able to weigh vehicles accurately at low speeds. Data below a set speed

threshold are generally discarded and this threshold may be higher than that for loop detectors.

Figure 5.8 shows that filtering significantly affects both the maximum and the average values at the highest bottleneck strength, $\Delta Q = 1164$ veh/h. In fact, while for lower bottleneck strengths the number of vehicles crossing at very low speed is rather low, most data is filtered out during very heavy congestion, thus leading to a large under-estimation. Except for the strongest bottleneck, the errors in the average density are very low and the errors in maxima (Tables 5.7 and 5.8) remain roughly the same as for the unfiltered data.



(a) Average density



(b) Maximum density

Figure 5.8 – Actual and filtered estimates of density statistics for a 200 m observed length. Note that the filtering significantly affects only the strongest bottleneck strength.

Table 5.7 - Relative error of density from filtered measurement (200 m observed length).

Bottleneck strength (veh/h)	Relative error (%)									
	162		363		665		897		1164	
Number of detectors	1	2	1	2	1	2	1	2	1	2
Average	-0.3	0.1	1.6	0.7	2.2	2.1	-0.1	-0.5	-97.6	-97.7
Maximum	-5.2	-14.3	7.8	-5.2	-1.8	-2.2	7.9	3.4	-55.0	-49.9
Coefficient of variation	-3.0	-9.2	36.0	0.2	30.4	23.6	61.1	56.6	4924	5246
Cross-correlation*	3.37	2.87	4.16	2.47	0.25	0.13	0.2	0.19	80.5	80.5

* Relative error defined as $1 - (\text{perfect cross-correlation} - \text{actual cross-correlation})$ expressed as percentage.

Table 5.8 - Relative error of density from filtered measurement (1000 m observed length).

Bottleneck strength (veh/h)	Relative error (%)									
	162		363		665		897		1164	
Number of detectors	1	2	1	2	1	2	1	2	1	2
Average	0.9	0.1	0.5	-0.4	2.1	-0.3	-1.4	-2.4	-97.6	-99.1
Maximum	87.1	39.5	37.0	3.2	2.5	2.3	5.9	1.3	-55.0	-67.2
Coefficient of variation	340	162	349	122	14.3	23.0	49.0	37.8	4557	6239
Cross-correlation*	7.5	2.66	3.51	0.64	0.22	0.1	0.23	0.12	82.5	87.4

* Relative error defined as 1 (perfect cross-correlation) minus the actual cross-correlation expressed as percentage

5.6 Summary and conclusions

5.6.1 Summary

Traffic density is important for traffic applications and infrastructure management. Common practice makes use of the fundamental equation of traffic for estimating density from a point detector (usually a loop detector). A micro-simulation tool is used here to generate traffic with different congestion strengths. One or two loop detectors are used to infer density over four stretches of road spanning from 100 to 1000 m. The behaviour of real loop detectors which do not collect data at very low speed is also simulated.

5.6.2 Conclusions

Three different congestion ranges are found to be relevant for density accuracy. When congestion is light (bottleneck strength < 500 veh/h), average density values from single point measurements can be used up to 1000 m and the effect of the detector inaccuracy at low speeds is small. Maximum density values are best inferred at about 200 m; for shorter distances they are under-estimated, whereas for longer distances they are significantly over-estimated. A proposed approach helps to achieve better maximum estimates over a longer section. It requires unaggregated vehicle-by-vehicle data as input. However, if peak accuracy is important, it is advisable to place multiple detectors not further than 200 m apart or consider using cameras ‘looking’ over the stretch of road.

When congestion is heavy (bottleneck strength 500 – 1000 veh/h), traffic is not oscillating significantly and the effect of the detector inaccuracy at low speeds is modest. Then, both average and maximum values can be accurately inferred.

When congestion is extremely heavy (bottleneck strength > 1000 veh/h), traffic is not oscillating but the speeds are below the minimum working speed of the detector. It is not possible to obtain even acceptable average values. In these rare cases, it is advisable to resort to other detectors, such as cameras.

To conclude, it is apparent that it is easier to infer spatial information from point measurements when the bottleneck strength is high, but just as long as speeds do not fall under the minimum working speed of the point detector. In fact, as the bottleneck gets stronger, the implicit assumption of constant speed in the fundamental equation of traffic becomes more realistic.

5.6.3 Implications for bridge traffic loading applications

The contents of this paper have important implications for bridge loading applications, although no trucks are accounted for. The results are useful for quantifying the theoretical errors implied in using common traffic measurements during congestion. While the focus here is on density accuracy, it is important to note that accurate density estimates are an essential condition for accurate load calculations. If the total number of vehicles present on a stretch of road (i.e. a bridge) is incorrect, so will be the load. In particular, extreme loading congested scenarios, and therefore maximum values of density, are of interest. The estimation of these values is shown to be more problematic than the estimation of average values.

Heavy congestion (bottleneck strength > 500 veh/h) is the most critical condition for bridge loading applications, as shown in Chapter 2. The use of real congested traffic measurements is possible without significant errors, until the speed is not low enough to fall below the detector minimum working speed. However, this is quite a rare case, as it corresponds to a very slow speed, of the order of 5 km/h, with the current technology. Note that current weigh-in-motion systems generally have a higher threshold. On the other hand, progress in technology may result in a drop of both thresholds, with beneficial effects on estimation. If values below the detector minimum working speed are thought essential, it is advisable to resort to cameras or

other spatial detectors. Finally, in the extreme case of full stop conditions, the use of point detectors is problematic, as they can only detect moving vehicles.

Significant errors in the maximum density may arise in oscillatory traffic (bottleneck strength < 500 veh/h). However, this is not the most critical case for bridge loading, as shown in Chapter 2. Simulation results show that a span of 200 m gives the best match between the estimated and actual maximum density. Results are then under-estimated for shorter spans and over-estimated for longer ones.

It is apparent that if one wants an optimal result from the theoretical point of view considered here, spatial detectors have to be used. This has been taken into account in this research, as SIMBA has been updated to calculate the load effects from the exact vehicle positions, thus avoiding any error due to position estimates. Further details are reported in Appendix E and F.

Chapter 6

The effect of controlling heavy vehicle gaps on long-span bridge loading

Authors:

Colin C. Caprani

Eugene J. OBrien

Alessandro Lipari

Paper Status:

Ready for submission. Minor modifications are done in the text in order to minimise repetition and to fit into the context of the thesis.

Note to the Reader:

The work in this chapter is entirely the work of the author under the supervision of Prof OBrien and Dr Caprani.

6.1 Introduction

During congestion, heavy vehicles can get quite close to each other, thus giving potential critical loading events for a long-span bridge. If such a distance could be limited, there would be less need for restricting a bridge to trucks or posting a weight limit, as there will always be a maximum possible number of trucks on the bridge, even during congestion. Moreover, single over-loaded trucks do not generally produce a critical event for a long-span bridge.

The minimum distance should be adjusted in relation to the site-specific traffic features and to the safe load capacity of the bridge. The minimum distance can allow for other variables, such as future increase in truck weights, heavy traffic volumes, or even for bridge deterioration, as the structural capacity of the bridge will inevitably decrease in time.

Current regulations about gaps between vehicles are mainly concerned about safety requirements to prevent crashes. They are usually expressed in terms of safe time gap (for instance the 2- or the 3-second rule), which can be obviously adapted to any speed. However, for bridges it is important to keep the load apart and hence a *space* gap is of interest, rather than a time gap. Some European countries prescribe a minimum distance of 50 m for trucks (Austria and Germany), or for vehicles when following heavy vehicles (France) (Conference of European Directors of Roads, 2010). A European Union directive prescribes a minimum of 5 m to the front vehicle, in case of stop in tunnels (The European Parliament and the Council of the European Union, 2004). In the United States, no regulation exists about a minimum space gap, whereas in Australia heavy vehicle drivers must follow another HGV at a minimum of 60 m in single-lane roads (Roads and Maritime Services, 2011). However, at the moment it is still very difficult to enforce these limits.

In this chapter, we assume that different percentages of trucks respond to a warning whenever the gap to the front vehicle falls below a certain threshold, which is a safe distance for bridge loading. Such a device can operate in the area preceding a bridge. The device may receive a wireless signal from a transmitter located close to the bridge (*infrastructure-to-vehicle communication*), indicating to the driver the minimum gap value to respect. A sensor in the truck computes the distance between the front vehicle and the driver is warned if the gap is below the threshold. Violations of the limit may be recorded and fined. In the first implementation phase, it may be beneficial to promote the use of the gap control device

among truck operators by providing incentives, such as a higher weight allowance or toll discounts. Finally, progress in *Adaptive Cruise Control* (ACC) (Naranjo et al., 2003; Kesting et al., 2010) may also *prevent* truck drivers from getting too close to the front vehicle, by taking over the control of the truck in such controlled areas.

Here, it is shown how the implementation of the described system can beneficially reduce the load on a sample long-span bridge and study the implications on traffic congestion. The task is carried out by means of single-lane micro-simulation, which is a powerful tool to replicate and analyse congested scenarios, as seen in the previous chapters.

6.2 Micro-simulation

The *Intelligent Driver Model* (Treiber et al., 2000) is used in this chapter. The focus here is a preliminary assessment of the impact of a system that warns truck drivers when not keeping a set minimum distance to the front vehicle.

Single-lane micro-simulations are carried out considering a high inflow rate, representative of peak hour traffic. Truck percentage is set to 20%, which is typical of a busy highway. Different percentages of trucks are taken to respond to the gap control system, in order to simulate both the market penetration of the device and the compliance of truck drivers to the device instructions. Two different congestion types are generated and the total load is studied on a 200 m span. Note that such a single-lane approach may also represent the slow lane of a multi-lane roadway, when lane changes are restricted in the controlled area.

6.2.1 The Intelligent Driver Model

The Intelligent Driver Model has been introduced in Section 2.2.1. The main equations are repeated here for convenience:

$$\frac{dv(t)}{dt} = a \left[1 - \left(\frac{v(t)}{v_0} \right)^4 - \left(\frac{s^*(t)}{s(t)} \right)^2 \right] \quad (6.1)$$

$$s^*(t) = s_0 + Tv(t) + \frac{v(t)\Delta v(t)}{2\sqrt{ab}} \quad (6.2)$$

Equations (6.1) and (6.2) are discretised into 250 ms steps.

6.2.2 Congested Traffic States

As done in previous chapters, flow-conserving inhomogeneities are used to generate congestion. The inhomogeneity is generated by increasing the safe time headway T downstream to T' . An important parameter in determining the congested states outlined in Table 6.1 is the bottleneck strength ΔQ , whose definition is reported here:

$$\Delta Q(T') = Q_{\text{out}}(T) - Q'_{\text{out}}(T') \quad (6.3)$$

Table 6.1 - Definitions of various traffic states

Acronym	Explanation of traffic state
FT	Free traffic
MLC	Moving localized cluster
PLC	Pinned localized cluster
SGW	Stop and go waves
OCT	Oscillating congested traffic
HCT	Homogeneous congested traffic

6.2.3 Implementation of the control gap

The *control gap* g^* produces an additional inhomogeneity in the traffic stream, effectively decreasing the vehicular density in the controlled area. A modification in the motion Equation (6.1) must be introduced for trucks responding to the gap control device, so that truck drivers tend to keep a gap reasonably close to the control gap. Importantly, such a gap must be independent of the speed. Caprani (2012a) modifies the safe time headway T with partially satisfactory results, as the modification would not be independent on the speed. It is also apparent that a simple modification of the minimum jam distance s_0 cannot give the expected results, as it will equally increase the desired minimum gap s^* at any speed.

Several tests have been performed to find the most suitable modification to implement the control gap g^* . Three selected possible solutions are:

1. the term $s_0 + Tv(t)$ in Equation (6.2) is limited to be equal or greater than g^* ;
2. the desired minimum gap s^* in Equation (6.2) is limited to be equal or greater than g^* ;

3. a truck behaves as if its leader were closer than it actually is; in other words the current gap in Equation (6.1) is artificially reduced to $s(t) = s_{\text{actual}}(t) - (g^* - Tv(t))$, while the desired minimum gap s^* is kept unchanged.

In fact, the capping of the desired minimum gap s^* (solutions 1 and 2) may not suffice to ensure that the control gap g^* is respected, as the acceleration depends also on the speed ratio (Equation 6.1) and a vehicle tends to brake when the gap s is equal to the desired minimum gap s^* :

$$\frac{dv(t)}{dt} = -a \cdot \left(\frac{v(t)}{v_0} \right)^4 \quad (6.4)$$

In solution 3, the control gap is then diminished by the safe distance $Tv(t)$, which is roughly the distance a vehicle would keep anyway to its leader.

Figure 6.1 shows a truck going at 80 km/h while approaching another truck going at 50 km/h. The initial gap is 100 m and the control gap is 50 m. The IDM parameters are reported in Table 6.2. It can be seen that solutions 1 and 3 cause the truck to keep a gap slightly larger than the control gap, which is desirable, whereas solution 2 makes the truck speed oscillate around the control gap (Figure 6.1a). The deceleration rates of solutions 1 and 3 are also quite smooth and similar (Figure 6.1b).

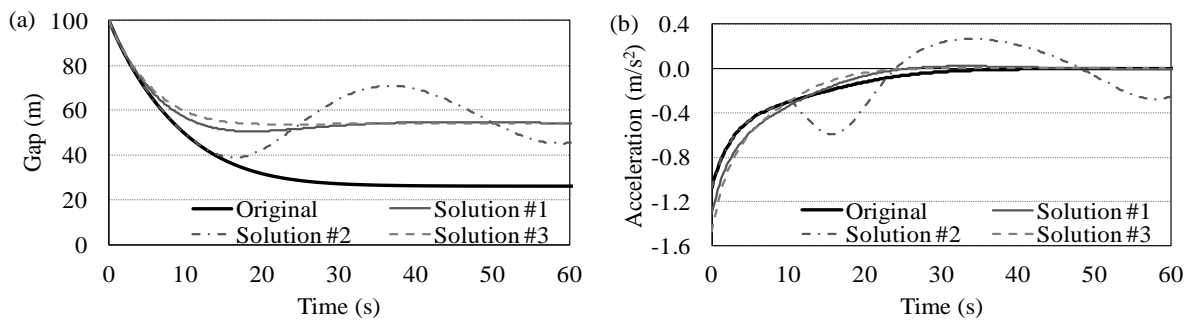


Figure 6.1 - Gap (a) and acceleration (b) of a truck approaching a slower vehicle.

However, when considering a truck going at 50 km/h and approaching an obstacle positioned at 100 m, the results are quite different. The original formulation would make the truck stop at a gap very close to the minimum jam distance s_0 . Figure 6.2a shows that solutions 1 and 2 make the truck overshoot at a gap much closer than it should, while solution 3 makes the

truck stop at a value reasonably close to the 50 m control gap. This of course comes at cost of a stronger deceleration rate (Figure 6.2b). Although the deceleration has a single simulation step peak of 9 m/s^2 , the average deceleration is about 2.5 m/s^2 , which is a reasonable deceleration rate considering that the truck is approaching a standstill object (Harwood et al., 2003). The other solutions have a soft deceleration rate ($1.5\text{-}1.6 \text{ m/s}^2$), which is in the order of the comfortable deceleration b (Table 6.2).

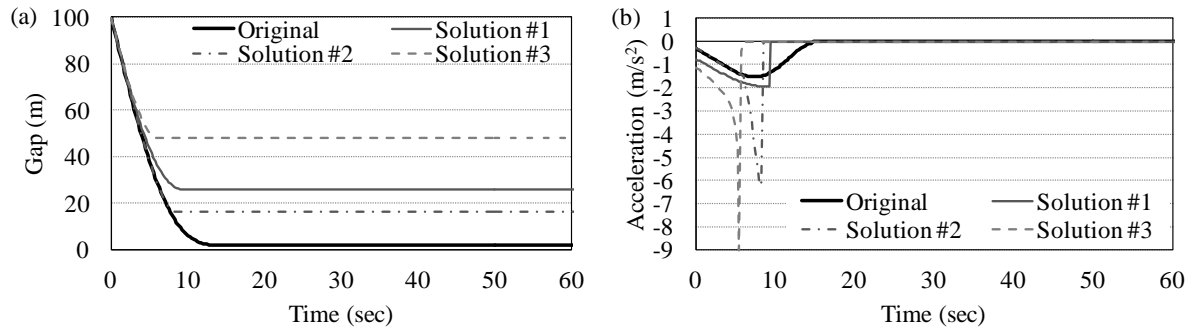


Figure 6.2 - Gap (a) and acceleration (b) of a truck approaching an obstacle.

In conclusion, solution 3 is adopted for modelling the trucks compliant with the gap control device, based upon the observed and required behaviours.

6.3 Model and Simulation Parameters

6.3.1 Traffic stream

The same set of parameters reported in Chapter 2 is used here. They are summarized in Table 6.2 for convenience. The GVW distribution is not meant to represent actual traffic, but it serves to show the benefits of the gap control device, which will be more beneficial for bridges carrying heavy traffic. The truck distribution should be adjusted to site-specific traffic features.

It is assumed that 0 (*base condition*), 10, 50 and 90% of the trucks comply with the gap control instructions and that the compliant trucks are randomly distributed in the traffic stream. The control gap is set to 20 and 50 m.

Table 6.2 – Model parameters.

Parameter	Car	Truck
Desired speed, v_0	120 km/h	80 km/h
Safe time headway, T	1.6 s	1.6 s
Maximum acceleration, a	0.73 m/s ²	0.73 m/s ²
Comfortable deceleration, b	1.67 m/s ²	1.67 m/s ²
Minimum jam distance, s_0	2 m	2 m
Vehicle length, l	4 m	12 m
Gross Vehicle Weight (GVW)	20 kN	432 kN ¹

¹ Normally distributed with CoV = 0.1.

6.3.2 Road geometry and bottleneck strength

A single-lane 5000 m long road is used in this work. The safe time headway is T from 0 to 2700 m (see Table 6.2), then increases gradually to the value T' at 3300 m. Two values of T' are considered: 2.2 and 4.0 s, which return a reduced dynamic capacity Q'_{out} equal to 1230 and 760 veh/h. The dynamic capacity Q_{out} is 1590 veh/h (Table 2.4) and is found by means of simulations, as the outflow coming out of a queue, as described in Section B.2. The inflow Q_{in} is set equal to the dynamic capacity, Q_{out} , then the bottleneck strengths ΔQ are 360 veh/h and 830 veh/h (Equation 6.3).

A 200 m long bridge is centred at 2000 m. The gap control area starts 1 km ahead of the bridge (at 900 m). The control gap is implemented gradually so that it simulates the adaptation of the truck driver behaviour to the control system, thus avoiding hard braking manoeuvres. Finally, it is assumed that the road is recurrently affected by one hour of congestion each day of a 250-working-day year, as assumed in Section 2.3.2. One year of congested traffic is simulated for each bottleneck strength, control gap and percentage of compliant trucks, for a total of 3500 hours of congestion generated and analysed.

6.4 Traffic results

6.4.1 Spatio-temporal congestion patterns

As introduced in Section 2.4.1, spatio-temporal speed plots are useful for visualizing congested patterns. The space mean speed is collected as one-minute harmonic averages at four virtual point detectors placed between 1000 and 2500 m. Figure 6.3a shows the OCT

state generated with $T' = 2.2$ s. The waves are clearly visible as peaks. Note that drivers do not fully recover speed between the waves, unlike the lighter SGW state. OCT is a quite frequent congested state (Treiber et al., 2000; Schönhof and Helbing, 2007). Figure 6.3b shows the HCT state resulting from $T' = 4.0$ s. Small oscillations are present upstream and fade away approaching the inhomogeneity. The average speed in the congested area is about 9 km/h. This is a rarer state that usually occurs after serious incidents (Schönhof and Helbing, 2007).

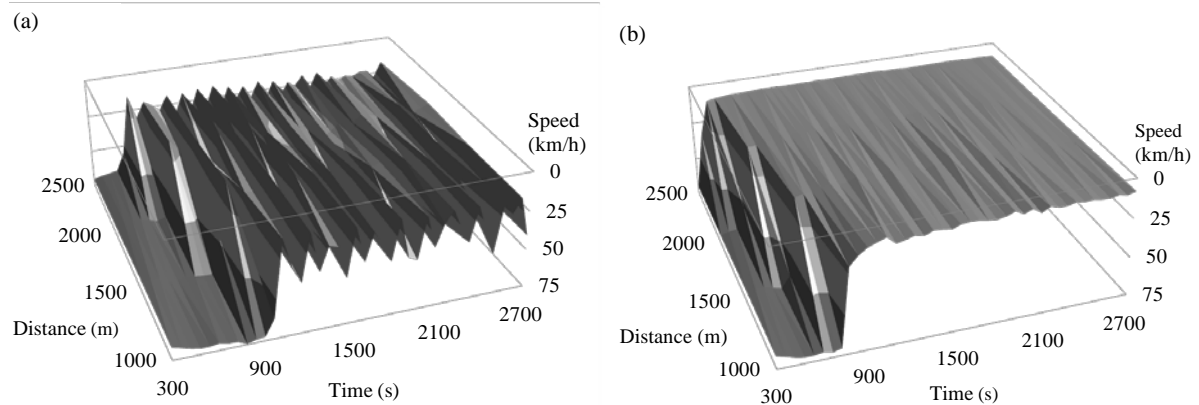


Figure 6.3 - Spatio-temporal speed plots of OCT (a) and HCT (b).

6.4.2 Implementation of the control gap

It is interesting to see how much the introduction of the control system disrupts the traffic further. Since trucks are now forced to keep a higher gap, the outflow from the controlled area will be reduced and the higher the gap, the smaller the outflow.

Figure 6.4a compares the flow computed at a virtual detector placed at 1500 m (that is, within the controlled area) to the flow at the same point when there are no compliant trucks (base conditions). It can be seen that the flow drops by less than 2%, indicating that the introduction of the system does not significantly increase the severity of congestion.

It is also interesting to consider the traffic oscillation properties and see how they change with the introduction of the control system (Figure 6.4b). A greater coefficient of variation of the speed indicates prominent oscillatory behaviour. Indeed the lightest bottleneck strength shows a high coefficient of variation, which is not significantly changed by the gap control system. On the other hand, the gap control enhances the speed oscillations at the strongest bottleneck,

actually changing the congestion type. This is expected because trucks need to slow down harder to reach the control gap, as discussed earlier, effectively generating shockwaves.

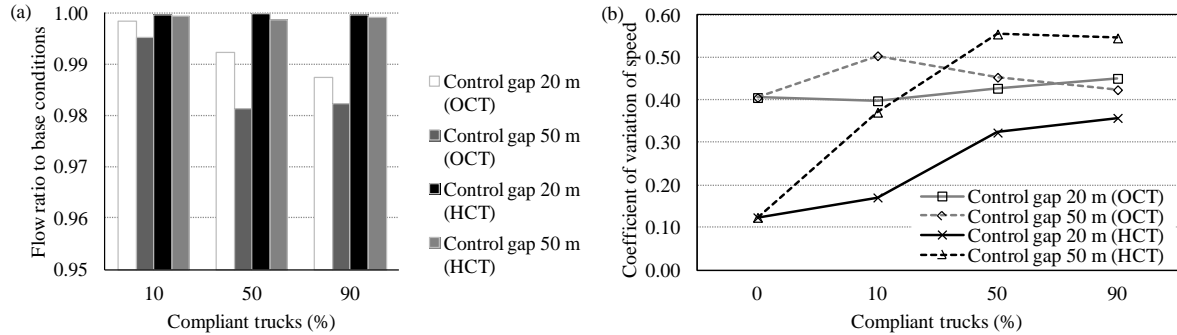


Figure 6.4 - Flow (a) and average coefficient of variation of speed (b) in the congested area.

6.5 Load results

6.5.1 Introduction

In this section, the total load on a 200 m bridge is computed. The maximum total load for each one-hour congestion event, which occurs every working day, is captured. The hourly/daily maximum values of the total load are extrapolated to determine 5-year characteristic values. Note that 5 years is the representative period of time for bridge assessment in the United States (AASHTO, 2011; Moses, 2001).

As introduced in Section 2.5.1, the Generalised Extreme Value (GEV) distribution is fitted to the simulated hourly/daily maximum total loads:

$$F(z) = \exp \left\{ - \left[1 + \xi \left(\frac{z - \mu}{\sigma} \right) \right]^{\frac{1}{\xi}} \right\} \quad (6.5)$$

The GEV parameters are inferred through maximum likelihood estimation. The target probability of non-exceedance for the maximum-per-day data is $P(z^*) = 1 - 1/1250 = 0.9992$ and its y-axis value on the probability paper is 7.13.

6.5.2 Results

The probability paper plot of the base condition (no trucks compliant) is shown in Figure 6.5, as well as the 5-year characteristic daily maximum values z^* . It can be seen that the two congestion types are well separate from each other, with the stronger congestion returning greater total load. The distribution for the combination of the two congestions is also plotted and it is addressed in the next section.

Table 6.3 indicates that, except for one single case of compliance to the Gumbel distribution ($\zeta = 0$), the curves slightly tend upwards, suggesting compliance with the Weibull distribution ($\zeta < 0$).

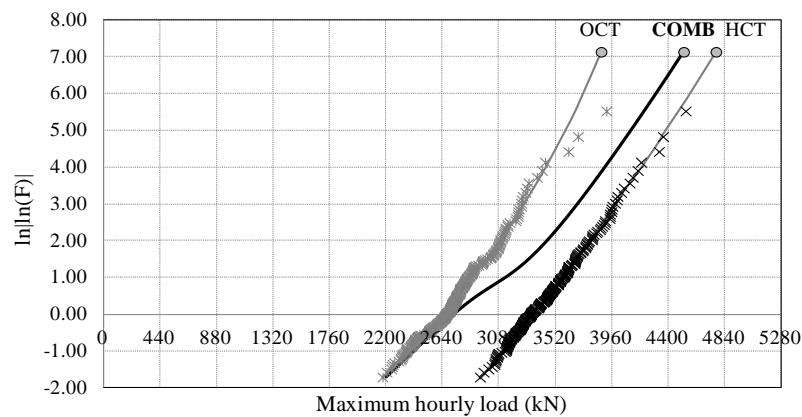


Figure 6.5 - Probability paper plot of base conditions (no compliant trucks); each vertical gridline approximately represents the weight of one average truck.

Figure 6.6 shows the effect of the gap control on the 5-year total load for the two bottleneck strengths considered, indicated as ratio to the total load in base conditions. It can be seen that the case of 10% compliant trucks does not return a significant reduction in the lighter bottleneck. Reductions become higher at the stronger bottleneck; that is, when total load is greater and therefore a reduction becomes more beneficial. It can be also noted that at the lower bottleneck strength the extrapolated load with the 50 m control gap is higher than the one with control gap 20 m. This is not due to an actual higher mean of the load, but instead to a higher curvature ζ of the 20 m extrapolation curve (see Table 6.3). When the percentage of compliant trucks increases to 50%, reductions are more interesting, as the reductions in total load lie between 26 and 36%. When most trucks are compliant, reductions are rather large, as they go up to 48%, and the actual control gap imposed plays a bigger role. It must be noted

that such reductions are attained with exactly the same traffic; that is, without posing any weight restriction to trucks.

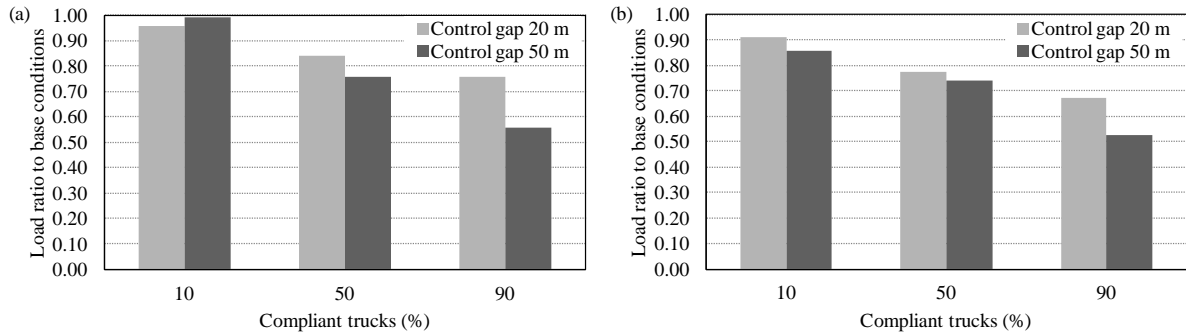


Figure 6.6 - Ratio of the 5-year load to the base conditions for OCT (a) and HCT (b).

Table 6.3 - Parameters and extrapolated values of the GEV distribution.

Compliant trucks (control gap)	OCT				HCT			
	μ	σ	ζ	z^*	μ	σ	ζ	z^*
0%	2644	247.1	-0.106	3880	3344	226.5	-0.035	4774
10% (50 m)	2490	226.4	-0.051	3845	3178	227.6	-0.181	4089
50% (50 m)	1828	216.2	-0.097	2940	2406	210.3	-0.086	3529
90% (50 m)	1461	97.7	0.000	2158	1760	144.5	-0.096	2506
10% (20 m)	2582	236.3	-0.122	3708	3244	230.7	-0.120	4350
50% (20 m)	2294	199.3	-0.118	3255	2831	193.8	-0.144	3696
90% (20 m)	2022	179.0	-0.099	2939	2334	126.5	-0.004	3222

6.5.3 Combination of congestions

Real world observations have shown that many types of congestion can occur. Intuitively, light forms of congestion are more frequent than strong ones. In line with data reported in Schönhof and Helbing (2007), we assume that the OCT congestion events (or lighter congestions) occur on 75% of the working days in one year, whereas the heavy HCT occurs on the remaining 25% of the working days.

It is then necessary to statistically combine the two different congestion types, either of which can occur with the assigned probabilities. This is done by applying the law of total probability, as presented in Section 2.6.2. The probability P that the load does not exceed z is:

$$P(z) = \sum_j F_j(z) \cdot f_j = F_{OCT}(z) \cdot f_{OCT} + F_{HCT}(z) \cdot f_{HCT} \quad (6.6)$$

where F_j is the cumulative distribution function for the maximum daily load for the j th congestion type (either OCT or HCT, Equation 6.5) and f_j is the assigned probability of occurrence for that type (either 0.75 or 0.25). An example of the combined distribution function $P(z)$ is shown in the probability paper plot of Figure 6.5.

Figure 6.7 shows the 5-year characteristic values, as ratio to the base condition. The reduction lies in between the two congested cases, but slightly closer to the heavier (although rarer) HCT state.

A small percentage of compliant trucks reduces the total load by approximately 10%, which may be desirable in a first implementation phase of the system. When half of the trucks are compliant, reductions get to about 25%. Finally, the control gap value starts making a large difference only when most trucks are compliant.

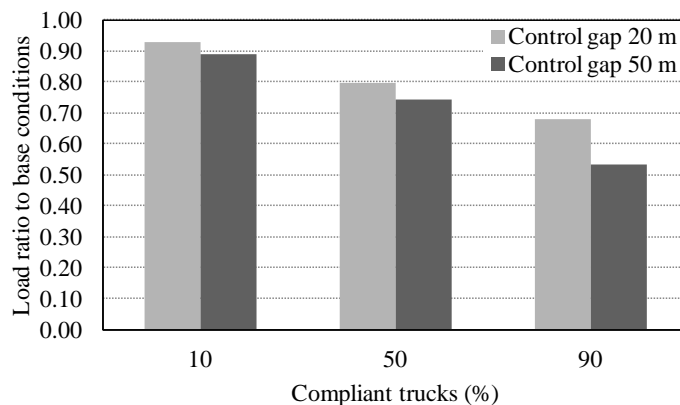


Figure 6.7 - Comparison of characteristic total load to the base conditions.

6.6 Conclusions

This chapter uses single-lane micro-simulation to investigate the effects on bridge loading of a gap control device which limits the gap between a truck and its leader during congested conditions. In fact, during congestion heavy vehicles can get very close to each other, thus giving potentially critical loading events for long-span bridges.

Results show that when only 10% trucks respond appropriately to the device, it is possible to attain a 10% reduction in the total load on a 200 m span. If 90% of the trucks respond, this

reduction can be as high as 47%. On the other hand, it is beneficially found that the introduction of the system does not significantly increase the traffic disruption.

It must be emphasised that this system does not require any weight restriction to the traffic, unlike the current practice. The control gap value should be adjusted to the site-specific traffic features and to the load that the bridge is able to carry safely, thus accounting for future increase of truck weights or heavy traffic volumes, or even deterioration of the bridge.

Chapter 7

Conclusions

This thesis investigates the traffic loading on long-span bridges by means of traffic micro-simulation, which models the motion of individual vehicles. Traffic loading on long-span bridges is governed by congested traffic. Collection and analysis of congested traffic data is problematic, and this is reflected in the fact that most previous research considers simplified traffic models, typically a queue of vehicles at minimum bumper-to-bumper distances. Thus, they neglect other observed forms of congestions. They also assume conservative frequencies of occurrence of congestion.

A broad framework including different congestion patterns as well as the actual frequencies of congestion occurrence is thus lacking. In this research, site-specific traffic information can be introduced in a methodology to compute a more accurate load, which is useful to support more efficient maintenance planning on existing bridges.

Traffic micro-simulation is a suitable tool to simulate different congestion patterns and analyse their effects on bridge loading. The car-following *Intelligent Driver Model* is used throughout this thesis. Such a model has been found able to reproduce observed congested patterns on several motorways by simulating a traffic stream made up of identical vehicles. However, trucks are the largest source of load on bridges and are then introduced. The IDM is combined with the lane-changing model MOBIL. Both models are implemented in an in-house program, which simulates traffic on a stretch of roadway. As a first, MOBIL is calibrated against lane change rates available in the literature for similar layouts.

The load resulting from the simulated congested events has been statistically analysed to find the characteristic traffic loading corresponding to given *return periods*.

The research presented in this thesis supported the following conclusions:

- the queue of vehicles at a standstill, widely used in previous research, is not always the most critical congested state for long-span bridge loading (Chapter 2). In fact, also slow-moving traffic can be critical for relatively short spans. This is due to the fact that full stop queues involve only one realisation of vehicles per congestion event, which actually reduces the probability of finding an extreme loading scenario. Moreover, it has been taken into account that lighter forms of congestions, such as *stop-and-go waves*, are more frequent than heavy congestion. A methodology for computing the characteristic load from a combination of congestion states has also been proposed.
- the load does not significantly depend on the inflow, as long as congestion is triggered, implying that critical loading events may occur also out of rush hours (Chapter 3). The car-following model has been extended with the lane-changing model MOBIL, thus allowing the consideration of the changes in the car-truck mix due to the overtaking manoeuvres and the subsequent observed formation of truck-only platoons. Finally, the effects of the distribution of trucks between lanes and the influence of cars have been also analysed and quantified.
- flows with high truck percentage, typically occurring at night-time in combination with low flows, largely affect the characteristic load, even though congestion in such conditions is quite rare. In comparison, other traffic features, such as total and truck daily flow and hourly flow distributions do not contribute as much. For sites with low traffic demand, congestion is caused by unpredictable events, such as incidents. The inclusion of site-specific traffic data, such as incident patterns and hourly flow distributions, has been considered in a new methodology to compute the characteristic load for road bridges with no excessive traffic demand. The methodology has been applied to traffic data available from the literature.
- traffic data collected from point detectors show that estimates of maximum traffic density, necessary to identify critical loading events, can be significantly different from the actual density values (Chapter 5). The number of vehicles on a stretch of road

(*density*) is in fact estimated from such point measurements. The density estimates from point-detectors are usually reliable when traffic is free, but they may be not during congestion.

- an application of micro-simulation to bridge loading control indicates that significant reductions in bridge loading can be attained with a system that warns truck drivers when the gap to the front vehicle falls below a certain threshold (Chapter 6). This system does not pose any weight restriction to the heavy vehicles and disrupts the traffic only marginally.

Appendix A

A comparative study of a bridge traffic load effect using micro-simulation and Eurocode load models

Authors:

Alessandro Lipari

Colin C. Caprani

Eugene J. OBrien

Paper Status:

Paper presented at the *6th International Conference on Bridge Maintenance, Safety and Management* (Stresa, 8-12 July 2012). Minor modifications are done in the text in order to minimise repetition and to fit into the context of the thesis.

Note to the Reader:

The work in this chapter is entirely the work of the author under the supervision of Prof OBrien and Dr Caprani.

A.1 Introduction

Since April 2010, the Eurocodes are the legal standards for structural design throughout the European Union. Eurocode 1 - Part 2 (European Committee for Standardization, 2003) deals with bridge loading. Its provisions apply only to the design of new bridges with spans up to 200 m. No provisions are made for longer span, or regarding the traffic loading for bridge safety assessment; this is still the responsibility of the relevant authority.

For longer spans in ≤ 200 m range, Eurocode 1 was calibrated assuming that congested conditions govern (Flint and Jacob, 1996; Prat, 2001). Small axle-to-axle distances were assumed in truck-only scenarios (Prat, 2001).

The single-lane micro-simulation approach described in Chapter 2 is used to generate traffic congestion. However, in this appendix, truck weights are not based on an assumed distribution, as done in Chapter 2, but come from data collected from a weigh-in-motion station in Poland.

The characteristic load effects on three sample bridges are calculated from traffic micro-simulations of 1000 hours of congestion, deemed to represent 1 year of traffic (250 working days and 4 congested hours per day). The results are then extrapolated to 75-year (for bridge assessment) and 1000-year return periods (for new bridge design, to compare with Eurocode 1).

A.2 The Eurocode load model

The Eurocode load models are based on one-week traffic data collected on the A6 motorway near Auxerre (France), deemed to be representative of European traffic (Prat, 2001). The Load Model 1 for general and local verifications of bridges up to 200 m consists of:

- a characteristic uniformly distributed load (UDL) q_{ik} ;
- a characteristic tandem system (TS) load, where the two axles are spaced 1.20 m apart, each with load Q_{ik} (Figure A.1).

Their values depend on the notional lane number i . The notional lane is 3 m wide. Therefore, there are often more loaded lanes than actual driving lanes.

For the first lane $i = 1$, the values are $q_{1k} = 9 \text{ kN/m}^2$ and $Q_{1k} = 300 \text{ kN}$. For other lanes, the characteristic values reduce, reaching a minimum of $q_{ik} = 2.5 \text{ kN/m}^2$ and $Q_{ik} = 0 \text{ kN}$ in the fourth and subsequent lanes (Table A.1). The characteristic values correspond approximately to a 1000-year return period (5% probability of exceedance in 50 years).

Adjustment factors, α_{Qi} and α_{qi} , are decided at national or network level and depend on the traffic features, if such information is known. Their default values are unity. The methodology implemented here may be used to quantify the adjustment factors for a given bridge or group of bridges.

For shorter spans, the Eurocode load model includes an allowance for dynamic amplification. However, since congestion governs for spans in excess of about 50 m (Flint and Jacob, 1996), no dynamic amplification has been allowed for (Bruls et al., 1996b; Prat, 2001).

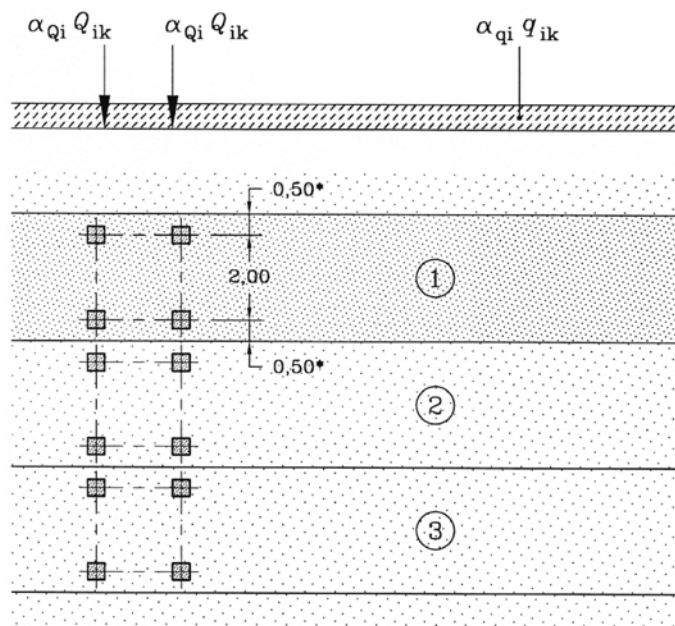


Figure A.1 - Eurocode load model 1

Table A.1 - Characteristic load values (adapted from Eurocode 1, 2003).

TS = Tandem System; UDL = Uniformly Distributed Load.

Lane number	TS Q_{ik} (kN)	UDL q_{ik} (kN/m ²)
1	300	9
2	200	2.5
3	100	2.5
4 or more	0	2.5

A.3 Model and simulation parameters

A.3.1 Traffic stream

For this study, the input vehicle stream is made up of traffic recorded over 91 days on the transcontinental A4/E40 near Wroclaw (Poland), provided courtesy of IBDIM (Warsaw) within the FP7 ASSET project. The original flow is quite low (Caprani et al., 2012a) and it is manipulated in order to increase the inflow Q_{in} up to 1500 veh/h, while keeping the original truck and car proportions.

The inflow rises from 0 up to Q_{in} in the first 30 minutes, then it is kept constant for the next two hours. After that, there is no inflow for the next 4 hours, in order to allow the discharge of the traffic queue (Figure A.2). It is assumed that such a congestion event occurs once per working day. In order to obtain 1 year of traffic, 250 congestion events are simulated under the assumption of 250 working days per year.

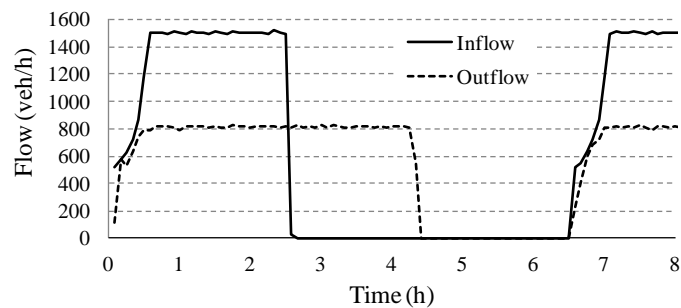


Figure A.2 - Example of simulated inflow and outflow from congestion (aggregation time 5 min).

As commonly assumed in this thesis, the traffic stream is classified into two vehicle classes: cars and trucks. Here, a car is defined as a vehicle weighing less than 3.5 tonnes. All the other vehicles are classified as trucks. A total of 842 500 vehicles are injected; 21.1% of which are, by this definition, trucks. Only 24% of the trucks have four or more axles. The histogram of truck gross vehicle weights is shown in Figure A.3. There is a high proportion of light trucks weighing less than 50 kN. However, magnification of the overloaded trucks (over 440 kN) shows that there are trucks weighing up to 737 kN. Note that this weight distribution is on average much lighter than the one assumed in Section 2.3.1.

The *Intelligent Driver Model* (IDM) is used to simulate traffic congestions (Section 2.2.1). The IDM parameters are taken from Treiber et al. (2000), where trucks are assigned a smaller desired speed than cars, reflecting their lower speed limit. The parameters are shown in Table A.2 and are the same used in Chapters 2.

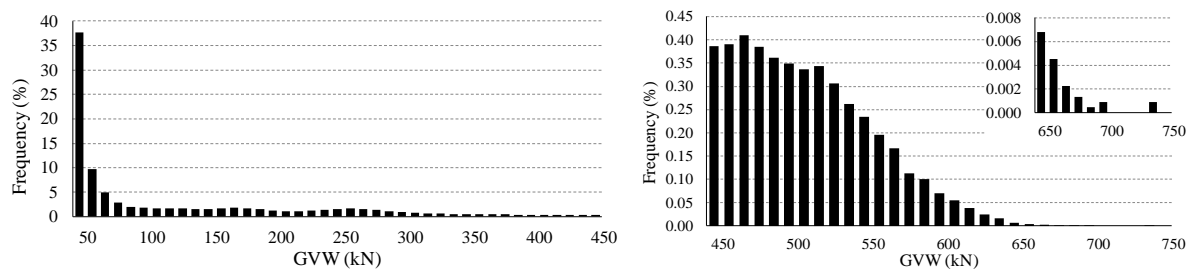


Figure A.3 - Truck GVW histogram: GVW < 450 kN (left) and GVW > 440 kN (right).

Table A.2 - Model parameters of IDM.

	Cars	Trucks
Desired velocity, v_0	120 km/h	80 km/h
Safe time headway, T	1.6 s	1.6 s
Maximum acceleration, a	0.73 m/s ²	0.73 m/s ²
Comfortable deceleration, b	1.67 m/s ²	1.67 m/s ²
Minimum jam distance, s_0	2 m	2 m

A.3.2 Road capacity estimation

It is not straightforward to calculate the static and dynamic traffic flow capacities Q_{\max} and Q_{out} of a road for real traffic (Treiber et al., 2000; Treiber and Kesting, 2012). Treiber et al.

(2000) calculate the dynamic capacity Q_{out} for single-lane simulations with the car parameter set shown in Table A.2 and a vehicle length of 5 m. However, the truck presence decreases the road capacity. In order to compute the dynamic capacity for the traffic with 21.1% of trucks, $Q_{out,21.1\%}$, a simplified approach is used here. It is assumed that the introduction of 21.1% trucks reduces the dynamic capacity $Q_{out,0\%}$ by the same proportion in which the static capacity Q_{max} is reduced:

$$\frac{Q_{out,21.1\%}}{Q_{out,0\%}} = \frac{Q_{max,21.1\%}}{Q_{max,0\%}} \quad (\text{A.1})$$

In fact, the static capacities Q_{max} can be computed or estimated analytically, while there is no analytical expression for the dynamic capacities Q_{out} , as described in Appendix B. The static capacity $Q_{max,0\%}$ for identical vehicles can be computed analytically, by imposing equilibrium traffic and maximizing the flow. The equilibrium gap s_e for a particular speed v is:

$$s_e(v) = (s_0 + vT) \cdot \left[1 - \left(\frac{v}{v_0} \right)^4 \right]^{\frac{1}{2}} \quad (\text{A.2})$$

Then, the equilibrium flow Q_e can be found using the fundamental equation of traffic, which links flow Q and density k by means of the speed v , and the so-called “*micro-macro link*”, which links density k and gaps s (Treiber et al., 2000):

$$Q_e(v) = k(v) \cdot v = \frac{v}{s_e(v) + l} \quad (\text{A.3})$$

where l is the length of the vehicles. The equilibrium flow Q_e can be then numerically maximised to find the static capacity. Doing so, the static capacity $Q_{max,0\%}$ for identical vehicles with the car parameters shown in Table A.2 and assuming 5 m length is 1743 veh/h. The dynamic capacity for the same parameters set is reported in Treiber et al. (2000) and is $Q_{out,0\%} = 1689$ veh/h.

The capacity $Q_{max,21.1\%}$ for mixed traffic can be estimated with a similar procedure, by considering an average length and the slower truck desired speed, as detailed in Section B.2.6.

The introduction of 21.1% of longer vehicles assumed to be 12 m long, decreases $Q_{\max,21.1\%}$ to 1680 veh/h (-3.6%). Finally, the dynamic capacity is scaled by the same factor (Equation A.1), thus obtaining $Q_{\text{out},21.1\%} = 1628$ veh/h.

A.3.3 Road geometry and bottleneck strength

A single-lane 5000 m long road is considered. The safe time headway is T , from 0 to 3400 m (see Table A.2), then increases linearly until it reaches the value $T' = 6.4$ s at 4000 m. As illustrated in Figure A.2, this procedure creates about 4 hours of congestion. The average outflow from congestion Q'_{out} is 798 veh/h, then the bottleneck strength $\Delta Q = Q_{\text{out}} - Q'_{\text{out}} = 830$ veh/h.

This bottleneck strength value can be seen as being equivalent to the injection of an on-ramp flow equal to ΔQ into the main traffic, which is considered here as a recurrent heavy congestion scenario. A lower bottleneck strength value is likely to return smaller load effects, as seen in Section 2.5, whereas greater values are likely to be too strong to realistically happen every working day (see also Figure 2.9), as they usually come as a consequence of a serious accident (Schönhof and Helbing, 2007).

A.3.4 Congestion pattern

The spatio-temporal speed plot of the congestion state is shown in Figure A.4. A virtual detector is placed every 500 m and aggregates the individual speeds over 1 min. The resulting congested pattern is a combination of Homogeneous Congested Traffic (Table 2.2) near the inhomogeneity and Oscillating Congested Traffic further upstream. The average speed around the HCT area is 7.5 km/h.

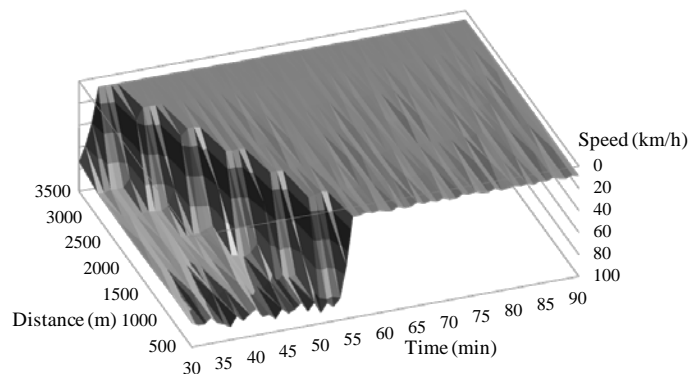


Figure A.4 - Spatio-temporal speed plot.

A.3.5 Sample bridges

Three simply-supported continuous beams are considered:

- a 50-m long single-span;
- a 100-m long bridge made up of two 50 m spans;
- a 200-m long bridge made up of three spans, respectively 58, 84 and 58 m long.

The load effects considered are sagging moment in the single-span (Load effect 1), and hogging moments at the central support for the multi-span bridges (Load effects 2 and 3), as illustrated in Figure A.5-7. The bridges are centred at 3000 m on the road, in the area preceding the inhomogeneity, and are affected by the HCT state.

A.4 Eurocode-based design

The Eurocode load model 1 is placed in the worst position for the relevant load effect, according to the influence line theory. It is assumed that the bridge is as wide as the notional lane (3 m), then the UDL applied is 27 kN/m.

The shape of the influence lines and the location of the imposed traffic loading are depicted in Figure A.5-8. The characteristic design values are shown in Table A.3. Notably, load effect 3 (200 m long bridge) is not included among the influence lines for the Eurocode calibration (Prat, 2001).

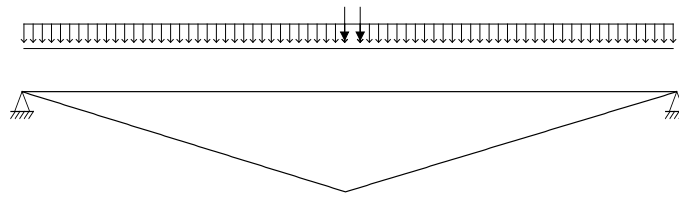


Figure A.5 - Influence line and load position for mid-span bending moment (Load effect 1 – 50 m bridge).

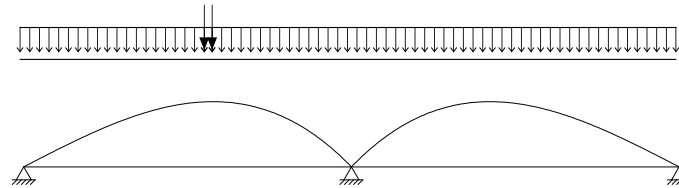


Figure A.6 - Influence line and load position for hogging moment at central support (Load effect 2 – 100 m bridge).

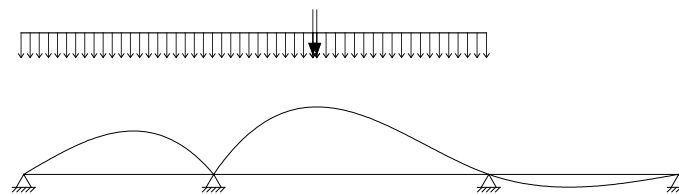


Figure A.7 - Influence line and load position for hogging moment at central support (Load effect 3 – 200 m bridge).

Table A.3 - Eurocode-based design values.

Bridge	Spans (m)	Load effect	Characteristic value (kNm)
50 m	50	1 Sagging moment	15 758
100 m	50 + 50	2 Hogging moment	11 322
200 m	58 + 84 + 58	3 Hogging moment	20 616

A.5 Microsimulation-based design

A.5.1 Introduction

In order to compute the 1000-year return period required in the Eurocode 1 (2003) and the 75-year return period typical for bridge assessment, it is necessary to extrapolate the generated traffic data. The maximum load effect per each congestion event (or day) is captured. Table A.4 gives some basic statistical results for the maximum-per-day load effects.

Table A.4 - Statistics from the simulation (values in kNm).

Bridge	Mean	Standard deviation	Max
50 m	7134	784	9451
100 m	5258	677	7370
200 m	8369	1131	11 606

A.5.2 Estimation

After filtering some outlying low values, the daily maximum data is fitted using the Generalized Extreme Value (GEV) distribution (Equation 2.5), whose Probability Density Function (PDF) is:

$$f(z; \theta) = F(z; \theta) \cdot \sigma^{-1} \left\{ 1 - \xi \left(\frac{z - \mu}{\sigma} \right) \right\}^{\frac{1}{\xi} - 1} \quad (\text{A.4})$$

where θ is the parameter set (ξ, μ, σ) . Maximum likelihood is used to estimate the parameters of the GEV distribution. The parameter set θ that is most likely to yield the n observed data points, y_i , is determined by maximizing the likelihood function:

$$L_y(\theta; y) = \prod_{i=1}^n f(y_i, \theta) \quad (\text{A.5})$$

Maximization of the log-likelihood function is equivalent, since the logarithm is a monotonic function. Hence, maximization is carried out using:

$$\log[L(\theta; y)] = \sum_{i=1}^n \log[f(y_i; \theta)] = -n \log \sigma - \left(1 - \frac{1}{\xi}\right) \cdot \sum_{i=1}^n \log z_i - \sum_{i=1}^n z_i^{1/\xi} \quad (\text{A.6})$$

where:

$$z_i = 1 - \xi \left(\frac{y_i - \mu}{\sigma} \right) \quad (\text{A.7})$$

See Coles (2001) for further details on the estimation procedure used.

A.5.3 Statistical extrapolation

The target probabilities P of the load effect values z_{1000} and z_{75} corresponding to 1000-year return period (250 000 working days) and 75-year return period (18 750 working days) are:

$$P(z_{1000}) = 1 - \frac{1}{T(z_{1000})} = 0.999996 \quad (\text{A.8})$$

$$P(z_{75}) = 1 - \frac{1}{T(z_{75})} = 0.999947 \quad (\text{A.9})$$

The corresponding Standard Extremal Variates for use with Gumbel probability papers (Section 2.5.1) are:

$$SEV_{1000} = -\log[-\log(0.999996)] = 12.43 \quad (\text{A.10})$$

$$SEV_{75} = -\log[-\log(0.999947)] = 9.85 \quad (\text{A.11})$$

With the parameters of the distributions estimated, the extrapolated load effects are determined using Equations (A.8) and (A.9) and the inverse of Equation (2.5). The results are given in Table A.5 along with the distribution parameter estimates. An example extrapolation on Gumbel probability paper is given in Figure A.8.

Table A.5 - Parameters of the GEV distributions and estimated 1000-year and 75-year characteristic values (kNm).

Bridge	μ	σ	ξ	z_{1000}	z_{75}
50 m	6842	624.9	-0.075	11 896	11 192
100 m	9124	482.7	-0.068	9124	8538
200 m	8163	780.7	-0.071	14 620	13 698

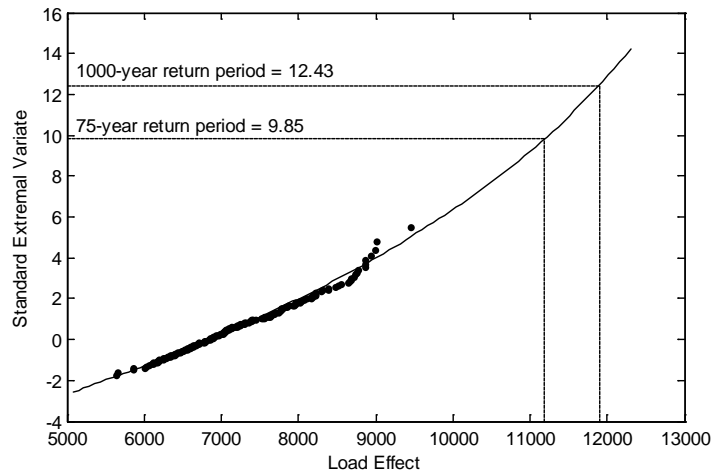


Figure A.8 - Example extrapolation on Gumbel probability paper for load effect 1.

A.6 Comparison

To compare the results of the micro-simulation to the Eurocode values, Notional Load Model Ratio (NLMR) are used (OBrien et al., 2006). The NLMR is the characteristic load effect calculated from the simulations (Table A.5), divided by the corresponding value found using the notional model (Eurocode) (Table A.3). These values are given in Table A.6 and plotted in Figure A.9.

Table A.6 - Notional Load Model Ratio for 1000-year and 75-year load effect.

Bridge	Load effect	NLMR ₁₀₀₀	NLMR ₇₅
50 m	1 Sagging moment	0.75	0.71
100 m	2 Hogging moment	0.81	0.75
200 m	3 Hogging moment	0.71	0.66

Although heavy congestion is applied for as much as 4 hours per working day, it can be seen that the extrapolation leads to values 29% to 19% lower than the Eurocode's for the design of new bridges. The value for the safety assessment of existing bridges allows a further reduction by roughly 5%. A site-specific analysis of the congestion frequency, as described in Chapter 4, may allow for further reductions.

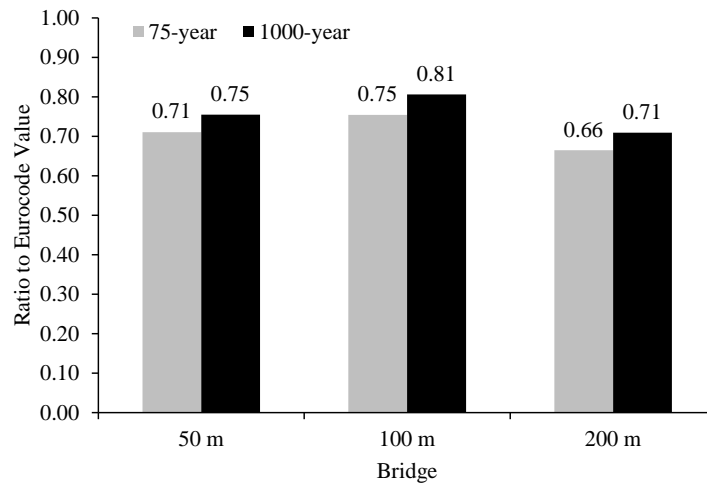


Figure A.9 - Ratio of micro-simulation to Eurocode values for 75- and 1000-year return periods.

A.7 Summary

In this appendix, real traffic weight data is used in single-lane micro-simulations. The load effects on three sample long-span bridges are computed. A total of 1000 hours of heavy congestion is simulated, deemed to represent 1 year of traffic on a busy single-lane road, with an inflow at about 90% of the road capacity. The load effects are extrapolated to 75 years, which is a typical return period for bridge assessment, and to 1000 years, in order to draw a comparison with the Eurocode load model, while preserving the required safety level.

It is found that the extrapolated values are about 25% less than the Eurocode provisions for the design of new bridges, whereas the values for bridge assessment allow for a further 5% reduction, thus suggesting that traffic micro-simulation is a valuable approach for the design and assessment of bridge traffic loading.

Appendix B

Multi-class traffic simulations

B.1 Introduction

Treiber et al. (2000) reproduce observed congested patterns on several motorways in Germany using micro-simulation of single-lane traffic and identical vehicles, even though motorways are not single-lane, nor actual traffic is made up of identical vehicles. In the present research, it is not sufficient to deal only with a single vehicle class, but it is essential to introduce trucks, as they constitute the actual load for bridges. However, trucks have different (and more restricted) operational properties than passenger cars and they negatively affect the road capacity: the higher the truck percentage, the smaller the capacity (Transportation Research Board, 2010). The capacities should thus be computed for any traffic composition considered, in order to calculate the bottleneck strength, which is a critical parameter for determining the congested states, as seen in Chapter 2.

The static capacity of single-class traffic can be calculated analytically when using the IDM. For mixed traffic, this calculation cannot be carried out exactly. On the other hand, the dynamic capacity cannot be calculated analytically, whether for single- or multi-class traffic. In this appendix these two aspects are dealt with and several means to calculate the dynamic capacity are tested and presented.

B.2 Capacity of mixed traffic

B.2.1 Static capacity of single-class traffic

The static capacity of traffic made up of identical vehicles can be calculated analytically. The static capacity, Q_{\max} , can be reached only in spatially homogeneous equilibrium traffic. The

equilibrium traffic implies $dv/dt = 0$ in Equation (2.1) and $\Delta v = 0$ in Equation (2.2). Equation (2.2) is then substituted into Equation (2.1) and solved for the gap, s . Hence the equilibrium gap s_e for a particular speed v is (Treiber et al., 2000):

$$s_e(v) = \frac{(s_0 + vT)}{\sqrt{1 - \left(\frac{v}{v_0}\right)^4}} \quad (\text{B.1})$$

Note that there is no longer a dependence on time, as typical of an equilibrium state. The only IDM parameters that affect the equilibrium gap are the minimum jam distance s_0 , the desired speed v_0 , and the safe time headway T . As may be expected for equilibrium traffic, no acceleration a or deceleration b parameters are involved. Equation (B.1) is plotted in Figure B.1 for the parameter set used by Treiber et al. (2000) (Table B.1). The equilibrium space headways h_e is simply:

$$h_e(v) = s_e(v) + l \quad (\text{B.2})$$

where l is the vehicle length. In Equation (B.1), when the speed $v \rightarrow 0$, the equilibrium gap $s_e \rightarrow s_0$. On the other hand, when $v \rightarrow v_0$, the equilibrium gap $s_e \rightarrow \infty$, which leads to an unrealistic spreading of vehicles. Treiber and Kesting (2010) propose a modification to overcome this limitation, and it is reported in Section D.4. However, they state that this limitation does not affect the traffic dynamics and this is expected, as congested speeds are much lower than the desired speed v_0 .

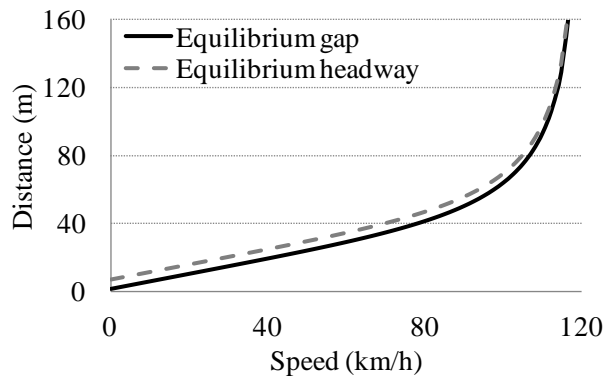


Figure B.1 - Equilibrium distance.

Table B.1 – IDM parameters from Treiber et al. (2000).

Parameter	Value
Desired speed, v_0	120 km/h
Safe time headway, T	1.6 s
Maximum acceleration, a	0.73 m/s ²
Comfortable deceleration, b	1.67 m/s ²
Minimum jam distance, s_0	2 m
Vehicle length, l	5 m

Figure B.2 shows the equilibrium *time* gaps and headways. They are given by Equations (B.1) and (B.2), divided by the speed v . The time headway is an important quantity, as it is the inverse of the flow. The analytical expression of the equilibrium flow Q_e is:

$$Q_e(v) = \frac{1}{\frac{h_e(v)}{v}} = \frac{v}{s_e(v) + l} = \frac{v}{(s_0 + vT) \cdot \sqrt{1 - \left(\frac{v}{v_0}\right)^4} + l} \quad (\text{B.3})$$

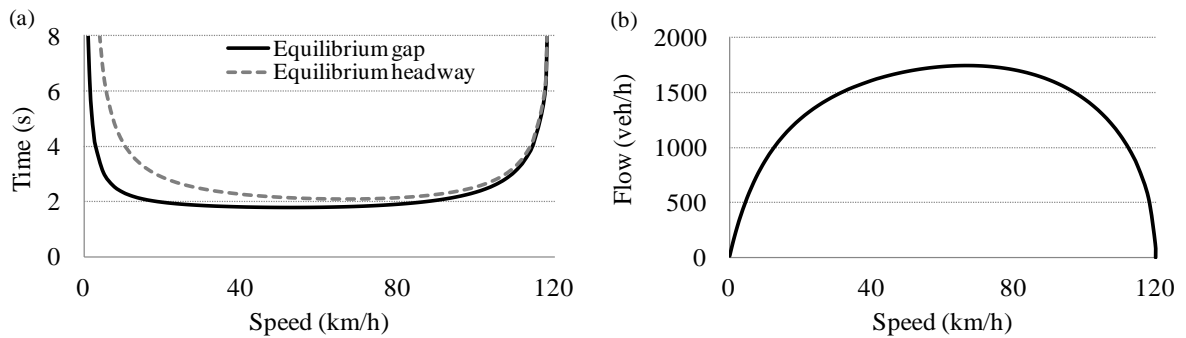


Figure B.2 - Equilibrium conditions: (a) time gap and headway, and (b) flow.

The maximum value of the equilibrium flow can be found numerically and corresponds to the static capacity Q_{\max} . Table B.2 shows the capacity for the parameter set in Treiber et al. (2000) (Table B.1), as well as when the vehicle length l is decreased to 4 m, and when both desired speed is decreased to 80 km/h and length is increased to 12 m. This latter case is deemed to be representative of truck-only traffic. Any mix between these vehicle classes will have an intermediate capacity.

Table B.2 – Capacity for single-class traffic.

Desired speed v_0 (km/h)	Vehicle length l (m)	Equilibrium gap s_e (m)	Equilibrium speed v (km/h)	Capacity Q_{\max} (veh/h)
120	5	33.4	66.8	1743
120	4	32.3	65.0	1790
80	12	28.7	53.4	1311

B.2.2 Multi-class traffic in the Highway Capacity Manual

The Highway Capacity Manual (Transportation Research Board, 2010) prescribes *passenger-car equivalents* E_T for converting mixed traffic into the reference traffic of 100% cars. The passenger-car equivalent for trucks and buses E_T represents "the number of passenger cars that would use the same amount of freeway capacity as one truck/bus under prevailing roadway and traffic conditions" (Transportation Research Board, 2010). For a *basic freeway segment* and *level terrain*, such equivalent is 1.5 (Chapter 11). Then, a *heavy vehicle adjustment factor* f_{hv} can be computed to adjust the capacity:

$$f_{hv} = \frac{1}{1 + P_T(E_T - 1) + P_R(E_R - 1)} \quad (\text{B.4})$$

where P_T is percentage of trucks and buses. P_R and E_R refer to recreational vehicles, which are not of interest in this research. Table B.3 shows the heavy vehicle adjustments factors calculated with Equation (B.4). They are applied to the capacities of the traffic stream with parameters as in Table B.1, where the static capacity Q_{\max} is 1743 veh/h (Table B.2), and the dynamic capacity Q_{out} is 1689 veh/h, as stated in Treiber et al. (2000). It can be seen that the 100% case is different from the truck-only value in Table B.2.

Table B.3 - Heavy vehicle adjustment factors according to HCM.

Truck percentage (%)	Heavy vehicle adjustment factor f_{hv}	Static Capacity Q_{max} (veh/h)	Dynamic Capacity Q_{out} (veh/h)
0	1.00	1743	1689
10	0.95	1660	1609
20	0.91	1585	1535
30	0.87	1516	1469
50	0.80	1394	1351
100	0.67	1162	1126

B.2.3 Vehicle length and truck percentage

The 5 m length used in Treiber et al. (2000) is apparently too long for a typical passenger car, and this value is likely to account for a proportion of trucks. Data for that study comes from the A5 motorway near Frankfurt and from the A8 and A9 motorways near Munich in 1998. According to Schönhof and Helbing (2007), the average truck fraction in the A5 motorway near Frankfurt is between 10% and 15% during rush hours. Their observations ran from January to September 2001, that is 3 years after the data collected by Treiber et al. (2000) on the same motorway. Thus, the study on the A5 motorway of Treiber et al. (2000) is likely to include a similar proportion of trucks. In fact, if car length is 4 m, and there is 12.5% of trucks 12 m long, the equivalent average length results equal to the 5 m used in Treiber et al. (2000). Therefore, a car length of 4 m and a truck length of 12 m are used throughout this work (see for instance Table 2.1).

B.2.4 Generation of input files for SIMBA

Suitable input files for SIMBA can be generated with the in-house program *BTLS package* (*BridgeTrafficLoadSim*). For this, it is necessary to set an injection speed, or *congested speed*, v , and a space gap between vehicles at injection, or *nominal congested spacing*, g (see also Section F.4). A vehicle i is then generated and injected with time headway Δt_i :

$$\Delta t_i = \frac{g + l_{i-1}}{v} \quad (\text{B.5})$$

where l_{i-1} is the length of the previous/front vehicle $i-1$. An implicit assumption of constant speed is made in Equation (B.5). However, when vehicles are injected in SIMBA, they are free to change their speed: in most cases, the actual space gap at injection is higher than the one set as input in BTLS package.

Furthermore, a *minimum space for next vehicle* s_{\min} must be set in the SIMBA program settings, in order to avoid vehicle overlapping when congestion goes back to the beginning of the road. If that happens, a vehicle injection is put in stand-by until the minimum space s_{\min} is available. The following vehicles are injected according to their set time headways (Equation B.5). In this case, the inflow will be actually reduced and the total number of vehicles generated will be spread over a longer time. This situation should be avoided in simulations, by choosing a sufficiently long road.

Care must be taken in setting the minimum space s_{\min} , as it may strongly affect inflows. First of all, the minimum space for next vehicle must be smaller than the gap at injection, used for generating the input file:

$$s_{\min} < g \tag{B.6}$$

otherwise the vehicles will simply not enter the road with the desired injection gap g . Then, it is important to take into account the simulation step, specifically how long a vehicle travels within a single simulation step. For instance, at 66.8 km/h (and assuming no acceleration), a vehicle would travel 4.6 m in a simulation step of 250 ms. A vehicle will be then injected at a distance which is the first multiple of 4.6 m greater than s_{\min} . This distance may be undesirably higher than g , effectively putting vehicles in stand-by and leading to inflows smaller than the desired one.

B.2.5 Dynamic capacity for single-class traffic

Firstly, it is checked if the theoretical static capacities can be correctly generated in SIMBA. For vehicle length 5 m, the capacity is 1743 veh/h, with an equilibrium gap of 33.4 m and speed of 66.8 km/h (Table B.2). This inflow is generated with BTLS package and injected in SIMBA. A minimum space for next vehicle $s_{\min} = 32.5$ m does not allow for full flow,

limiting the flow to 1703 veh/h, whereas smaller values of s_{\min} allow for the full capacity flow (Figure B.3). This is due to the simulation step used (250 ms), as discussed above.

On the other hand, when injecting a flow with smaller gaps at the same speed (66.8 km/h), more vehicles are generated but the road capacity is exceeded and therefore a cluster of vehicles forms at the beginning of the road. The generation of higher inflows (that is with smaller gaps at injection) does not change the value of the outflow from the cluster, as can be seen on the left part of Figure B.3. This outflow is deemed to be the dynamic capacity Q_{out} and is very much dependent on the minimum space for next vehicle s_{\min} . In fact, there is congestion at the beginning of the road and vehicles are injected only when the s_{\min} is available. The minimum space for next vehicle s_{\min} affects the inflow, and therefore also the outflow, as there cannot be more vehicles exiting than the ones entering:

$$Q_{\text{out}} \leq Q_{\text{in}} \quad (\text{B.7})$$

Therefore, the minimum space for next vehicle s_{\min} should be chosen in order to have the maximum flow in (and out of) the cluster, but it should not be too high to prevent the formation of the cluster itself. For instance, in Figure B.3, with a minimum space of 30 m the static capacity Q_{max} is 1743 veh/h, as expected, and the dynamic capacity is 1662 veh/h, whereas smaller values of s_{\min} reduce the outflow. Note that the dynamic capacity of 1662 veh.h is slightly smaller than the 1689 veh/h from Treiber et al. (2000).

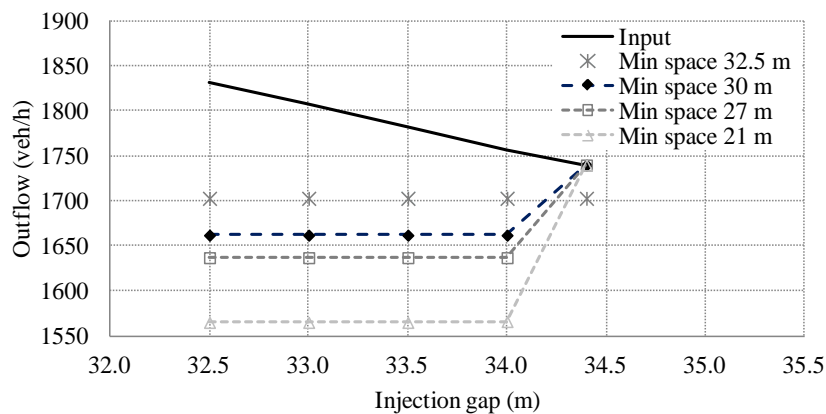


Figure B.3 – Outflow for vehicle length 5 m.

For vehicle length 4 m, the static capacity is 1790 veh/h (Table B.2). Unfortunately, there is no possibility to generate this flow in SIMBA, as the flow gets congested. Possibly, the inflow is so high that any small numerical approximation causes instability and traffic breakdown. This can be solved by using a slightly higher injection gap of 32.5 m, which helps reaching a stable flow of 1781 veh/h. The outflows are only slightly higher than the ones obtained for car length 5 m (Figure B.4).

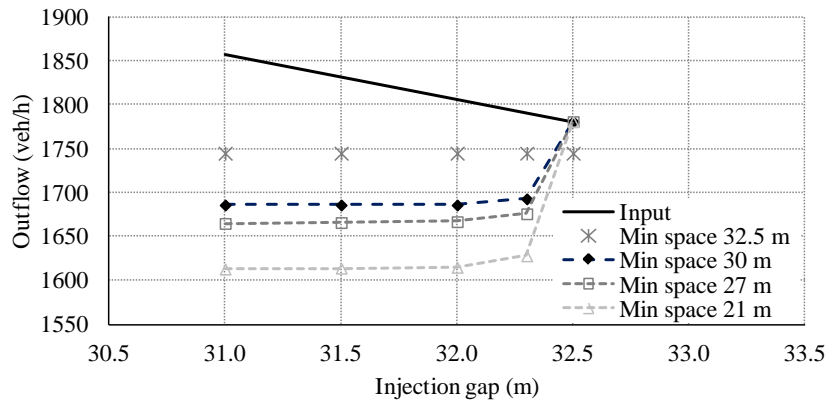


Figure B.4 – Outflow for vehicle length 4 m.

B.2.6 Static and dynamic capacity for multi-class traffic

In the case of multi-class (or mixed) traffic, it is not straightforward to find the theoretical static capacity. In fact, trucks are slower (lower desired speed v_0) and longer than other vehicles. The different lengths can be considered by using an average equivalent length \bar{l} in Equation (B.1), but the reduced desired speed is more difficult to handle since it is a model parameter. It seems reasonable to consider the truck desired speed $v_{0, \text{truck}}$, since trucks are slower and impose their behaviour on the followers. Under this assumption, the equilibrium flow Q_e is:

$$Q_e(v) = \frac{v}{s_e + \bar{l}} \approx \frac{v}{(s_0 + vT) \cdot \sqrt{1 - \left(\frac{v}{v_{0, \text{truck}}}\right)^4} + \bar{l}} \quad (\text{B.8})$$

Using the parameter set in Table 2.3, where cars are 4 m long and trucks have desired speed $v_0 = 80$ km/h and are 12 m long, the theoretical static capacities calculated with Equation B.8 are as in Table B.4.

Table B.4 – Theoretical static capacity for different truck percentages.

Truck percentage (%)	Average vehicle length \bar{l} (m)	Equilibrium gap s_e (m)	Equilibrium speed v (km/h)	Capacity Q_{\max} (veh/h)
10	4.8	24.6	47.4	1610
20	5.6	25.2	48.3	1567
30	6.4	25.8	49.2	1529
40	7.2	26.3	49.9	1492
50	8.0	26.7	50.6	1457

However, simulations with SIMBA show that it is possible to get a flow higher than the theoretical capacity by reducing the gap at injection (Figure B.5). For 20% trucks, the actual capacity is 4% higher than the theoretical value ($1630 > 1567$ veh/h). The dynamic capacity is the maximum outflow found in the flat part of the diagram. In this case, it is 1590 veh/h and is generated with a minimum space for next vehicle s_{\min} of 21 m.

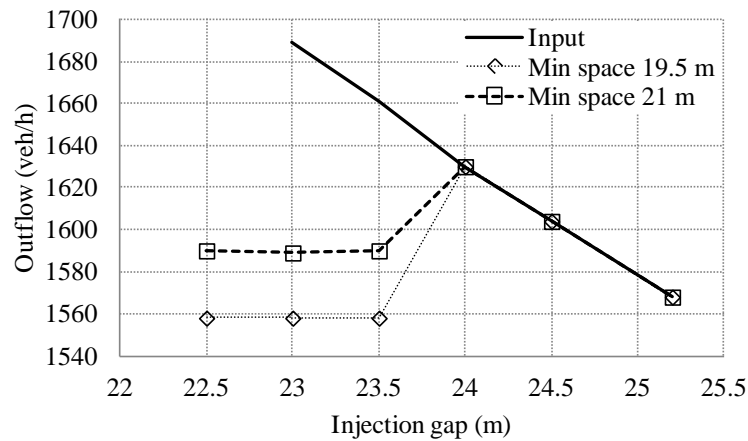


Figure B.5 – Outflow for 20% trucks.

Figure B.6 shows the outflow when there are 50% trucks. Again, it is possible to get a flow higher than the theoretical capacity by reducing the injection gap to 26 m. Note that when the minimum space for next vehicle is 23.5 m, there is no peak, because the minimum space s_{\min} actually prevents the input vehicles from starting on-time on the road.

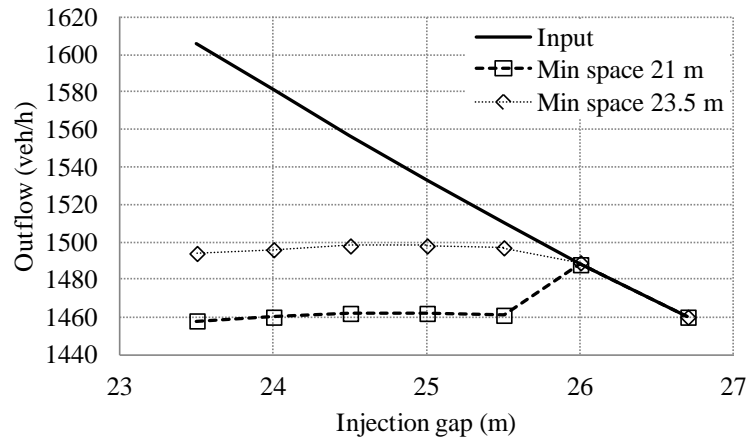


Figure B.6 - Outflow for 50% trucks.

B.2.7 Heavy vehicle adjustment factors based on IDM simulations

Table B.5 sets out heavy vehicle adjustment factors f_{hv} for computing mixed traffic capacity when using the IDM with the parameters in Table 2.3. The adjustment factor is the ratio of the capacity Q (whether static or dynamic) to the same equivalent capacity of the traffic with no trucks Q_{eq} :

$$f_{hv} = \frac{Q}{Q_{eq}} \quad (\text{B.9})$$

The adjustment factors are reasonably close to the ones set out in HCM (Table B.3). Note that the static capacities are lower than observed values (Knoop et al., 2008; Transportation Research Board, 2010). There is little data to compare the dynamic capacity with. Kerner and Rehborn (1996) observe values from 1100 veh/h (40% trucks) to 1800 veh/h (1% trucks), while Knoop et al. (2009) computes a higher value of 2167 veh/h.

The capacity drop is also reported, and it is defined as:

$$CD = 1 - \frac{Q_{out}}{Q_{max}} \quad (\text{B.10})$$

The values are again smaller than the ones observed in real traffic (Kerner and Rehborn, 1996; Cassidy and Bertini, 1999). This can be also noticed in Treiber et al. (2000) and Kesting et al. (2010), and it may be due to the IDM lower static capacity. Moreover, the

capacity drop for identical vehicles is greater than that for mixed traffic, as also reported in the simulations by Kesting et al. (2010). However, the IDM has been calibrated to reproduce observed congested states, rather than uncongested flows close to capacity.

Table B.5 – Heavy vehicle adjustment factors from simulations.

Truck percentage	Equivalent capacity	Theoretical capacity		Capacity Q_{\max} from simulations		Dynamic capacity Q_{out} from simulations		Capacity drop
		veh/h	f_{hv}	veh/h	f_{hv}	veh/h	f_{hv}	
0	1790	1790	1.00	1781	1.00	1686	1.00	0.06
20		1568	0.88	1630	0.92	1590	0.94	0.02
50		1460	0.82	1489	0.84	1462	0.87	0.02
100		1311	0.73	not tested				

B.2.8 Congested states

When using traffic with different truck percentages, the same inhomogeneities $\Delta T = T - T'$ (or simply T') should return similar congested states, in order to allow for a meaningful comparison between different traffic compositions. It is then necessary to use the equivalence set out in Table B.5, otherwise the same inflow Q_{in} may return different congested states. For instance, say it is required to inject 1590 veh/h with 20% trucks, and then with a truck proportion of 50%; in the latter case, the flow would be congested even with $\Delta T = 0$, because the inflow exceeds the capacity corresponding to the 50% truck percentage (Table B.5). Although both cases share the same total inflow, it would not be possible to make a comparison on the loading, because the traffic states are different: free traffic for the former, congestion for the latter. On the other hand, consider a case with 1462 veh/h with 50% trucks. In this case, any small inhomogeneity would make the traffic congested, because it is at its capacity (Table B.5). However, if in the same flow the truck proportion were 20%, the same small inhomogeneity would not be enough to get the flow congested. In fact, a greater inhomogeneity would be needed to generate congestion. Therefore, the procedure described in the following aims at adjusting the inflow in order for the same inhomogeneity ΔT to return similar congested states, or similar *equivalent bottleneck strengths*.

The inflows Q_{in} are those corresponding to the dynamic capacity (Table B.5) and congestion is generated with inhomogeneities $T' = 1.9, 2.2, 2.8, 4.0, 6.4$ s. Figure B.7a shows the reduced outflows Q'_{out} as recorded from the simulations. The outflows are then scaled according to the adjustment factors f_{hv} for the dynamic capacity (Table B.5) and the results are depicted in Figure B.7b.

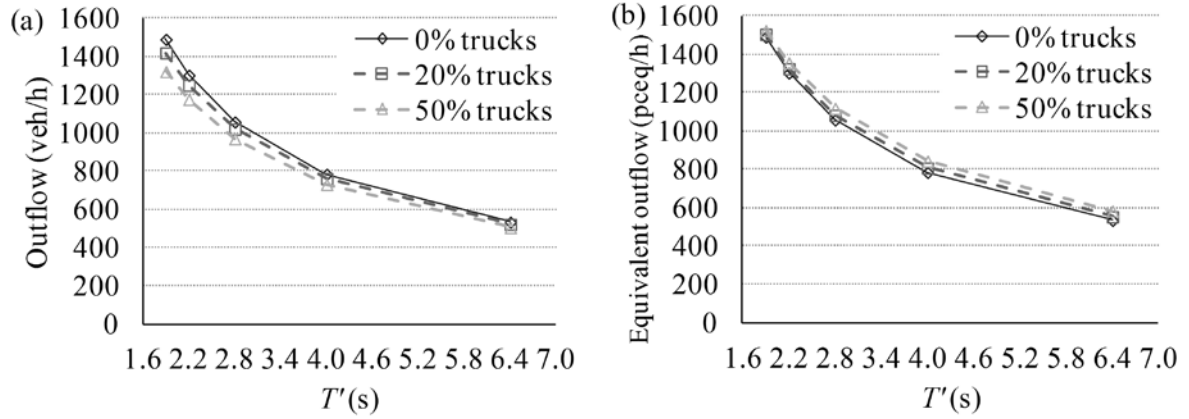


Figure B.7 - Outflow (a) and equivalent outflow (b) from simulations of congestions.

The equivalent bottleneck strength ΔQ_{eq} corresponding to the applied inhomogeneity T' can be then computed:

$$\Delta Q_{eq}(T') = Q_{out,eq}(T) - Q'_{out,eq}(T') = \frac{Q_{out}(T) - Q'_{out}(T')}{f_{hv}} = \frac{\Delta Q(T')}{f_{hv}} \quad (\text{B.11})$$

Figure B.8 shows the equivalent bottleneck strengths ΔQ_{eq} for the inhomogeneities considered. The values are quite similar across the different truck percentages. Note that the highest equivalent bottleneck strength values derive from the condition with no trucks. This procedure has been used to derive Figure 2.3.

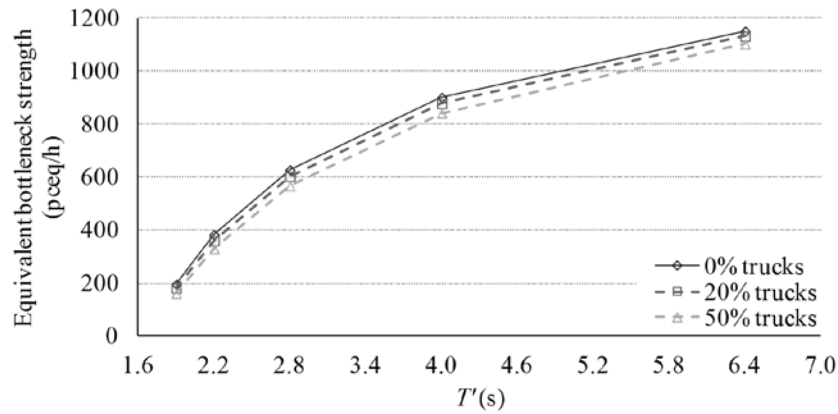


Figure B.8 - Equivalent bottleneck strength.

Figure B.9a shows the average congested speed for the different truck percentages. It can be seen that there is no large difference among the curves. Surprisingly, the condition with no trucks is, in most cases, the one with the slowest speed despite the fact that trucks have a slower desired speed. This probably derives from the slightly higher equivalent bottleneck strength of the 0% truck case in Figure B.8.

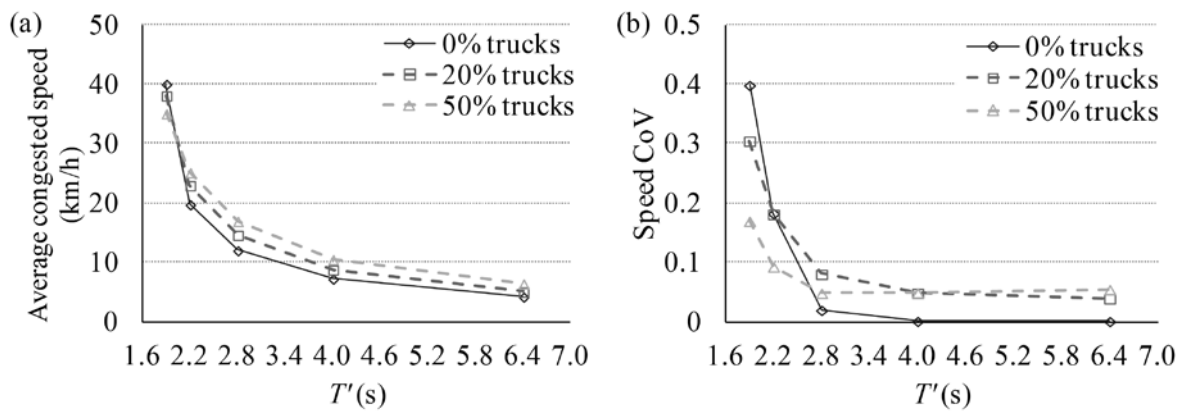


Figure B.9 - Congested speed: (a) average and (b) coefficient of variation.

Figure B.9b shows the coefficient of variation of the congested speed for different truck percentages. It can be seen that for lighter congestions trucks "dampen" the oscillations, while for stronger congestions they introduce a sort of "disturbance" to the homogeneous congestion.

Note that in Section 3.7, a different approach is used to compare the same flow with different truck percentages. In that case, the inflow Q_{in} is kept the same, while the inhomogeneities are

changed in order to obtain the same congested state. This is possible because the inflow $Q_{in} = 1250$ veh/h is well below the capacity.

B.2.9 Extension to multi-lane simulations

The same procedure can be applied to find the static and dynamic capacity of multi-lane traffic. In this case, an analytical formulation is not possible, due to the effects of the lane change manoeuvres. Figure B.10 shows the outflow for 2-lane traffic and 20% trucks with the parameters used in Chapter 3 and 4 (Table 3.2), where all the trucks are injected in the slow lane. The static capacity is $Q_{max} = 3220$ veh/h, while the dynamic capacity Q_{out} is about 3070 veh/h. Note that the outflow is not exactly constant with small injection gaps. This may be due to the fact that the variations in the injection gap actually change the truck percentage over the traffic stream, as discussed in Section F.4. Note also that the capacity is slightly less than twice the single-lane values calculated for the stream with the same truck percentage (Table B.5). In other words, the per-lane capacity is smaller for a two-lane flow than for a single-lane flow.

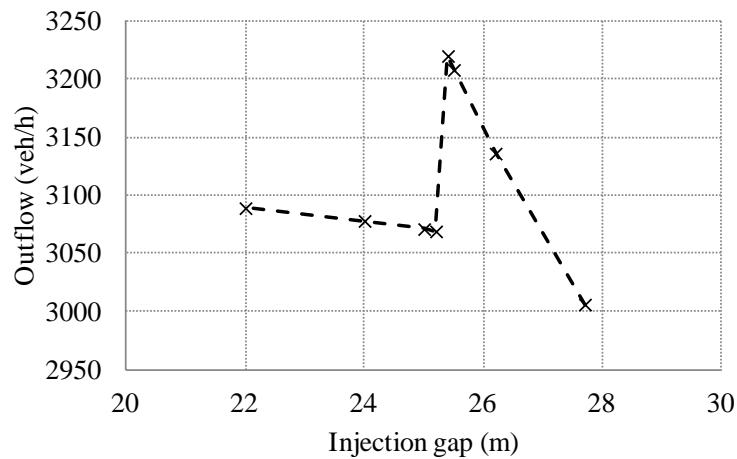


Figure B.10 - Outflow for 2-lane traffic (20% trucks).

B.2.10 Summary

It is not straightforward to calculate the capacities Q_{max} and Q_{max} for multi-class traffic. It is possible to analytically estimate the static capacity by considering the truck parameters (trucks govern the traffic) and an equivalent length. However, simulations show that it is

possible to obtain flows higher by 2-4% than the theoretical static capacity, by slightly reducing the injection gap. Reducing the injection gap further allows the derivation of the dynamic capacity Q_{out} . However, its value strongly depends on the SIMBA program setting *minimum space for next vehicle*. Moreover, the dynamic capacity found is slightly smaller than the one reported in Treiber et al. (2000) for equal conditions. The procedure described here can be applied to find the static and dynamic capacity of multi-lane traffic.

Finally, heavy vehicle adjustment factors for the capacity of multi-class traffic are derived. Consideration of these factors allows traffic with different truck percentages to return similar congested states.

B.3 Alternative means of computing the dynamic capacity

In this section, other means of computing the dynamic capacity for identical vehicles are tested, to check if it is possible to reproduce the dynamic capacity $Q_{out} = 1689$ veh/h stated in Treiber et al. (2000). For this purpose, IDM parameters are as per Table B.1 and simulation step is 100 ms. Five different methods to work out the outflow are developed in MATLAB and reported. The road layout is either open (stretch of road, as in SIMBA) or closed, that is a ring road, as in Treiber et al. (2000).

B.3.1 Open system

First, a start of a standstill queue is simulated ("traffic light" start, *Method 1*). A virtual point detector is placed 500 m in the front of the first car. Figure B.11 shows that the time headways are relatively large for the first vehicles, then become moderately stable after about 50 vehicles and constant after 500 vehicles, converging to 2.07 s. The vehicles start from the queue roughly every 1.6 s. This corresponds to a wave speed of about -15 km/h, as 7 m of road are freed up every 1.6 s, in line with most field observations (Kerner and Rehborn, 1996; Treiber et al., 2000).

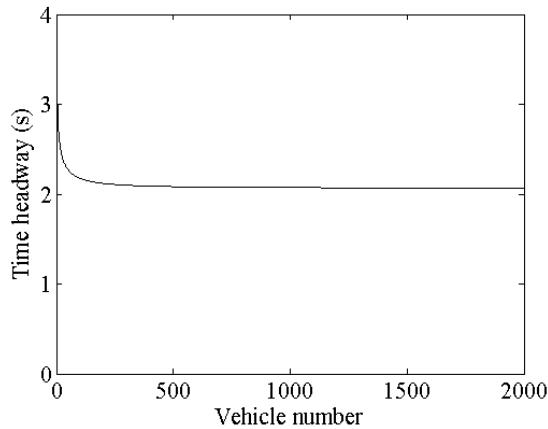


Figure B.11 - Time headways at the detector

Figure B.12a shows the average and maximum flow at the detector for different numbers of vehicles. The maximum flow is found at the end of simulation, as the time headways steadily decrease (Figure B.11). The flow is calculated at the passage of every vehicle i , as the inverse of the time headway Δt_i , that is the *microscopic flow* q_i :

$$q_i = \frac{3600}{\Delta t_i} \quad (\text{B.12})$$

in which q_i is expressed in vehicles per hour and Δt_i in seconds. The average “macroscopic” flow Q is the harmonic mean of the microscopic flow (Treiber and Kesting, 2013):

$$Q = \frac{N}{\sum_i \Delta t_i} = \frac{N}{\sum_i \frac{3600}{q_i}} = \frac{1}{3600} \frac{N}{\sum_i \frac{1}{q_i}} \quad (\text{B.13})$$

where N is the number of vehicles crossing the detector.

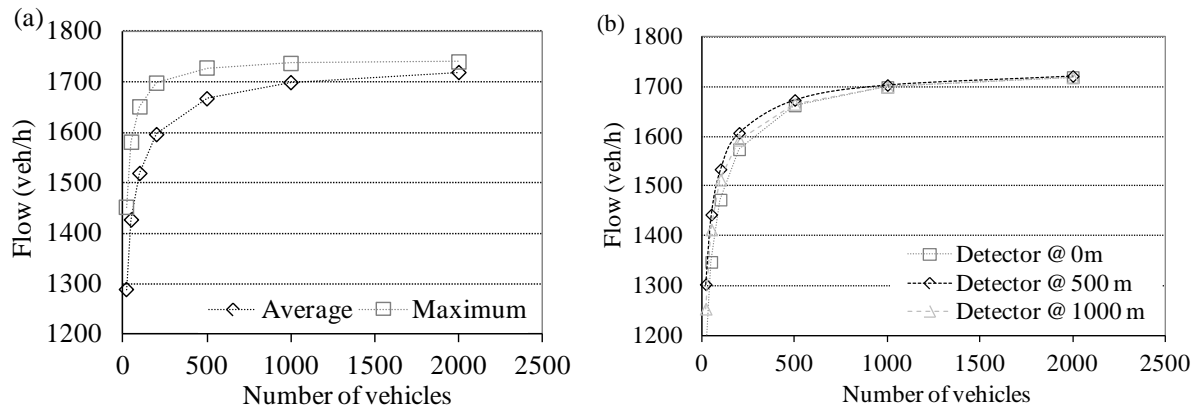


Figure B.12 – Outflow from a start from a standstill: (a) for different number of vehicles and (b) at different detector positions.

Values of the same order of the $Q_{out} = 1689$ veh/h stated in Treiber et al. (2000) can be found between 100 and 1000 vehicles, which seem like a long queue. A convergence can be seen for very high number of vehicles, but this rather converges to the static capacity $Q_{max} = 1743$ veh/h (Table B.2). Figure B.12b shows that for a small number of vehicles N , the detector location affects the measured outflow.

Figure B.13a shows the average outflow when the vehicle length is decreased to 4 m. The ratios between the average outflow and the capacity Q_{max} (as per Table B.2) remain quite the same, regardless of the vehicle length (Figure B.13b).

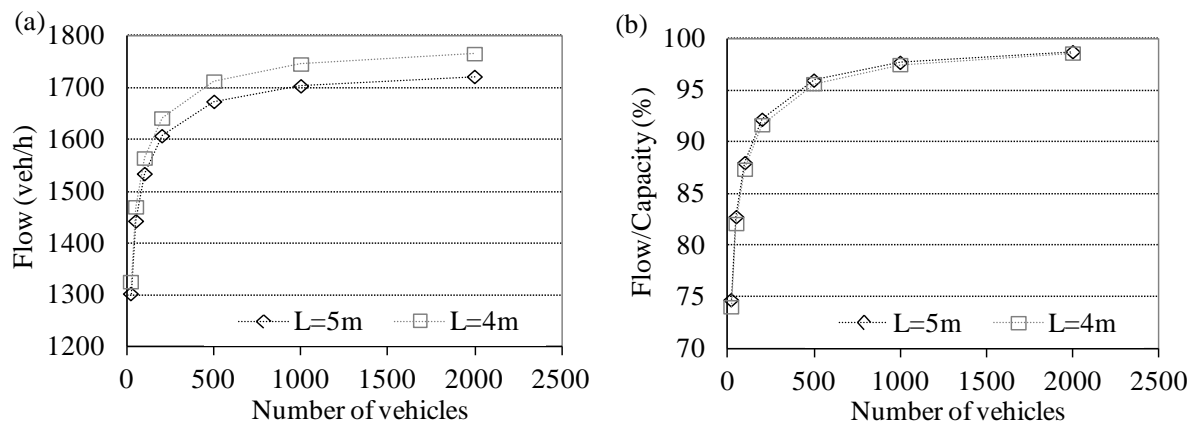


Figure B.13 – Comparison of vehicle lengths: (a) outflow and (b) ratio to capacity.

B.3.2 Ring road

Treiber et al. (2000) state that the dynamic capacity "*can be determined from fully developed stop-and-go waves in a closed system, whose outflow is constant in a rather large range of average densities (20-60 veh/km)*". Therefore, a closed system (i.e. a ring road) is modelled here. The density corresponding to Q_{\max} is 26 veh/km.

A simplified and artificial ring road is first simulated. A queue of vehicles on a stretch of road 1 km long is simulated, must stop at the end of the road, just like if the vehicles met another queue in a ring road (*start-and-stop, Method 2*). The detector is placed halfway. 20 vehicles return an average flow of 1304 veh/h (max 1455) and 50 vehicles return an average flow of 1423 veh/h (max 1563). These values are similar to the ones found in the fully open road for the same number of vehicles. However, if the road were longer (which means longer distance between congestion clusters), while keeping the same density values, the flow would be higher (Figure B.14).

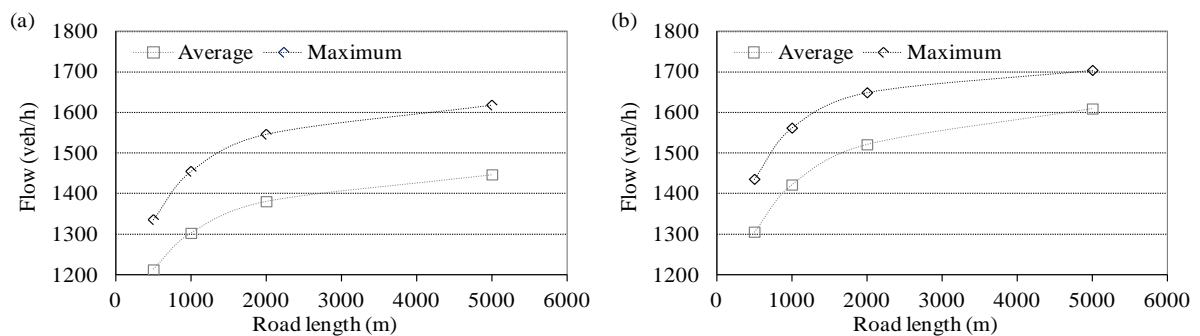


Figure B.14 – Flow from start-and-stop conditions for density (a) 20 veh/km and (b) 50 veh/km.

Then, a full 1 km long ring-road is simulated, where all the vehicles start at the minimum jam distance s_0 (*Method 3*). This initial condition can be seen as a consequence of a large perturbation. In fact, if all the vehicles started equally spaced, they would reach an uncongested equilibrium state.

Figure B.15a shows the time headways at a virtual point detector when there are 50 vehicles in the ring. The peaks represent the crossing of the vehicle clusters. Figure B.15b shows the average and maximum flow at the detector. For the case of 20 veh/km, the traffic stabilizes into free traffic after a short while and its maximum flow is actually the static capacity Q_{\max} .

Then, there is a flat region at 30 and 40 veh/km. The average flows, which comprises also the peaks, are still smaller than the value from Treiber et al. (2000), whereas the maximum flows are not too far. The maximum flow corresponds to the lowest time headway values in Figure B.15a. When considering only the average flow between clusters, for instance when time headways are smaller than 3 s, the average flows would be higher by only 4-8% than the one depicted in Figure B.15b, while the maxima remain unchanged, as they already come from the flow between clusters.

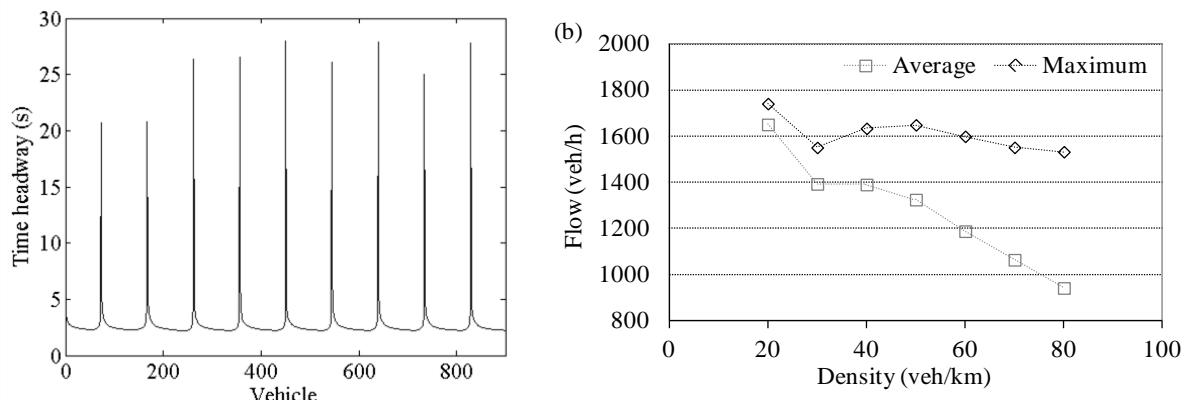


Figure B.15 – Ring road: (a) time headways with density 50 veh/km and (b) flow at different densities.

The flow Q can be also calculated from the density on a section of the road ρ through the fundamental equation of traffic (*Method 4*):

$$Q = \rho \cdot v_s \quad (\text{B.14})$$

Where v_s is the *space mean speed*, calculated as the average speed of the vehicles in the stretch of road at a given time. The results are shown when the monitored section is 250 m long and centred at the point detector. However, it must be noted the flow estimation may not be reliable, because of the use of the fundamental equation during congestions (see also Section 5.2).

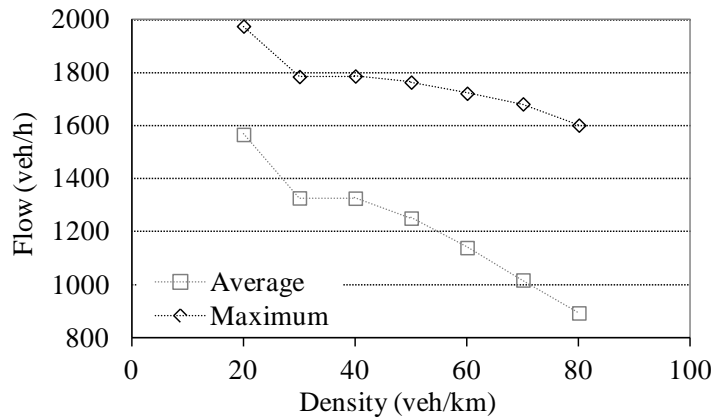


Figure B.16 – Outflow from ring road (flow estimated from density).

Another procedure is to differentiate between standstill vehicles in clusters (for which $Q \approx 0$ and $\rho \approx \rho_{\max}$) and vehicles flowing between clusters, as done in Treiber et al. (2000) (*Method 5*). The flow is again computed from the fundamental equation of traffic (Equation B.14), but it is expected to be more reliable, as traffic conditions are more homogeneous than in Method 4. The speed threshold chosen for differentiating vehicles in and between clusters is 1 m/s (3.6 km/h). There is a small dependence of the flow between clusters on the speed threshold chosen (Figure B.17a). The results for a range of density show that the flow between clusters is rather constant in the range 30-50 veh/km (Figure B.17b), but still quite lower than the values stated in Treiber et al. (2000). The vicinity of the average and maximum values shows the increased flow homogeneity.

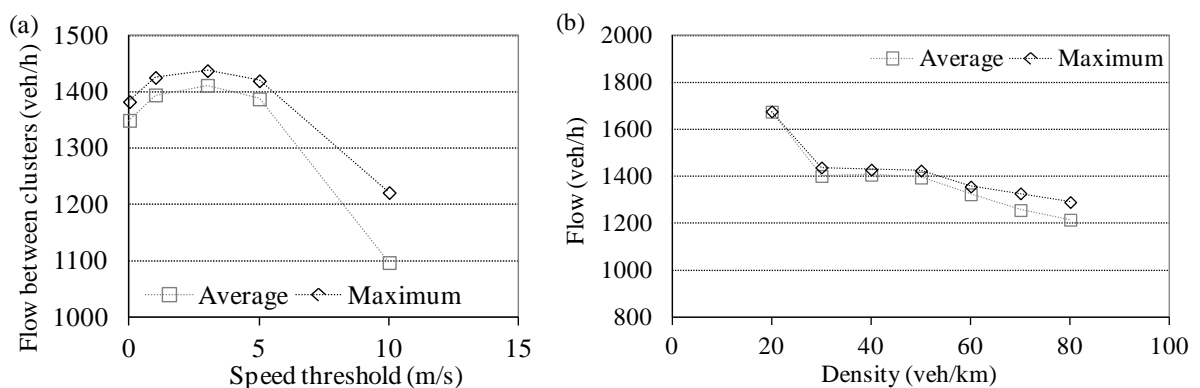


Figure B.17 – Flow between clusters: variation with (a) speed threshold and (b) density.

B.3.3 Summary

None of the five methods tested returns the outflow of 1689 veh/h stated in Treiber et al. (2000). The average and maximum flow values are shown in Figure B.18 for 50 vehicles. Only the maximum flow derived from a ring road (Method 3) is quite close to that of Treiber et al. (2000), while the others are generally below.

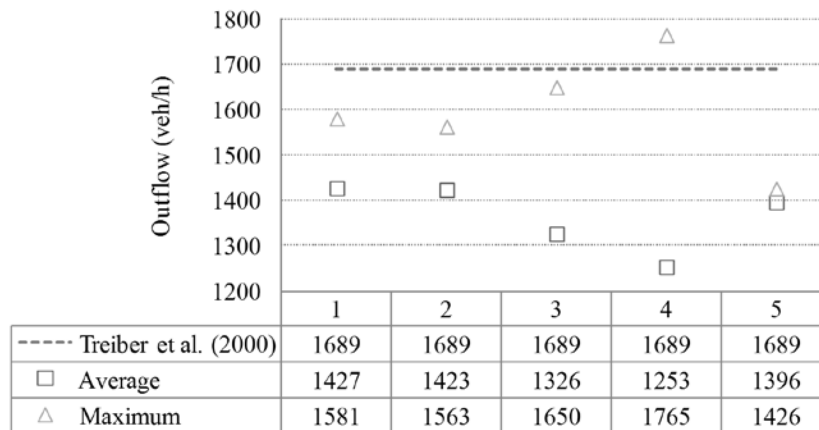


Figure B.18 – Comparison between different methods to calculate the dynamic capacity.

In conclusion, the closest value to the one in Treiber et al. (2000) remains the one computed by means of SIMBA simulations for the same conditions in Section B.2.5 (1662 veh/h).

B.4 Conclusions

The use of micro-simulation for bridge loading requires the explicit modelling of trucks. The introduction of trucks reduces the road capacity, which needs to be calculated for multi-class traffic in order to determine the expected congested conditions.

The static capacity for mixed traffic may be computed theoretically for single-lane traffic. However, the values found in simulations are slightly higher than the theoretical ones. The dynamic capacity values are found by simulations, by causing congestion at the beginning of the road and computing the outflow from the vehicle clusters. This approach is used also for computing the static and dynamic capacity of multi-lane traffic.

Several other methods are tested for computing the dynamic capacity, in order to reproduce a value found in literature (Treiber et al., 2000). However, they are not as close as the values obtained by simulations in SIMBA. Therefore, the dynamic capacity values used throughout this thesis have been derived from SIMBA simulations with the procedure described in this Appendix.

Appendix C

Micro-simulation modelling of congestion due to lane closures

Authors:

Alessandro Lipari

Colin C. Caprani

Eugene J. OBrien

Paper Status:

Paper presented at the *Irish Transport Research Network Conference* (Belfast, 29-30 August 2012). Minor modifications are done in the text to minimise repetition and to fit into the context of the thesis.

Note to the Reader:

The work in this chapter is entirely the work of the author under the supervision of Prof OBrien and Dr Caprani.

C.1 Introduction

Incident/accident clearance and road works often require the closure of one or more of the available lanes on a highway. Data from the UK and the USA suggests that about one third of all incidents results in a lane closure (Rodgers et al., 2006; Tasnim et al., 2008). Besides, there may be a particular geometric road layout that has a permanent lane.

A lane-closure causes a significant capacity reduction, which disproportionately affects the capacity (Knoop et al., 2009; Transportation Research Board, 2010). When the flow demand exceeds such reduced capacity, congestion forms upstream of the closure, as vehicles approaching the closure merge into the open lane. A better understanding of the driver behaviour when approaching a lane closure requires a realistic simulation of the merging manoeuvres of vehicles occurring in the proximity of the lane closure.

Micro-simulation is a suitable tool for studying traffic merging, as it simulates the behaviour of individual vehicles. Trucks are also included in the traffic stream. The lane closure is first explicitly modelled in SIMBA. Then, an equivalent flow-conserving inhomogeneity is applied, as done elsewhere in this thesis. The effects on the traffic resulting from the two ways of modelling the lane closures are compared.

C.1.1 Previous research on merging manoeuvres and lane closures

Lane closures are strictly related to merging manoeuvres. Merging manoeuvres can be classified as mandatory lane changes, as opposed to discretionary lane changes, which are modelled in Chapters 3 and 4.

On-ramp merging has been relatively more studied than lane closures. In fact, it is possible to select an area of study for a long time (for instance, a junction), whereas lane-closure locations are often not known, as they are a consequence of incidents or roadwork. Moreover, the merging manoeuvres are not limited to a restricted area (for instance across the on-ramp lane), but merges may occur well before the actual closure. Bertini and Leal (2005) carry out an empirical analysis of two lane drops in the UK and the USA; Laval and Daganzo (2006) reproduce the macroscopic features of the UK lane drop. Knoop et al. (2009) observe some

lane closures on several Dutch motorways. These studies focus on the macroscopic features of traffic, such as queue discharge flow, capacity reduction and traffic oscillations.

In these studies, no information is given about traffic composition, such as the truck percentage. Moreover, no details were available about lane change activities, as data was collected from loop detectors. A more rigorous approach would require the use of cameras for capturing the manoeuvres of the many vehicles involved in a lane change. However, this approach is still not practicable in many situations. Hidas (2005) analyses 4 hours of traffic including 73 lane changes and classifies the observed lane changes into free, forced, or cooperative. Chodhury et al. (2006) build up a complex model for forced and cooperative merging, based on 540 observed merging manoeuvres.

C.2 Micro-simulation models

As mentioned in Section 3.1, car-following models are relatively more established than lane-changing models, since suitable data for analysing the complex lane-changing manoeuvres is modest. Although some car-following models are used to describe the global effects of multi-lane traffic (Treiber et al., 2000; Schönhof and Helbing, 2007), they would not be suitable for capturing the merging manoeuvres. As done elsewhere in this thesis, the Intelligent Driver Model is used, as introduced in Section 2.2.1, and is combined with the lane-changing model MOBIL, presented in Section 3.2.2.

C.3 Traffic stream and model parameters

As commonly assumed throughout this thesis, the vehicle stream is made up of two vehicle classes: cars and trucks. The IDM parameters are based on those used by Treiber et al. (2000) and are the same used in Chapter 3 (Table C.1). All the parameters are constant, except for the desired speed, which is uniformly distributed. Trucks comprise 20% of the total flow and are randomly injected between cars in the slow lane.

Table C.1 - IDM parameters.

	Cars	Trucks
Desired speed, v_0	120 km/h*	80 km/h*
Safe time headway, T	1.6 s	1.6 s
Maximum acceleration, a	0.73 m/s ²	0.73 m/s ²
Comfortable deceleration, b	1.67 m/s ²	1.67 m/s ²
Minimum jam distance, s_0	2 m	2 m
Vehicle length, l	4 m	12 m

*uniformly distributed within $\pm 20\%$ (cars) and $\pm 10\%$ (trucks).

The lane-changing parameter set is initially based on Kesting et al. (2007) (left column of Table C.2), in which an on-ramp was simulated. However, when this set is applied to a lane closure, a growing queue forms on the closed lane and traffic remains free on the open one, which is clearly unrealistic. In fact, congestion is expected to form in both lanes with vehicles caught in the closed lane merging into the open one. Therefore, a modification of the parameters is proven necessary.

In proximity to the lane closure, the lane change parameter set is appropriately modified in order to allow the merging. Several tests showed that effective merging manoeuvres can be achieved by (right-hand column of Table C.2):

- not taking into account the disadvantage imposed to the neighbouring vehicles in considering the lane change execution ($p = 0$); note that in this way b_{safe} becomes the parameter which effectively controls the aggressiveness and safety of the manoeuvres;
- imposing a very high maximum allowable braking b_{safe} , equal to the maximum vehicle capability $b_{\text{max}} = 9 \text{ m/s}^2$;
- increasing the bias acceleration Δa_{bias} towards the open lane, in order to prevent vehicles from moving to the closed lane.

It must be noted that this modified parameter set does not necessarily imply an extremely aggressive behaviour. The resulting manoeuvres can also be seen as a cooperation of the follower to the merging vehicle in front. In fact, the strong deceleration rate "imposed" on the

follower generally lasts only the time of a simulation step. In the real world, vehicles would "spread" their deceleration to let the merging vehicle cut in.

Table C.2 - MOBIL parameters.

	0 - 4000 m	4000 - 8000 m
Politeness factor, p	0.15	0
Changing threshold, Δa_{th}	0.1 m/s ²	0.1 m/s ²
Safe braking, b_{safe}	9 m/s ²	9 m/s ²
Bias for the slow lane, Δa_{bias}	0.3 m/s ²	3.0 m/s ²

A two-lane same-direction 8000 m long road is considered. The lane closure is applied on the fast lane at 6000 m until the end of the road. The modified parameter set is introduced 2000 m before the lane closure. This takes into account that vehicles further upstream may not be aware of the lane closure ahead and therefore drive normally and use both lanes.

The dynamic capacity Q_{out} of the road is 3080 veh/h. This value is computed by injecting a high inflow, which causes a cluster localised at the beginning of the road. The average outflow from such a cluster is deemed to be the dynamic capacity Q_{out} , as detailed in Section B.2. Note that for this calculation, the MOBIL parameter set should not be modified. The reduced dynamic capacity due to the lane closure Q'_{out} is 925 veh/h. Therefore, the capacity reduces by 70%, which is close to available real-world observations (Transportation Research Board, 2010). As per Equation (3.6), the bottleneck strength ΔQ is then 2155 veh/h.

The difference between applying an actual lane closure and applying an inhomogeneity over both lanes is also investigated. The reduced dynamic capacity due to the lane closure Q'_{out} is obtained by increasing the safe time headway to $T' = 7.0$ s. The flow-conserving inhomogeneity increases linearly from T to T' in the section 5700 - 6300 m. Note that the MOBIL parameter set (Table C.2) is left unchanged in order to maintain most merging manoeuvres into the slow lane.

Four inflows Q_{in} are considered: 1500, 2000, 2500, 3000 veh/h. For each inflow Q_{in} , eight simulations of one hour of traffic are run, in order to account for the randomness involved in the truck injection and vehicle desired speed.

C.4 Results

The capacity reduction caused by a lane closure is rather strong. According to Treiber et al. (2000), the expected congested state is the heavy HCT type. Both lanes are actually heavily congested, as a consequence of the merging manoeuvres (Figure C.1).



Figure C.1 – Screenshot of SIMBA near the lane closure showing plan view of traffic (small black bars = cars; longer gray bars = trucks; white line = closure).

Lane-averaged space-time speed plots are useful to visualise the spatio-temporal evolution of congestion. Figure C.2 shows that the congestion patterns are quite similar for a lane closure and inhomogeneity. The main difference is that some small oscillations arise when the lane closure is explicitly modelled (Figure C.2a), whereas these are hardly noticeable when the inhomogeneity is applied (Figure C.2b).

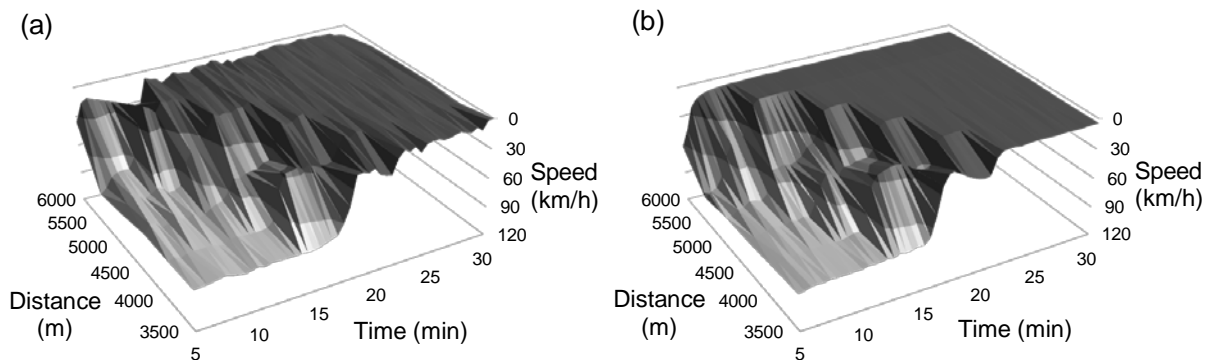


Figure C.2 – Space-time speed plots when applying:
(a) lane closure and (b) inhomogeneity ($Q_{in} = 3000$ veh/h).

A detailed analysis of the one-minute aggregated speed at a virtual detector placed at 5000 m (that is, 1 km upstream of the lane closure) shows that when the lane closure is explicitly modelled, the open lane is, on average, faster than the closed one, even though still rather slow (Figure C.3a). On the other hand, when the inhomogeneity is applied, the speeds are roughly the same in both lanes and they are slightly less than the average of the two lanes when the lane closure is modelled. The analysis of the coefficient of variation of speed confirms the reduced oscillations when the inhomogeneity is applied (Figure C.3b); when the

lane closure is explicitly modelled, the merging vehicles cause oscillations, as can be also seen in Figure C.2b.

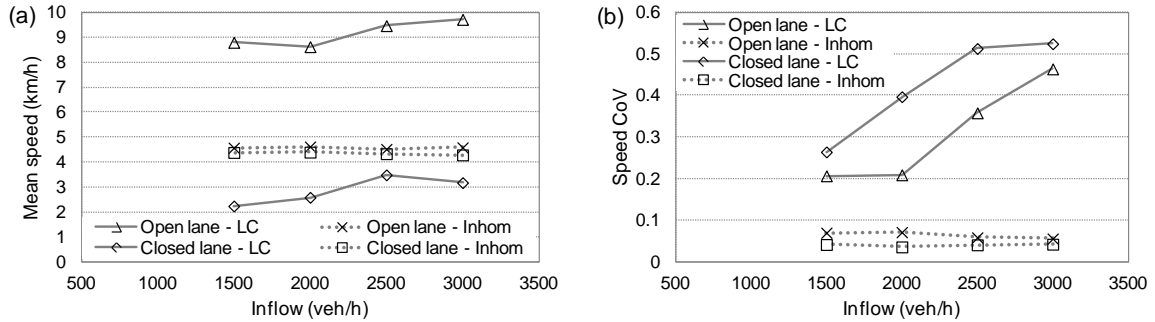


Figure C.3 – Speed at 5000 m for lane closure (LC) and inhomogeneity (Inhom):
(a) mean and (b) coefficient of variation.

Figure C.4 shows the lane change rates, separated for the space-time area in which the traffic is still uncongested (that is, before approaching the queue) and in proximity of the lane closure, where traffic is congested and merging manoeuvres take place. In the former case, it can be seen that the inhomogeneity returns a slightly lower lane change rate for high inflows. However, such lane change rates are in the range of the available observations for uncongested traffic on two-lane motorways (Sparmann, 1979; Yousif and Hunt, 1995). In the latter case, the explicit modelling of the lane closures brings greater lane change rates, which again match available observations (Sparmann, 1979). As merging manoeuvres are not fully modelled with the inhomogeneity, the lane change rate is expectedly much lower.

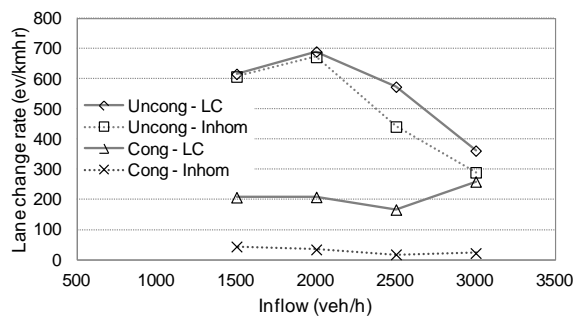


Figure C.4 – Lane change rates in the uncongested and congested area for lane closure (LC) and inhomogeneity (Inhom).

Finally, it is interesting to analyse the behaviour of the truck traffic. Figure C.5a shows that the application of the inhomogeneity results in a higher proportion of truck traffic in the

closed lane, whereas in the explicit modelling of the lane closure, more trucks stay in the open lane. Figure C.5b shows the number of lane changes performed by trucks. This percentage is rather constant across the inflows and is slightly higher when the inhomogeneity is applied, which is consistent with Figure C.5a, as trucks are all injected in the slow lane.

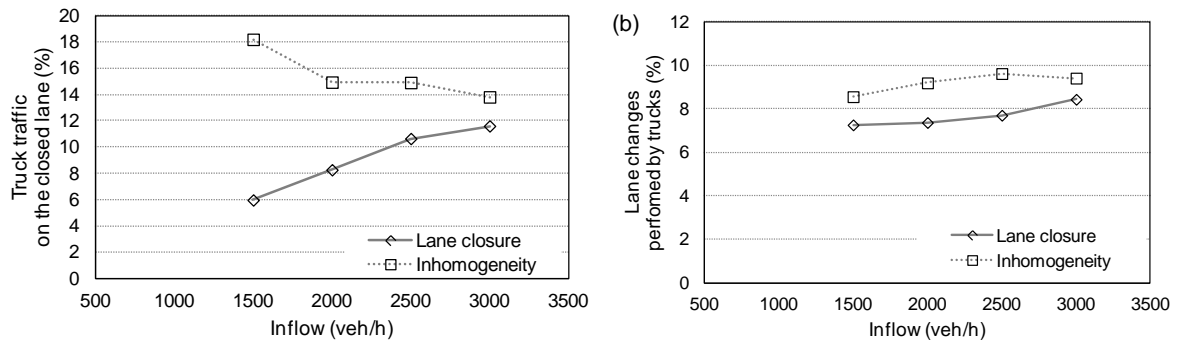


Figure C.5 – Behaviour of truck traffic: (a) percentage of trucks in the closed lane at the 5000 m detector and (b) number of lane changes performed by trucks.

C.5 Conclusions

This appendix focuses on the modelling of mandatory merging manoeuvres occurring in proximity of a lane closure. The IDM is combined with the lane-changing model MOBIL, and the lane closure is explicitly modelled in SIMBA. The application of an available parameter set would not replicate any merging manoeuvre in proximity of the lane closure. Therefore, it is necessary to appropriately modify the lane-changing parameters in order to simulate the merging manoeuvres.

The explicit modelling of the lane closure is compared to the application of an equivalent flow-conserving inhomogeneity, used elsewhere in this thesis. It is found that such inhomogeneity can replicate the overall congestion pattern. However, the inhomogeneity cannot fully catch details of the traffic in proximity of the lane closure, such as lane change activity or distribution of trucks between lanes.

Appendix D

Refinement and calibration of the lane-changing model

D.1 Introduction

Kesting et al. (2007) present the lane-changing model MOBIL and analyse the lane changes due to an on-ramp scenario (*mandatory lane changes*). In their work, no focus is given to the resulting congested patterns. However, the reproduction of observed congested patterns is an essential pre-requisite of this research. It is then essential to verify that the introduction of the lane-changing model does not limit the characteristic capability of the car-following IDM to replicate such congestion patterns. The lane-changing model needs to be calibrated to return realistic lane change rates in the scenario modelled in SIMBA, i.e. a stretch of motorway with no on- or off-ramps (*discretionary lane changes*).

The introduction of the lane-changing model requires refinements also in the car-following IDM, since MOBIL is based on an acceleration advantage strategy, where all the accelerations are still calculated with the IDM. For instance, vehicles may over-react to cut-in manoeuvres of vehicles moving from adjacent lanes. This situation clearly cannot happen in single-lane simulations, but nevertheless involves a modification of the IDM. It is important that these refinements do not significantly increase the computational burden, as bridge loading applications require the simulation of quite long periods of time.

In this appendix, the procedures and the tests carried out for refining the model and determining the final parameters used in Chapter 3 and 4 are detailed. For this purpose, field observations available in the literature are used.

D.2 MOBIL formulation

The incentive criterion of MOBIL used in Chapter 3 and 4 is reported here for a slow-to-fast and for a fast-to-slow lane changes under asymmetric rules:

$$\tilde{a}_c(t) - a_c(t) > \Delta a_{th} + \Delta a_{bias} + p(a_n(t) - \tilde{a}_n(t)) \quad (D.1)$$

$$\tilde{a}_c(t) - a_c(t) > \Delta a_{th} - \Delta a_{bias} + p[(a_n(t) - \tilde{a}_n(t)) + (a_o(t) - \tilde{a}_o(t))] \quad (D.2)$$

For ease of reference, Figure D.1 reports the vehicles involved in a lane change manoeuvre, as shown in Section 3.2.2.

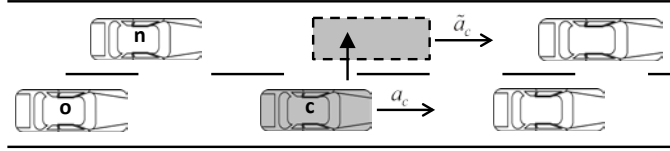


Figure D.1 - Vehicles involved in a lane-changing manoeuvre (adapted from Kesting et al. (2007)).

Kesting et al. (2007) do not include the disadvantage to the new target follower, $a_n - \tilde{a}_n$ in the fast-to-slow lane-changing (D.2), but only the (negative) disadvantage to the current ‘pushy’ follower $a_o - \tilde{a}_o$:

$$\tilde{a}_c(t) - a_c(t) > \Delta a_{th} - \Delta a_{bias} + p(a_o(t) - \tilde{a}_o(t)) \quad (D.3)$$

Note that the disadvantage imposed to the new follower $a_n - \tilde{a}_n$ is always included under symmetric passing rules (Treiber and Helbing, 2002; Kesting et al., 2007; Treiber, 2011):

$$\tilde{a}_c(t) - a_c(t) > \Delta a_{th} + p[(a_n(t) - \tilde{a}_n(t)) + (a_o(t) - \tilde{a}_o(t))] \quad (D.4)$$

However, under asymmetric rules, it seems appropriate to include the disadvantage to the new follower for fast-to-slow lane changes, otherwise this would be set only with the safety criterion (Equation 3.5), in fact imposing strong decelerations to the new follower. The exclusion of the pushy follower o is then “*a correct strategy for drivers on the right-hand lane, while the full MOBIL should be considered for drivers on the left-hand lane*” (Treiber, 2011), where the right-hand lane is the slow lane (asymmetric passing rules – continental

European usage). This reasoning leads to the implementation and used of Equations (D.1) and (D.2) throughout this thesis.

Kesting et al. (2007) suggest the application of a "mixed" passing rule for asymmetric rules, where under a certain "*critical speed*" the driving behaviour switches from asymmetric to symmetric. This mixed rule is not implemented in SIMBA, so the rule can be either symmetric ($\Delta a_{bias} = 0$) or asymmetric ($\Delta a_{bias} > 0$). However, during congestions (i.e. under the critical speed), the number of lane changes drops considerably and for bridge loading applications it is crucial to model the lane changes occurring *before* approaching congestions. Therefore, asymmetric rules are used throughout this thesis. An application of symmetric rules to bridge loading calculation is presented in Caprani et al. (2012b). No qualitative differences are found in lane change rates and traffic loading from the simulations shown in Chapter 3 for similar conditions.

Finally, the safety criterion is unmodified as in Equation (3.5). The effect of the safety criterion is addressed in Section D.6.

D.3 Combination of IDM and MOBIL: cut-in manoeuvres

SIMBA simulations show that the combination of the IDM and MOBIL returns an unrealistic behaviour in the fast-to-slow lane changes. Specifically, overtaking vehicles cut in front of vehicles on the slow lane allowing for an inconsistent gap. Figure D.2 shows the acceleration resulting from a speed difference Δv and a gap to the front vehicle s . According to the IDM, vehicles at small gaps react strongly when the front vehicle is slower ($\Delta v > 0$), as this is a critical emergency situation. However, there is also a region where vehicles over-react when the front vehicle is close ($s < \sim 10$ m) but faster ($\Delta v < 0$), which is just a mildly critical situation. Moreover, for certain speed differences, there is hardly any reaction. This inconsistency is due to the desired minimum gap, s^* (Equation 2.2), which may get unrealistically below zero for negative values of speed difference Δv , and consequently return inconsistent accelerations in Equation (2.1). This situation seldom happens in single-lane simulations, where the speed difference between two consecutive vehicles is typically within a limited range, but it is common in multi-lane traffic, where merging or cut-in manoeuvres can occur frequently.

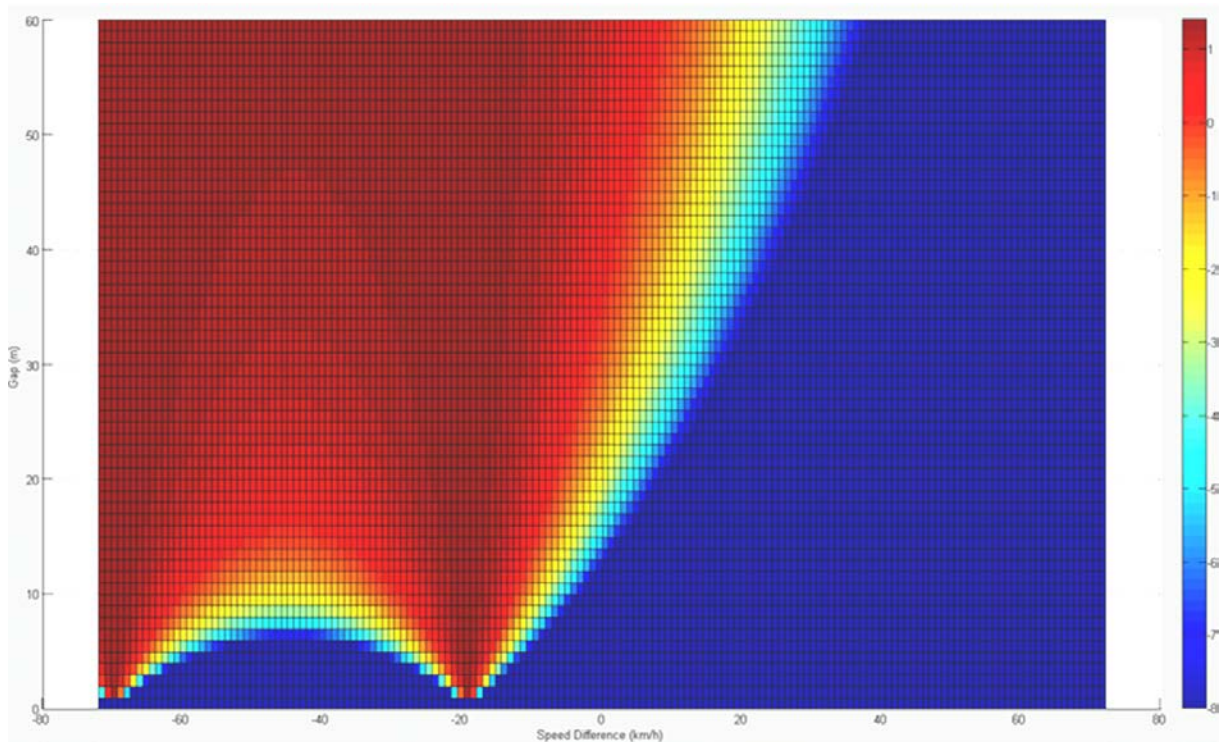


Figure D.2 – IDM acceleration resulting from given speed difference and gap.

D.3.1 Data

Field observations show that vehicles accept gaps shorter than usual when a vehicle that cuts in is faster (Hidas, 2005; Federal Highway Administration, 2005; Chodhury et al., 2006). In fact, drivers rely on the front vehicle not changing its behaviour and therefore react only mildly with little or even no deceleration. The micro-simulation models based on the above field observations allow for a gap close to the bumper-to-bumper distance when the cut-in vehicle is faster (Hidas, 2005; Chodhury et al., 2006).

Figure D.3 shows data taken from the US-101 dataset of the NGSIM project (Federal Highway Administration, 2005). This dataset contains 45 minutes of video recording over 640 m of the US-101 6-lane freeway. The layout includes an on- and an off- ramp, with an auxiliary lane in between. The video data was collected from 7:50 to 8:35 am on 15 June 2005. The subset from 7:50 to 8:05 am shows the highest number of lane changes, which occurs during the congestion build-up. After that, the traffic is primarily congested and the number of lane changes significantly drops, as expected.

In total, 396 lane changes are considered; 64 lane changes are discarded because they involve motorcycles and a further 527 removed because either the NGSIM tracking algorithm misplaced some vehicles or a vehicle aborted a lane-changing manoeuvre. Vehicles are discarded if 1 s after changing lane, they have either not moved transversally more than 0.6 m or moved back to the initial lane.

Figure D.3a shows the observed relationship between the speed difference of the new follower and the lane-changing vehicle, and the gap between the same vehicles. It can be seen that some very close cut-in manoeuvres occur when the relative speed is less than zero (i.e. the lane-changing vehicle is faster), while the minimum gap seems to increase linearly with the speed difference when the follower is faster (the dotted lines are just indicative). Figure D.3b shows the observed relationship between the absolute speed of the follower and the same gap as above. It can be noticed that small gaps occur also when the follower speed is high, confirming that the driver behaviour in lane-changing is different from the one in car-following (Hidas, 2005).

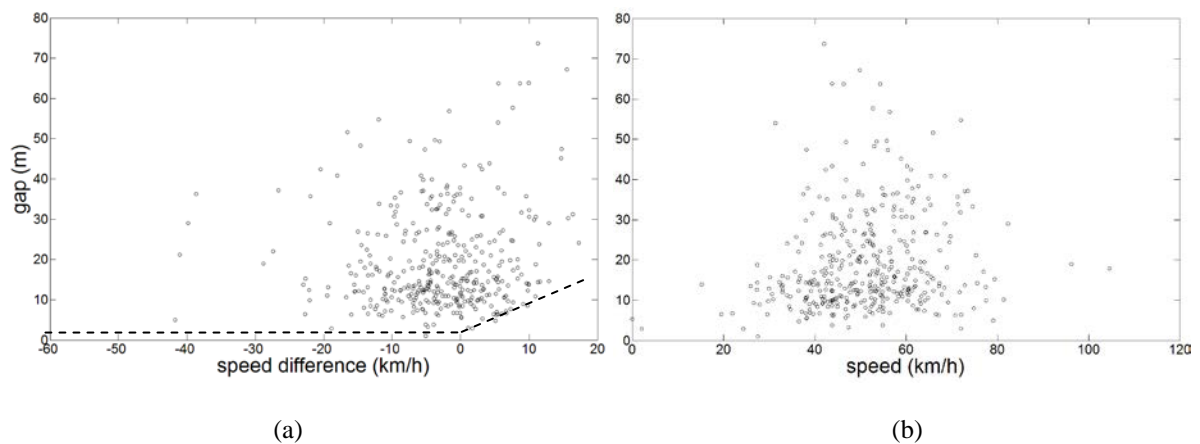


Figure D.3 - Relation between (a) gap and speed difference and (b) gap and follower speed.

D.3.2 IDM modifications

Kesting et al. (2010) acknowledge the problem of the IDM over-reaction and find an analytical formulation in the field of the *Adaptive Cruise Control* (ACC). They combine the IDM with a *constant-acceleration heuristic* model (CAH). This latter model considers the acceleration of the leading vehicle and leads to a more relaxed behaviour. The ACC differs from the IDM when the two vehicle speeds are comparable, while leads to a similar behaviour

when the cut-in vehicle is slower, which represents a seriously critical situation. The ACC model requires the introduction of a new parameter, named the *coolness factor*. However, the combination of the ACC and MOBIL would be likely to lead to an increase in complexity and computational demand. This is an important requirement for bridge loading applications, as it is necessary to simulate long periods of time.

We therefore consider two alternative formulations to the IDM, which only modify Equation (2.2) when the speed difference is negative ($\Delta v < 0$). They both do not require any new parameter and do not add significant computational complexity.

The vehicle stream is made up of two vehicle classes: cars and trucks. The parameters for each class are shown in Table 3.1. They are taken from Kesting et al. (2007), where the politeness factor is set to 0.5. No parameter randomness is accounted for. A two-lane 5000 m long road is considered. The total inflow is 1425 veh/h, 20% of which are trucks. The whole inflow is injected in the slow lane and then vehicles are allowed to change lane. The flow is uncongested with a density of about 7 veh/km/lane.

Table D.1 - Model parameters of IDM and MOBIL.

	Parameter	Cars	Trucks
IDM	Desired speed, v_0	120 km/h	80 km/h
	Safe time headway, T	1.2 s	1.2 s
	Maximum acceleration, a	1.5 m/s ²	1.5 m/s ²
	Comfortable deceleration, b	2.0 m/s ²	2.0 m/s ²
	Minimum jam distance, s_0	2 m	2 m
	Vehicle length, l	4 m	12 m
MOBIL	Politeness factor, p	0.5	0.5
	Changing threshold, Δa_{th}	0.1 m/s ²	0.1 m/s ²
	Maximum safe deceleration, b_{safe}	4 m/s ²	4 m/s ²
	Bias for the slow lane, Δa_{bias}	0.3 m/s ²	0.3 m/s ²

Figure D.4 shows the original formulation (Equation 2.2) and two proposed modifications, in terms of desired minimum gap s^* resulting from a speed difference Δv . The original Equation (2.2) is linear with the speed difference Δv and its slope is:

$$\frac{d s^*(t)}{d \Delta v(t)} = \frac{v(t)}{2\sqrt{ab}} \quad (\text{D.5})$$

The first modification simply caps Equation (2.2) to the minimum jam distance s_0 (*Case 1*), providing a sharp discontinuity at -16 km/h:

$$s^*(t) = \max\left(0, s_0 + Tv(t) + \frac{v(t) \cdot \Delta v(t)}{2\sqrt{ab}}\right) \quad (\text{D.6})$$

The second one provides a softer exponential function (*Case 2*):

$$s^*(t) = s_0 + Tv(t) \cdot \exp\left(\frac{\Delta v(t)}{2T\sqrt{ab}}\right) \quad (\text{D.7})$$

Equation (D.7) has the following desirable properties:

- when $\Delta v \rightarrow -\infty$, it has asymptote at s_0 ;
- at $\Delta v = 0$, it has same value ($s^* = s_0 + Tv$) and slope of the original formulation:

$$\frac{d s^*(t)}{d \Delta v(t)} = \frac{v(t)}{2\sqrt{ab}} \cdot \exp\left(\frac{\Delta v(t)}{2T\sqrt{ab}}\right) \quad (\text{D.8})$$

$$\left. \frac{d s^*(t)}{d \Delta v(t)} \right|_{\Delta v(t)=0} = \frac{v(t)}{2\sqrt{ab}} \quad (\text{D.9})$$

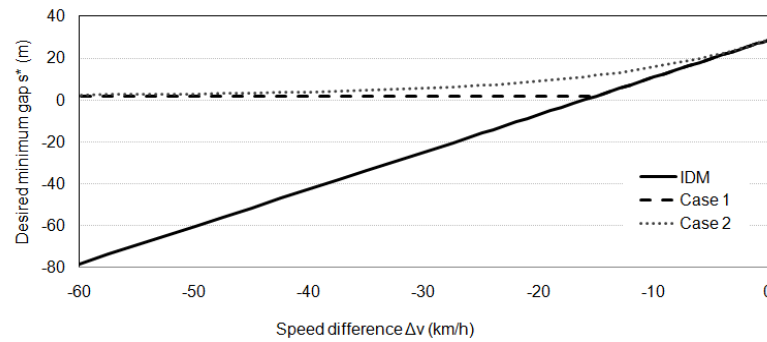


Figure D.4 - Proposed modifications of the IDM model.

D.3.3 Microscopic results

From Equation (D.2) it can be found that the acceleration imposed to the new follower n in order for the current vehicle c to perform a fast-to-slow cut-in manoeuvre must be:

$$\tilde{a}_n \geq \frac{\Delta a_{th} - \Delta a_{bias} - (\tilde{a}_c - a_c)}{p} + (a_o - \tilde{a}_o) + a_n \quad (D.10)$$

If a vehicle cuts in at its desired speed, v_0 , it has no acceleration advantage, then $\tilde{a}_c - a_c = 0$. If the new follower n is also going steadily, then $a_n = 0$. Finally, if there is no pushy follower o , then $a_o - \tilde{a}_o = 0$. In this case, the imposed deceleration \tilde{a}_n depends only on the model parameters (Table 3.1) and must be:

$$\tilde{a}_n \geq \frac{\Delta a_{th} - \Delta a_{bias}}{p} = -0.4 \text{ m/s}^2 \quad (D.11)$$

Figure D.5 illustrates the minimum gap allowed for a lane change, when a car cuts in the slow lane at its desired speed $v_{0,car}$ in front of a slower vehicle, e.g. a truck going at its slower desired speed $v_{0,tr} = 80$ km/h, so that the imposed deceleration \tilde{a}_n can be calculated according to Equation (D.11). A rearrangement of Equation (2.1) when $v = v_0$ allows the calculation of the resulting minimum gap s :

$$s \geq s^* \cdot \sqrt{-\frac{a}{\tilde{a}_n}} = s^* \cdot \sqrt{\frac{a \cdot p}{\Delta a_{bias} - \Delta a_{th}}} \quad (D.12)$$

where the desired minimum gap s^* is according to the original formulation in Equation (2.2) or to the modifications (D.6) and (D.7). The desired speed of the car, $v_{0,car}$, is varied from 80 to 140 km/h, so that $\Delta v = v_{0,tr} - v_{0,car}$. As expected, the IDM does not show a steady trend. After a speed of about 96 km/h, the faster the car cuts in, the bigger the gap allowed for, which is clearly unrealistic. If $v_{0,car} = 120$ km/h, as in Table 3.1, the car would allow for 82.5 m gap to go back to the slow lane. The modified cases 1 and 2 show a steady trend instead.

It can be seen that when the speed difference Δv is limited, the gaps in Figure D.5 are quite large compared to the field observations, in which the observed discontinuity is at about 0 km/h (Figure D.3a). This aspect is deliberately not taken into account in order to not

drastically change the IDM model and because the US-101 observations may include some mandatory lane changes, where the necessity of following the planned path may force drivers to accept or impose very short gaps.

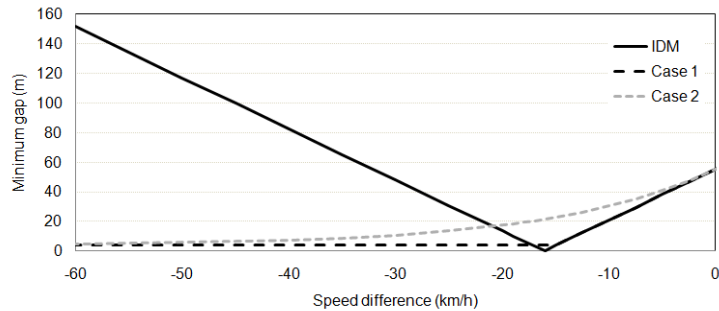


Figure D.5 - Minimum gap allowed for to the follower vehicle.

Note that using the fast-to-slow lane-changing formulation in Kesting et al. (2007) (Equation D.3), the car would cut in allowing for a smaller gap, but imposing a deceleration $b_{\text{safe}} = 4 \text{ m/s}^2$ to the truck. This seems too strong compared to the field observations and it may even lead to flow instability. In fact, the US-101 lane changes analysed above show that the deceleration of the new follower was stronger than the comfortable deceleration $b = 2 \text{ m/s}^2$ in only 26 cases (5.5%).

Finally, it must be noted that the slow-to-fast lane changes (Equation D.1) are affected by the proposed modifications as well. However, in this case, it is mainly the front gap that the current vehicle allows for to be affected. It represents a gentler manoeuvre than the cut-in described above. Figure D.4 can also be qualitatively regarded as the lead gap allowed for when a vehicle moves to the fast lane. In fact, with the proposed formulations, a vehicle will generally allow for a shorter gap when its new leader in the fast lane is faster.

D.3.4 Macroscopic results

Figure D.6a shows the difference between the IDM and its two modifications in terms of number of lane changes during a 30-min simulation with the parameters shown in Table 3.1. The IDM returns almost half of the number of lane changes compared to the two modification cases. This is due to the large gap required in order to undertake a lane-changing manoeuvre (Figure D.5). If the desired speed, $v_{0,\text{car}}$, is chosen to be 96 km/h, the number of lane changes

for the IDM is roughly the same of the case with $v_{0,car} = 120$ km/h, while it is expected to have fewer. Conversely, this does happen in the two modifications. Finally, the exponential modification leads to 10% fewer lane changes than the IDM because of the larger gaps (see Figure D.5 around $\Delta v = -16$ km/h).

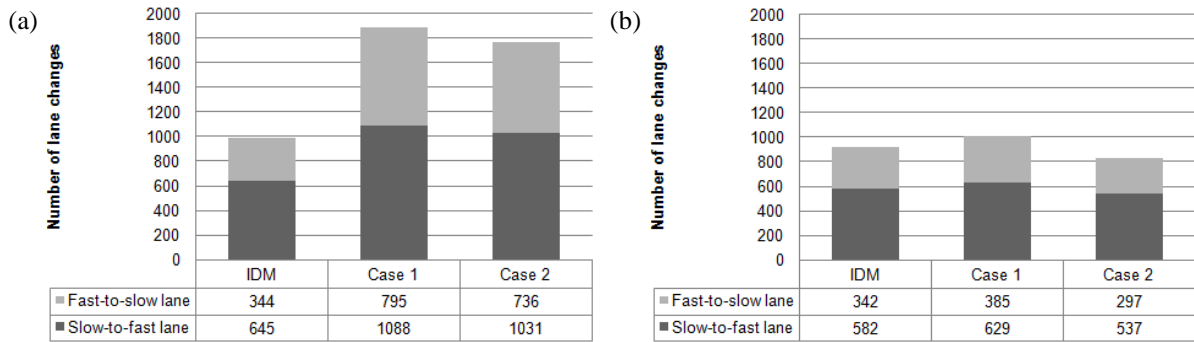


Figure D.6 - Number of lane change events for (a) $v_{0,car} = 120$ km/h and (b) $v_{0,car} = 96$ km/h.

Finally, it is interesting to see to which extent the proposed modifications affect the simple IDM car-following behaviour. Since the proposed modifications affect the driver response only when there is a speed difference between two consecutive vehicles, free traffic is not suitable for testing. Therefore congestion is introduced by increasing the inflow to 2190 veh/h and increasing the safe time headway, T , downstream. The safe time headway is $T = 1.2$ s from 0 to 2700 m (see Table 3.1), then increases linearly to 3300 m where it reaches the value $T' = 1.8$ s. Figure D.7 plots the density in the area next to the inhomogeneity (from 2000 to 2500 m) during the 30-minute simulation.

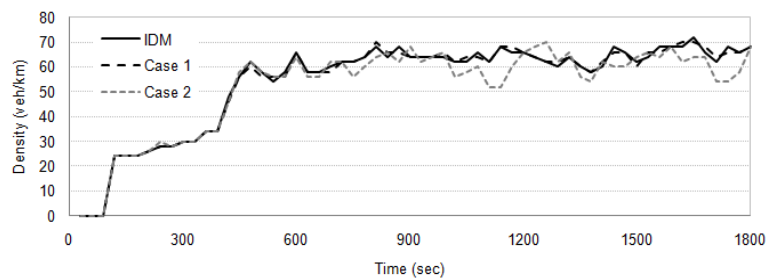


Figure D.7 - Density in single-lane congested traffic.

It can be seen that the difference is negligible for Case 1 and modest for the exponential decay. In the latter case, the maximum difference in a single value is 23.5%, while on average the density is lower by 3%. This happens because the speed differences are limited during the

single-lane simulations and in this range case 1 is similar to the IDM, while case 2 provides higher gaps (Figure D.5).

D.3.5 Summary

The use of the IDM coupled to MOBIL returns some unrealistic behaviour. In fact, MOBIL is based on an acceleration advantage criterion, with all the accelerations calculated according to the IDM. In particular, this leads to an inconsistent trend in the allowed gaps during lane change manoeuvres when a vehicle cuts in faster in front of another, which is quite a common situation in multi-lane simulations.

Available field observations are used in order to define possible modifications. Two simple modifications are tested: they reflect real driver behaviour, do not significantly increase model and computational complexity and do not twist the model concept. One modification limits the desired minimum gap s^* to the minimum jam distance s_0 (Equation D.6), while the other propose an exponential formulation for the desired minimum gap s^* (Equation D.7). They both lead to similar results, providing a consistent lane-changing behaviour, whereas they do not significantly change the car-following behaviour in single-lane traffic. Equation (D.6) is then used for the simulations carried out in this thesis, as it is simpler and allows faster simulations.

D.4 Combination of IDM and MOBIL: platoon modification

As shown in Section B.2.1, when a vehicle approaches its desired speed $v \rightarrow v_0$, the IDM equilibrium gap $s_e \rightarrow \infty$, which leads to an excessive spreading of platoons. Treiber and Kesting (2010) outline a modification to solve the unrealistic spreading of vehicles close to the desired speed. Such a modification is reported and tested in the following. The modified IDM formulation depends on the ratio between the desired minimum gap s^* and the actual gap s . If the desired minimum gap s^* is greater than the actual gap s , which is clearly not a comfortable situation, the acceleration is:

$$\frac{dv(t)}{dt} = a \left[1 - \left(\frac{s^*(t)}{s(t)} \right)^2 \right] \text{ for } \frac{s^*(t)}{s(t)} > 1 \quad (\text{D.13})$$

If the desired minimum gap s^* is smaller than the actual gap s , which is a comfortable situation, the acceleration is:

$$\frac{dv(t)}{dt} = a_{free}(t) \cdot \left[1 - \left(\frac{s^*(t)}{s(t)} \right)^{\frac{2a}{a_{free}(t)}} \right] \text{ for } \frac{s^*(t)}{s(t)} < 1 \quad (\text{D.14})$$

where a_{free} is the acceleration on a free road, as in the original IDM formulation (Equation 2.1) when $s \rightarrow \infty$:

$$a_{free}(t) = a \left[1 - \left(\frac{v(t)}{v_0} \right)^4 \right] \quad (\text{D.15})$$

Figure D.8 shows the time-history of the acceleration and the gap resulting from two vehicles starting at 50 km/h and 50 m apart. They both approach their desired speed $v_0 = 80$ km/h. The other parameters are as in Table 2.3. The accelerations of the two vehicles are shown in Figure D.8a. The lead vehicle (Vehicle 1) approaches its desired speed according to Equation (D.15), while the follower (Vehicle 2) accelerates according to Equation (D.14), as it results $s^*/s < 1$. As it can be seen in Figure D.8b, the gap increases indefinitely in the original formulation, while in the modified formulation the gap stabilises shortly.

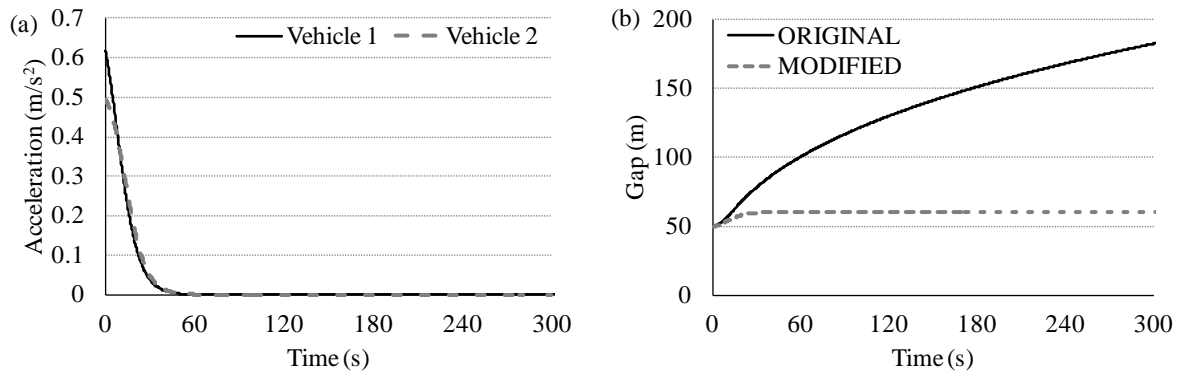


Figure D.8 - IDM modification: (a) acceleration of leader and follower and (b) gap.

There is hardly any difference in braking situations. In this case, Equation (D.13) governs. In fact, when $v \rightarrow 0$, the original formulation tends to Equation (D.13).

The equilibrium gap s_e can be found imposing $dv/dt = 0$ in Equation (D.13) and $\Delta v = 0$ in the desired minimum gap s^* (Equation 2.2):

$$s_e(v) = s_0 + Tv \quad (\text{D.16})$$

Equation (D.16) leads to a linear relation between the equilibrium gap and speed. Field observations show that the equilibrium gap follows a quasi-linear trend, as speed increases (Brackstone et al., 2002). The equilibrium gap is shown in Figure D.9a for identical vehicles with parameters as in Treiber et al. (2000) (Table B.1). Figure D.9b shows that the equilibrium time gap flattens out as speed increases.

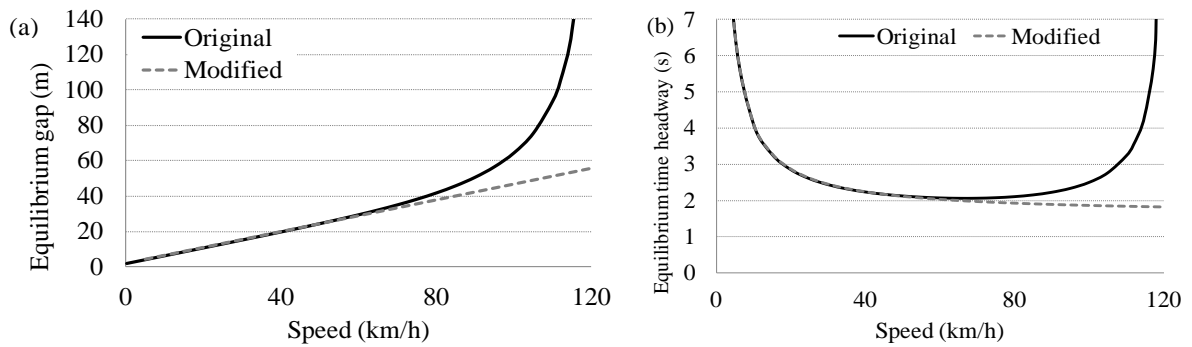


Figure D.9 - IDM modification: (a) equilibrium space gap and (b) time gap.

The equilibrium flow $Q_e(v)$ is given by:

$$Q_e(v) = \frac{v}{s_e(v) + l} = \frac{v}{s_0 + Tv + l} \quad (\text{D.17})$$

It has no peak anymore (Figure D.10a) and the maximum value, that is the static capacity Q_{\max} , occurs at the desired speed v_0 . The modification involves also a change of shape of the fundamental diagram (Figure D.10b). The static capacity Q_{\max} is now higher by 14% (1986 veh/h).

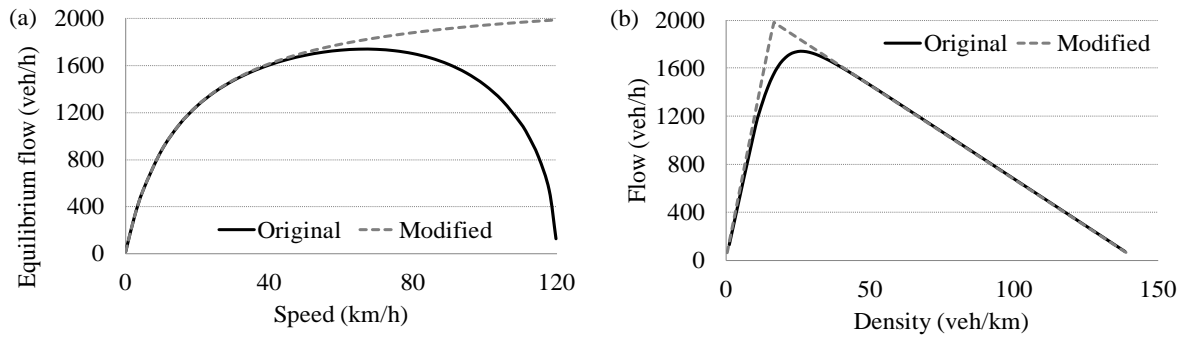


Figure D.10 – IDM modification: (a) equilibrium flow and (b) fundamental diagram.

In conclusion, the introduction of this modification should not affect congestion, since congested speeds are much lower than the desired speed v_0 and the congested branch of the fundamental diagram remains unchanged (Figure D.10b). However, it may affect the car-following behaviour in busy traffic close to capacity.

The issue of the large gaps at speeds close to the desired speed v_0 may be limited by introducing random distributions of desired speed, in order to decrease the chances of having a vehicle following its leader at its desired speed.

Therefore, the modification has not been implemented in SIMBA, as it would also certainly increase the computational burden. Further research may implement the modification and test it with full traffic simulations, with special regards to the truck platoon formation at flows close to capacity.

D.5 Calibration of the lane-changing model

The IDM parameters used in Kesting et al. (2007) (Table D.1) differ from the ones used in Treiber et al. (2000) (Table B.1). They have lower safe time headway T , which leads to a higher capacity, and greater maximum acceleration a , which leads to a more stable flow. Table D.2 shows that the static capacities Q_{\max} calculated with the IDM parameters in Kesting et al. (2007) are greater than the ones using the IDM parameters in Treiber et al. (2000). Capacities are calculated according to Equations (B.3) and (B.8), where trucks are 12 m long and have desired speed $v_0 = 80$ km/h. Note that the 2-lane capacity is generally less than twice the single-lane capacity, due to the effects of lane change manoeuvres.

Table D.2 – Static capacity for single-lane traffic.

Car length l (m)	Trucks (%)	Q_{\max} Kesting et al. (2007)	Equilibrium gap (m)	Equilibrium speed (km/h)	Q_{\max} Treiber et al. (2000)
5	0	2192	27.0	70.1	1743
4	0	2263	26.2	68.3	1790
4	10	1994	20.1	49.6	1610
4	20	1932	20.6	50.5	1567
4	30	1875	21.0	51.4	1529
4	40	1823	21.4	52.1	1492
4	50	1773	21.8	52.8	1457

Most importantly, with the parameter set in Kesting et al. (2007) it is not possible to reproduce stop-and-go waves. The parameters are as in Table D.1, where the politeness factor p is set to 0.15. Figure D.11a shows the speeds resulting from the capacity flow $Q_{\text{in}} = Q_{\max} = 1932$ veh/h/lane (20% trucks, Table D.2) and the application of a small inhomogeneities $\Delta T = 0.15$ s, that is where oscillatory traffic is expected to arise. As it can be seen there are no waves, but the congested speeds are rather constant, suggesting homogeneous congested states (HCT).

Figure D.11b shows the speeds when all the trucks are injected in the slow lane. The inflow is generated according to Table D.2 for the case of 40% trucks: therefore in the slow lane is $Q_{\text{in},1} = Q_{\max} = 1823$ veh/h/lane, whereas in the fast lane results $Q_{\text{in},2} = 2040$ veh/h/lane. The same small inhomogeneity $\Delta T = 0.15$ s is applied. It can be seen that the slow lane (Lane 1) goes to a HCT state, similarly to Figure D.11a, whereas the faster Lane 2 remains uncongested.

Therefore, the MOBIL parameters are calibrated using the IDM parameters based on Treiber et al. (2000), in order to reproduce the observed congestion patterns. The parameters are the same used in Chapter 2, where trucks are introduced with desired speed $v_0 = 80$ km/h (Table D.3).

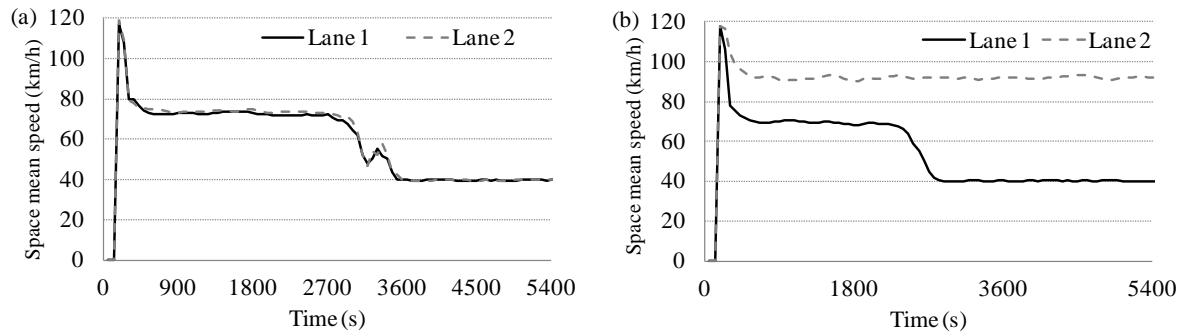


Figure D.11 - Space mean speed with parameters from Kesting et al. (2007): (a) trucks equally injected in the two lanes and (b) only in the slow lane.

Table D.3 - IDM parameters.

Parameter	Cars	Trucks
Desired speed, v_0	120 km/h	80 km/h
Safe time headway, T	1.6 s	1.6 s
Maximum acceleration, a	0.73 m/s ²	0.73 m/s ²
Comfortable deceleration, b	1.67 m/s ²	1.67 m/s ²
Minimum jam distance, s_0	2 m	2 m
Vehicle length, l	4 m	12 m

The version of SIMBA used for calibration is the 1.3.0, released on 30 May 2012. Such release features a reorganization of the sequence of updating vehicle accelerations, lane changes, and positions. Tests with previous versions showed a high sensitivity of lane change rates with the simulation steps, which was not detected in Kesting et al. (2007), and these issues are resolved in SIMBA 1.3.0 (see also Section F.2).

In Kesting et al. (2007), vehicle speeds are uniformly distributed over the range $\pm 20\%$, as this introduces heterogeneity in the flow and thus enhances lane changes, as illustrated in Figure D.12 for free traffic. The introduction of randomness in the desired speed also limits the spreading of platoon, which occur when two vehicles are going at the same desired speed (Section D.4).

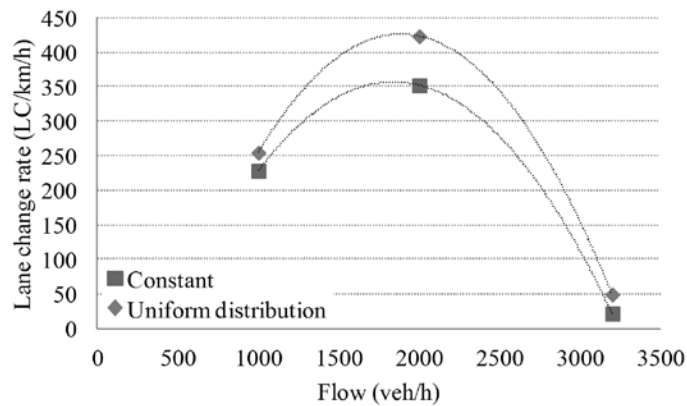


Figure D.12 - Lane change rates with constant and uniformly distributed desired speed.

However, experience and research suggest that trucks typically have a smaller range of speeds than cars (Knospe et al., 2002). Figure D.13 shows the speed histogram of about 260 000 vehicles (25% trucks) crossing several WIM stations in Sweden in 2004. 81% of the trucks have speed included in a 4 m/s range (14.4 km/h), while cars are spread over a wide range. Therefore, the truck desired speed range is dropped to $\pm 10\%$.

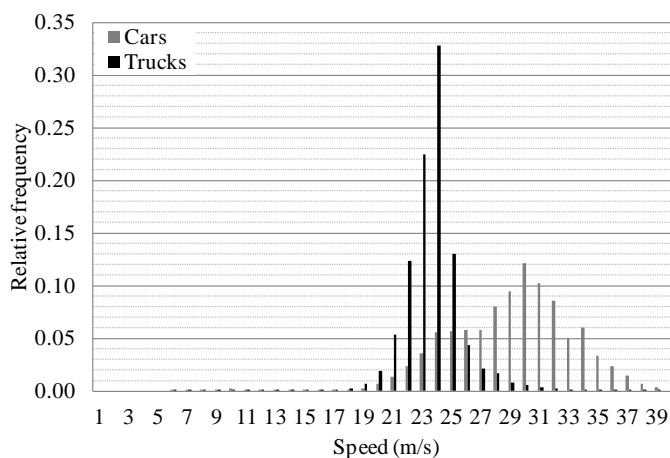


Figure D.13 - Speed histogram of vehicles from WIM stations in Sweden.

Five MOBIL parameters sets are tested and reported in Table D.4. The first part of the calibration involves the acceleration threshold Δa_{th} and the bias acceleration Δa_{bias} ; the politeness factor p is then chosen in order to reproduce the observed peak of between 550 and 650 LC/km/h at 2000 veh/h (Sparmann, 1979; Yousif and Hunt, 1995); the safe braking is initially taken constant as $b_{safe} = 4 \text{ m/s}^2$, as in Kesting et al. (2007), and it will be calibrated later.

A first constraint is $\Delta a_{\text{bias}} \geq \Delta a_{\text{th}}$ (Kesting et al., 2007). Secondly, the acceleration that a car following a truck going at its desired speed $v_{0,\text{tr}} = 80$ km/h can gain would be at most 0.58 m/s^2 . Therefore, it is necessary to ensure that $\Delta a_{\text{th}} + \Delta a_{\text{bias}}$ is well below 0.58 m/s^2 , otherwise most lane changes will be prevented.

In Set 1, Δa_{bias} and Δa_{th} are taken from Kesting et al. (2007). Since $\Delta a_{\text{bias}} > \Delta a_{\text{th}}$, vehicles move back to the slow lane, even though this may lead to an acceleration loss. This can be seen from Equation (D.2), where the acceleration gain $\tilde{a}_c - a_c$ must be greater than $\Delta a_{\text{th}} - \Delta a_{\text{bias}} = -0.2 \text{ m/s}^2$, when $p = 0$ or there are no disadvantages for the followers n and o . During busy traffic it might be unlikely that a car would move back to the slow lane at a cost of a disadvantage. In Set 2, Δa_{bias} and Δa_{th} are taken from Treiber (2011). In this case $\Delta a_{\text{bias}} = \Delta a_{\text{th}}$: vehicles move back to the slow lane only if this generally implies no acceleration loss ($\Delta a_{\text{th}} - \Delta a_{\text{bias}} = 0 \text{ m/s}^2$). In the following we say that Set 1 is “*strongly asymmetric*” and more asymmetric than Set 2. Set 4 is another strongly asymmetric set, while 3 and 5 are not. Note that Set 4 and 5 differ only for the bias acceleration Δa_{bias} .

Table D.4 – MOBIL parameter sets for calibration.

Parameter	Set				
	1	2	3	4	5
p	0.15	0.1	0.15	0.2	0.2
$\Delta a_{\text{bias}} \text{ (m/s}^2\text{)}$	0.3	0.2	0.15	0.15	0.1
$\Delta a_{\text{th}} \text{ (m/s}^2\text{)}$	0.1	0.2	0.15	0.1	0.1
$b_{\text{safe}} \text{ (m/s}^2\text{)}$	4	4	4	4	4

D.5.1 Free Traffic

Eight hours of simulation are run for each parameter set and the average lane change rates are reported in Figure D.14. The traffic stream includes 20% trucks, which are all injected in the slow lane. It is found that lane change rates are rather sensitive to the inflow, when this is approaching capacity. An inflow 1% smaller than the 3000 veh/h reported in Figure D.14 increases the lane change rates by about 50% (not shown in the figure). It does appear that as traffic approaches capacity, the lane change rates decrease drastically.

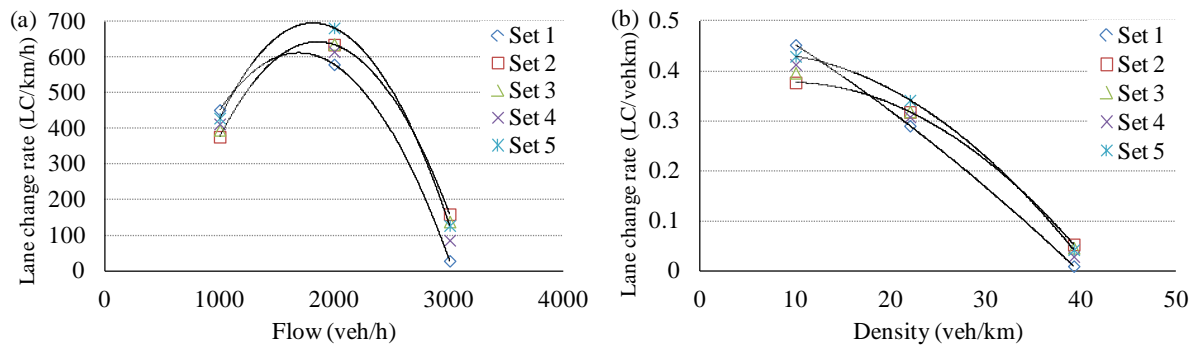


Figure D.14 – Lane change rates per km and per hour (a) and per vehicle km travelled (b).

The lane change rates (LC/km/h) show a good match with the available observations at 1000 and 2000 veh/h, but they are under-estimated at 3000 veh/h, where lane change rates between 250 and 400 LC/km/h are reported (Sparmann, 1979; Yousif and Hunt, 1995). In fact, the traffic flow is close the IDM capacity, and limited gaps are available. However, the IDM capacity is lower than most capacities observed (Transportation Research Board, 2010) and this may explain the discrepancy.

When compared to Knoop et al. (2012), lane change rates (in LC/vehkm) are slightly under-estimated at 2000 veh/h. Knoop et al. (2012) have no data available for density greater than 30 veh/km in the Dutch site. The British M42 site has some data of busy traffic (up to 70 veh/km), but lane change rates are on the whole rather high, possibly due to mandatory lane changes.

In general, the strongly asymmetric Set 1 has a high rate at low inflows, while the lowest at other inflows. Set 2 (low p) has the highest LC rate at high inflows and therefore it is the closest set to the observations. It is set 5 (low Δa_{bias} and Δa_{th}) to have the highest lane change rate at medium inflows. It seems that the politeness factor p mainly affects lane-changing at high inflows, where the interaction between vehicles is strong.

Simulations have shown that in some cases immediately after a lane change takes place, the new follower changes lane, effectively performing a *lane swap*. This can be seen in Figure D.15, where the position and time of all the lane changes on a sample simulation are plotted. Lane swaps can be recognised as a bunching of data points, which indicates that many lane changes are taking place at the same time and point. This may be noticed also in the online applet (Treiber, 2011).

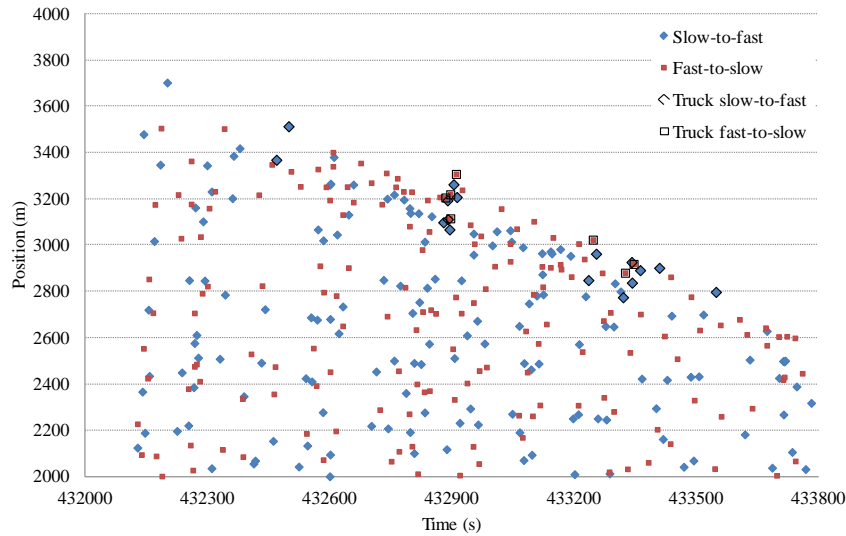


Figure D.15 - Evidence of lane-swapping (note the few truck lane changes).

The percentage of trucks moving to the fast lane gives a rough indication of the lane-swapping, as the slower trucks are expected to stay in the slow lane. If the lane swaps are excessive, several trucks end up in the fast lane, and faster vehicles may overtake them in the slow lane, especially in busy flows. Therefore, another indicator of lane-swapping is the speed difference between lanes.

The strongly asymmetric sets 1 and 4 have the least trucks on the fast lane and the highest speed difference at any inflow (Figure D.16). This is expected, as the condition $\Delta a_{\text{bias}} > \Delta a_{\text{th}}$ lets more trucks stay in the slow lane. Set 5 has the smallest thresholds Δa_{bias} and Δa_{th} and the highest percentage of trucks in the fast lane at 1000 veh/h and 2000 veh/h. Set 4 has fewer trucks and greater speed differences than set 5, due to the highest bias acceleration Δa_{bias} . Set 2 (small p) has the highest number of trucks in the fast lane among 3000 veh/h and the smallest speed difference between lanes.

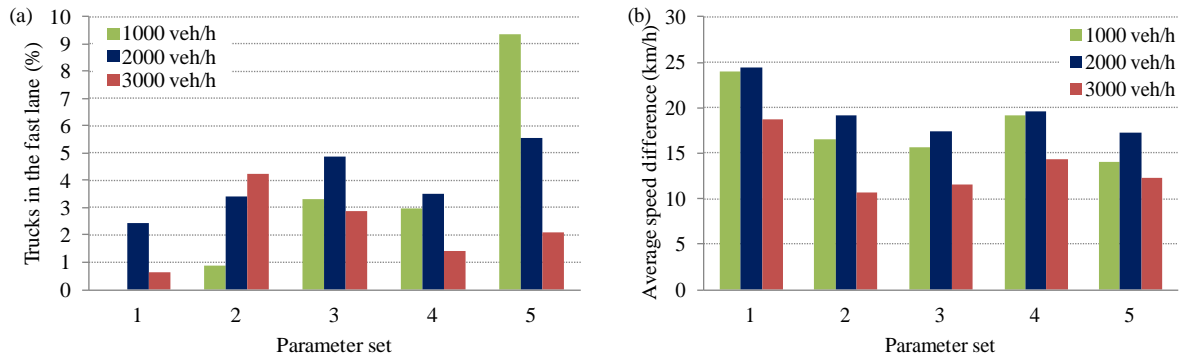


Figure D.16 - Percentage of trucks on the fast lane (a) and speed difference between lanes (b).

Cumulative frequency plots can be used to represent the truck platoons. They give the percentage of trucks travelling in platoons equal or smaller than a given size. The truck platoons in the slow lane for the flow of 2000 veh/h are shown in Figure D.17. Set 2 (low p) is the most platooning, with 15.2% trucks travelling in platoons of 6 or more (11.8% 7+). Set 5 is the least platooning with 8.5% in 6+ platoons (3.7% 7+).

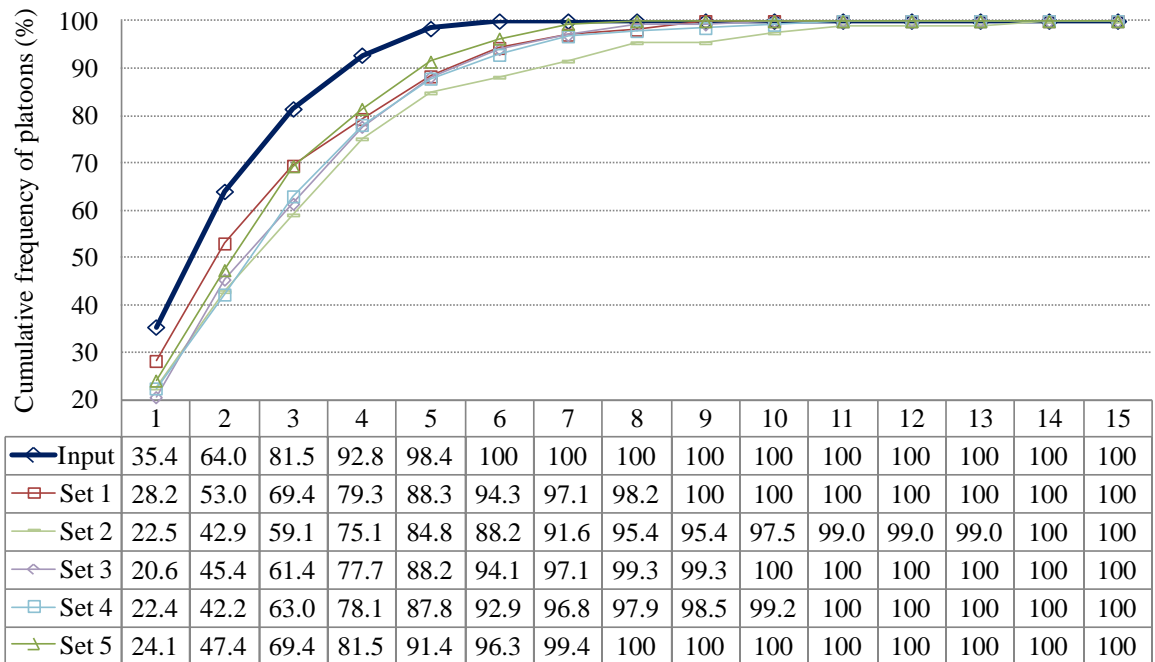


Figure D.17 - Cumulative frequency of truck platoons (2000 veh/h).

Figure D.18 shows the cumulative frequency of truck platoons, at inflow 3000 veh/h. It can be seen that the platooning effect is not as strong as when the inflow is 2000 veh/h. Set 2 is not

the most platooning anymore (it has only 1% of 7+ platoons): it is the set with the highest lane change rate at 3000 veh/h (Figure D.14) and possibly this greater activity makes the trucks go to the fast lane and break the platoons. Set 3 is the most platooning (4.7% of 7+ platoons), followed by Set 5 (3.8% of 7+).

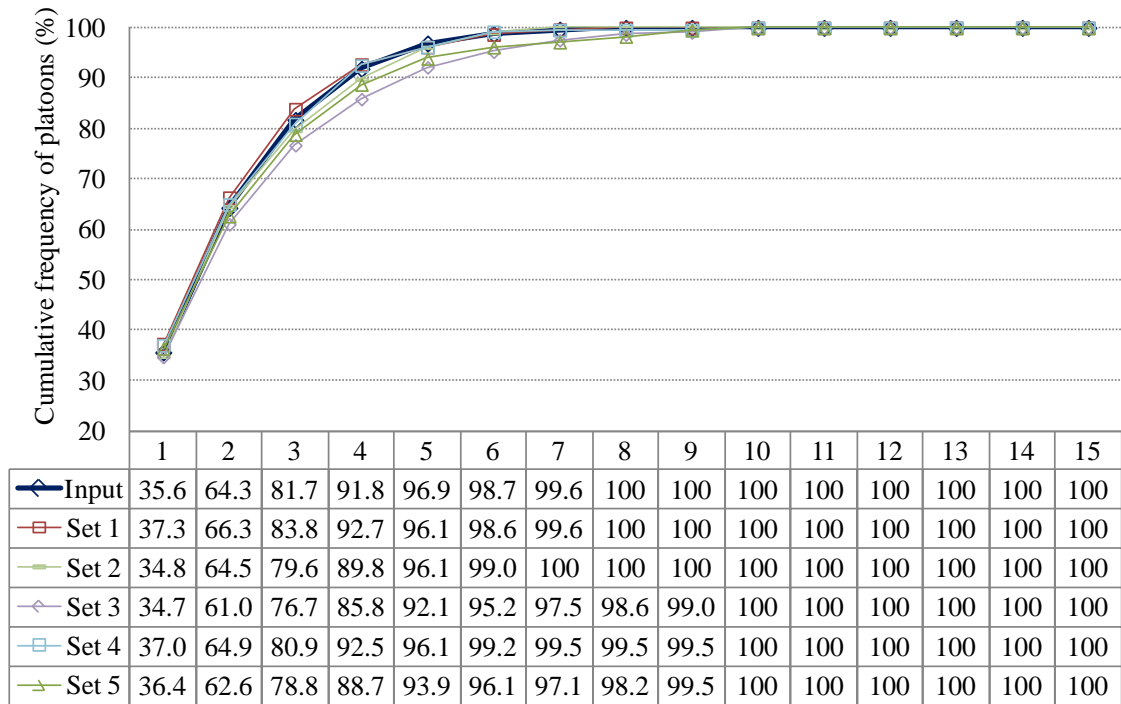


Figure D.18 - Cumulative frequency of truck platoons (3000 veh/h).

D.5.2 Congestion

To examine congestion under each parameter set, 8 one-hour simulations are run for each set. Three congestion levels are generated with inflow $Q_{in} = 3000$ veh/h and inhomogeneities $\Delta T = 0.3, 0.6$ and 1.2 s, which return reduced dynamic capacity $Q'_{out} = 2800, 2465$ and 1985 veh/h. The congested states are SGW, OCT and HCT/OCT, confirming that the introduction of the lane-changing model does not limit the ability of the IDM to reproduce congested states. Figure D.19 shows that the lane change rates are expectedly smaller than the free traffic case (Figure D.14a). The strongly asymmetric sets return the lowest lane change rates, as it was in the free traffic case for the same inflow of 3000 veh/h.

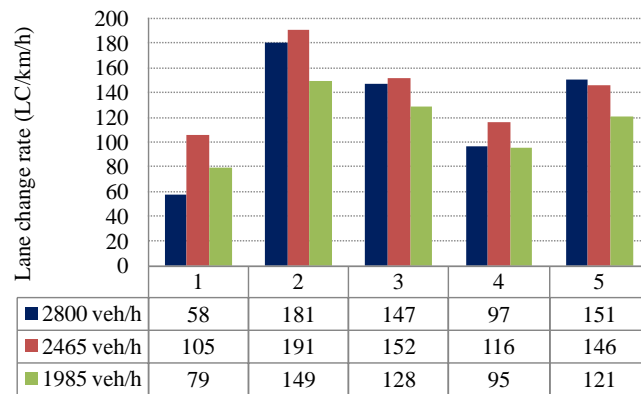


Figure D.19 - Lane change rates for different congested outflows for each MOBIL parameter set.

The percentage of trucks in the fast lane reflects the free traffic findings, that is highest with Set 2 (low p) and lowest for sets 1 and 4 (Figure D.20a). The plot of the average speed difference between lane 1 and 2 shows that, for stronger congestions, the slow lane is actually faster (Figure D.20b).

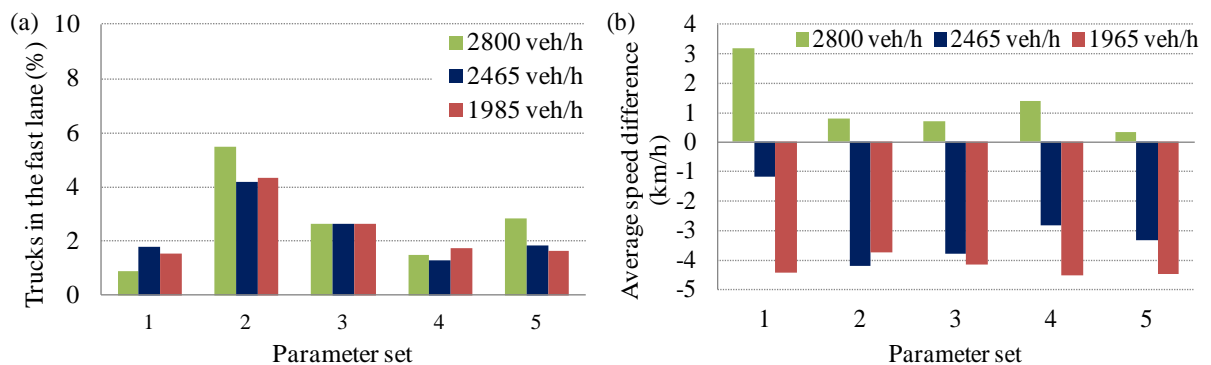


Figure D.20 - Percentage of trucks in the fast lane (a) and speed difference between lanes (b) for different congested outflows.

Regarding the platooning effect, there is hardly any difference between the sets, as they do not lead to a strong truck platoon formation (Figure D.21). Set 3 offers slightly more platooning, while the longest platoon size occurs with Set 4.

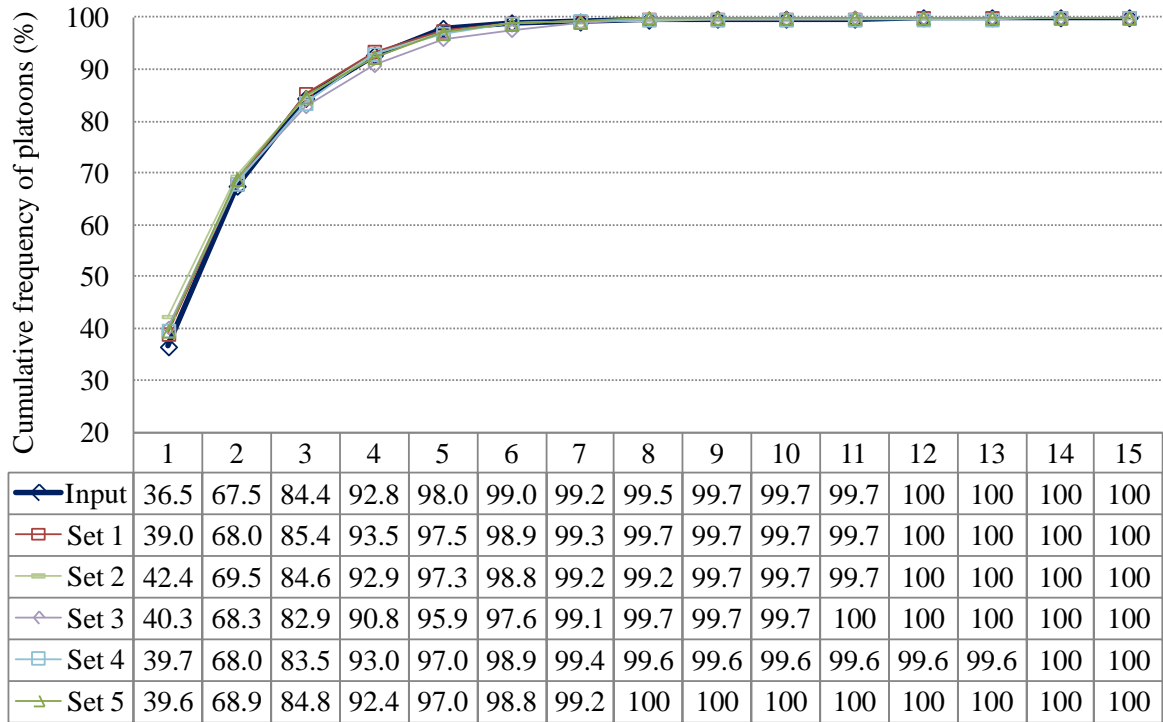


Figure D.21 - Cumulative frequency of platoons ($Q'_{out} = 2800$ veh/h).

The hourly maxima of total load on a 200 m span are captured for each congested outflow Q'_{out} and parameter set for the two lanes separately and combined. The load on the slow lane and on both lanes show little difference in the average values among different parameter sets (Figure D.22a,e): results are all within a $\pm 3.4\%$ range. The load in the fast lane is considerably lower and more erratic, due to the small proportion of trucks driving on that lane (Figure D.22c,d).

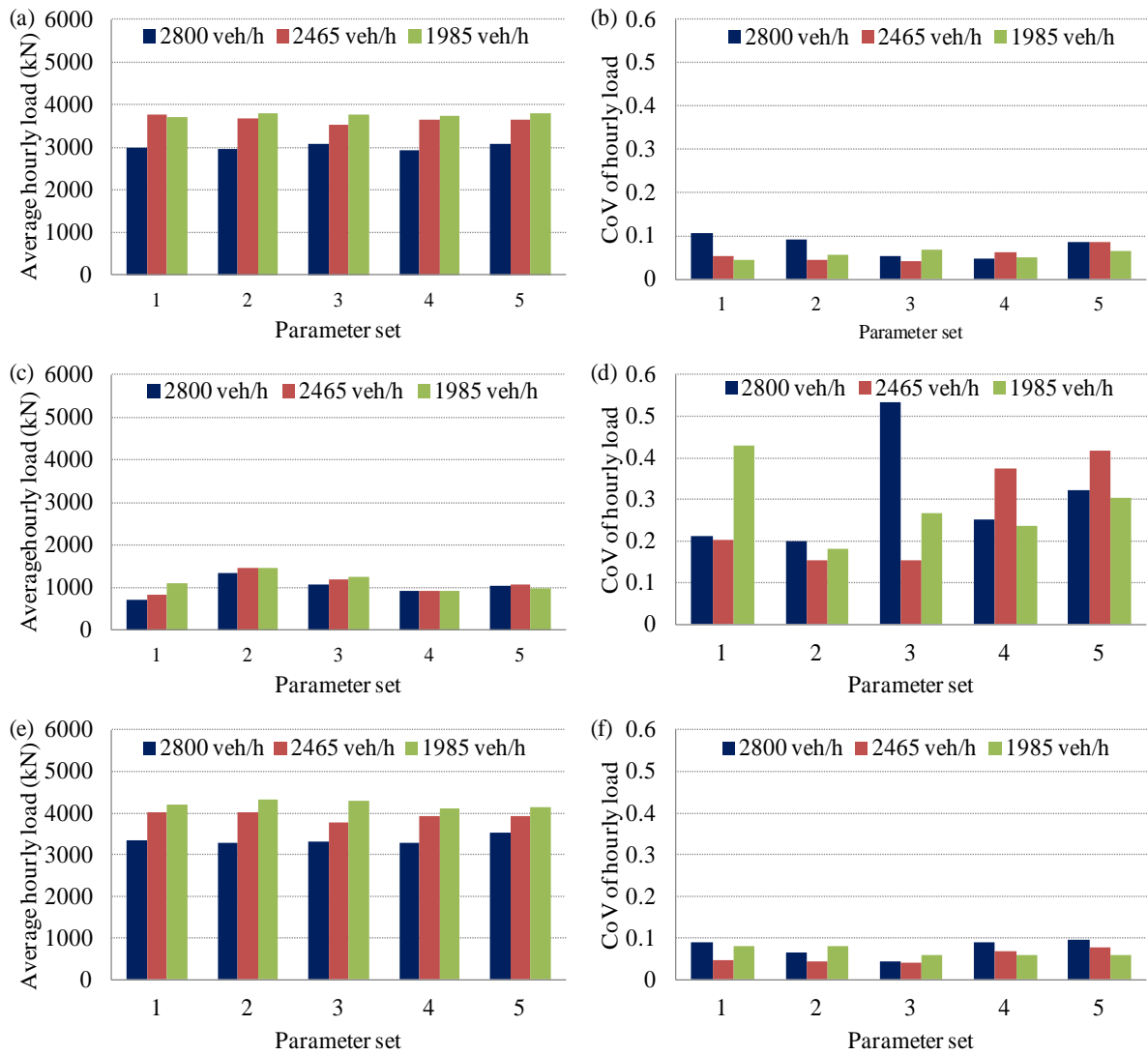


Figure D.22 - Total load on a 200 m span: average and coefficient of variation of hourly load for (a, b) slow lane, (c, d) fast lane and (e, f) both lanes.

To see the effects on extreme values, 96 one-hour simulations are run for each parameter set and with $Q'_{out} = 2800$ veh/h. Figure D.23a,b,c shows the probability paper plots of the hourly maxima of the load. As can be seen, the points are mostly superimposed. Figure D.23d shows the 5-year extrapolated values with the Gumbel distribution, assuming 250 hours of congestion for year. For details about probability paper and extrapolation, refer to Section 2.5.1. Set 2 seems to be the most critical, but differences are on the whole rather small (within $\pm 3.1\%$ for the slow lane, $\pm 5.2\%$ for the total load), except for the fast lane.

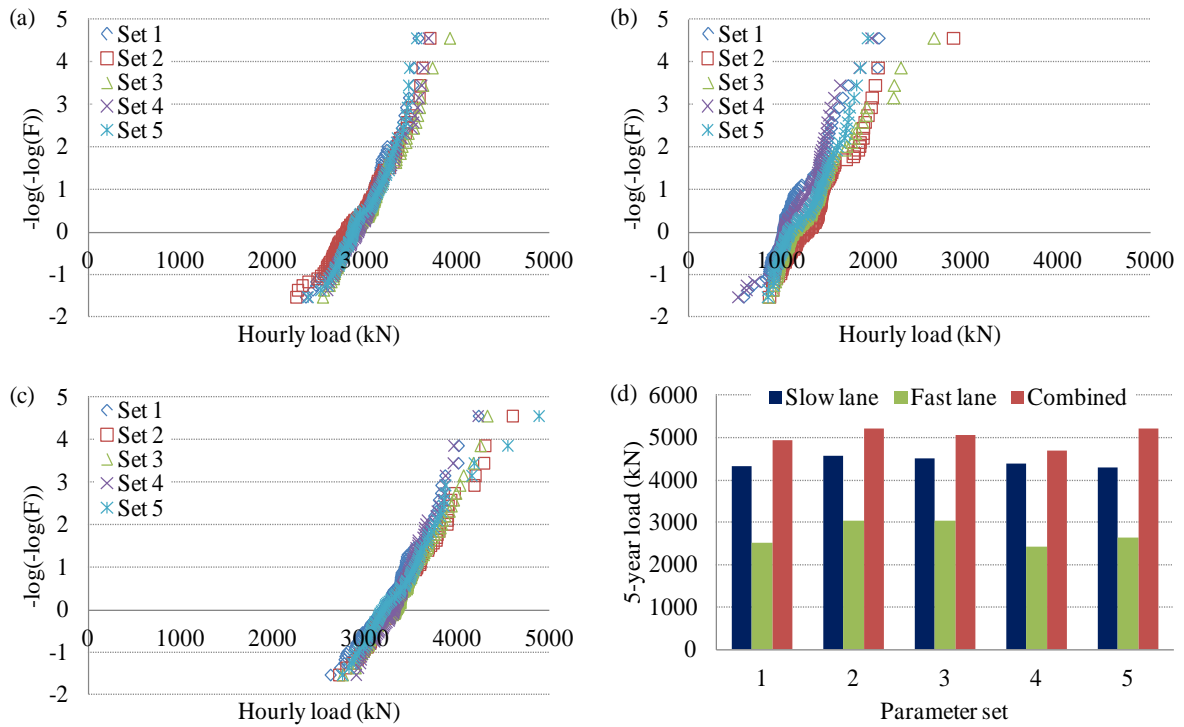


Figure D.23 - Probability paper of the total load on (a) slow lane, (b) fast lane and (c) combined lanes, and (d) 5-year extrapolated load.

D.5.3 Injection of trucks in the fast lane - Free traffic

In the previous analyses, all trucks are injected in the slow lane; here, 25% of the truck traffic is injected in the fast lane. Although the injection of trucks in the fast lane at low inflows is not realistic, it is tested for comparison. As shown in Figure D.24, the lane change rates have similar values of the case when trucks are all injected in the slow lane (Figure D.14a), except for the strongly asymmetric sets 1 and 4, which are now higher.

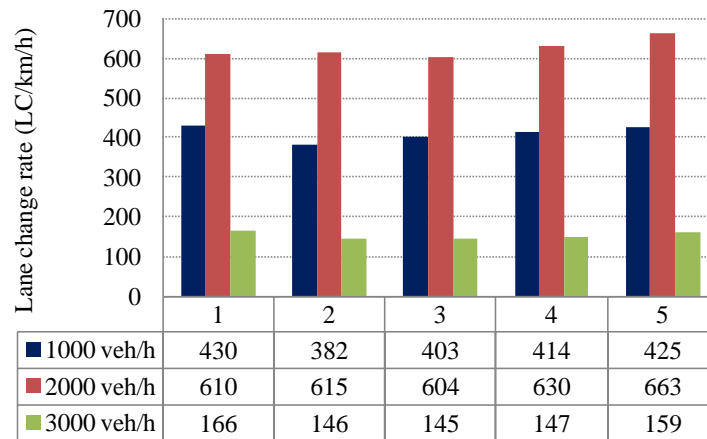


Figure D.24 - Lane change rates (25% trucks injected in the fast lane).

Figure D.25 shows that strongly asymmetric sets (1 and 4) bring more trucks back to slow lane. However, this does not happen at high inflow, where most trucks remain in the fast lane. Also the speed difference between the two lanes is low for high inflows, with no sharp difference between the sets. This is possibly to the blocking effect of trucks driving side-by-side.

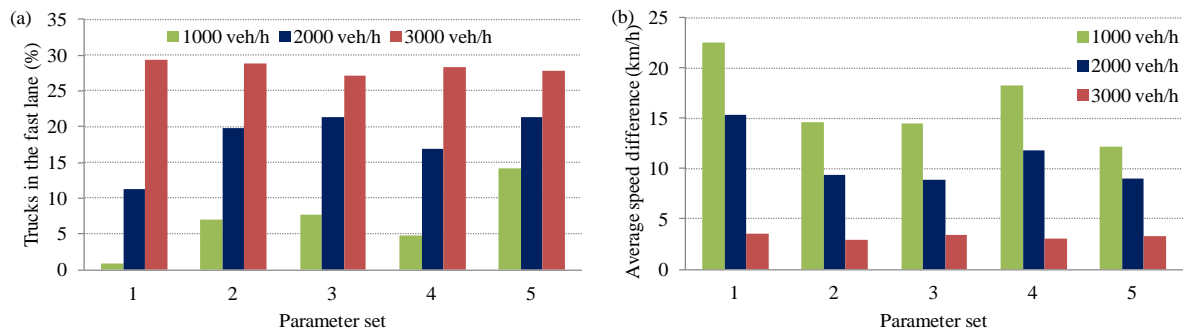


Figure D.25 - 25% trucks injected in the fast lane: (a) percentage of trucks on the fast lane and (b) speed difference between lanes.

D.5.4 Injection of trucks in the fast lane - Congestion

Figure D.26 shows the lane change rates for different reduced dynamic capacities Q'_{out} . When compared to the case of trucks injected only in the slow lane (Figure D.19), there is an increase for the strongly asymmetric sets 1 and 4, while the rates have the same order of magnitude for other sets, similarly to the free traffic case described in the previous section.

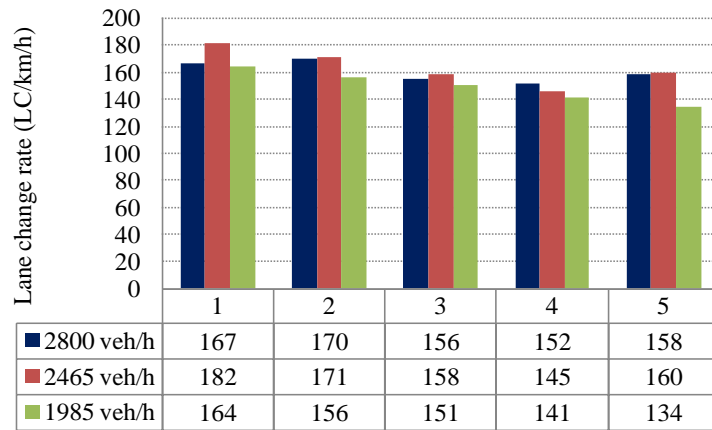


Figure D.26 - Lane change rates during congestion (25% trucks injected in the fast lane).

Trucks do not come back to the slow lane, with little difference between different sets (Figure D.27a), as seen for the free traffic with inflow 3000 veh/h (Figure D.25a). Figure D.27b shows that the "fast lane" is actually slightly slower, with small differences among sets.

A comparison of Figure D.28 with Figure D.22 shows that the slow lane is not significantly less loaded, while the fast lane is expectedly much more loaded. However, the load of the combined lanes becomes higher, with increases more significant for the strongest congestions.

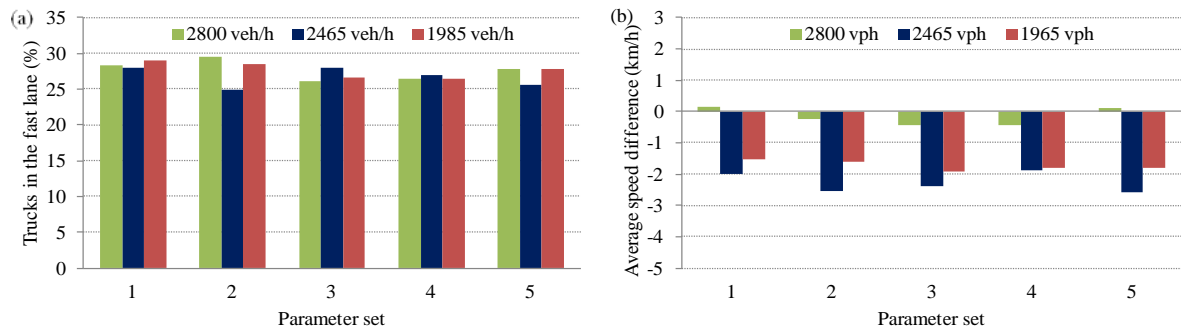


Figure D.27 - 25% trucks injected in the fast lane: (a) percentage of trucks on the fast lane and (b) speed difference between lanes for different reduced capacities.

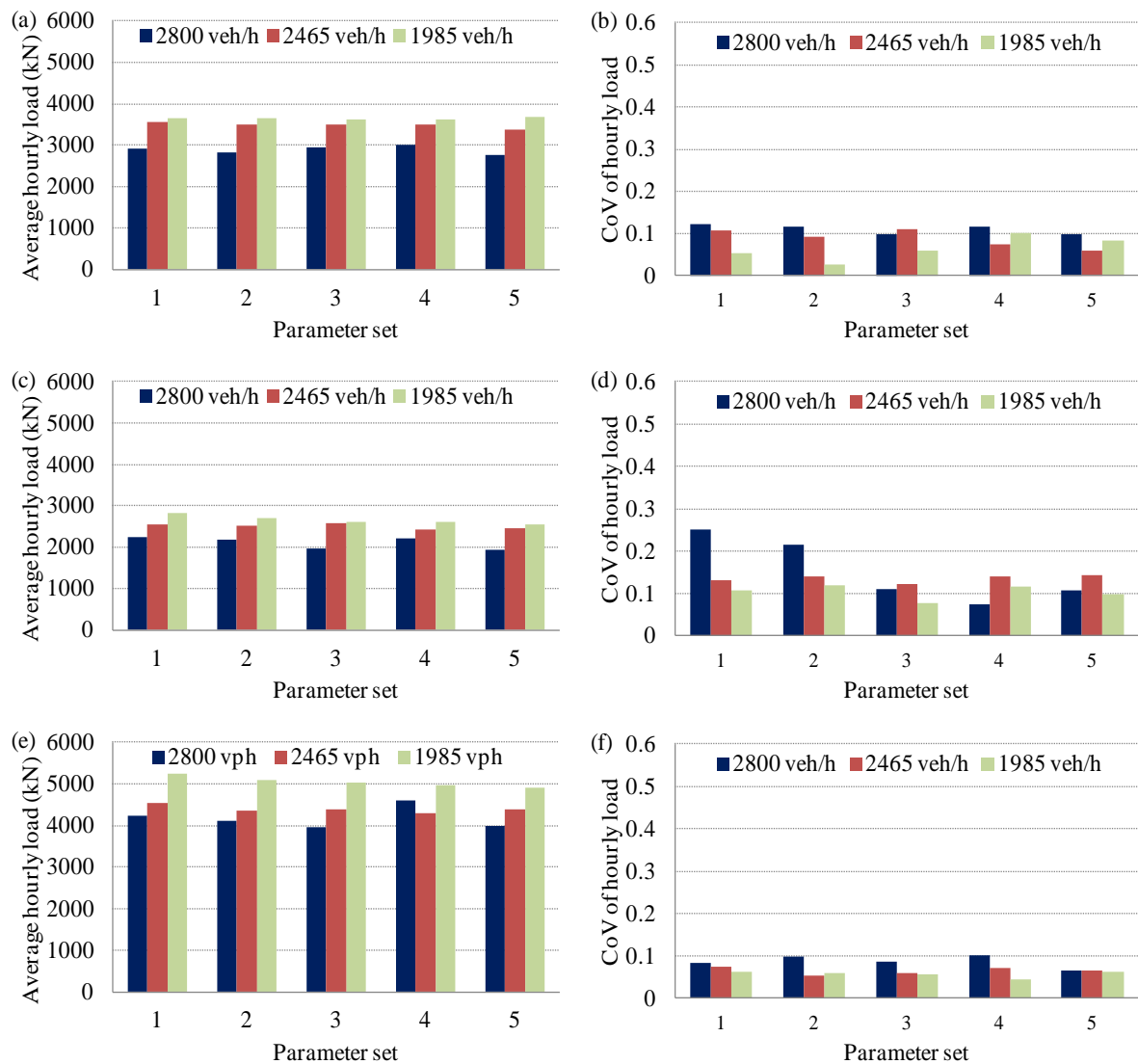


Figure D.28 - Total load on a 200 m span (25% of trucks injected in the fast lane): average and coefficient of variation of hourly load for (a, b) slow lane, (c, d) fast lane and (e, f) both lanes.

D.5.5 Summary

Five MOBIL parameter sets are tested for calibration. They are tested under free traffic conditions (1000, 2000 and 3000 veh/h) and under three congestion levels with inflow 3000 veh/h. Generally speaking, there is not a large difference among different sets. Some general remarks can be made:

- the politeness factor p seems to govern at high inflows, where the tested sets underestimate the field observations; indeed the set with the lowest p (Set 2) is the closest to the observations;

- the presence of trucks in the fast lane can be controlled by using a parameter set with $\Delta a_{\text{bias}} > \Delta a_{\text{th}}$ (Set 1 and 4); however these sets return low lane change rates at high inflows and during congestions;
- truck platooning is strong at 2000 veh/h, but at 3000 veh/h and during congestions is not; there is no large difference between sets;
- there are no large differences in the total load among parameter sets;
- when trucks are injected also in the fast lane, trucks do not go back to the slow lane at 3000 veh/h and during congestions; the load on the slow lane slightly decreases, while the load on both lanes increase.

D.6 Safe braking calibration

Simulations with the safe braking value suggested in Kesting et al. (2007) (Table D.4) have shown good match with available data at low and medium inflows, while lane change rates are under-estimated at high inflows (Figure D.14a). Calibration of the safe braking value is carried out here with the less asymmetric sets 2, 3 and 5, which are the ones closest to the observations.

The safe braking regulates the *safety criterion*:

$$\tilde{a}_n(t) > -b_{\text{safe}} \tag{D.18}$$

It is reasonable to expect that the safety criterion applies only at busy flows, as when traffic is lighter, there is no need to impose strong decelerations to the new follower and a lane-changing manoeuvre can be controlled with the incentive criteria (D.1) and (D.2). The situations when the safety criterion applies are first analysed, in particular the situations when the incentive criterion is passed, but the safety is not.

The imposed deceleration \tilde{a}_n depends not only on the parameter set, but also on the acceleration advantage of the current vehicle $\tilde{a}_c - a_c$ in performing the lane change. To pass the incentive criterion for a slow-to-fast lane change, the imposed acceleration \tilde{a}_n must be:

$$\tilde{a}_n \geq \frac{\Delta a_{th} + \Delta a_{bias} - (\tilde{a}_c - a_c)}{p} + a_n \quad (\text{D.19})$$

As it can be seen, the deceleration disadvantage that can be imposed on the new follower \tilde{a}_n linearly depends on the current vehicle advantage $\tilde{a}_c - a_c$, as the other parameters are set. Figure D.29 shows the relation under the assumption that $a_n = 0$.

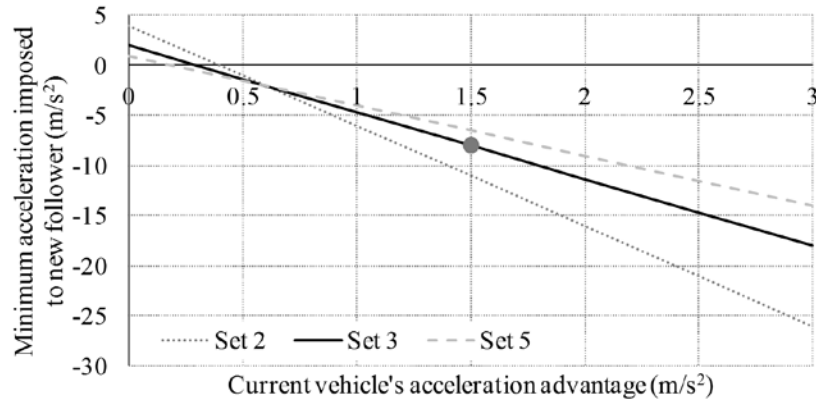


Figure D.29 - Minimum acceleration impossible to the new follower.

The results of Figure D.29 mean that, with Set 3, if the current vehicle acceleration advantage $\tilde{a}_c - a_c$ is 1.5 m/s^2 , the incentive criterion will be passed as long as it does not impose a deceleration \tilde{a}_n stronger than 8 m/s^2 , which is already rather high and close to the maximum possible deceleration. It is then the safety criterion to come into action and prevent the hard braking at the b_{safe} value. Moreover, there is more acceleration to gain when speeds are low, due to the non-linear relationships between speed and acceleration in the IDM, as the maximum acceleration a occurs at $v = 0$ (Equation 2.1). A great advantage can also arise when there is the opportunity to fill a gap in the fast lane.

A microscopic analysis of the vehicle motions over 1 km and 8 hours (collecting data every 3 s) shows that with inflow 3000 veh/h the actual strongest deceleration is 7.2 m/s^2 , when setting $b_{safe} = 9 \text{ m/s}^2$ (with only 26 instances with braking harder than the comfortable deceleration b), while it is 3.6 m/s^2 when setting $b_{safe} = 4 \text{ m/s}^2$. At 2000 veh/h, the strongest deceleration is 4.1 m/s^2 when setting $b_{safe} = 9 \text{ m/s}^2$, with 31 instances with braking harder than the comfortable deceleration b ; when setting $b_{safe} = 4 \text{ m/s}^2$, the strongest deceleration is again

3.6 m/s² with 27 instances with braking harder than the comfortable deceleration b . Therefore, this confirms that the safe braking value only affects the traffic behaviour at high inflows.

Figure D.30a shows the lane change rates with Set 3 and different safe braking b_{safe} values. It can be seen that high b_{safe} enhances lane change manoeuvres, but expectedly only at high flows. Figure D.30b shows the percentage of trucks moving to the fast lane. Again, the differences are significant only at high inflows, where the greater b_{safe} enhances the movement of trucks to the fast lane, possibly as a consequence of lane-swapping manoeuvres.

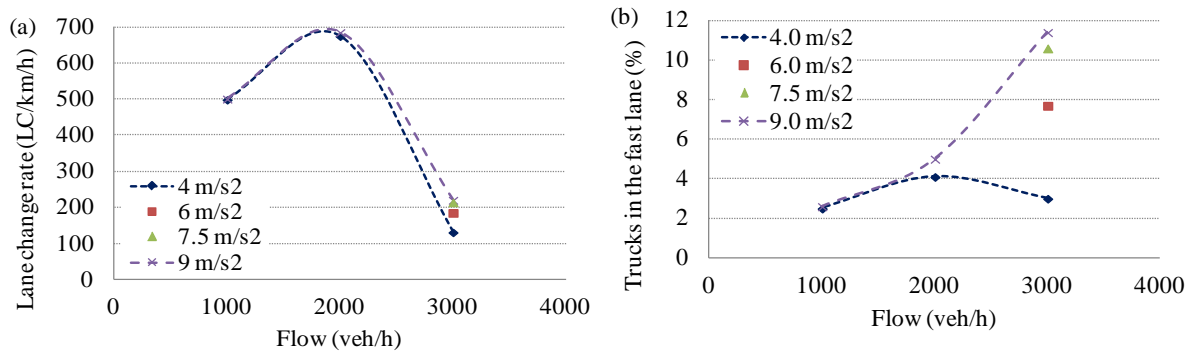


Figure D.30 – (a) Lane change rates and (b) truck traffic in the fast lane with Set 3 and different safe braking values.

Figure D.31 shows the effect of the safe braking b_{safe} on the lane change rates and on the percentage of trucks moving to the fast lane at the inflow of 3000 veh/h for Set 2 and 3. The effect of b_{safe} is non-linear and the lane change rate and truck percentage stabilise after a certain b_{safe} . When using Set 2, the safe braking values can be increased less than Set 3 to reach the lower bound of the observed lane change rates (250 LC/km/h).

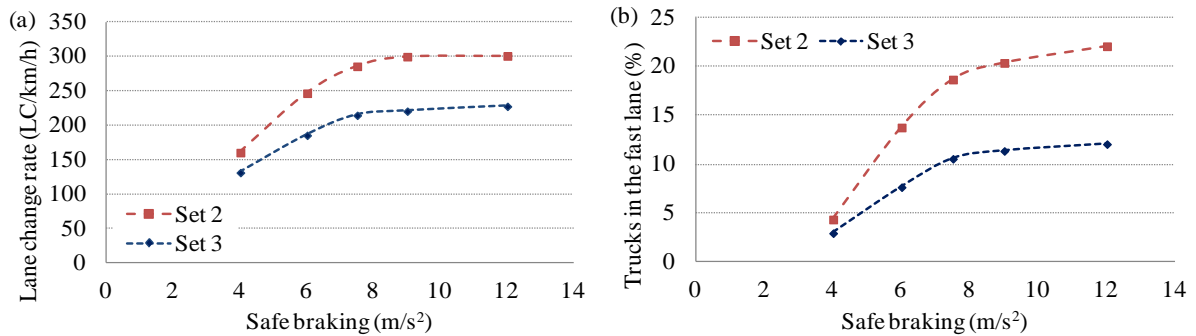


Figure D.31 – (a) Lane change rates and (b) truck traffic in the fast lane with Set 3 and 2.

D.6.1 Summary

Set 2 returns the closest match with observed lane change rates. However, these are underestimated at high inflows. The braking safe value affects the lane changes only at high inflows, therefore it is a suitable parameter to adjust. The safe braking value is then increased to $b_{\text{safe}} = 6 \text{ m/s}^2$, which return a lane change rate of 247 LC/km/h and 13.8% trucks on the fast lane. The final lane-changing parameter set is then based on Set 2 with $b_{\text{safe}} = 6 \text{ m/s}^2$ and it is reported in Table 3.2.

D.7 Lane distribution

This section analyses the effects of the lane-changing model on the distribution of traffic flow between lanes, for which there is available data in free traffic. The load distribution between lanes is also analysed under a variety of congestion states.

D.7.1 Flow distribution between lanes - Free traffic

Yousif and Hunt (1995) record a variable distribution of flow between lanes with the total flow for two-lane motorways in the United Kingdom. When traffic is light, the slow lane is mostly used. At 1500 veh/h, the split between lanes is about 50-50%. Over this flow, the fast lane carries a higher flow. At 3000 veh/h, 2/3 of the flow is in the fast lane. This may be due to the slowest speeds and to the influence of trucks in the slow lane. However, there are not many data points at high inflows to prove that in general.

Data about flow distributions in 2-lane motorways is modest. Wu (2006) indicates similar proportions from data from Germany up to 4000 veh/h. Lee and Park (2012) suggest similar trends in the US and relate lane distribution to density instead of flow, which is better for congested traffic. More data is available for 3-lane motorways (Golias and Tsamboulas, 1995; Knospe et al., 2002; Duret et al., 2012).

SIMBA simulations are carried out to check the lane distribution split. The split is checked at 5000 m over the total length of 8000 m and there are no inhomogeneities applied, as the available data does not include congestions.

In BTL5 package it is not possible to set different injection gaps and speeds across lanes for generating input files. However, when most trucks are injected in the slow lane, the slow lane flow is smaller, due to the greater length of trucks (see also Section F.4). For 20% trucks, all of which are injected in the slow lane, this typically results in an inflow split of about 47.5-52.5% across the two lanes. In this case, when injecting an inflow of 3000 veh/h, the outflow at the virtual detector returns about 46-54%, which is more balanced than that observed.

When injecting an inflow of 3000 veh/h with a lane split of 40-60%, generated with the combination of two single-lane inflows, the outflow split is about 44.5-55.5%. The inflow split is on purpose slightly more balanced than the observed 2/3 - 1/3, because the flow for the fast lane would exceed the capacity attainable with the IDM with only cars (Table B.2). Minimal changes are found across different MOBIL parameter sets.

At 1000 veh/h, the split is about 60-40% (Yousif and Hunt, 1995). This split is generated with two different single-lane flows and injected in SIMBA. The outflow split is rather balanced, 49-51% with set 3 and 5. The strongly asymmetric Set 1 makes the split 56-44%, due to the higher bias acceleration that brings cars back to the slow lane. When injecting the same total inflow with the same parameters across lanes, the outflow splits remain unchanged at 49-51% (Set 3 and 5) and 56-44% (Set 1).

In conclusion, the injection of flows with lane split closer to observations does not make a large difference in the outflow lane split from simulations. The outflow split is more balanced than the ones observed in real traffic and none of the tested MOBIL set could reproduce the observed lane distribution. Moreover, the injection of flow according to the observed data would require a re-calibration of the IDM parameters because for busy flows the fast lane may exceed the IDM capacity. Therefore, throughout this thesis, inflows are generated with the same injection parameters across lanes.

D.7.2 Flow distribution between lanes - Congestion

Figure D.32 shows the distribution of flow between lanes for the simulations reported in Section 3.3 with inflow $Q_{in} = 3000$ veh/h. The input file has 20% trucks, injected in the slow lane, and a lane split of 47.5-52.5%. It can be seen that there is no large difference between congested states.

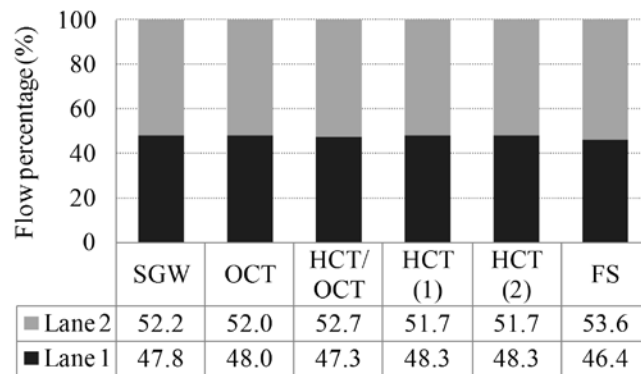


Figure D.32 - Flow lane distribution during congestion.

Figure D.33 shows the percentage of trucks over the slow lane traffic for the same simulations. It can be seen that there is no large variation among congested states: the 20% truck percentage on the total flow leads to an average 38% trucks in the slow lane.

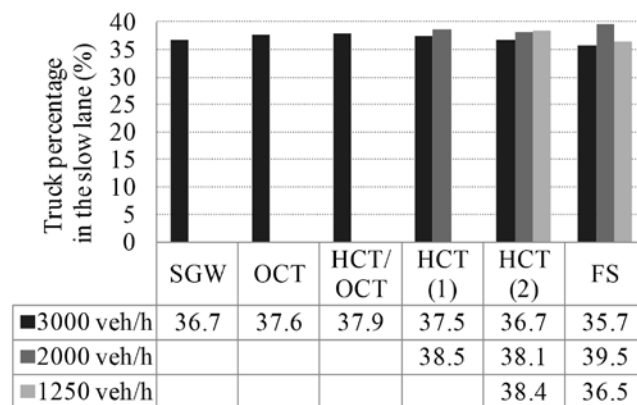


Figure D.33 - Truck percentage in the slow lane during congestion

D.7.3 Load distribution between lanes

This section reports the load distributions separately for the slow and fast lane for the simulations presented in Section 3.5.

Figure D.34 shows the probability paper plots of the load in the slow and fast lane, for the 200 m span and inflow 3000 veh/h. The distributions in the slow lane resemble the ones when the lanes are combined (Figure 3.8), except for the full stop condition, which is now the most critical case. For the fast lane, results are more erratic and the distributions overlap. This may be due to the small number of trucks driving on the fast lane (Figure 3.5).

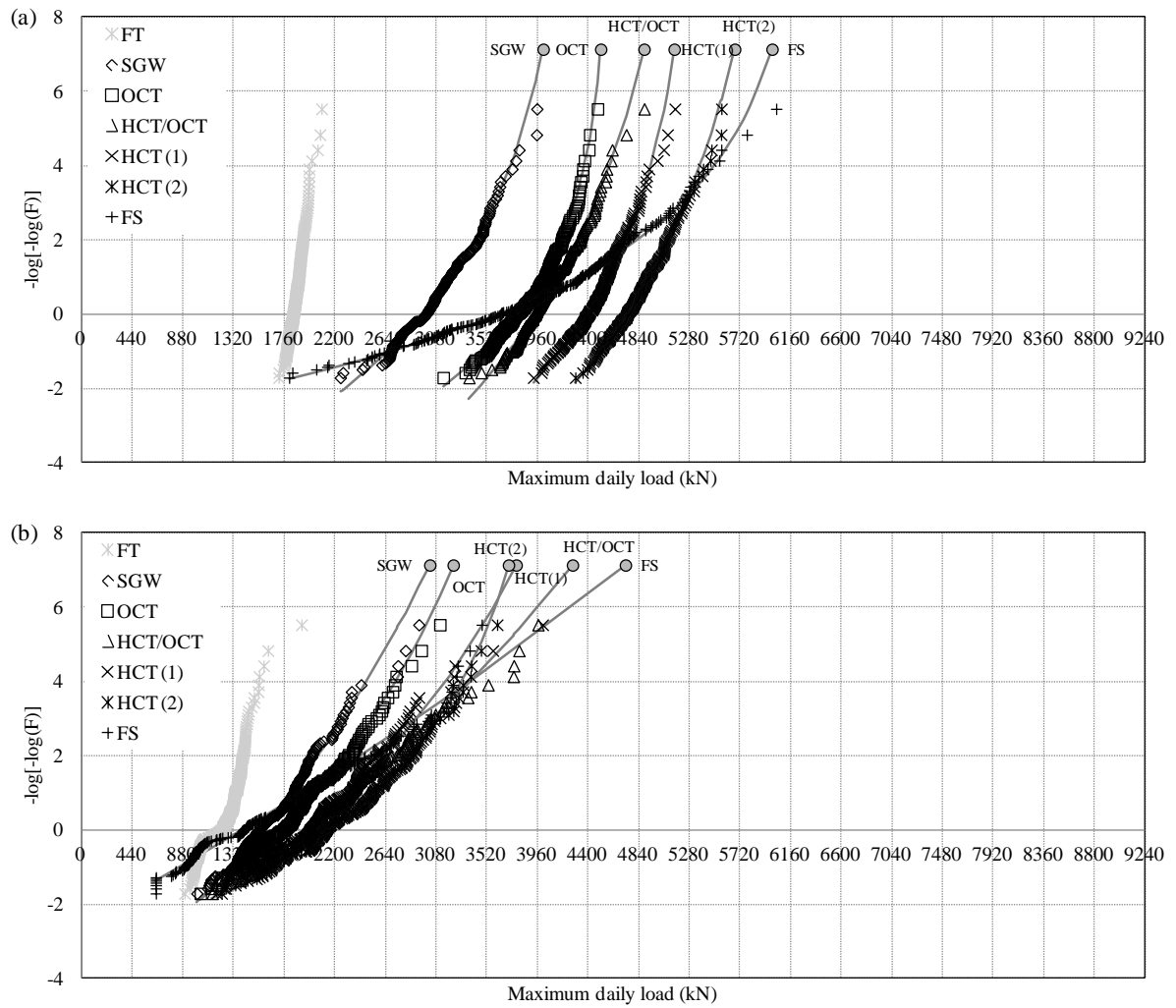


Figure D.34 - Probability paper of total load (200 m span) in (a) slow lane and (b) fast lane.

Table D.5 reports the 5-year characteristic load for slow, fast and combined lanes. The slow lane EUDL is between 19.3% and 33% lower than the EUDL for the combined lanes, whereas the fast lane EUDL is around half of the one for the combined lanes, in spite of the small proportion of trucks driving in the fast lane. Similar proportions are found in the EUDL for the other inflows (Table D.6). Note that when the truck percentage is 48%, lower proportions, but higher loads, are found for the slow lane.

Table D.5 - EUDL on the 200 m span for different lanes (inflow 3000 veh/h).

Traffic state	Combined lanes (kN/m)	Slow lane (kN/m)*	Fast lane (kN/m)*
SGW	24.84	20.06 (80.7%)	15.13 (60.9%)
OCT	30.07	22.55 (75.0%)	16.15 (53.7%)
HCT/OCT	36.79	24.44 (66.4%)	21.33 (58.0%)
HCT(1)	37.32	25.74 (69.0%)	18.88 (50.6%)
HCT(2)	42.33	28.37 (67.0%)	18.55 (43.8%)
FS	41.73	29.99 (71.9%)	23.63 (56.6%)

*In parenthesis, the ratio to the load in the combined lanes.

Table D.6 - EUDL on the 200 m span for different lanes.

Inflow - Traffic state	Combined lanes (kN/m)	Slow lane (kN/m)*	Fast lane (kN/m)*
2000 veh/h - HCT (1)	37.11	25.51 (68.7%)	19.84 (64.4%)
2000 veh/h - HCT (2)	38.72	27.63 (71.4%)	20.80 (53.5%)
2000 veh/h - FS	37.79	30.04 (79.5%)	18.46 (48.9%)
1250 veh/h - HCT(2)	34.15	26.17 (76.6%)	17.45 (51.1%)
1250 veh/h - FS	38.77	28.60 (73.8%)	17.00 (43.9%)
1250 veh/h (48% trucks) - HCT(2)	46.49	28.69 (61.7%)	22.17 (47.7%)
1250 veh/h (48% trucks) - FS	49.45	32.64 (66.0%)	21.79 (44.1%)

*In parenthesis, the ratio to the load in the combined lanes.

Figure D.35 shows the probability paper plots of the load in the slow and fast lane, for the 1000 m span presented in Section 3.5. Both lanes are characterised by a clearer separation between different states, similarly to the plot when the two lanes are combined (Figure 3.10). Table D.7 reports the 5-year EUDL for slow, fast and combined lanes. The slow lane load is between 9.6% and 21.6% lower than the combined load, a smaller percentage than for the 200 m span, while the fast lane EUDL is always less than half of EUDL for the combined lanes. Similar proportions are found in the EUDL with smaller inflows (Table D.8). Again, when the truck percentage is 48%, lower proportions, but higher loads, are found for the slow lane.

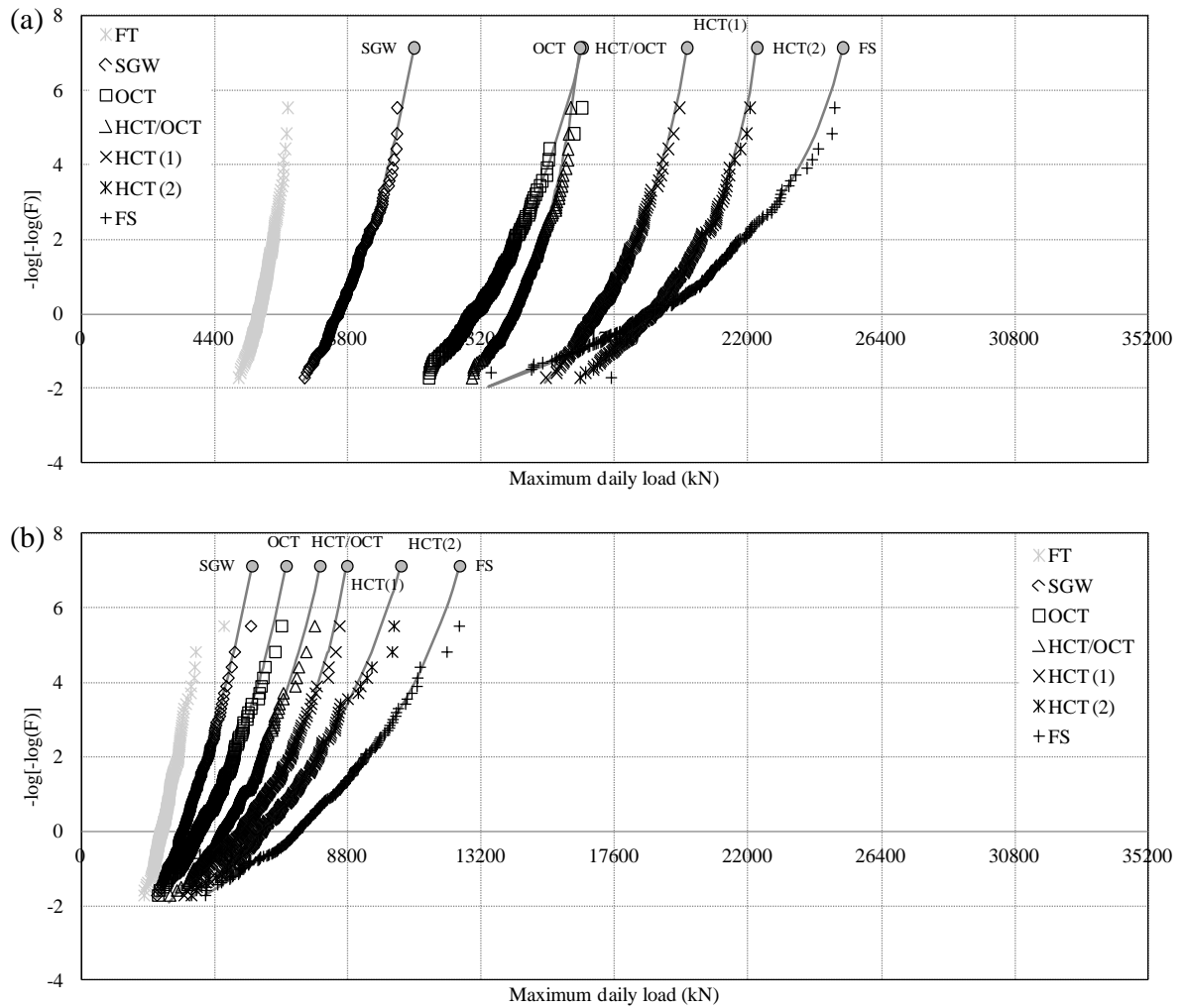


Figure D.35 - Probability paper of total load (1000 m span) in (a) slow lane and (b) fast lane.

Table D.7 - EUDL on the 1000 m span for different lanes (inflow 3000 veh/h).

Traffic state	Combined lanes (kN/m)	Slow lane (kN/m)*	Fast lane (kN/m)*
SGW	12.57	10.97 (87.3%)	5.63 (44.8%)
OCT	18.29	16.53 (90.4%)	6.76 (37.0%)
HCT/OCT	20.44	16.45 (80.5%)	7.87 (38.5%)
HCT(1)	25.03	19.98 (79.8%)	8.77 (35.0%)
HCT(2)	27.06	22.29 (82.4%)	10.55 (39.0%)
FS	32.04	25.12 (78.4%)	12.48 (39.0%)

*In parenthesis, the ratio to the load in the combined lanes.

Table D.8 - EUDL on the 1000 m span for different lanes.

Inflow - Traffic state	Combined lanes (kN/m)	Slow lane (kN/m)*	Fast lane (kN/m)*
2000 veh/h - HCT (1)	23.49	18.60 (79.2%)	9.34 (39.8%)
2000 veh/h - HCT (2)	27.14	20.68 (76.2%)	9.52 (35.1%)
2000 veh/h - FS	32.17	25.24 (78.5%)	10.88 (33.8%)
1250 veh/h - HCT(2)	18.55	13.95 (75.2%)	6.26 (33.7%)
1250 veh/h - FS	32.71	23.27 (71.1%)	11.41 (34.9%)
1250 veh/h (48% trucks) - HCT(2)	37.81	25.30 (66.9%)	15.81 (41.8%)
1250 veh/h (48% trucks) - FS	45.87	30.10 (65.6%)	18.97 (41.4%)

*In parenthesis, the ratio to the load in the combined lanes.

Finally, Table D.9 shows the characteristic load when 25% of the trucks are injected in the fast lane (Split 75-25). The simulations are presented in Section 3.6. For the 200 m span, the difference between the EUDL in the slow lane and in the fast lane is not quite strong, although most trucks are still in the slow lane. The difference is sharper for the 1000 m span (Table D.10).

Table D.9 - EUDL on the 200 m span for different lanes (Split 75-25).

Traffic state	Combined lanes (kN/m)	Slow lane (kN/m)*	Fast lane (kN/m)*
SGW	27.11	20.55 (75.8%)	18.17 (67.0%)
OCT	32.84	24.34 (74.1%)	23.34 (71.1%)
HCT/OCT	33.28	24.14 (72.5%)	20.69 (62.2%)
HCT(1)	35.13	24.82 (70.7%)	21.80 (62.1%)
HCT(2)	39.21	26.15 (66.7%)	21.69 (55.3%)
FS	40.41	27.56 (68.2%)	23.35 (57.8%)

*In parenthesis, the ratio to the load in the combined lanes.

Table D.10 - EUDL on the 1000 m span for different lanes (Split 75-25).

Traffic state	Combined lanes (kN/m)	Slow lane (kN/m)*	Fast lane (kN/m)*
SGW	13.82	10.02 (72.5%)	7.03 (50.9%)
OCT	19.29	15.87 (82.3%)	10.39 (53.9%)
HCT/OCT	21.36	15.74 (73.7%)	10.79 (50.5%)
HCT(1)	25.41	17.71 (69.7%)	12.30 (48.4%)
HCT(2)	27.69	19.04 (68.8%)	13.56 (49.0%)
FS	33.36	22.05 (66.1%)	16.27 (44.8%)

*In parenthesis, the ratio to the load in the combined lanes.

D.8 Conclusions

The lane-changing model is calibrated in order to return realistic lane change rates in the scenario considered for the present research, i.e. a stretch of motorway with no on- or off-ramps. To have a good match with available observations at high flow, it is necessary to increase the safe braking from the value suggested in Kesting et al. (2007). The final parameter set is then used in Chapters 3 and 4, in combination with the IDM parameters used in Chapter 2, in order to keep the desirable property of reproducing the congestion patterns characteristic of the IDM model.

The introduction of the lane-changing model requires refinements in the single-lane model. It is necessary that the refinements do not significantly increase the computational burden. Two solutions for solving the over-reaction due to cut-in manoeuvres are proposed and tested. It is found that a simple capping of the desired minimum gap s^* (Equation D.6) can solve the problem.

Traffic data collection for bridge loading applications

E.1 Introduction

In Section 5.2, it was shown that in traffic theory there are temporal and spatial quantities. *Temporal quantities* give information on the traffic at a certain point in space and return quantities such as flow or time headway. On the other hand, *spatial quantities* give information on the traffic over a certain location, returning quantities such as density or space headways.

For bridge loading applications, spatial quantities are by far the more important: it is the distance between two heavy vehicles that affects bending moment etc., rather than their time gap. Therefore, accurate estimation of spatial quantities is an essential prerequisite for load effect calculations. It is also apparent that data on vehicle weights is a key element in any calculation of bridge load effects.

Regrettably, most traffic data comes from point measurements and therefore spatial quantities can only be estimated. This is commonly done under an assumption of constant speed, which rarely holds in congestion, as discussed in Section 5.2. For a traffic engineer, an average value of density is usually of interest (i.e., average number of vehicles on a given length of road), while peak values are more significant for bridge loading applications (i.e., maximum number of vehicles on a bridge or maximum concentration of load in a given length). Chapter 5 shows that the average density estimates from point measurements are very close to the actual values, while this is not always the case for maximum density values.

This appendix firstly outlines the work that led to the content of Chapter 5, emphasising the differences implied in different ways of estimating spatial traffic quantities (and load effects)

from point measurements. In fact, an initial version of the micro-simulation tool, SIMBA, calculated spatial traffic quantities and load effects from point measurements (*virtual detectors*), as was done in previous bridge loading studies (for instance, in Eymard and Jacob (1989)). This is acceptable for free traffic conditions, when the speed is approximately constant, but not always for congestion.

The evidence of differences in the density estimation from point detectors during congestion has led to deep modifications in the micro-simulation tool, which has been upgraded to include the direct calculation of spatial quantities and load effects, by means of virtual *snapshots* (see also Appendix F). This makes it possible to draw an interesting comparison between the two approaches and a quantification of the error implied in the estimation of spatial quantities. The comparison for the estimation of density is made in Chapter 5. Here, additional information and the implications for load calculations are reported. This appendix refers to the analysis of unaggregated vehicle-by-vehicle data from point measurements, which are typically available from combined WIM and loop detector stations (at least for heavy vehicles, and more frequently also for cars). Instead, Chapter 5 mainly deals with the use of aggregated data.

Finally, some considerations for real-world applications are made and the concept of a camera system for bridge loading applications is developed. The system should be able to recognise vehicle bumpers and wheels during congestion. Fundamentals of image processing are given and the most promising techniques are described and applied to two sample pictures. Fundamentals of optics are also given and final recommendations are made for choosing the most suitable optical system and image processing techniques for data collection.

E.2 Calculation of load effects from point measurements

In order to calculate load effects on a bridge, it is first essential to know the total number and the positions of the vehicles, which come from spatial quantities. When these are directly output, the spatial distribution of vehicles is known and therefore it is straightforward to calculate the load effects on a bridge, provided that the vehicle loads are also known. However, comparisons with real vehicle distributions would require uncommon traffic detectors (e.g. cameras) and weight measurements, by their nature, come from point detectors.

On the other hand, the use of point measurements implies that the required spatial quantities must be estimated to derive vehicle positions and then load effects. In fact, for longer spans, if it is assumed that vehicles keep a constant speed equal to that recorded when crossing the point detector, it is likely that unrealistic overlapping of vehicles will occur in non-stationary conditions, as a faster vehicle may ‘pass through’ a slower one. Therefore, it is preferable to set a constant speed, thus effectively ‘freezing’ the *time headways*¹. However, such a constant speed is not straightforward to set. For instance, a sensible option would be to choose an average speed. In this case, this method provides reliable results when the actual velocity is close to the average one, but in non-stationary conditions, where there can be a wide range of velocities, two cases are likely to occur:

- the actual speed is lower than the average (for instance, in a stop-and-go wave): then the space headways will be over-estimated and the load effects under-estimated. In this case, critical pieces of information may be missed;
- the actual speed is higher than the average (for instance, during free-flowing traffic between waves): then the space headways will be under-estimated and the load effects over-estimated, which may be even higher than during congestion.

As will be shown later, the under- or over-estimation can be significant, so that the assumption of constant speed is quite sensitive to the average speed chosen. It is expected that estimation errors increase with increasing speed oscillations and no errors are expected when actual speeds are constant, which suggests that the estimation is reliable for free traffic and homogeneous congestion. An advantage of this method is that traffic data can be compared with the widely available data collected from common real traffic measurements (e.g., induction loops and WIM stations).

¹ The *time headway* of a vehicle α is defined as the difference between the time stamps of the current vehicle α and the front one, $\alpha-1$. Likewise, the *space headway* (or *spacing*) of a vehicle α is defined as the difference between the position of the current vehicle α and the front one $\alpha-1$.

E.2.1 Proposed approach based on individual speeds

In this section, a new approach based on point measurements is introduced. This method is similar to the method named *micro-estimation* in section 5.5.2. A spatial vehicle distribution is found by multiplying the time headways, Δt_i between the current vehicle i and the front one $i-1$ by the current vehicle's own speed, v_i , thus effectively "freezing" the *space* headways h_i . It is assumed that the current vehicle i keeps its speed v_i , and therefore space headways h_i^{est} at time t_i are estimated as follows:

$$h_i^{est}(t_i) = v_i(t_i) \cdot \Delta t_i \quad (E.1)$$

There is still, to some degree, an approximation, as a vehicle may still change its speed, but the approximation of a constant speed for all the vehicles is dropped. Therefore, the estimates can be beneficially adapted to the different kinds of traffic, as individual speeds are considered, unlike the case of setting a global average speed. The estimated gaps s_i^{est} can be found by subtracting the front vehicle length l_{i-1} from the estimated space headways h_i^{est} :

$$s_i^{est}(t_i) = h_i^{est}(t_i) - l_{i-1} = v_i(t_i) \cdot \Delta t_i - l_{i-1} \quad (E.2)$$

As a result of this approach, for each vehicle i passing over a point detector, the space headways h^{est} between the current vehicle i and as many following vehicles as fit on the bridge length, L is found. Moreover, rather than passing the whole traffic data across the bridge, the current leading vehicle i is positioned over the last bearing, and does not affect the load. This means that the positions are reconstructed looking at the next vehicles $i + 1, i + 2, i + j, \dots, i + u$ crossing the detector, where $i + u$ is the farthest vehicle still on the bridge. The total number of vehicles on the bridge is therefore equal to u and satisfies the condition:

$$\sum_{j=1}^u h_{i+j}^{est} < L \quad (E.3)$$

This assumption significantly reduces the amount of data, but may be non-conservative in free-traffic, as the assumption that the first vehicle i is on the farthest bearing, does not generally provide the worst loading position in free traffic. However, as the number of

vehicles on the bridge increases, this difference becomes smaller and smaller, providing reliable results for congested traffic.

Once the vehicle positions are known, it is straightforward to calculate the load effects. An example of the mid-span bending moment calculation at time 890 s is shown in Table E.1.

Table E.1 – Example of load effect calculation from time stamps and individual speeds.

Time stamp	Speed	Speed	Time headway	Space headway	Position	Moment
s	m/s	km/h	s	m	m	kNm
890	7.3	26.28	n/a	n/a	0	0
892.99	6.3	22.68	2.99	18.84	18.84	188
896.09	5.2	18.72	3.1	16.12	34.96	350
899.41	4.1	14.76	3.32	13.61	48.57	486
903.21	2.6	9.36	3.8	9.88	58.45	416
909.37	0.6	2.16	6.16	3.7	62.15	379
934.47	2	7.20	25.1	50.2	112.35	0
Total						1818

E.2.2 Consideration of different congestion patterns

In this section, load effects are calculated on a sample bridge with 100 m span. The traffic stream is 1580 veh/h and is passed over a road 5000 m long. The stream is made up of identical vehicles, each of which is represented as a single concentrated load of 2 t (19.6 kN). The IDM parameters used are reported in Table C.2 and are based on Treiber et al. (2000). Note that vehicle length l and minimum jam distance s_0 are different from those used in Chapter 5 (Table 5.2). However, the results are still comparable, because the stability of the traffic is determined by the maximum acceleration a , the desired deceleration b , and the safe time headway T (Treiber et al., 2000), while the maximum density (and the fundamental diagram) depends on the sum $l + s_0$, which is the same in both cases.

Table E.2 - IDM model parameters

Parameter	Value
Desired speed, v_0	120 km/h
Safe time headway, T	1.6 s
Maximum acceleration, a	0.73 m/s ²
Comfortable deceleration, b	1.67 m/s ²
Acceleration exponent, δ	4
Minimum jam distance, s_0	3 m
Vehicle length, l	4 m

Eight 30-minute periods of congestion are generated with inhomogeneities $\Delta T = 0.3, 0.45, 0.6, 0.9, 1.2, 1.8, 2.4$ and 3.0 s, applied from 2700 m on. The bridge spans from 1900 to 2000 m. It is taken to be simply-supported and the bending moment at mid-span is calculated using its influence line. Some typical shapes of influence lines are shown in Figure E.1. Note that the total load may be regarded as a *load effect* with rectangular influence line. It is important to note that in this case of single-span and identical vehicles, density is *quantitatively* proportional to total load and *qualitatively* proportional to load effects. If it were not a single span, density would still have been quantitatively proportional to total load, but the load effects would depend on the span configuration. Most importantly, the results shown in Chapter 5 about accuracy of density estimates in congestion can be regarded as accuracy in computing the total load of a bridge, with the length of the observed stretches considered in Chapter 5 (100, 200, 500 and 1000 m).

Data is collected at the virtual point detector placed at 2000 m with four different methods:

- constant speed taken as the average of the full simulation (1);
- constant speed taken as the average of the congested part of the simulation (2);
- variable speed (3);
- estimation from individual speeds as for section E.2.1 (4).


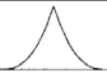
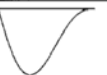
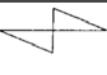

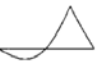
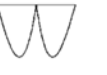
Shape	Description
	Bending moment at midspan : simply supported beam
	Bending moment at midspan : double fixed beam with strongly varying inertia
	Maximum bending moment at the support of former double fixed beam
	Shear forces at midspan (maximum and minimum) : simply supported beam
	Total load
	Minimum and maximum bending moment : two-span continuous beam
	Bending moment on central support of former continuous beam

Figure E.1 - Typical influence lines (adapted from Prat (2001)).

In order to illustrate the differences in the various estimation methods, a full simulation with inhomogeneity, $\Delta T = 3.0$ s, is first analysed in detail. Figure E.2 (left) shows the one-minute aggregated space mean speed at three point detectors. It can be seen that at the 2000 m detector in the first 7 minutes, traffic is free, then congestion builds up to an OCT state with rather small oscillations. Note that it is not always straightforward to determine when congestion is starting, especially during strongly oscillating conditions. At the same detector, the average space mean speed of the full simulation is 31.1 km/h. Until minute 7, the average space mean speed is 99.4 km/h, while after minute 8, it drops to 13.3 km/h. Note that after minute 14, the space mean speed stabilises at about 8 km/h.

Figure E.2 (right) plots individual vehicle speeds. In this case, the average speed is 20.1 km/h (from minute 8) and 10.4 km/h (from minute 14), both greater than the average of the

aggregated space mean speeds. This should be taken into account because averaging individual speeds, rather than averaging aggregated space mean speeds, leads to higher gaps and lower loads.

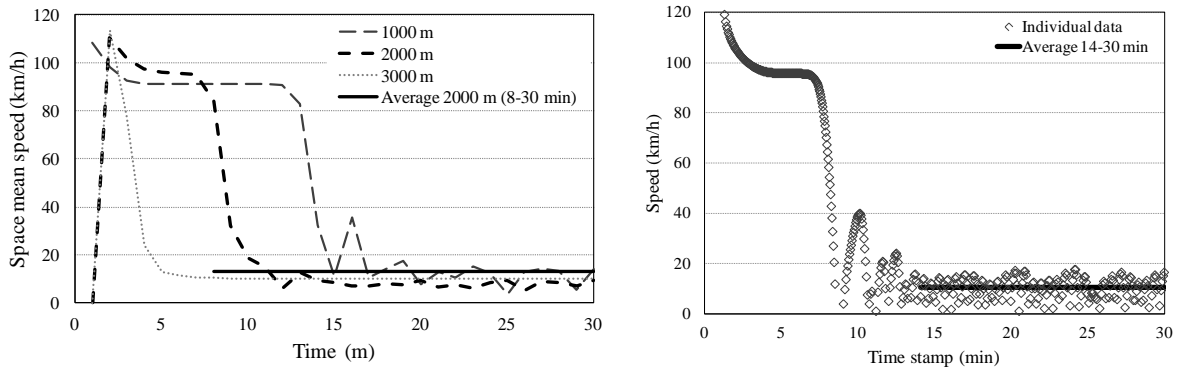


Figure E.2 - Aggregated space mean speed (left) and non-aggregated speeds at the 2000 m detector (right).

Figure E.3 shows the time-history of the mid-span bending moment for a full simulation with applied inhomogeneity $\Delta T = 3.0$ s. The maximum moment in free traffic can be hand-calculated and it is 500 kNm. Significant differences between the four methods can be noticed:

- the variable speed (3) returns high values in congestion, while they are accurate in free traffic;
- the constant speed taken as the average of the full simulation (1) returns low values in congestion, while they are overestimated in free traffic;
- the constant speed taken as the average of the congested part of the simulation (2) returns intermediate values in congestion, but unrealistically high values in free traffic, remarkably even higher than in congestion; note also the difference between the moments calculated with 13.3 km/h and 10.4 km/h;
- the estimation from individual speeds (4) can be beneficially adapted to the different traffic types.

Note that, in the second part of the simulation (minutes 14-30), the values found with method (4) are very close to those found with method (2) by using the average of the individual congested speed 10.4 km/h (as per Figure E.2b). This happens because speed oscillations are

reduced, and the average speed is quite close to the actual one, so that the estimation is more reliable.

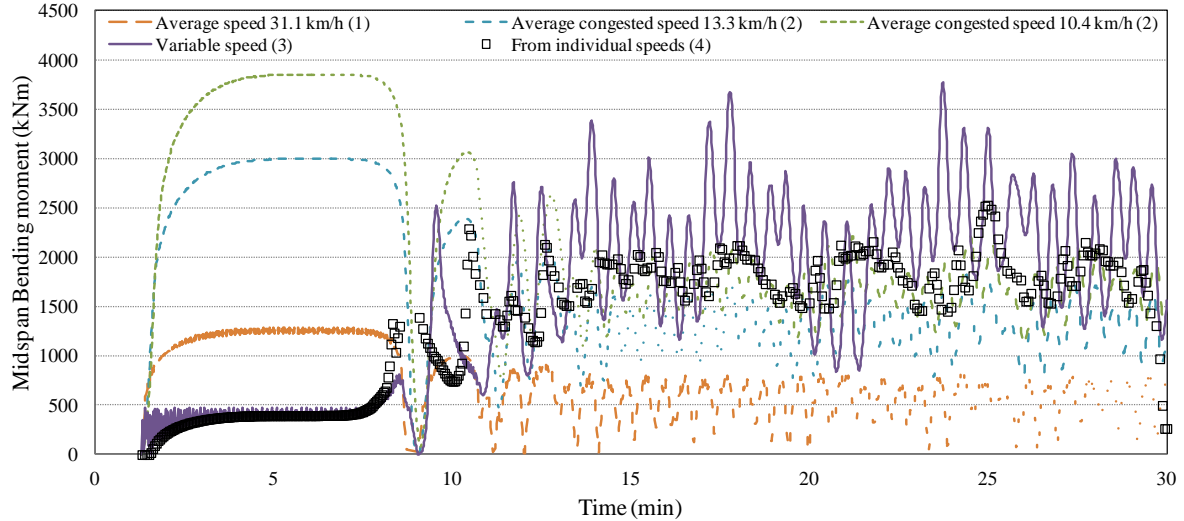


Figure E.3 – Comparison of a time-history of bending moment.

Figure E.4 shows that the maximum bending moment for the different applied inhomogeneities ΔT . It can be seen that there are significant differences between the four methods, except in free traffic. The variable speed (3) returns unrealistically high values due to vehicle overlapping (there are up to 30 cars in the 100 m span, even though a car is 5 m long).

It is expected that method (2) will be the most accurate when there are negligible oscillations (FT and HCT). Note that when both free traffic and congestion occur, the free traffic values have been discarded. For oscillatory traffic SGW and OCT, it is difficult to say which one is more correct and this will be dealt with further in Section E.3. Using a constant speed for the full simulation, (1), returns under-estimated values for congestion.

However, it can be said that both (2) and (4) have an expected increasing trend between the correct estimates of FT and HCT and therefore they look like the most realistic ones.

Table E.3 summarises the different estimation methods for free traffic only (FT), oscillatory traffic (SGW/OCT), homogeneous congested traffic (HCT), and free traffic preceding congestion.

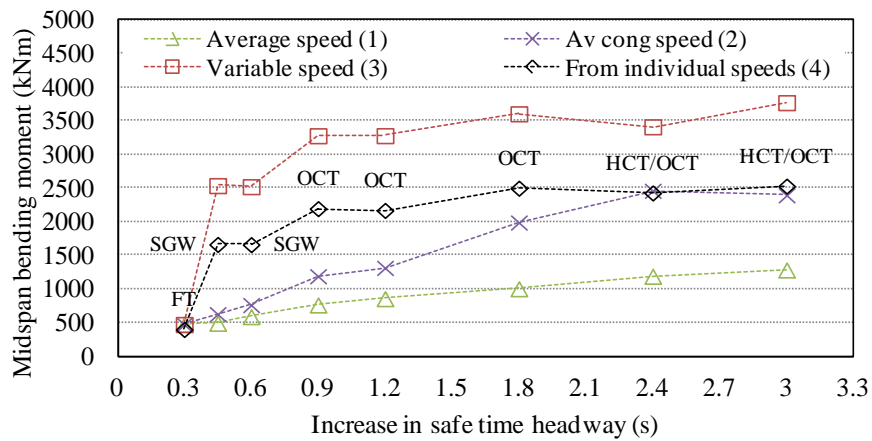


Figure E.4 – Comparison of load effects calculated with different methods.

Table E.3 – Estimation of maximum load effects from point measurements (+: over-estimated; ++: highly over-estimated; -: under-estimated; --: highly under-estimated).

Method	Free Traffic	Oscillatory Traffic	Homogeneous congested traffic	Free Traffic before congestion
(1)	OK	--	--	++
(2)	OK	-	OK	++
(3)	OK	++	++	OK
(4)	-	+	OK	-

E.2.3 Methods of headway estimations from individual speeds

Thiemann et al. (2008) use a slightly different way of estimating inter-vehicle gaps and headways from time stamps and individual speeds. The space headway between the current vehicle i and the leading vehicle $i-1$ can be estimated from their time headway Δt_i and speed v_{i-1} :

$$h_i^{est}(t_i) = v_{i-1}(t_{i-1}) \cdot \Delta t_i \quad (\text{E.4})$$

This formula underlies the assumption that the *leading* vehicle $i-1$ keeps a constant speed v_{i-1} during Δt_i , whereas Equation (E.1) assumed that the *current* vehicle i keeps its speed v_i .

It is also possible to use the average speed between the current i and the leading vehicle $i-1$:

$$h_i^{est}(t_i) = \left[\frac{v_i(t_i) + v_{i-1}(t_{i-1})}{2} \right] \cdot \Delta t_i \quad (E.5)$$

In this case, the estimated headways will lie exactly in between the ones estimated with Equations (E.1) and (E.4). In order to illustrate the difference between the application of Equations (E.1) and (E.4), it is useful to analyse a stop-and-go wave (Table E.4). The first group of vehicles crosses the virtual detector with decreasing speed, while the last one speeds up. The large time headway of 25.1 s suggests that the platoon came to a full stop and then a small space headway is expected, close to minimum jam distance, $s_0 = 3$ m. The first column estimates the space headways calculated according to Equation (E.1) (named LCO, from Lipari et al. (2010), where the proposed method was applied), while the second according to Equation (E.4) (named TTK, from Thiemann et al. (2008)). The platoon position on a virtual bridge is also calculated, being the first vehicle on the farthest bearing (the position is the backward distance from the farthest bearing).

Table E.4 – Different positions from micro-estimation.

Time stamp	Speed	Speed	Time headway	Space headway (LCO)	Position	Space headway (TTK)	Position
s	m/s	km/h	s	m	m	M	m
890	7.3	26.28	n/a	n/a	0	n/a	0
892.99	6.3	22.68	2.99	18.84	18.84	21.83	21.83
896.09	5.2	18.72	3.10	16.12	34.96	19.53	41.36
899.41	4.1	14.76	3.32	13.61	48.57	17.26	58.62
903.21	2.6	9.36	3.80	9.88	58.45	15.58	74.20
909.37	0.6	2.16	6.16	3.70	62.15	16.02	90.22
934.47	2.0	7.20	25.1	50.2	112.35	15.06	105.28
939.20	3.1	11.16	4.73	14.66	127.01	9.46	114.74
943.16	4.0	14.4	3.96	15.84	142.85	12.28	127.02
946.78	4.8	17.28	3.62	17.38	160.23	14.48	141.50
950.18	5.4	19.44	3.40	18.36	178.59	16.32	157.82
953.45	6.0	21.60	3.27	19.62	198.21	17.67	175.49

As expected, in the braking phase, TTK values are greater (as they consider the leader's speed, which is greater), while in the accelerating phase LCO values are higher (as they consider the greater current vehicle's speed).

Notably, LCO values returned an unrealistic space headway (3.7 m), because it is shorter than the vehicle length (4 m), while the following one is quite high (50.2 m). On the other hand, TTK has returned the smallest value (9.46 m) in the acceleration phase, which sounds unrealistic.

On the whole, TTK placed the same vehicles in a length that was 23 m shorter. The estimated mid-span bending moment of the 100-m span at 890 s would be 1818 (LCO) and 1402 kNm (TTK).

E.3 Comparison with actual load effects

The previous section has shown that there are significant differences in estimating the density or load effects from point measurements. This was the basis that led to the upgrade of SIMBA (not by the author) with the introduction of virtual snapshots and to the analyses described in Chapter 5. The analyses carried out here compare the point-estimated load effects with the actual values.

Furthermore, in the previous section, it is assumed that the point detector is placed on the farthest bearing of the bridge. Therefore, the traffic has been analysed looking backward at the vehicles on the bridge. As is shown below, this approach is not the only possible one.

E.3.1 Influence of detector position

In this section, a platoon made up of 24 vehicles is analysed. The congestion condition is *oscillating congested traffic* (OCT) and is generated by injecting 1200 veh/h and applying an inhomogeneity $\Delta T = 1.2$ s. The IDM parameters are as per Table C.2.

The first speed drop is studied. The speed at the detector decreases steadily from 25 (vehicle #1) to 5 km/h (vehicle #8) and then increases to 31 km/h (vehicle #23). Conversely, time headways increase steadily from 2.75 (vehicle #1) to 9.5 s (vehicle #8) and then decreases to about 3 s (vehicle #24). This indicates that traffic almost stopped just before vehicle #8 passed the detector, as vehicle #8 passed with the slowest speed and with greater time headway than the average (Figure E.5).

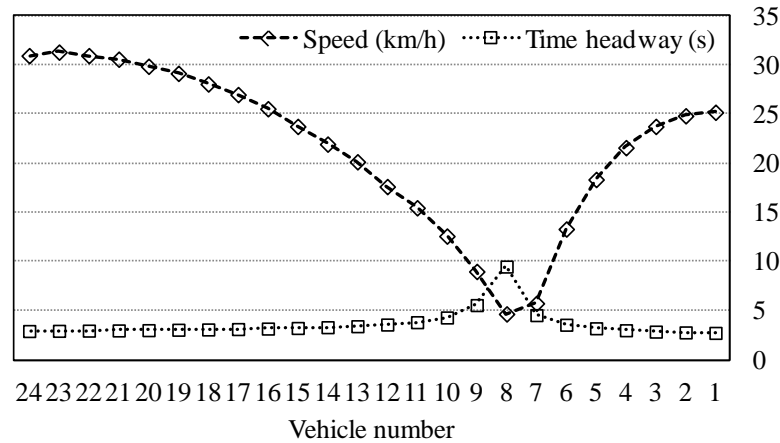


Figure E.5 – Vehicle data at the 2500 m point detector.

Space headways are estimated according to Equation (E.1) (LCO) and Equation (E.4) (TTK). The estimates are used to derive a spatial distribution of vehicles, according to section 0. Then, these two estimated spatial distributions *at a certain point in time* are compared to the actual spatial distribution at that time. Three points in time are considered for the actual values: when the first (#1, at 1437.46 s), the last (#24, 1512.78 s) or the slowest vehicle (#8, 1457.52 s) passes over the detector placed at 2500 m. Figure E.6 shows, for each vehicle, the actual and estimated space headways.

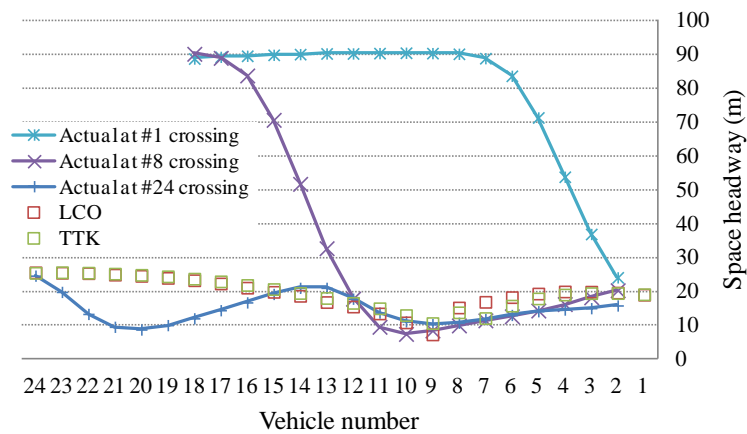


Figure E.6 – Vehicle headway comparison.

First of all, it can be seen that there is not a large difference between the estimates according to LCO and TTK. Then, it can be seen that, if the actual distribution at the time when vehicle #1 crosses the detector is considered - which is equal to placing a bridge *behind* the detector,

with the detector and vehicle #1 on the farthest bearing (as assumed in section 0) – it is found that the actual headways are much higher, tending to the equilibrium gap of about 90 m. This occurs because traffic is still free behind the detector at 2500 m (see Figure E.7) and the speed used for estimation is much lower than the actual one, as vehicles are slowing down while approaching the detector. In this case, space headways are under-estimated and loading would be over-estimated. In fact, on a bridge 100 m long, 5 vehicles are estimated as opposed to the actual number of 3.

Vehicle #: .. 14 13 12 11 10 9 8 7 6 5 4 3 2 1

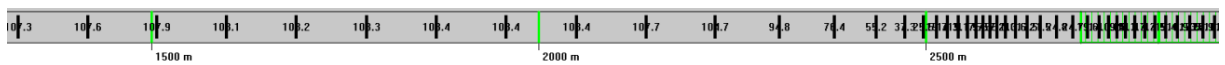


Figure E.7 – Snapshot at vehicle #1 crossing the 2500 m detector.

If we consider the actual distribution at the time when vehicle #8 crosses the detector - which is equal to placing the detector *in the middle of* the bridge - we find that headways around #8 are fairly well estimated (Figure E.6), and so are vehicle positions (Figure E.8). We can see that LCO estimates the braking phase better (vehicles #1-8), while TTK estimates the accelerating one better (vehicles #8-13). This is valid until vehicle #14, as the traffic further upstream is free (see Figure E.9), as discussed above. Assuming again a bridge 100 m long, we have 8 vehicles estimated against the actual 9. However, for longer bridges the error increases.

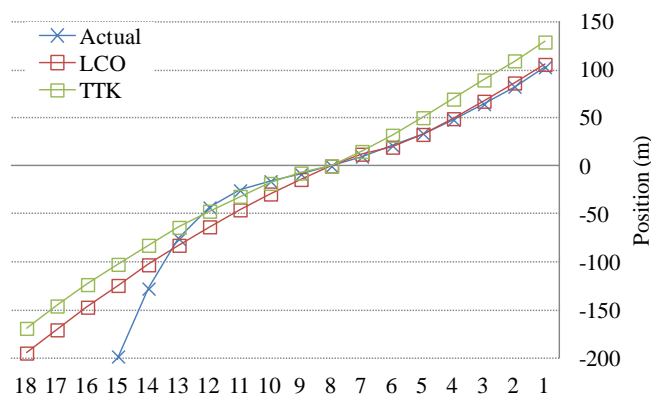


Figure E.8 – Vehicle positions when #8 crosses the detector.

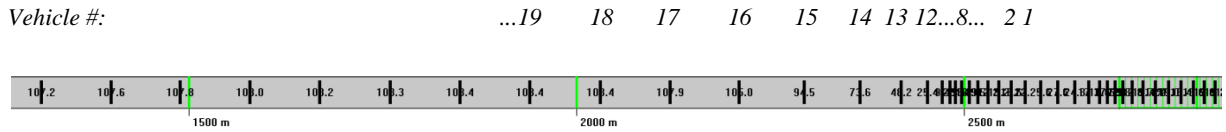


Figure E.9 – Snapshot at vehicle #8 crossing the 2500 m detector.

Finally, if we consider the actual distribution at the time when vehicle #24 crosses the detector - which is equivalent to placing a bridge *in front of* the detector, with the detector and vehicle #24 on the nearest bearing - we find that the first gap (#24) is accurately estimated, but then the actual gaps are much lower, for the following 8 vehicles (vehicles #16-23). This is due to the fact that those vehicles slowed down again because of a second stop-and-go wave (see Figure E.11). We do not have information about this further wave, so this effect cannot be considered. In this case, loading would be under-estimated. In fact, assuming a bridge 100 m long, we would have 4 vehicles estimated against the actual 8 (Figure E.10). Note that this is the only method that could be applied in real-time applications, as it is based on data of vehicles that have already crossed the detector.

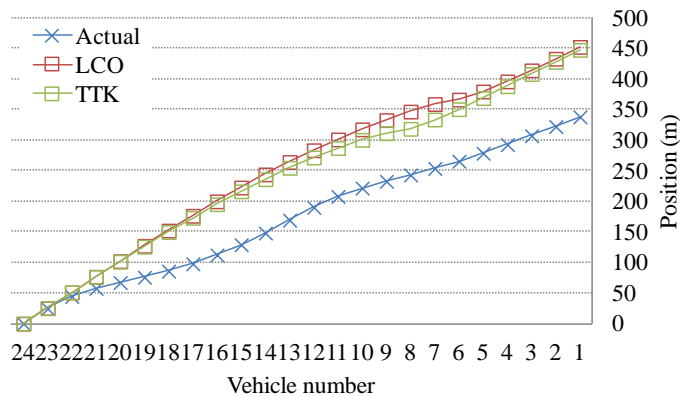


Figure E.10 – Vehicle positions when vehicle #24 crosses the detector.

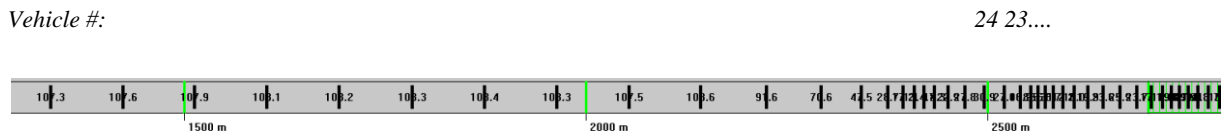


Figure E.11 – Snapshot when vehicle #24 crosses the 2500 m detector.

It can be concluded that spacing estimates are usually reliable only for the initial vehicles. Further vehicle estimates are often unreliable, because vehicle data is collected only when it

passes the detector. The further we move away from the detector, the more likely it is that a vehicle changes its speed which results in a wrong spacing estimate. This may significantly affect the loading on a long-span bridge. A reasonable compromise is to consider the time when the slowest vehicle passes the detector and look at both directions, which means to place the detector in the middle of the bridge.

E.3.2 Comparison with actual spacing

Thiemann et al. (2008) show that gaps estimated from temporal data are larger than real gaps in jammed traffic, while there are small differences for less congested traffic states. The comparison is made on NGSIM data (Federal Highway Administration, 2005).

In Figure E.12, the actual load calculated from traffic snapshots has been superimposed on the most successful methods depicted in Figure E.3. The virtual detector is placed on the farthest bearing of the bridge (i.e. the bridge spans from 1900 to 2000 m). The actual values have the same order of magnitude of methods (2) and (4) but are globally higher. This means that the proposed method (2) is slightly non-conservative and qualitatively agrees with the findings about density shown in Chapter 5.5.2 for the 100 m span (Table 5.4).

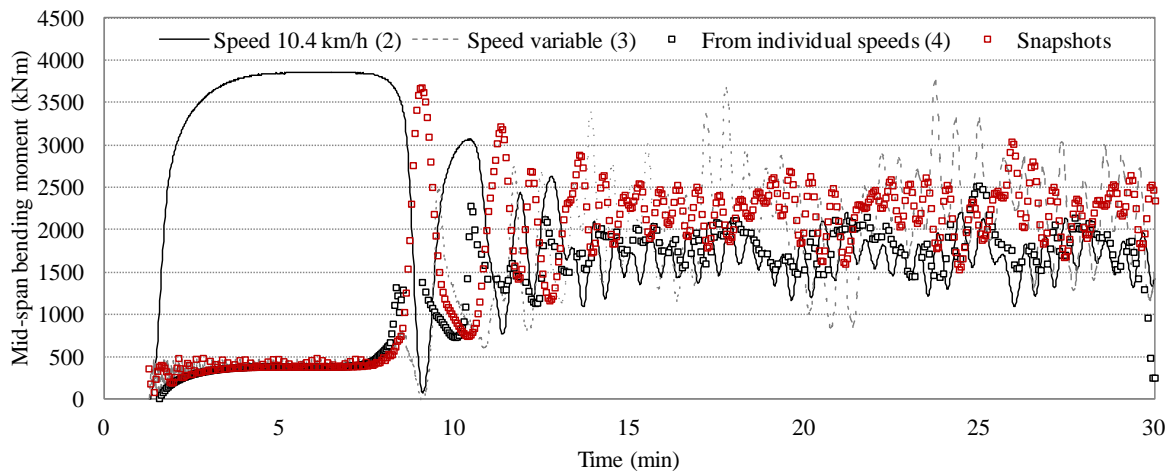


Figure E.12 - Comparison of actual and estimated bending moments (bridge behind the detector).

As can be seen, there is a peak at the beginning of the congestion (at around 9 minutes), which could not be fully caught with any point estimates from individual speeds (Method 2). This corresponds to a situation of standstill traffic, as confirmed by the large time gap between the estimates. In fact, since a piece of information is taken every time a vehicle

passes over the detector; there is no information when the traffic is in standstill and all the vehicles are very close to each other. The bridge is actually filled up with 15 vehicles (Figure E.13), and the estimates from individual speeds could catch only five of them. The other estimates performed worse.

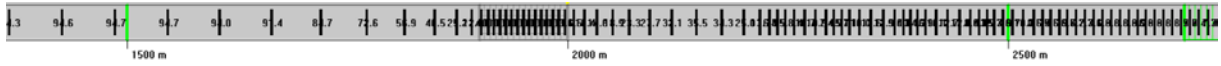


Figure E.13 - Snapshot of the cluster at 2000 m.

When placing the detector in the middle of the bridge, there are no large differences in the moment time-history, but now some dots are better superimposed (Figure E.14). Note that this is the detector position used in Chapter 5.

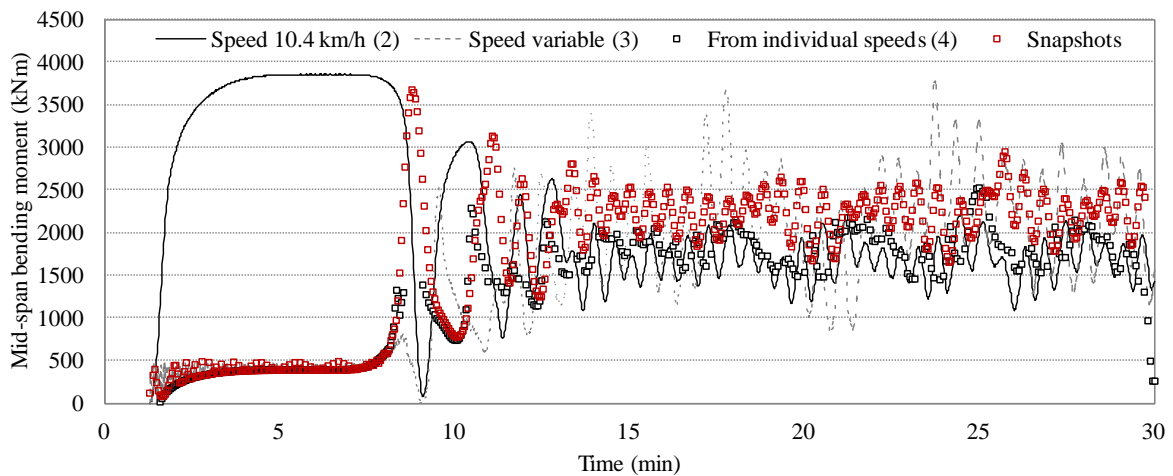


Figure E.14 – Comparison of actual and estimated bending moments (detector in the centre of the bridge).

E.3.3 Summary

It is apparent that there are difficulties in estimating vehicle positions from point measurements, especially during traffic oscillations. In this situation, the estimates are usually reliable for the very first vehicles. However, in long-span bridges it is essential to have accurate vehicle position estimates over a significant length. Such difficulties are related to theoretical problems, rather than to estimation methods, and therefore they cannot be fully overcome (Hall, 1994). Moreover, if a vehicle comes to a standstill, which corresponds to a situation of short gaps and high load, no information can be collected with a point detector.

E.4 The development of a camera system for bridge loading applications

The previous section concluded that there are theoretical difficulties when estimating vehicle positions from point measurements. The use of *spatial detectors*, such as cameras, can help to overcome such theoretical difficulties, but poses some practical ones. In particular, cameras involve the transmission of huge amounts of data and then require intensive image processing (Klein et al., 2006). Outdoor use involves further complications compared to indoor applications, such as dealing with changing illumination conditions and inclement weather. Furthermore, every vehicle has a different shape and colour. So, the object to identify is always changing, as well as the illumination conditions. To this end, cameras are mostly deployed for research purposes and very often used to collect aerial pictures to track vehicles (Treiterer and Myers, 1974; Coifman et al., 1998; Hoogendoorn et al., 2003; Federal Highway Administration, 2005; Kovvali et al., 2007). Nevertheless, the technology is developing rapidly and many of these problems may be overcome in the near future.

As seen in Chapter 2, the minimum bumper-to-bumper gap is a critical parameter in bridge loading studies, as full stop queues are often considered (Ivy et al., 1954; Buckland et al., 1980; Harman et al., 1984; Flint and Neill Partnership, 1986; Ditlevsen and Madsen, 1994; Nowak et al., 2010). The minimum bumper-to-bumper gap at a standstill can be detected only with a camera, as point detectors can measure only moving vehicles. Nevertheless, this value has often been based on little or no data. Among the quoted work, only Buckland et al. (1980) and Nowak et al. (2010) state that they have used video recordings as a basis for their load models.

E.4.1 Background and requirements

In order to compute gaps, it is first necessary to detect vehicle bumpers and then measure the distance between the following vehicle's front bumper and leading vehicle's rear bumper. It would also be desirable to collect some other bridge-sensitive vehicle features, such as axle spacings and overhangs, and to do so, it is necessary to identify wheels as well. In this case, the camera has to be placed perpendicular to the traffic, thus ruling out aerial cameras.

No literature has been found about bumper detection from roadside cameras, whereas there are some applications of wheel detection. For instance, Fung et al. (2007) present an

application of wheel detection for toll collection. However, the camera is focussed on a small area and environmental conditions could be controlled.

As a further step, it would be desirable to compute speeds and accelerations of slow-moving vehicles and relate them to gaps. This will be needed to *microscopically* calibrate the full micro-simulation model. Note that the minimum bumper-to-bumper distance at a standstill corresponds to the *minimum jam distance* parameter s_0 in the IDM model.

The first choice to make for the development of the camera system regards the use of video or still images. The use of video is not recommended, as this will unnecessarily increase the amount of data. Typical video systems take 25 (PAL) or 29.97 (NTSC) frames per second. Since the traffic is at a standstill or slow-moving, the use of still pictures at a lower frequency rate than video can work well. For instance, the Federal Highway Administration (2005) uses 10 frames per second (Cambridge Systematics Inc., 2005b; Cambridge Systematics Inc., 2005a). Then, it is not necessary to use colour images, as the aim is to detect shapes of no particular colour. The use of greyscale images beneficially reduces the amount of data.

The camera system should ideally be portable and inexpensive. The image acquisition can be easily carried out with a standard laptop. No particular performance is required, as it is not necessary to process the images in real-time. Indeed, the image processing can be carried out after the image acquisition on a more powerful computer.

In this section, several image-processing techniques relevant to bumper and wheel detections are first investigated and applied to sample pictures. Then, some optic fundamentals are recalled and two possible site setups are outlined. Finally, some conclusive recommendations are made.

It is acknowledged that the content of this section is just a first approach to the topic and needs further development.

E.4.2 Definitions

A *monochrome* image is a two-dimensional matrix function $f(x, y)$. The amplitude of f at each point (*pixel*) is called *grey level* or *intensity*. *Colour* images are formed by a combination of

individual images, typically by three monochrome images. If the amplitude values are discrete, it is called a *digital image*. Such values are typically quantised in the interval [0, 255] (8-bit) or [0, 65535] (16-bit). A *binary image* is an image whose intensity is either 0 (black) or 1 (white).

The total number of pixels is often called *resolution*, although this definition is not strictly correct. It is expressed in the number of pixel columns and rows (e.g. 640×480) or their total number (1 MP, megapixel). A high resolution implies greater detail, at the cost of an increased amount of data. For our applications, the objects to recognise are not particularly small; therefore very high resolution should not be needed. The resolution intended as a count of pixels should be more correctly referred to as *pixel resolution*, whereas the *resolution* represents the number of pixels (or dots) per unit of length, usually called *dpi* (dots per inch). Hence, it is not a mere characteristic of the image itself, but depends also on the size of the printed or visualized image.

E.4.3 Image processing

Image segmentation is an image processing technique whose aim is to subdivide an image into objects. The input is an image, but the outputs are attributes extracted from those images. Image segmentation is useful for detecting edges (such as bumpers) or objects with a given shape (such as wheels). These are the most common image segmentation techniques:

- edge detection;
- thresholding;
- line (or circle) detection with the Hough transform;
- background subtraction
- region-based segmentation;
- watershed segmentation.

For traffic applications, the most interesting approaches are *edge detection*, *thresholding* and the *Hough transform*, which are dealt with more extensively. *Background subtraction* is a technique widely used in traffic applications to identify moving objects. *Region-based segmentation* and *watershed segmentation* may not be very useful for traffic applications, and so they are just briefly outlined. Each of these techniques has in turn several different sub-techniques.

Image segmentation techniques are applied to a sample picture using *MATLAB 7.6.0*. A second sample picture is later used, in order to test the efficacy and sensitivity of the most promising techniques. For further details about these techniques and their implementation, the reader is referred to the book by Gonzalez et al. (2009).

Background subtraction

Background subtraction is a popular technique in image processing of moving objects (Hoogendoorn et al., 2003; Cheung and Kamath, 2004; Cathey and Dailey, 2005; Atkočiunas et al., 2005; Wang et al., 2008). It compares a picture with a given background and classifies pixels as belonging to either the *foreground* or the *background*. Thus, moving objects can be identified.

However, there are some drawbacks for its applications in traffic. For instance, the background updating is usually a difficult task in congested areas, as stationary vehicles may end up in the background. Conversely, shadows or moving leaves (from trees) could be detected as foreground. Cheung and Kamath (2004) present a valuable overview of background subtraction techniques applied to traffic and the reader is referred to their paper for further details. Background subtraction techniques are usually applied only to greyscale images. Colour image processing is much more complex, but is becoming more common as it helps the identification of shadows.

The background subtraction techniques can be divided into:

- *recursive methods*: some previous frames are stored in the buffer;
- *non-recursive methods*: only one background is recursively updated based on each input frame.

Among the recursive methods, the most interesting ones (for traffic applications and computational simplicity) are the *Frame Differencing* (FD) and *Median Filtering* (MF) methods. *Approximated Median Filtering* (AMF) is the most popular among the non-recursive techniques. Other techniques are more complex and sometimes offer little improvement in results, such as the *Mixture of Gaussian* (MoG) method (Cheung and

Kamath, 2004). Benton (2008) published online a sample video analysed with FD, AMF and MoG. Only frame differencing techniques are tested here.

Once the foreground is separated from the background, it is advisable to set a threshold in order to discard pixels with small variations:

$$\left| I_t(x, y) - B_t(x, y) \right| > T \quad (\text{E.6})$$

in which $I_t(x, y)$ is the pixel intensity and $B_t(x, y)$ is the intensity of the background at the time t . The use of the absolute difference is not the only possible choice, as will be shown later. Notably, the background subtraction is very sensitive to the threshold set (Cheung and Kamath, 2004; Benton, 2008; Zaurin and Catbas, 2010).

There are some applications of background subtraction in aerial traffic pictures. Cheung and Kamath (2004) use four publicly available videos with different weather and traffic conditions. Significantly, one is called *busy* and represents a jam at a traffic light (*Nibelungen-Platz, Frankfurt*) (Insitut für Algorithmen und Kognitive Systeme, 1995). In this case, MF and AMF returned results similar to more sophisticated methods.

Mirth (2008) suggests analysing *detection lines* to find vehicles from aerial pictures, thus reducing the background subtraction problem to just one dimension. However, there may be problems with shadows (as shown in Figure E.15).



Figure E.15 – Detection lines (after Mirth (2008)).

A sample picture is analysed with the *Matlab Image Processing Toolbox* and compared to its real background (Figure E.16). The pictures have been provided courtesy of PEC, Feldkirchen in Kärnten (Austria).

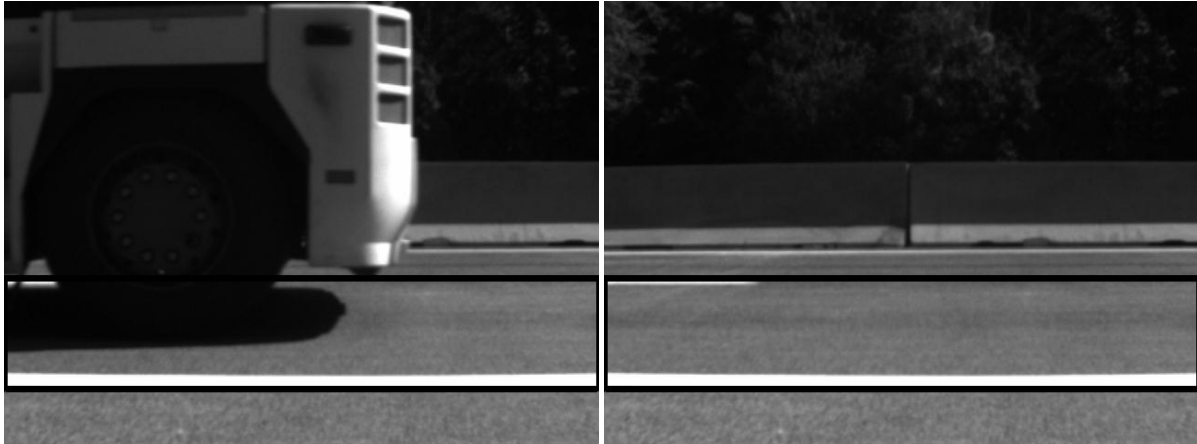


Figure E.16 - Sample picture (left) and background (right).

Both pictures have resolution 646×480 pixels (*VGA resolution*) and are 8-bit (MATLAB class *uint8*), that is, grey intensities vary from 0 (black) to 255 (white). Unfortunately, the images are corrupted with a black rectangle. As may be seen, there is no apparent intensity difference between the tyre and the shadow, but there is some difference between the wheel and the tyre, as well as between the bumper and the background.

The image is tested with the frame differencing technique. FD uses the frame at time $t-1$ as background for the frame at time t (Cheung and Kamath, 2004). In the sample case of Figure E.16, the background is not the image corresponding to the immediately preceding frame. In general, it must be noted that the use of a fixed background cannot cope with likely illumination changes.

Figure E.17 shows the results of background subtraction with frame differencing (as we have only one background available), setting a threshold T equal to 10 and 20 pixels² (Equation E.6). The background is set to be white. As can be seen, the bumper can be clearly identified.

² In MATLAB, the image must be first converted into *double* class through the function *mat2gray*. Otherwise arithmetical operation out of the *uint8* range $[0, 255]$ would not be allowed, as needed for intermediate steps of background subtraction. In *double* class gray intensities vary from 0 to 1.

However, the trees over the barrier have the same colour as the wheel, so it is partially recognized as background, making a “hole” in the truck (this phenomenon is known as the *aperture problem*). The presence of a uniform background may help avoid the aperture problem, provided that the vehicle is not at a standstill.

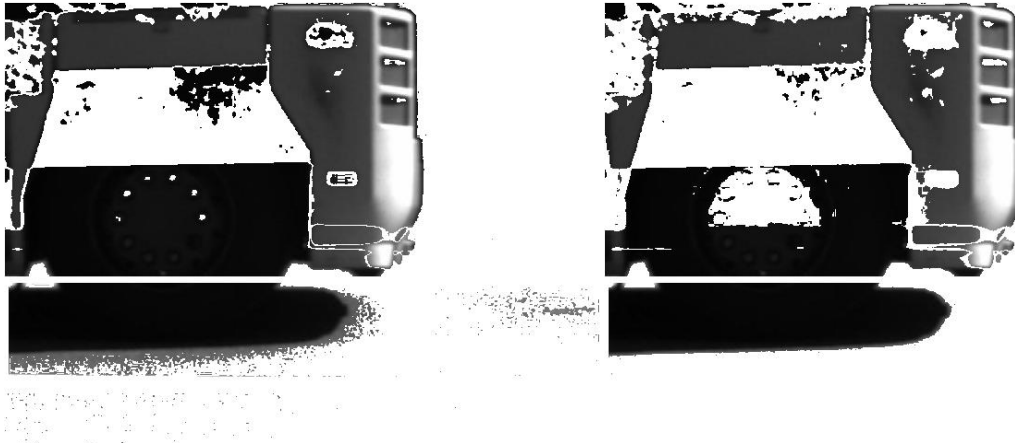


Figure E.17 – Background subtraction with frame differencing with threshold:
(left) 10 and (right) 20 pixels.

The subtraction can be also computed through normalized statistics (Cheung and Kamath, 2004):

$$\frac{|I_t(x, y) - B_t(x, y) - \mu_d|}{\sigma_d} > T \quad (\text{E.7})$$

where μ_d and σ_d are the mean and the standard deviation of $I_t(x,y) - B_t(x,y)$ for all spatial locations (x, y) . Zaurin and Catbas (2010) use another statistical procedure for colour images, which is adapted here for grey-scale images:

$$\frac{(I_t(x, y) - \mu_b)^2}{\sigma_b} > T \quad (\text{E.8})$$

where μ_b and σ_b are the mean and standard deviation of the background frames $B_t(x,y)$. Furthermore, Fuentes and Velastin (2003) use the relative difference, in order to emphasise the contrast in dark areas:

$$\frac{|I_t(x, y) - B_t(x, y)|}{B_t(x, y)} > T \quad (\text{E.9})$$

Figure E.18 shows the subtraction with normalized statistics (Equation E.7) and relative difference (Equation E.9) (both thresholds are equal to 50 pixels). The wheel is still not clearly recognisable and there is more noise compared to Figure E.17.

More usually, the background subtraction outputs a binary image, with white foreground and black background (Gonzalez and Woods, 2002; Sonka et al., 2008; Zaurin and Catbas, 2010). Figure E.19 shows the results with absolute (threshold 20 pixels) and relative difference.

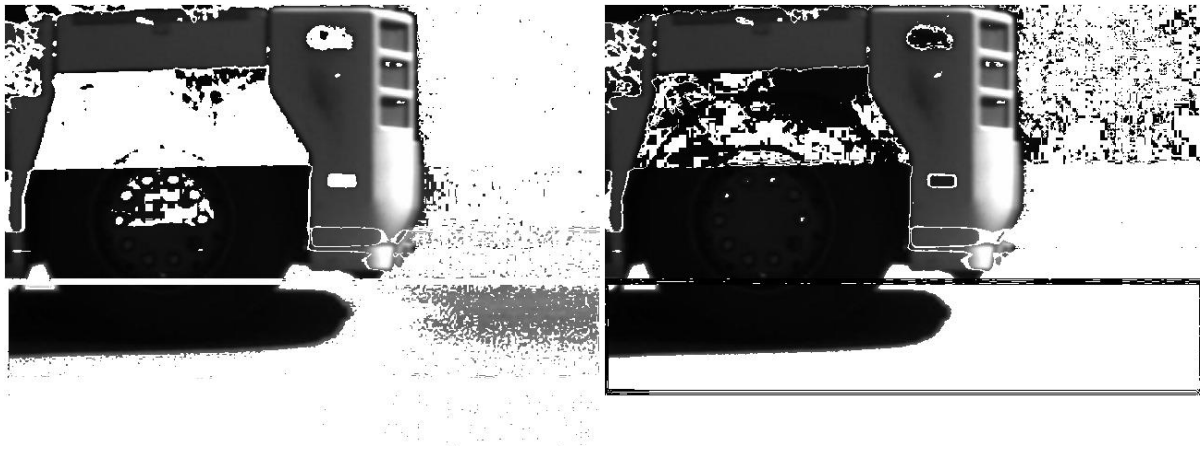


Figure E.18 – Background subtraction with normalized statistics (left) and relative difference (right).

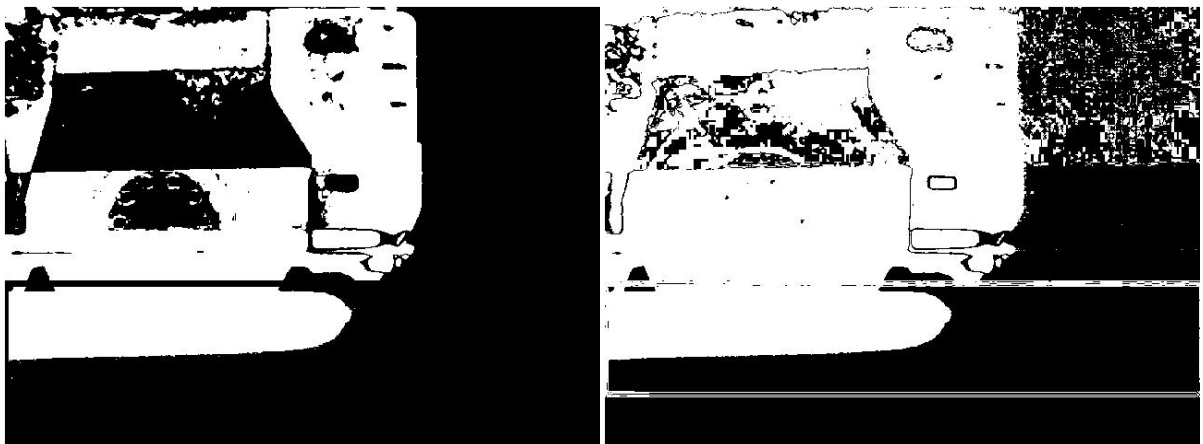


Figure E.19 – Background subtraction with absolute (left) and relative difference (right) as a binary image.

Edge detection

Edge detection looks for “meaningful” discontinuity by using derivatives (first and/or second order). Several methods have been proposed in the literature. In each of them, at least one threshold has to be set.

Sobel, *Prewitt* and *Roberts* methods use a mask to approximate derivatives. All the coefficients sum to 0, allowing them to give a response of 0 in areas of constant grey levels, as expected of a derivative operator. The Sobel method should be preferred, because it has slightly superior noise-suppression characteristics.

The *Laplacian of Gaussian* (LoG) finds edges by looking for zero crossings after filtering the image with an LoG filter (the so-called *Mexican Hat*). This method is useful for noisy images. A standard deviation has to be set.

Canny is a more complex algorithm which includes smoothing through a Gaussian filter as well. This method needs two thresholds, as well as a standard deviation. The higher threshold sets the strong edges, while the lower one identifies weak edges, which are included in the final picture only if connected to strong edges (Gonzalez et al., 2009).

In the left-hand side of Figure E.20, there are Sobel, Laplacian of Gaussian and Canny methods with the threshold automatically computed by the MATLAB function *edge*. The thresholds are: Sobel 0.0909; LoG 0.0031; Canny 0.0188 and 0.0469. The standard deviations are, by default, 2 (LoG) and 1 (Canny). The initial image has to be greyscale (or binary) and the output is a binary image. As can be seen, the routines successfully detect the bumper, but not the wheel.

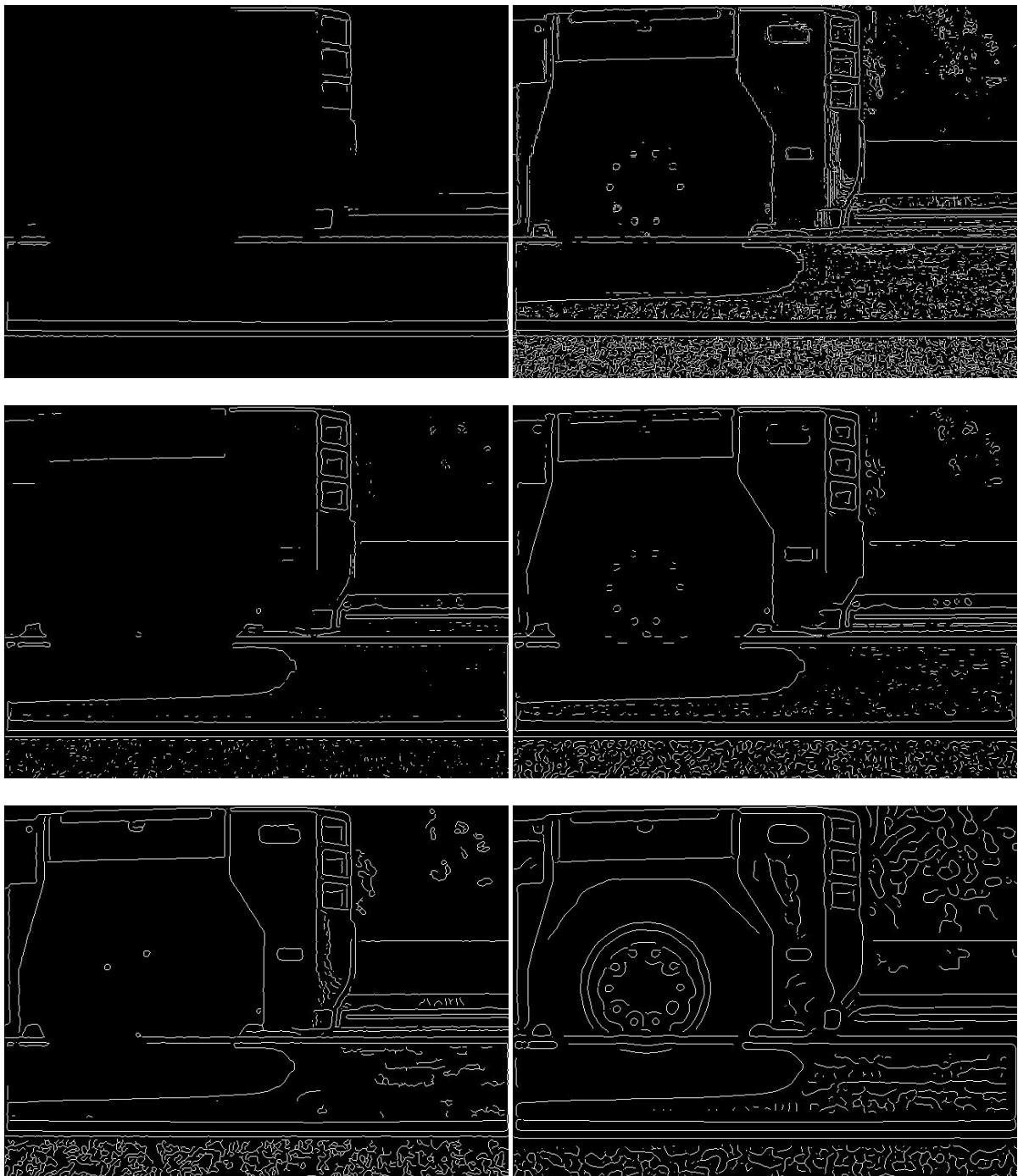


Figure E.20 – Edge detection with Sobel (top), Laplacian of Gaussian (centre) and Canny (bottom) with MATLAB default values (left) and adjusted values (right).

In the right-hand side of Figure E.20, the picture is processed with the same three methods, but with lower thresholds (in order to detect more edges) and standard deviations increased (in order to reduce noise). Sobel's threshold is dropped to 0.01. LoG's threshold is dropped to 0.001, while the standard deviation is slightly increased to 2.5. Canny's higher threshold is

dropped to 0.01 (lower threshold is by default 40% of the higher one) and standard deviation is increased to 3, thus providing the most successful result. In fact, Sobel and LoG fail again to find the wheel (unless by decreasing the threshold dramatically, at the cost of getting excessive noise), while Canny was able to identify the wheel quite clearly.

Thresholding

Thresholding is quite a popular method, because of its simplicity. Any image point with intensity higher than the threshold set is called a *foreground point*; otherwise it is called a *background point* (or the other way round), similarly to what was defined in background subtraction. Thresholding can be either *global* (when the threshold is a constant applicable over an entire image) or else *variable*. The output is a binary image, where 0 (black) is the background and 1 (white) is the foreground³.

Thresholding, with MATLAB default value 0.5 (128 in class *uint8*), is shown in Figure E.21 (left). The original picture is quite dark and, as a consequence, the thresholded image is quite dark as well. However, the bright front of the truck can be recognized.

A manual analysis shows that the wheel grey intensity is around 10-15, while the tyre intensity is around 5. The shadow has basically the same intensity as the tyre. Thus, it is not possible to separate the whole wheel, but we can differentiate the rim from the tyre, by choosing a threshold of 0.04 (10 in *uint8*). The result is shown on the right-hand side of Figure E.21.

³ The MATLAB function *im2bw* converts an image into a binary one and a threshold value between 0 and 1 (regardless of the class of the image) can be set.

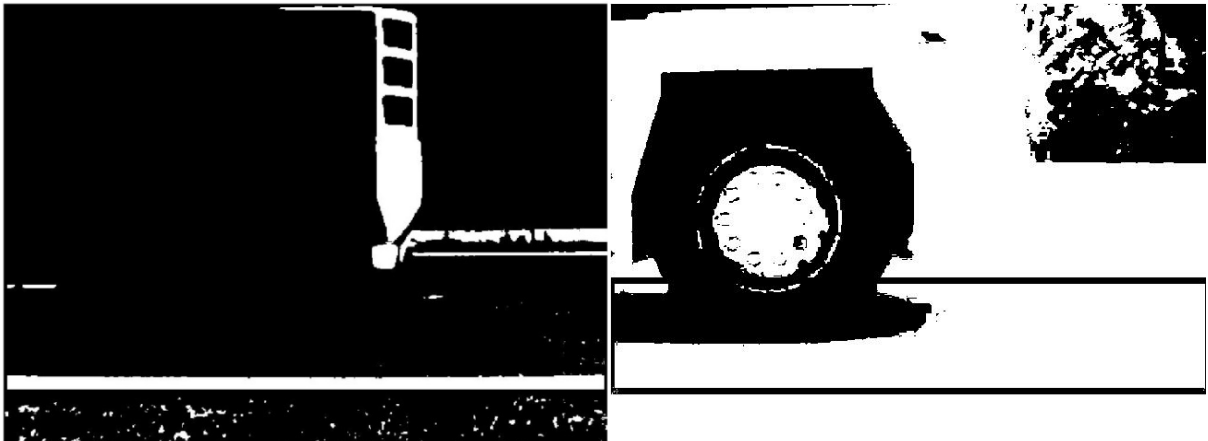


Figure E.21 – Global thresholding with threshold 128 (left) and 10 (right).

The threshold value can be automatically computed using Otsu’s method⁴, which maximises the so-called *between-class variance*. This parameter is related to the more intuitive *separability measure*, which spans from 0 for constant images to 1 for binary images. For details, refer to Gonzalez et al. (2009).

Figure E.22 (left) shows the histogram of the sample picture (Figure E.16). The histogram plots the total number of pixels that have a certain intensity level⁵. Figure E.22 (right) shows the image after thresholding with Otsu’s method. It returns a threshold 0.2902 (74 in *uint8*), which identifies the deepest and most separated valley in the histogram, and a separability measure 0.7343. However, it does not return the desired separation between the truck and the real background, as they mostly share the same intensity range.

⁴ The method is implemented in the MATLAB function *graythresh*.

⁵ In MATLAB, the histogram can be generated with the function *imhist*.

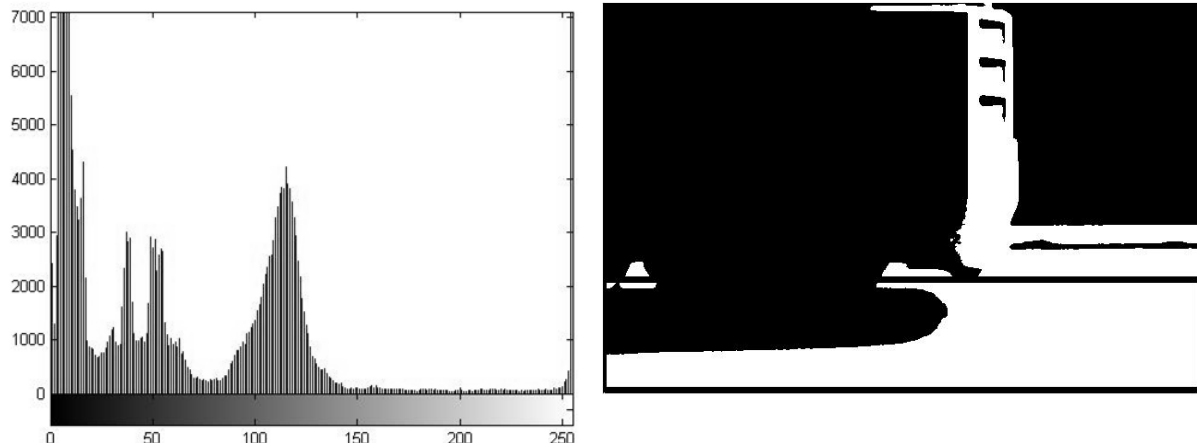


Figure E.22 - Histogram (left) and automatic thresholding with Otsu's method (right).

The chances of selecting a good threshold are enhanced considerably if the histogram peaks are tall, narrow, symmetric, and separated by deep valleys (for instance, when the histogram has a clearly bimodal distribution). Unfortunately, this is not often the case, but pre-processing (such as image smoothing or edge detection) may help global thresholding to succeed (Gonzalez et al., 2009).

Global thresholding methods typically fail when the background illumination is not uniform, as is usual in outdoor applications. In this case, *variable thresholding* can be used, i.e., the value of the threshold changes over the image. Among variable thresholding techniques, *local thresholding* computes a threshold value at every point (x, y) in the image, based on local statistics of neighbouring pixels. One common approach considers the mean m_{xy} and the standard deviation σ_{xy} in a neighbourhood. The global image mean, m_G can be used as well. The threshold can then be found by arithmetical (sum) or logical (*AND*) combination of the mean and the standard deviation⁶. For instance, Gonzalez et al. (2009) implement local thresholding with statistical parameters logically combined as follows (function *localthresh*):

⁶ In MATLAB, the local standard deviation σ_{xy} in a neighbourhood can be computed by the function *stdfilt*. The global mean m_G can be computed by the function *mean2* (in the sample picture is 58.5160), while the local mean m_{xy} can be computed using the custom function *localmean* in Gonzalez et al. (2009).

$$g(x, y) = \begin{cases} 1 & \text{if } f(x, y) > a\sigma_{xy} \text{ AND } f(x, y) > bm \\ 0 & \text{otherwise} \end{cases} \quad (\text{E.10})$$

where $g(x,y)$ is the segmented (output) image and $f(x,y)$ is the input image. The mean m can be either local m_{xy} or global m_G . The size of the neighbourhood (must be odd) and the two parameters a and b have to be set. The results of setting a 3×3 neighbourhood, $a = 10$ and $b = 0.2$ (as the image is quite dark) with global mean (left) and local mean (right) are shown in Figure E.23. The results are satisfactory as both the bumper and the wheel are quite clear and the noise is moderate.

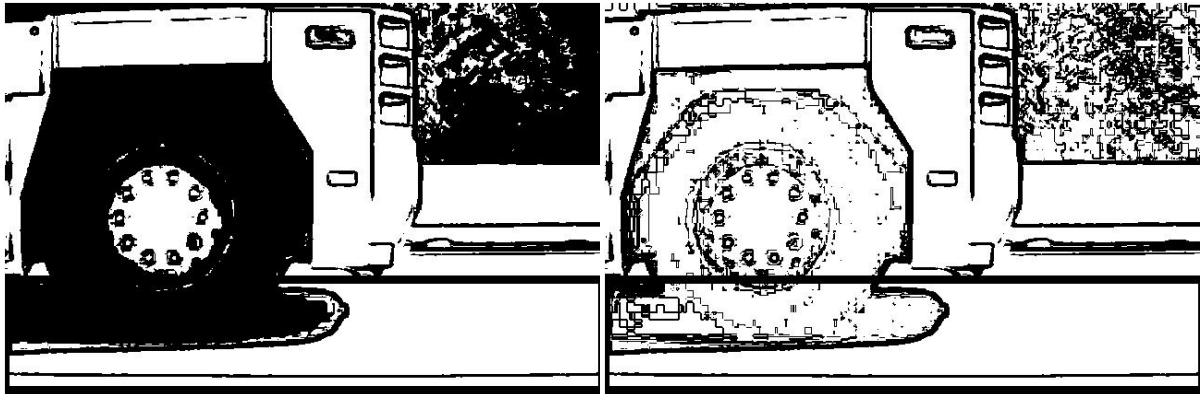


Figure E.23 - Local thresholding with global (left) and local mean (right).

Region-based segmentation

Region-based segmentation, as the name itself suggests, finds regions directly. *Region growing* groups pixels into larger regions starting from *seed points*. A priori knowledge of some points in the region (for example, the intensity of the seed points) is required. Unfortunately, this is not true of images of congested traffic, as vehicles and wheels can have many different intensities. Another sub-technique, *region splitting and merging*, only applies to square regions.

Watershed segmentation

Watershed segmentation uses a “hydrological” approach to images. The image is interpreted as a topographic surface (with the grey intensity representing the height), then regional minima are found in it (*catchment basin*) and finally the image is flooded from below by letting water rise. Whenever the flooding is about to flow into an adjacent basin, a dam is built to prevent the merging.

This method is mostly useful for extracting ‘blob-like’ objects from the background. Watershed segmentation, directly applied to images, often leads to over-segmentation. Gonzalez et al. (2009) suggest the use of a *gradient image* (left-hand side of Figure E.24) - which can be obtained by filtering with a Sobel approximation to the derivative, just like edge detection – but this still leads to over-segmentation (right-hand side of Figure E.24). The result is apparently not useful for vehicle detection purposes.

Image pre-processing through smoothing or morphological operations would tackle over-segmentation, but just leads to bigger blobs. More effectively, selected markers could be used for controlling over-segmentation, but, again, some a priori knowledge of the region property is required in order to place the markers properly.

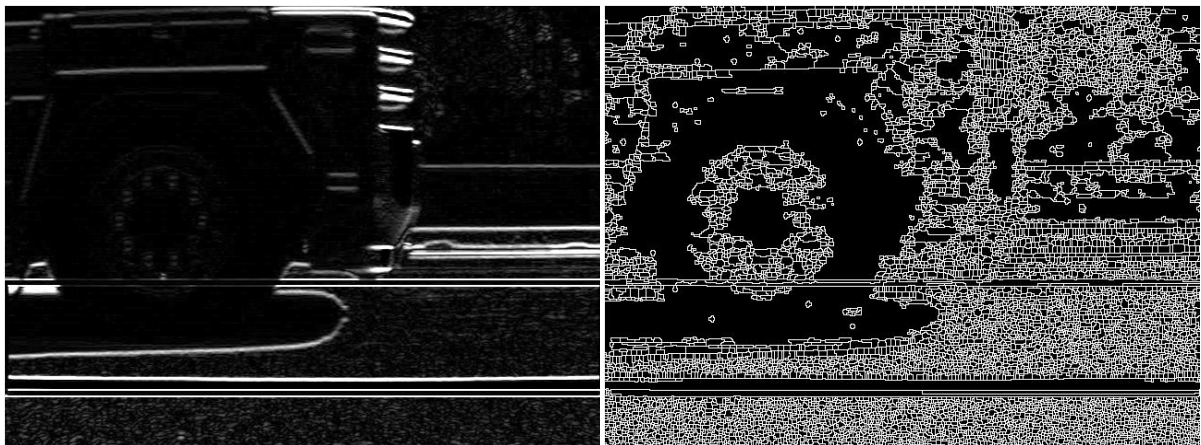


Figure E.24 - Gradient image (left) and watershed segmentation (right).

Line detection with the Hough transform

The *Hough transform* is a powerful method to detect lines in a binary image. The first step is to build up the *parameter space*, where for each non-zero point (x_i, y_i) the parameters of *all*

the possible lines with parameters (a, b) passing over (x_i, y_i) are plotted. They are, in turn, represented by a line:

$$y_i = ax_i + b \rightarrow b = -ax_i + y_i \quad (\text{E.11})$$

In practical applications, the polar representation of a line (ρ, θ) is used in order not to have $y = \infty$ for vertical lines:

$$x_i \cos \theta + y_i \sin \theta = \rho \quad (\text{E.12})$$

The parameter space (ρ, θ) is then divided into *accumulator cells*, the dimensions of which, $\Delta\rho$ and $\Delta\theta$, have to be set. The dimensions represent the precision at which the analysis is carried out. The parameter space starts as an empty matrix. Whenever a line corresponding to the parameters of a given point (x_i, y_i) falls into a cell, the cell value is incremented by one. When a cell is a *local maximum*, it means that many image points share the same parameters, i.e., that they are aligned. One of the advantages of this method is that it is not very sensitive to image noise and partial occlusion.

Figure E.25 shows the Hough method applied after Sobel edge detection (as for Figure E.20 top right), along with the parameter space (ρ, θ) ⁷. The brightest points correspond to higher value cells. Horizontal edges lie at both sides of the graph ($\theta = 0$ and $\theta = 180^\circ$), while vertical edges lie in the middle ($\theta = 90^\circ$) and in this case are weaker than the horizontal ones. The number of peaks to look for is set to 10 and the endpoints of the lines must be found⁸. In Figure E.25, only vertical lines are displayed (slope between 88 and 92°). Gaps between lines with the same parameters are filled if smaller than 50 pixels. The vertical line shown is the strongest vertical edge and is the actual bumper of the truck.

⁷ The parameter space can be generated with the MATLAB function *hough*.

⁸ The function *houghpeaks* finds the peaks and the function *houghlines* finds the endpoints of the lines.

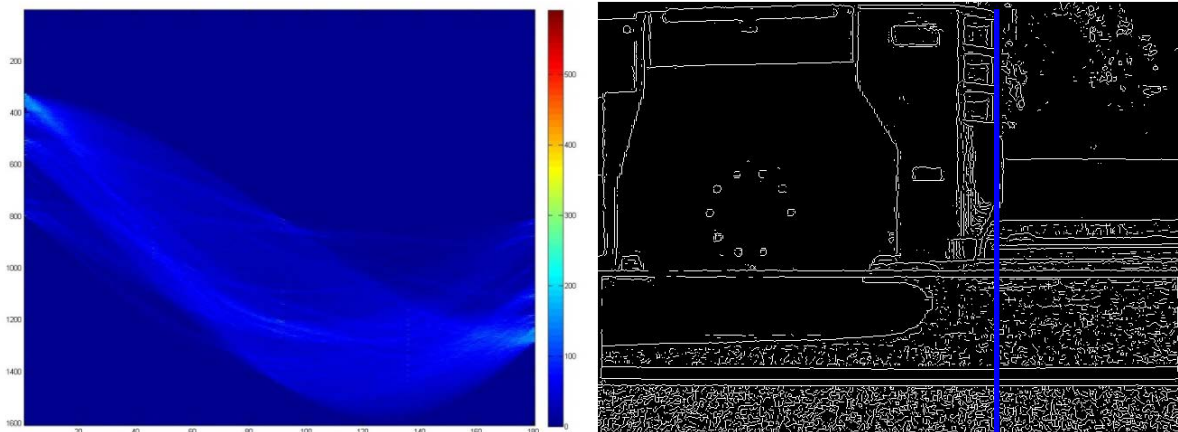


Figure E.25 – Parameter space (left) and bumper detection (right) after Sobel's edge detection.

Circle detection with the Hough transform

The Hough transform can be generalized to any shape (even with no analytical representation), although complexity increases considerably (Ballard, 1981). The circle detection would involve three parameters (the centre coordinates x_0 , y_0 and the radius r) and so the parameter space would be 3-D, which can be found from the equation of a circle:

$$(x - x_0)^2 + (y - y_0)^2 = r^2 \quad (\text{E.13})$$

This is already a computationally demanding task, but implementation becomes easier if one of three parameters is known (for instance the radius). A simple applet showing the application of the Hough transform for circle detection is available online (Schulze, 1996).

Figure E.26 shows the Hough transform for circle detection after Canny's edge detection (which was the only method successful at recognising the wheel), superimposed on the original image. The parameter space (x_0, y_0) is shown as well. The radius has to be preliminarily set to 82 pixels though, following a manual analysis of the image. The minimum number of pixels belonging to a circle has to be set as well. That has been set quite low (equal to the radius) in order to account for imperfections in the radius value and for possible shape warping. The procedure is successful, as it is quite easy to identify the centre of the wheel in the parameter space.

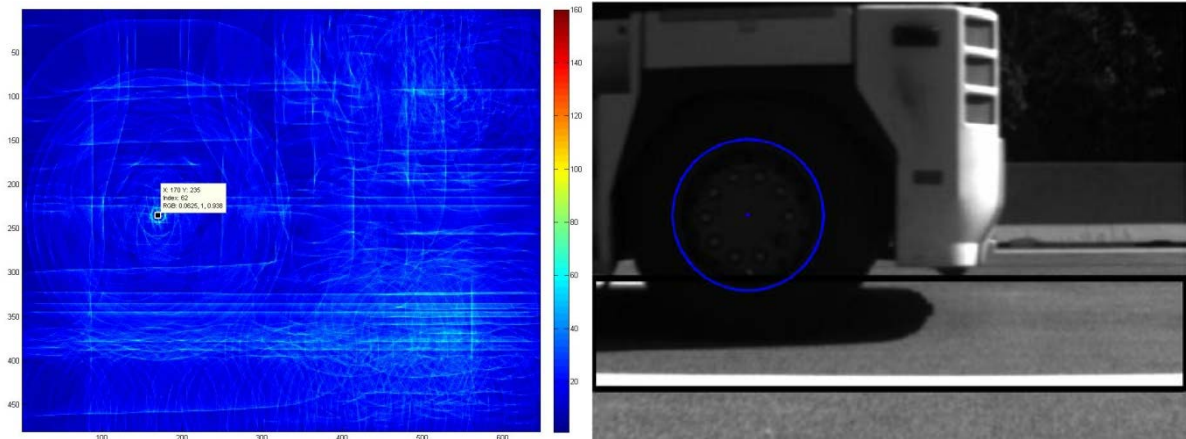


Figure E.26 – Parameter space (left) and circle detection (right) after Canny's edge detection.

It has been shown that local thresholding with local mean returns thin regions (Figure E.23). Thus, it can be processed further through the Hough transform after inverting the image (that is its *negative*), in order to have white edges on black background. However, the clusters of white pixels significantly increase the number of circles detected, leading to the detection of numerous fake circles (Figure E.27). The minimum number of pixels per circle has to be increased to twice the radius, in order to limit the detection of fake circles, but the wheel is not even the strongest circle. It is expected that when multiple radius values are considered, the interference from other objects will increase, leading to the detection of even more fake circles.

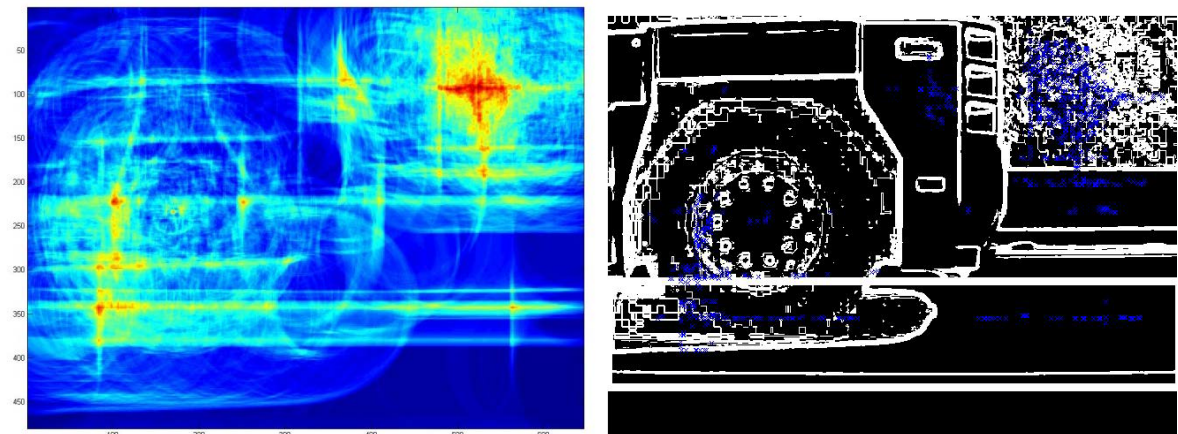


Figure E.27 – Parameter space (left) and circle detection after local thresholding (right; only the circle centres are shown).

Another picture

A second sample picture (Figure E.28) is analysed with the most promising techniques. The picture is slightly brighter than the previous one. It has better conditions for wheel recognition (higher contrast), but the rear bumper has a complex shape and may be more difficult to recognise. The parameters for the image processing are initially not changed, in order to test the robustness and the sensitivity of the tested techniques.

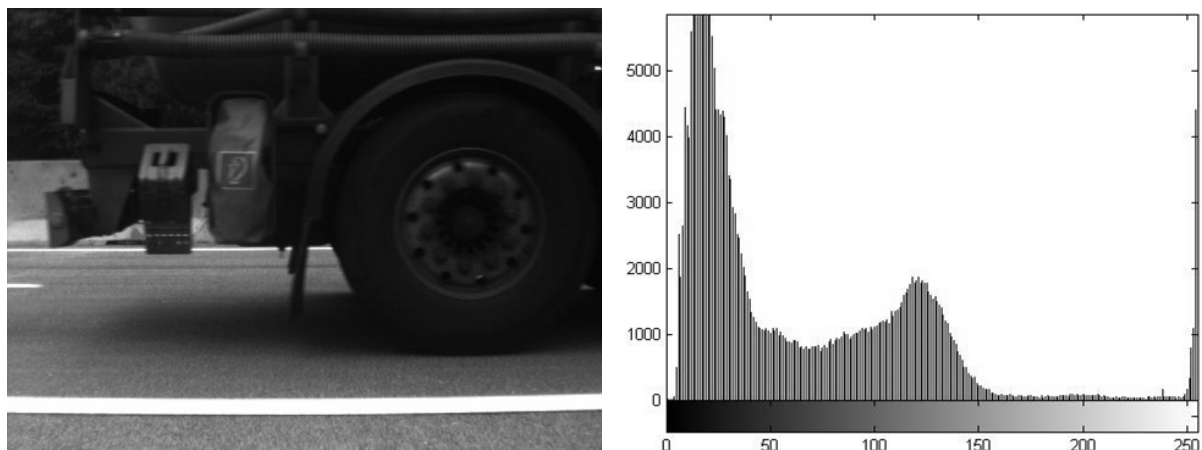


Figure E.28 - Second sample picture (left) and histogram (right).

Figure E.29 shows the application of edge detection. As in Figure E.20, the left-hand column shows the Sobel, LoG and Canny methods with MATLAB automatic thresholds⁹, while in the right-hand side there are the same methods with the same parameters used in the section on *Edge detection*.

All the methods (except for Sobel with automatic settings) succeed at recognising the wheel, although partially and with some noise, whereas the bumper can be seen only in four of them.

⁹ The thresholds automatically computed by MATLAB are: Sobel 0.0583, LoG 0.023 and Canny 0.0250 and 0.0625.

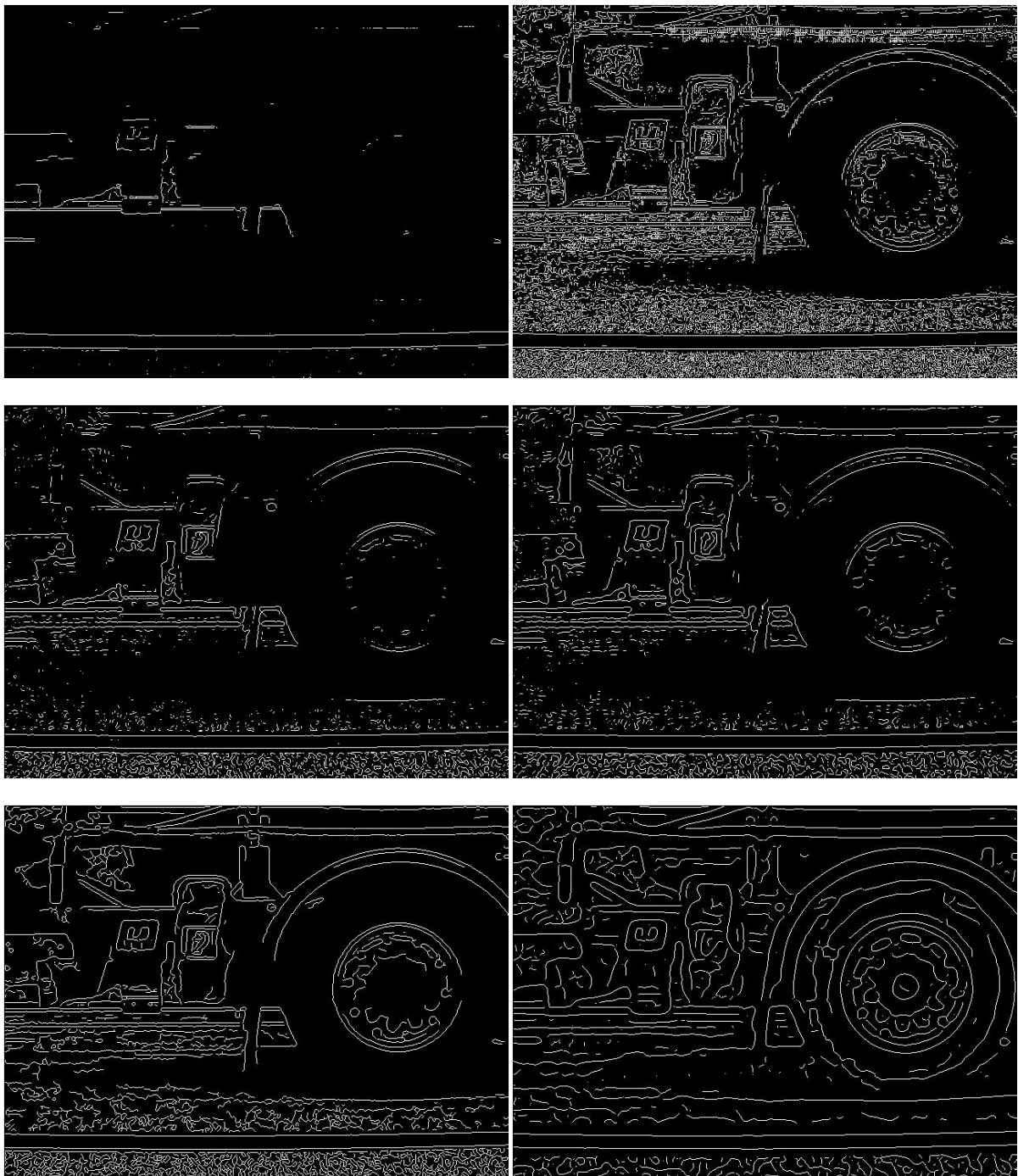


Figure E.29 - Edge detection of second picture with Sobel (top), Laplacian of Gaussian (centre) and Canny (bottom) with MATLAB default values (left) and adjusted values (right).

The parameter space of the Hough transform after Sobel edge detection is shown on the left-hand side of Figure E.30. In a first attempt, the Hough transform does not detect any vertical edge (as the bumper is not as clear as in the first image). However, increasing the number of peaks detected from 10 to 100 returned two vertical edges, one of which is the actual bumper

and the other is at left edge of the picture (Figure E.30). Another option may be to restrict the analysis to a region of the parameter space, for instance in the range 88-92 degrees.

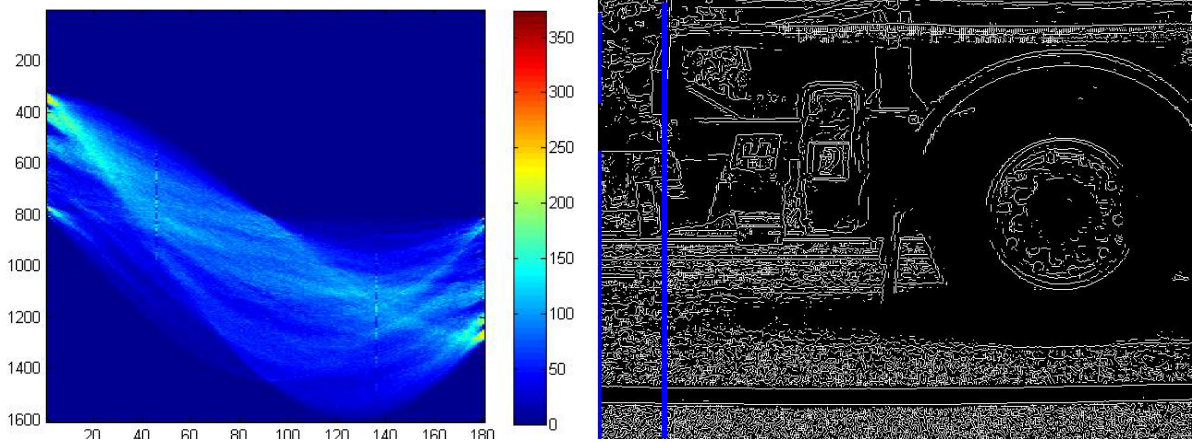


Figure E.30 – Parameter space (left) and vertical line detection (right) for the second picture.

On the other hand, the Hough transform for circle detection detects many “fake” circles. However, the strongest circle detected corresponds to the actual wheel, as can be seen in the parameter space (Figure E.31). However, it has been necessary to increase the minimum number of pixels of a circle (which was initially set equal to the radius, as in Figure E.26).

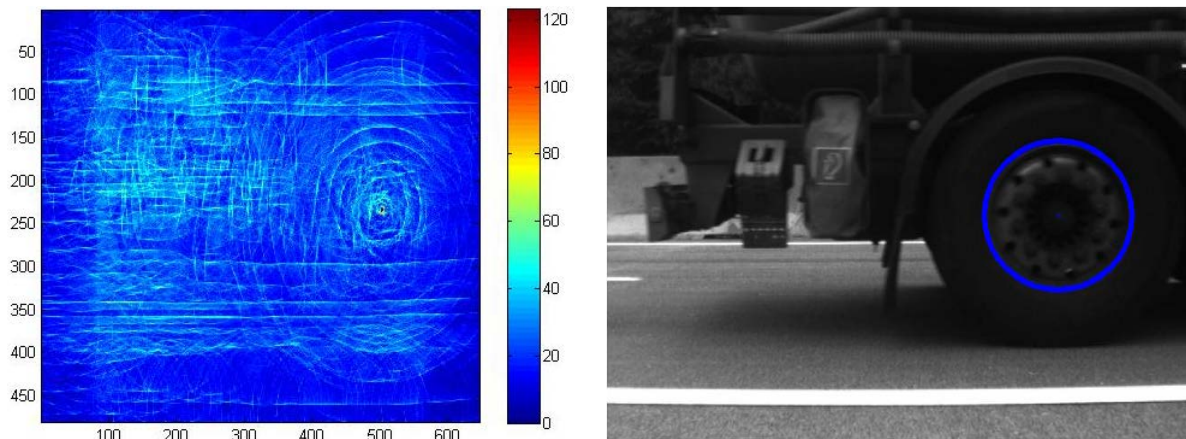


Figure E.31 – Parameter space (left) and circle detection after edge detection (right) of the second picture.

The application of global thresholding is shown in Figure E.32. The left picture has a threshold of 0.04 (10 in the MATLAB class *uint8*, as in Figure E.21 right) and in the right-hand side the threshold is computed by Otsu’s method, which returned 0.3098 (79 in *uint8*). The separability measure is 0.7257. Both images are clearly not satisfactory, although Otsu’s

method returns something similar to the actual difference between foreground (dark) and background (bright).

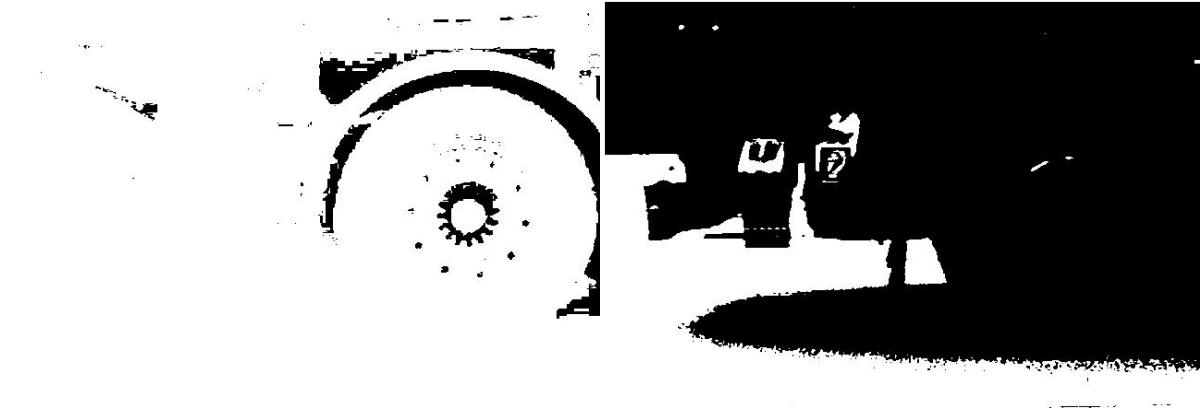


Figure E.32 - Global thresholding with manual (left) and automatic (right) settings of the second picture.

Local thresholding using the custom function, *localthresh* (Gonzalez et al., 2009) is shown in Figure E.33. The left-hand picture uses the global mean (59.5824), while the right-hand one the local mean. The wheels can be clearly identified.

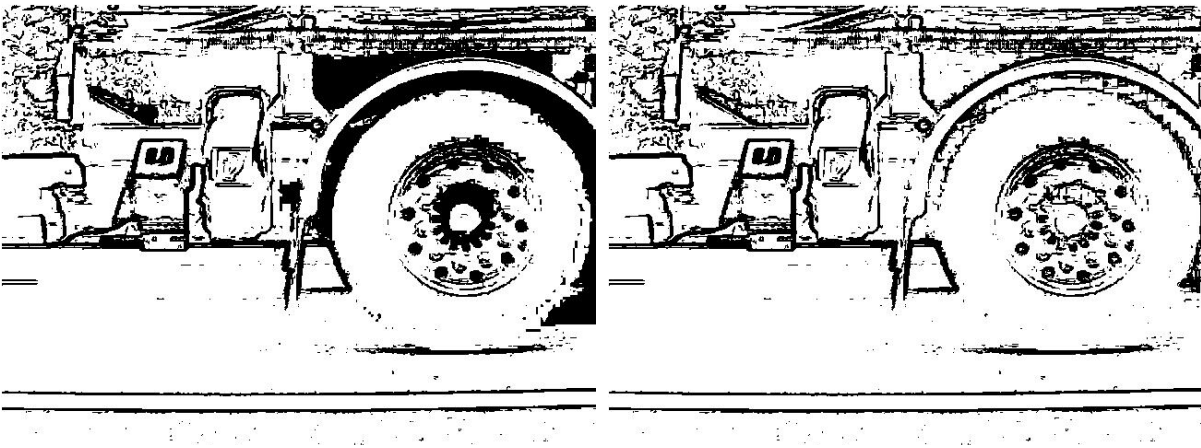


Figure E.33 - Local thresholding with global (left) and local mean (right) of the second picture.

The Hough transform applied to the local thresholding with local mean returns many fake circles (Figure E.34). However, the wheel is the strongest circle, so it is easily recognised. Again, it was necessary to increase the minimum number of pixels in a circle.

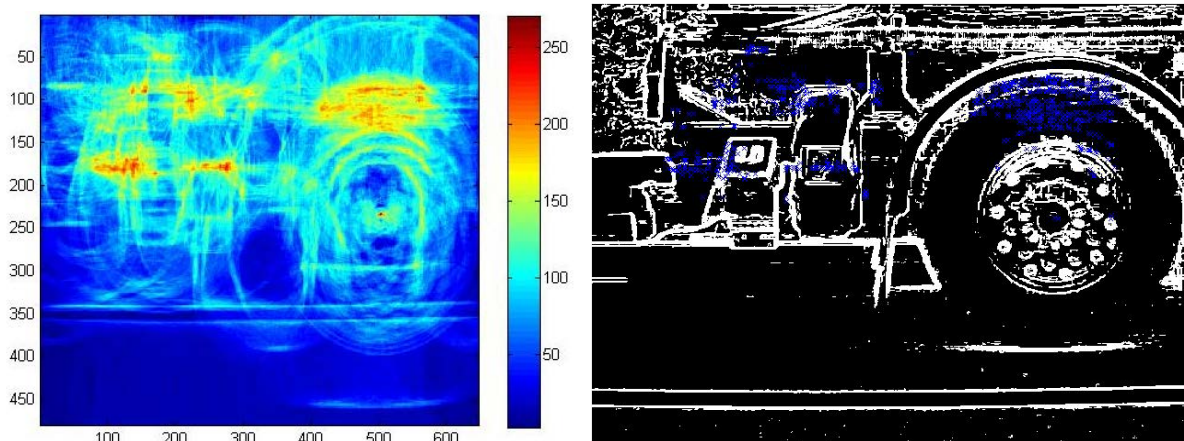


Figure E.34 – Parameter space (left) and circle detection after local thresholding of the second picture (right; only the centres are shown).

Pre-processing

Besides post-processing, image pre-processing may be helpful, such as *filtering* (to remove noise) and *morphological operations* (to remove small objects). Details of these techniques have been presented by Gonzalez et al. (2009). Pre-processing may significantly improve the quality of the final picture. For instance, Cheung and Kamath (2004) pre-process the images with erosion and a 3×3 spatial Gaussian filter, while Mirth (2008) pre-processes the 1-D signal with a low-pass filter.

Summary

It is clear that there is no single technique that can work with the same parameters, even for two sample pictures. The most promising approach seems to be the use of edge detection plus the Hough transform. Canny's method is the only edge detection technique which – when properly set – managed to detect the wheel edges in both pictures. The Hough transform for circle detection manages to find the wheel edges in both pictures, with minor adjustments. For bumper detection, a simpler Sobel filter can be used. Again, the processing succeeds in both pictures, with small adjustments. The drawback of the Hough transform may be the computational requirements. In particular, the circle detection algorithm may be quite computationally demanding, unless one of the three parameters is known (e.g., the radius of the wheel).

Global thresholding is quite simple and not computationally demanding. However, the threshold strongly depends on the picture features, which may vary because of vehicle colours and illumination changes. On the other hand, local thresholding with local mean returns clear and thin regions, which help further processing with the Hough transform. The use of this technique for circle detection succeeds only in one picture.

In general, wheels may be easier to identify, as they always have the same shape. However, they do not have the same size, which largely increases the computational requirements of the Hough transform. Bumpers may be more challenging. Front heavy vehicle bumpers look easier to identify, but other bumpers may not have a straight shape, as often happens in cars (Blacoe et al., 2012), or they may be just short (as in Figure E.28).

Background subtraction is a popular technique in identifying moving objects, but it does not turn out to be as successful as thresholding and edge detection. In fact, the background needs to be updated to cope with illumination changes, but in congested conditions slow vehicles may incorrectly end up in the background. Moreover, issues arise when vehicles have the same colour as the background, generating holes in the processed image.

E.4.4 Fundamentals of geometrical optics

In order to design a camera system for vehicle detection, it is essential to study some basic principles of *geometrical optics* applied to photography. Geometrical optics neglects the finite wavelength of visible light, as opposed to *physical optics*. In this case, light travels from its source along straight lines or *rays* (Pedrotti and Pedrotti, 1993). For further details, the reader is referred to reference books in optics, such as that of Pedrotti and Pedrotti (1993) or Hecht (2002), or applied optics, such as Ray (2002).

Thin lens equation

Although cameras are often made up of complex multiple lenses, their basic behaviour can be understood through the equation governing *thin lenses*¹⁰ in air, also called the *lensmaker's equation*:

$$\frac{1}{S_1} + \frac{1}{S_2} = \frac{1}{f} \quad (\text{E.14})$$

where S_1 is the distance between the real object and the lens, S_2 the distance between the lens and the image (i.e., the digital sensor, in modern cameras) and f the focal length (Figure E.35). The *focal length* is characteristic of an optical system and is a measure of how strongly a system converges light (in the case of the *convex* lenses used in photography).

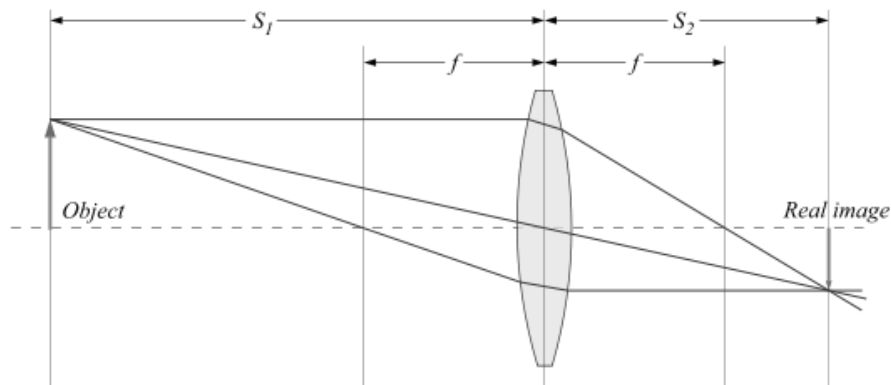


Figure E.35 - Thin lens property (taken from [http://en.wikipedia.org/wiki/Lens_\(optics\)](http://en.wikipedia.org/wiki/Lens_(optics))).

When an object is far away ($S_1 = \infty$), S_2 has to be equal to the focal length f , i.e., the lens has to be exactly at a distance f from the image. When the object is closer, S_2 must be increased (the lens has to be further from the image), as the ratio $1/f$ is often fixed (also called *optical power*). For instance, if we want to take a picture at infinity with a lens with focal length $f = 3.0$ mm, the distance between the lens and the object S_1 has to be 3.0 mm, just equal to f . If we want a picture at 100 mm, the lens has to be 3.09 mm away from the image plane.

¹⁰ A lens with negligible thickness compared to the object and image distances.

Longer focal lengths are associated with larger magnification and a narrower angle of view. Conversely, shorter focal lengths are associated with smaller magnification and a larger angle of view (*wide-angle lenses*). In *zoom* or *varifocal lenses* the focal length can be varied. They are usually described by the *zoom ratio*, that is the ratio of their largest to shortest focal length, for instance 4:1 or 4× (Ray, 2002).

In digital cameras, *image sensors* are needed to convert the optical signal into a digital signal. The most used digital sensors are the CCD (*charge-coupled device*)¹¹. From similar triangles one can also find the focal length required (thus the optical system) by knowing the distance from the object (S_1+S_2) and its width w_1 , as well as the width of the sensor w_2 :

$$f = \frac{w_2(S_1 + S_2)}{w_1 + w_2} \approx \frac{w_2 S_1}{w_1} \quad (\text{E.15})$$

The approximation is made considering that for traffic applications $S_1 \gg S_2$ and $w_1 \gg w_2$.

For example, if we want to take a picture 15 m wide from 5 m, with a CCD sensor ¼” then:

$$f \approx \frac{3.2 \cdot 5000}{15000} \approx 1 \text{ mm} \quad (\text{E.16})$$

Increasing the sensor size w_2 would increase the focal length required.

Another important parameter is the *angle of view* α (sometimes referred to as *field of view*). It describes the angular extent of a given scene that is taken by a camera. It can be found by means of a trigonometric ratio:

$$\alpha = 2 \arctan \frac{d}{2f} \quad (\text{E.17})$$

¹¹ The most common digital CCD sensor size are (in brackets the diagonal):

¼” 3.2 x 2.4 mm (4 mm)

⅓” 4.8 x 3.6 mm (6 mm)

½” 6.4 x 4.8 mm (8 mm)

The angle of view α can be computed horizontally, vertically or diagonally, depending on the dimension of the sensor, d chosen. For our purpose, the horizontal angle of view is by far the most important. For a CCD sensor 1/4" and 3.0 mm focal length, the (theoretical) horizontal angle of view is about 56°, which is quite a standard value. A greater angle (about 75-90°) characterises *wide-angle* lenses, while *fish-eye* lenses can reach as much as 180°.

Aperture

The *aperture* of a camera controls the amount of light reaching the sensor, along with the *exposure time* (or *shutter speed*). The aperture is typically adjusted by varying the size of a *diaphragm* and it is coordinated with the exposure time, which adjusts the time during which a camera shutter is open, thus determining the total exposure to light (Pedrotti and Pedrotti, 1993). Fast moving objects require fast shutter speeds. Dark objects require a high aperture or a high exposure time (= lower shutter speed).

The *relative aperture* A is the ratio between the aperture D and the focal length f :

$$A = \frac{D}{f} \quad (\text{E.18})$$

However, in photography the aperture is measured in *f-numbers*, typically 1 1.4 2 2.8 4 5.6 8 11 16 22, which are the inverse of the relative aperture (Hecht, 2002). For instance, *f*-number 4 or *f*/4 means an aperture 4 times *smaller* than the focal length. Those numbers are selected in such a way that the area of the diaphragm doubles, when moving from a given *f*-number value, a 'stop', to the next (lower) one.

Reducing the aperture (higher *f*-number) increases the *depth of field* (DOF), which describes the extent to which objects around the actual plane of focus appear to be in focus. In this case, the image will turn out to be globally sharper. On the contrary, small *f*-numbers allow for more light into the sensor, but decrease the depth of field. The two limits (*near* D_N and *far* D_F) of the depth of field DOF can be calculated from the following equation (Ray, 2002):

$$D_N, D_F \approx \frac{s \cdot f^2}{f^2 \pm N \cdot c \cdot s} \quad (\text{E.19})$$

with s the distance from the object, f the focal length, N the f -number, c the *circle of confusion*. The circle of confusion c can be set equal to the dimension of one pixel (about 5 μm). In summary, the smaller the focal length f , the greater the depth of field.

For instance, if we focus at 10 cm, with focal length 3.0 mm and aperture $f/1.4$, the depth of field spans from 9.3 to 10.8 cm, blurring all the objects not included in this range. If we use aperture $f/11$, the depth of field is expanded from 6.3 to 24.6 cm.

An important value involved in the depth of field is the *hyperfocal distance*, H (Ray, 2002):

$$H \approx \frac{f^2}{N \cdot c} \quad (\text{E.20})$$

Inserting Equation (E.20) into (E.19) shows that when focussing at the hyperfocal distance ($s = H$), the depth of field spans from $H/2$ to infinity.

Focussing at the hyperfocal distance results in the largest possible depth of field (for a given f -number). Focussing beyond the hyperfocal distance does not increase the far limit (which is already infinite), but decreases the total DOF. Thus, there is no advantage in the sharpness of the farthest objects (at least ideally).

For example, if we have a system with focal length $f = 3.0$ mm and large aperture $f/1.4$, the hyperfocal distance H is 1286 mm (Equation E.20). In this case, any object further than 643 mm is acceptably focussed. If the f -number is 11 (small aperture), H is much lower (164 mm). This implies that, for traffic applications - which may require large apertures, because of darkness or low shutter time - depth of field should not be a problem, as we usually need to focus on objects much farther than the lower limit of the depth of field.

Aberration

Spherical lenses do not have the ideal shape when light rays strike near its edge, but they have by far the easiest shape to make. *Aberration* results when the light is not in the so-called *paraxial region* of a lens, which is a small area around the lens symmetry axis (Hecht, 2002).

There are many kinds of aberration, but they can be broadly subdivided into *monochromatic* and *chromatic* aberrations. *Monochromatic aberrations* are caused by the geometry of the lenses. *Chromatic aberrations* are not of interest here, as we use greyscale pictures. Among monochromatic aberrations, some affect the sharpness (*spherical aberration*, *coma* and *astigmatism*), while others affect the shape (*field of curvature* and *distortion*). The latter sub-group is the most important for applications with wide-angle lenses, where it is particularly noticeable. Among this sub-group, quite common is the *barrel distortion*, in which the centre of the image is magnified more than the perimeter (see Figure E.36). The apparent effect is that the image has been mapped around a barrel. Since the barrel distortion is radial, the two central axes are not warped, so it is a good idea to make the part to measure (e.g., wheels and bumpers) lie in the middle of the picture. In any case, the image may be post-processed in order to correct barrel distortion (Vass and Perlaki, 2003). Or else, more expensive aspherical lenses may be used.

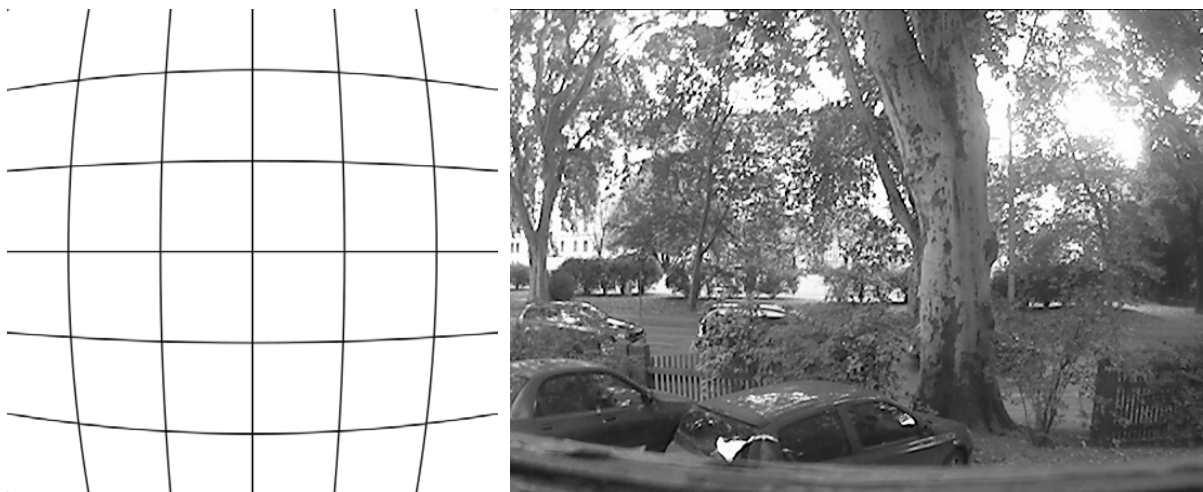


Figure E.36 - Example of barrel distortion.

E.4.5 Site setup

In this section, two possible site setups for data collection are outlined. Several tests have been carried out with the colour digital camera *Axis 221*, provided courtesy of *ROC Systemtechnik GmbH*, Graz (Austria). The *Axis 221* has a 1/3" CCD sensor (4.8 x 3.6 mm) with varifocal lens 3-8.0 mm.

One-camera setup

A possible setup option is to use one camera located next to the slow lane. In this case, it is useful to capture the widest picture possible, in order to fit long vehicles and allow wheel detection in a single picture. It would also allow the detection of gaps higher than those visible in standstill conditions. An image width of 15 m seems a reasonable initial target and several tests are performed with the Axis 221 to achieve the target width.

Axis 221 specifications declare that the maximum horizontal angle of view is 93° (Axis Communication, 2008). Hence, we have to step back from the object at a distance roughly half of the width of the object (7.5 m if the target width is 15 m). However, such a distance is not always available on site at the roadside, so the use of wider angle lenses would pose fewer constraints to the site choice. As mentioned in section E.4.4, in order to avoid barrel distortion, it is a good idea to take the picture in such a way that wheels or bumpers do not lie near the corners.

Axis 221's maximum resolution is 640×480 pixels (*VGA resolution*). If we have an object 15 m wide, one pixel represents about 2 cm. A standard car wheel would turn out to have a diameter of approximately 25 pixels and this should pose no problem for image post-processing.

Regarding the exposure time, at a typically fast value of $1/500^{\text{th}}$ s, a vehicle at 36 km/h moves 2 cm. This exposure time is quite low but seems appropriate, because it returns the same precision as the resolution. Thus, there would be no need to set slower exposure times, unless traffic were much faster. Moreover, there would be no need to increase the resolution, unless a smaller exposure time is required, for instance, because of darkness.

The maximum aperture is $f/1$, and in this case the hyperfocal distance is 1.80 m (Equation E.20). This suggests that there should be no blurring problem when focussing on objects farther than 90 cm, for the case where it is needed to take pictures in low light or low exposure time.

With this setup, it is not possible to collect data from other lanes. Actually, the detection of vehicles in the slow lane is likely to be disturbed by other vehicles queuing in the farther

lanes. This problem can be solved by inclining the camera and then selecting a *region of interest*. However, this means putting the camera higher than the road plane. Figure E.37 illustrates that taking a picture 7 m far from the slow lane and at 1.5 m high (i.e., a man standing) is not enough to solve this problem. In fact, any wheel in the fast lane would fall in the region of interest (red rays in Figure E.37). Furthermore, a small wheel in the slow lane appears with the same diameter as a big wheel in the fast lane. Therefore, the picture should be taken either from a high vantage point (e.g., a pole or a hill) or from closer, in the latter case with the disadvantage of reducing the overall width of the picture.

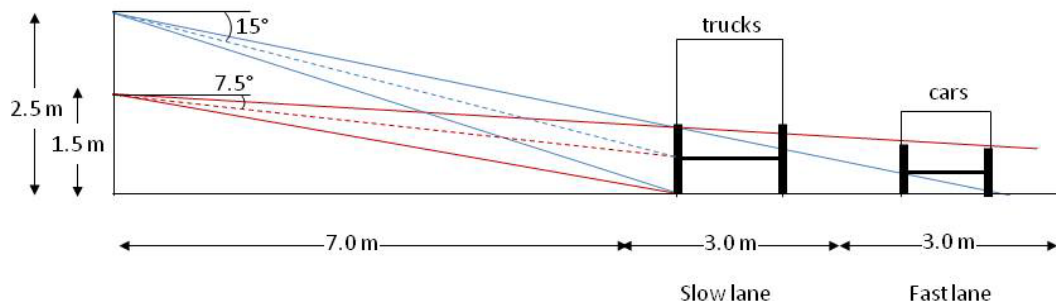


Figure E.37 - Camera inclination.

As a rough indication, an inclination of 15° or higher should avoid disturbance from farther lanes. Such an inclination can be achieved with a man standing less than 3.5 m far from the lane, or by putting the camera higher than 2.5 m if we stay 7 m far from the lane (blue rays in Figure E.37), in the latter case benefitting from a wider picture. However, with such an inclination, shape warping might pose issues for further circle detection.

In order to test shape warping, a sample picture has been taken from the *ROC* office in Graz (notably with little illumination, Figure E.38 left), converted into greyscale and then processed with edge detection and the Hough transform. The camera is about 15.5 m far from the wheel and 3.5 m high from the road plan, returning an inclination of about 13° .

For this image, a default Sobel filter works well for edge detection. The circular Hough transform with fixed radius (18 pixels) succeeds in detecting the wheel (Figure E.38), which actually was the strongest (and only) circle detected. This result confirms that the Hough transform is a powerful method to detect circles (or quasi-circular objects) and suggests that shape warping is not an issue for wheel detection with such inclinations.

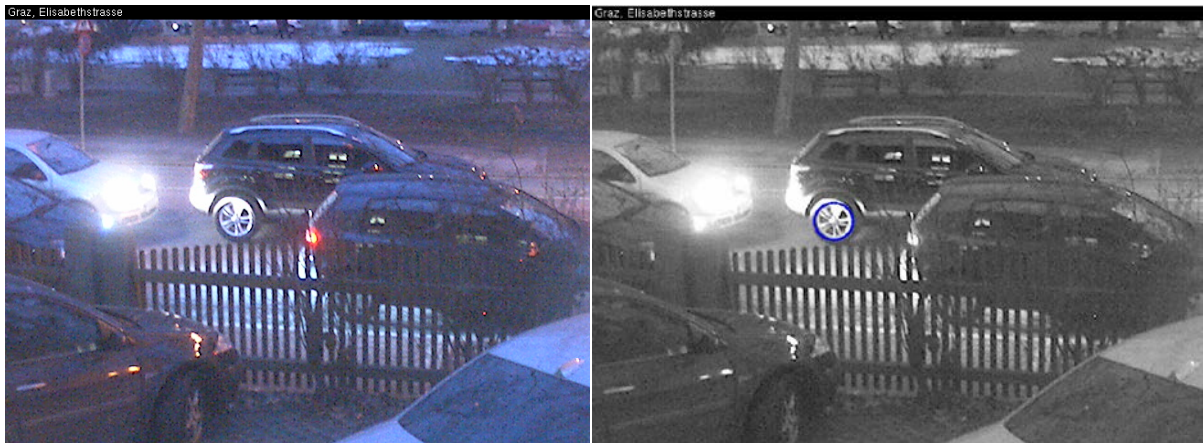


Figure E.38 – Original picture (left) and processed image for wheel detection (right).

The one-camera setup has the advantage of simplicity, portability and low costs, as it requires only a camera and a system for data acquisition (e.g., a laptop, better with a big hard disk to store the pictures). The demanding post-processing can be carried out after acquisition.

Finally, this setup could be also used to obtain speed-gap relationships in slow-moving traffic, which may be required for the calibration of the single-lane micro-simulation model. If this is the aim, two cameras in a row may help, effectively doubling the actual field of view. However, this option would be more computationally demanding, as speeds and accelerations need to be computed, possibly at a higher frame rate, and synchronization between the two cameras would be needed.

Two-camera setup

Another option is to use two different cameras, one on the roadside for detecting wheels and bumpers of the vehicles in the slow lane, and one aerial camera for detecting gaps in all the lanes. The aerial camera needs to be placed on a pole or over a bridge crossing the site, thus imposing constraints on the site choice.

The main advantage is that the aerial camera can provide gaps from all the lanes, which can be used to determine the micro-simulation model parameters, if related to speeds and accelerations. The information about wheels and bumpers would come from the roadside camera, similar to the one-camera setup. It may help to use an aerial camera with higher resolution, according to the stretch of road considered. However, occlusion of vehicles may

be a problem for automatic gap detection in congested conditions (Coifman et al., 1998). The measurements have to take account of the perspective and results may be less accurate than the one coming from the roadside camera. The two cameras have also to be synchronised for post-processing.

Finally, the overall cost is higher and the system is less portable. However, there is no need to use wide-angle lenses and two cameras with standard lenses can be used.

E.4.6 Recommendations and conclusions

The following recommendations can be made for choosing an optical system for bridge loading applications:

- colour images are not needed, as objects of no particular colour need to be identified;
- wide-angle lenses are useful, because there may not be available space on the roadside; in this case, aspherical lenses can be used to avoid barrel distortion;
- a very high resolution is not needed, as the objects to detect are relatively large;
- a particularly quick exposure time is not needed, nor a high frame rate acquisition, as the traffic is slow-moving;
- aperture and subsequent depth of field should not pose issues, as the objects to focus on are quite far;
- it is advisable to take a picture with an inclination of about 15° (or more), in order to avoid disturbance from vehicles in farther lanes.

Regarding the image processing, tests showed that:

- bumper detection can be challenging, as bumpers are rarely straight (except for front bumpers of heavy vehicles);
- circle detection is computationally demanding, unless the radius of the circle is known;

- the most promising image processing technique is Canny's edge detection plus Hough transform; a test with two sample pictures showed that the parameters needed to be adjusted for each picture;
- local thresholding may also be suitable, but it has succeeded only in one picture;
- background subtraction is not advised, mainly because still vehicles may end up in the background.

Appendix F

SIMBA overview

F.1 Introduction

SIMBA (*SIMulation for Bridge Assessment*) is the in-house micro-simulation tool used throughout the present research. The author of this thesis has been responsible for the software testing, identifying bugs, proposing upgrades and fixes, while the programming has been carried out by Dr Colin Caprani (DIT).

SIMBA implements the car-following *Intelligent Driver Model* and the lane-changing model MOBIL. It simulates traffic over a stretch of road of adjustable length with no on- or off-ramps. Lane closures may be applied. A screenshot is shown in Figure F.1.

SIMBA has numerous output capabilities, allowing a broad range of analyses. Output traffic features include:

- aggregated cross-sectional data, such as flow, space mean speed and time mean speed;
- aggregated spatial data, such as density or space mean speed;
- unaggregated cross-sectional data, such as speeds and time headways;
- unaggregated spatial data, such as speeds, accelerations, space headways and gaps.

Trajectory plots can be derived, such as the ones in Figure 2.1, although they are computationally quite heavy. Unique to SIMBA is the possibility of placing bridges and calculating static load effects from influence lines, either built-in or user-defined. The load effects can be output as time-history, block maxima or peaks-over-threshold.

F.2 Upgrades and releases

SIMBA derives from an older program called *EvolveTraffic*, whose initial development dates back to 2008 and did not have the capability to output load effects, nor to output spatial data. Only cross-sectional data was available. For the calculation of load effects, unaggregated traffic information was first captured at a single cross section. Then another in-house program, called *MarchTraffic*, was used to calculate load effects on a bridge by either assuming a constant speed or leaving the speed as recorded at the cross-section. However, as discussed in Section 5.2.5 and Section E.2, this procedure may lead to significant errors in bridge loading estimation under congested conditions.

Output of spatial data and calculation of load effects from actual vehicle positions have been introduced in the first release of SIMBA (version 1.0, released on 7 September 2011). Since then, SIMBA has been thoroughly tested and continuously upgraded. In particular, SIMBA 1.3.0 (released on 30 March 2012) features a significant upgrade with the reorganization of sequence of updating vehicle accelerations, lane changes, and positions. This release removed an undesired sensitivity of the lane change activity to the simulation step. Finally, SIMBA 1.4.0 (released on 21 July 2012) introduced the implementation of the gap control, used in Chapter 6.

F.3 Model formulations

The maximum possible deceleration b_{\max} , suggested in Treiber et al. (2000), is not implemented. Vehicles can undertake any deceleration needed by the traffic conditions. This is required because vehicles are all injected at the same speed and when congestion backs up to the beginning of the road, they may need hard deceleration in order not to overlap the leader. However, the MOBIL safe braking b_{safe} parameter, which controls the safety of lane change manoeuvres, is fully implemented.

Initial versions of *EvolveTraffic* did not take into account the pushy follower in the MOBIL formulation, but only the disadvantage to the new follower in the target lane. The pushy follower option was introduced in *EvolveTraffic* 1.3.1. The disadvantage to the new follower in target lane is always considered, and a fast-to-slow lane change formulation as suggested in

Kesting et al. (2007) cannot be implemented. This is discussed in more detail in Section D.2. There is no *critical speed* under which the asymmetrical lane-changing rules switch to symmetric ones, as suggested in Kesting et al. (2007).

F.4 Generation of input files

Single- and multi-lane input files can be generated with the in-house program BTLS (*BridgeTrafficLoadSim*) software package. As outlined in Section B.2, an injection gap and an injection speed must be appropriately set in order to generate the required inflow. However, these two parameters cannot be different among lanes. Formulas to estimate the injection parameters for generating the maximum flow of mixed traffic are given in Appendix B. Lower inflows can be generated by selecting a higher injection gap.

Cars are 4 m long and weigh 2 t. Trucks can be assigned normal distributions of GVWs and axle spacings. A truck percentage can be assigned to each lane. However, it must be taken into account that the presence of longer vehicles reduces the inflow. Typically, heavy vehicles are mostly injected in the slow lane. In this case, the slow lane inflow will be lower than the one on the fast lane. This aspect should be taken into account also when assigning the truck percentages. This can be best explained with an example. Say we want to inject a two-lane traffic stream with an overall truck percentage of 20%, where all the trucks are injected in the slow lane. The injection of 40% trucks in the sole slow lane will make the slow lane flow lower the car-only fast lane flow. Therefore, the actual percentage of trucks over the full traffic will result less than 20% and the initial truck percentage needs to be modified slightly upwards in order to return the desired overall truck percentage.

F.5 Program settings

SIMBA has some program settings that need to be carefully set, before running extensive simulations. The change of one of these parameters requires the restarting of the program.

The *minimum space for next vehicle* sets the minimum clear distance for a new vehicle to be injected at the start of the road. This value may affect the inflow, as discussed in Appendix B. In particular, it must be lower than the injection gap set in the input file. It has a strong

influence when there is congestion at the beginning of the road, which is a situation to avoid, unless done on purpose, for instance to calculate the dynamic capacity, as outlined in Section B.2.

The *safe braking* is one of the parameters of the MOBIL model. Kesting et al. (2007) suggest a value of 4 m/s², but Section D.6 shows that a better match with real data at high inflows may be attained using stronger deceleration values.

The *desired gap model* sets the formulation of the IDM desired minimum gap s^* , when the leader speed is faster, as discussed in Section D.3. It is recommended to use " s^* is limited to s_0 ", which is Case 1. The alternative exponential solution (Case 2) is implemented as "*Exponential decay*".

The *lane change minimum gap* sets the minimum lead and lag gap in the target lane necessary to perform a lane change. It is advised to set this parameter equal to the minimum jam distance s_0 .

The *lane change time delay* specifies the time gap until a new lane change event is permissible for a particular vehicle after a lane change has been performed. This parameter reflects the duration of real lane changes that are implemented in one time step in the program. If it is too high, it may affect the overall lane change rates. In SIMBA, overtaking manoeuvres take place within a simulation step, so it is advised that this value be greater than the actual duration of a lane change. Research suggests an average value of the lane change duration of about 4 s (Thiemann et al., 2008).

The *lane change follower* specifies whether the advantage to the current follower o (the so-called *pushy follower*) is considered in the decision of a lane change (see Section D.2). This parameter has a slight effect on the overall lane change rates. It is advised to set it to *true*.

The *lane change fast lane follower* restricts the consideration of the lane change follower to the fast lane only. It is advised to set it to *true* when using asymmetrical lane-changing rules and to *false* when using symmetrical rules (see Section D.2 for a detailed formulation).

The *road end buffer* sets the distance a vehicle considers clear as it approaches the end of the road. Tests showed that this parameter does not affect the overall outflow, but it may slightly affect the speed at which vehicles exit the road (the higher, the faster) and the lane change rates. Note that a road end buffer equal to zero does not allow any vehicle to exit the road, which is useful for generating full stop conditions.

F.6 Generation of inhomogeneities

Inhomogeneities can be generated by either decreasing the desired speed v_0 or increasing the safe time headway T , with comparable effects on traffic (Treiber et al., 2000). In the former case, a speed limit can be easily introduced in SIMBA. In the latter, there is no direct way to introduce variations of the safe time headway. However, they can be artificially created by setting an uphill gradient, following the process outlined here. In the SIMBA program settings, the IDM modifiers *A flag* and *B flag*, which set whether an uphill gradient would affect the IDM parameters maximum acceleration a and comfortable deceleration b , must be de-activated. Then, the parameter *VO slope*, which adjusts the rate at which the desired speed of vehicles is reduced due to an uphill gradient, must be set to a very low value. Finally, the *T slope* parameter should be adjusted in order to return the required variation of the safe time headway T due to the uphill gradient.

Either way, it is important to introduce inhomogeneities gradually, in order to avoid to impose drastic changes in the driver behaviour, which may lead to exaggerated hard braking.

Full stop can be generated by setting a null road end buffer. However, when multiple simulations are needed, this is often not a practicable way. Full stop conditions can be generated by setting a very high artificial uphill gradient with a strong effect on the safe time headway. In this way, speed can be brought very close to zero. However, since the speed is not exactly zero, the distance between vehicles at standstill is slightly higher than the minimum jam distance s_0 , which may lead to an under-estimation of load and density. Therefore, for full stop conditions, the IDM minimum jam distance s_0 can be slightly decreased in order to return the required minimum bumper-to-bumper distance at a standstill.

Note that the IDM formulation (Equations 2.1 and 2.2) does not cause a vehicle to stop exactly at the minimum jam distance s_0 , but rather to a distance slightly shorter. This should be taken into account when using relatively large values of s_0 .

Finally, it is important to recall that the purpose of an inhomogeneity is to reduce the outflow, which must be lower than the inflow in order to have congestion. In this case, vehicles queue and congestion lasts also after the last vehicle has entered the road. This must be taken into account when a specific duration of congestion is sought. For example, if one-hour of congestion is sought, then the inflow must be shorter than one hour, approximately by the ratio between outflow and inflow. The stronger the congestion, the shorter the inflow needs to be. In the extreme case of a full stop, the inflow can be just long enough to fill the bridge.

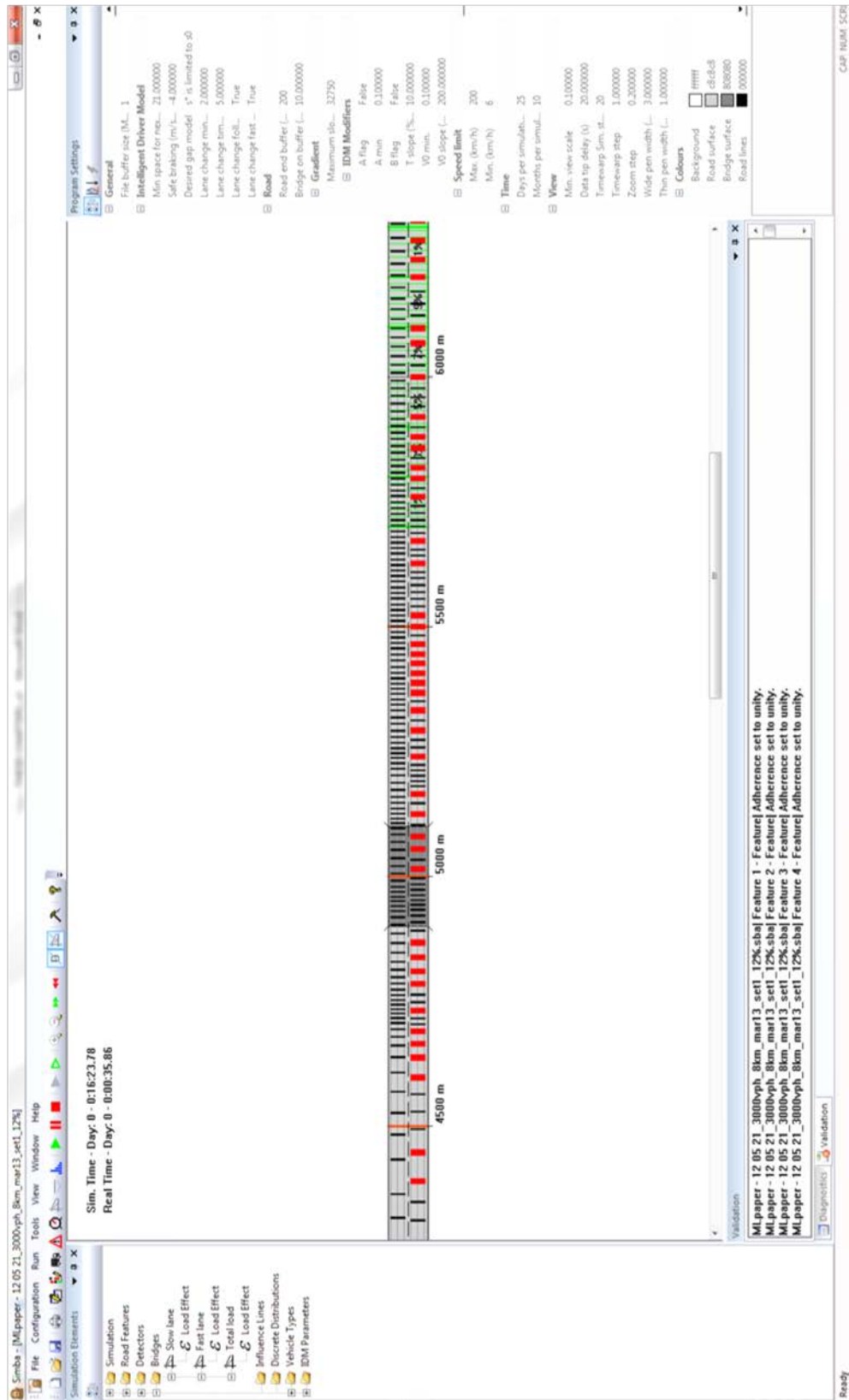


Figure F.1 - SIMBA screenshot.

References

- American Association of State Highway and Transportation Officials. *AASHTO Guide for Design of Pavement Structures. Part II Pavement design procedures for new construction or reconstruction*. American Association of State Highway and Transportation Officials, Washington, 1993
- American Association of State Highway and Transportation Officials. *Standard Specifications for Highway Bridges, 17th Edition*. American Association of State Highway and Transportation Officials, Washington, 2002
- American Association of State Highway and Transportation Officials. *AASHTO LRFD Bridge Design Specifications - Fifth Edition*. American Association of State Highway and Transportation Officials, Washington, 2010
- American Association of State Highway and Transportation Officials. *The Manual for Bridge Evaluation - Second Edition*. American Association of State Highway and Transportation Officials, Washington, 2011
- Ang, A. H.-S. & Tang, W. H. 2007. *Probability Concepts in Engineering: Emphasis on Application to Civil and Environmental Engineering, 2nd Edition*, Hoboken, Wiley.
- Atkočiunas, E., Blake, R., Juozapavičius, A. & Kazimianec, M. 2005. Image Processing in Road Traffic Analysis. *Nonlinear Analysis: Modelling and Control*, **10**, No. 4, 315-332.
- Axis Communication. 2008. *Axis 221 Network Camera* [Online]. Available: http://www.axis.com/products/cam_221/index.htm [Accessed 18 February 2013].
- Bailey, S. F. & Bez, R. 1999. Site Specific Probability Distribution of Extreme Traffic Action Effects. *Probabilistic Engineering Mechanics*, **14**, No. 1, 19-26.
- Ballard, D. H. 1981. Generalizing the Hough Transform to Detect Arbitrary Shapes. *Pattern Recognition*, **13**, No. 2, 111-122.
- Banks, J. H. 2002. Review of Empirical Research on Congested Freeway Flow. *Transportation Research Record: Journal of the Transportation Research Board*, **1802**, 225-232.
- Benton, S. 2008. *Background Subtraction, Part 1: Matlab Models* [Online]. EE times. Available: <http://www.eetimes.com/design/military-aerospace-design/4017685/Background-subtraction-part-1-MATLAB-models> [Accessed 28 February 2013].
- Bertini, R. L. & Leal, M. T. 2005. Empirical Study of Traffic Features at a Freeway Lane Drop. *Journal of Transportation Engineering*, **131**, No. 6, 397-407.

-
- Bertini, R. L., Rose, M. W. & El-Geneidy, A. 2005. Using Archived ITS Data Sources to Measure the Effectiveness of a Freeway Incident Response Program. *84th Annual Meeting of the Transportation Research Board*. Washington.
- Blacoe, S., Caprani, C. C., O'Brien, E. J. & Lipari, A. Determination of Minimum Gap in Congested Traffic. In: Caprani, C. & O'Connor, A., eds. *Bridge and Concrete Research in Ireland*, 6-7 September 2012 Dublin, 31-36.
- Brackstone, M. & McDonald, M. 1999. Car Following: A Historical Review. *Transportation Research Part F*, **2**, 181-196.
- Brackstone, M., Sultan, B. & McDonald, M. 2002. Motorway Driver Behaviour: Studies on Car Following. *Transportation Research Part F*, **5**, 31-46.
- British Standard. *Steel, Concrete and Composite Bridges. Part 2: Specification for loads*. British Standards Institution, London, 2006
- Brockfeld, E., Kühne, R. D. & Wagner, P. 2004. Calibration and Validation of Microscopic Traffic Flow Models. *Transportation Research Record: Journal of the Transportation Research Board*, **1876**, 62-70.
- Bruls, A., Calgaro, J.-A., Mathieu, H. & Prat, M. ENV 1991 - Part 3 : The Main Models of Traffic Loads on Road Bridges - Background Studies. *IABSE Colloquium*, 1996a Delft. 215-228.
- Bruls, A., Croce, P., Sanpaolesi, L. & Sedlacek, G. ENV 1991 - Part 3 : Traffic Load on Bridges - Calibration of Road Load Models for Road Bridges. *IABSE Colloquium*, 1996b Delft. 439-453.
- Buckland, P. G. 1991. North American and British Long-Span Bridge Loads. *Journal of Structural Engineering*, **117**, No. 10, 2972-2987.
- Buckland, P. G., Navin, F. P. D., Zidek, J. V. & McBryde, J. P. 1980. Proposed Vehicle Loading of Long-Span Bridges. *Journal of the Structural Division*, **106**, No. 4, 915-932.
- Cambridge Systematics Inc. 2005a. *NGSIM I-80 Data Analysis*. Oakland: Cambridge Systematics Inc.
- Cambridge Systematics Inc. 2005b. *NGSIM U.S. 101 Data Analysis*. Oakland: Cambridge Systematics Inc.
- Cambridge Systematics Inc. 2005c. *Traffic Congestion and Reliability: Trends and Advanced Strategies for Congestion Mitigation*.
- Caprani, C. C. 2012a. Bridge-to-Vehicle Communication for Traffic Load Mitigation. In: Caprani, C. & O'Connor, A. (eds.) *Bridge and Concrete Research in Ireland*. Dublin.
-

-
- Caprani, C. C. 2012b. Calibration of a Congestion Load Model for Highway Bridges Using Traffic Microsimulation. *Structural Engineering International*, **22**, No. 3, 342-348.
- Caprani, C. C. 2012c. Lifetime Highway Bridge Traffic Load Effect from a Combination of Traffic States Allowing for Dynamic Amplification. *Journal of Bridge Engineering*, **in print**.
- Caprani, C. C., Enright, B. & Carey, C. 2012a. Lane Changing Control to Reduce Traffic Load Effect on Long-Span Bridges. *In: Biondini, F. & Frangopol, D. M. (eds.) International Conference on Bridge Maintenance, Safety and Management*. Stresa: Taylor and Francis.
- Caprani, C. C., Lipari, A. & O'Brien, E. J. 2012b. Load Effect of Multi-Lane Traffic Simulations on Long-Span Bridges. *In: Biondini, F. & Frangopol, D. M. (eds.) 6th International Conference on Bridge Maintenance, Safety and Management*. Stresa: Taylor and Francis.
- Cassidy, M. J. & Bertini, R. L. 1999. Some Traffic Features at Freeway Bottlenecks. *Transportation Research Part B*, **33**, 25-42.
- Cathey, F. W. & Dailey, D. J. A Novel Technique to Dynamically Measure Vehicle Speed Using Uncalibrated Roadway Cameras. *Intelligent Vehicle Symposium*, 6-8 June 2005. IEEE, 777-782.
- Chen, C., Li, L., Hu, J. & Geng, C. Calibration of MITSIM and IDM Car-Following Model Based on NGSIM Trajectory Datasets. *International Conference on Vehicular Electronics and Safety*, 15-17 July 2010 QingDao, China. 48-53.
- Chen, S. R. & Wu, J. 2011. Modeling Stochastic Live Load for Long-Span Bridge Based on Microscopic Traffic Flow Simulation. *Computers and Structures*, **89**, No. 9-10, 813-824.
- Cheung, S.-C. S. & Kamath, C. Robust Techniques for Background Subtraction in Urban Traffic Video. *In: Panchanathan, S. & Vasudev, B., eds. SPIE, Visual Communication and Image Processing*, 18-22 January 2004 San Jose. SPIE, 881-892.
- Chodhury, C., Ben-Akiva, M., Toledo, T., Rao, A. & Lee, G. 2006. *NGSIM Cooperative Lane Changing and Forced Merging Model*. Washington: Federal Highway Administration.
- Coifman, B. 2003. Estimating Density and Lane Inflow on a Freeway Segment. *Transportation Research Part A*, **37**, 689-701.
- Coifman, B. 2006. Vehicle Level Evaluation of Loop Detectors and the Remote Traffic Microwave Sensor. *Journal of Transportation Engineering*, **132**, No. 3, 213-226.
- Coifman, B., Beymer, D., McLauchlan, P. & Malik, J. 1998. A Real-Time Computer Vision System for Vehicle Tracking and Traffic Surveillance. *Transportation Research Part C*, **6**, 271-288.
- Coles, S. 2001. *An Introduction to Statistics Modeling of Extreme Values*, London, Springer.
-

-
- Committee on Loads and Forces on Bridges of the Committee on Bridges of the Structural Division 1981. Recommended Design Loads for Bridges. *Journal of the Structural Division*, **107**, No. 7, 1161-1213.
- Conference of European Directors of Roads 2010. *Safe Distance between Vehicles*. Paris: CEDR.
- Consiglio Superiore dei Lavori Pubblici. *Norme Tecniche Per Le Costruzioni. Capitolo 5 - Ponti*. Consiglio Superiore dei Lavori Pubblici, 2008
- Ditlevsen, O. & Madsen, H. O. 1994. Stochastic Vehicle-Queue-Load Model for Large Bridges. *Journal of Engineering Mechanics*, **120**, No. 9, 1829-1847.
- Dowling, R., Skabardonis, A., Carroll, M. & Wang, Z. 2004. Methodology for Measuring Recurrent and Nonrecurrent Traffic Congestion. *Transportation Research Record: Journal of the Transportation Research Board*, **1867**, 60-68.
- Duret, A., Ahn, S. & Buisson, C. 2012. Lane Flow Distribution on a Three-Lane Freeway: General Features and the Effects of Traffic Controls. *Transportation Research Part C*, **24**, 157-167.
- Edie, L. C. 1974. Flow Theories. In: Gazis, D. C. (ed.) *Traffic Science*. New York: Wiley Interscience.
- Enright, B. & O'Brien, E. J. 2012. Monte Carlo Simulation of Extreme Traffic Loading on Short and Medium Span Bridges. *Structure and Infrastructure Engineering*, **in print**, 1-16.
- European Committee for Standardization. *Eurocode 1: Actions on Structures. Part 2: Traffic loads on bridges*. CEN, 2003
- Eymard, R. & Jacob, B. 1989. Un Nouveau Logiciel: Le Programme Castor Pour Le Calcul Des Actions Et Sollicitations Du Trafic Dans Les Ouvrages Routiers. *Bulletin de Liaison des LPC*, **164**, 64-77.
- Federal Highway Administration. 2005. *NGSIM Project* [Online]. Federal Highway Administration. Available: <http://www.ops.fhwa.dot.gov/trafficanalysistools/ngsim.htm> [Accessed 02 February 2012].
- Flint and Neill Partnership 1986. *Interim Design Standard: Long Span Bridge Loading* Crowthorne: Transport and Road Research Laboratory.
- Flint, A. R. & Jacob, B. Extreme Traffic Loads on Road Bridges and Target Values of Their Effects for Code Calibration. *IABSE Colloquium*, 1996 Delft.
- Fuentes, L. M. & Velastin, S. A. From Tracking to Advanced Surveillance. *International Conference on Image Processing*, 14-17 September 2003 Barcelona. IEEE, 121-4.
-

-
- Fung, Y.-f., Lee, H. & Ercan, M. F. 2007. Image Processing Application in Toll Collection. In: Ao, S. I., Gracia, A. M., Lee, J.-S. & Yu, K.-M. (eds.) *Recent Advances in Engineering and Computer Science*. Newswood Limited.
- Fwa, T. F. & Li, S. 1995. Estimation of Lane Distribution of Truck Traffic for Pavement Design. *Journal of Transportation Engineering*, **121**, No. 3, 241-248.
- Gazis, D. C. & Knapp, C. H. 1971. On-Line Estimation of Traffic Densities from Time-Series of Flow and Speed Data. *Transportation Science*, **5**, No. 3, 283-301.
- Geistefeldt, J. & Hohmann, S. 2013. Assessment of Different Design Hours for Freeways. *TRB 2013 Annual Meeting*. Washington.
- Giuliano, G. 1989. Incident Characteristics, Frequency, and Duration on a High Volume Urban Freeway. *Transportation Research Part A*, **23**, No. 5, 387-396.
- Golias, J. & Tsamboulas, D. 1995. Macrolevel Estimation of Highway Lane Usage. *Journal of Transportation Engineering*, **121**, 40-49.
- Gonzalez, R. C. & Woods, R. E. 2002. *Digital Image Processing, 2nd Edition*, Gatesmark Publishing.
- Gonzalez, R. C., Woods, R. E. & Eddins, S. L. 2009. *Digital Image Processing Using Matlab, 2nd Edition*, Gatesmark Publishing.
- Grave, S. A. J., O'Brien, E. J. & O'Connor, A. J. 2000. The Determination of Site-Specific Imposed Traffic Loadings on Existing Bridges. In: Ryall, M. J., Parke, G. a. R. & Harding, J. E. (eds.) *Bridge Management 4*. Thomas Telford.
- Greenshields, B. D. 1935. A Study of Traffic Capacity. *Highway Research Board Proceedings*, **14**, 448-477.
- Hall, F. L. 1994. Traffic Stream Characteristics. In: Gartner, N., Messer, C. J. & Rathi, A. K. (eds.) *Revised Monograph on Traffic Flow Theory*. Federal Highway Administration.
- Hallenbeck, M., Rice, M., Smith, B., Cornell-Martinez, C. & Wilkinson, J. 1997. *Vehicle Volume Distribution by Classification*. Federal Highway Administration.
- Harman, D. J., Davenport, A. G. & Wong, W. S. S. 1984. Traffic Loads on Medium and Long Span Bridges. *Canadian Journal of Civil Engineering*, **11**, No. 3, 556-573.
- Harwood, D. W., Torbic, D. J., Richard, K. R., Glauz, W. D. & Elefteriadou, L. 2003. *Review of Truck Characteristics as Factors in Roadway Design*. Washington: National Cooperative Highway Research Program.
- Hayrapetova, A. A. 2006. *Micro-Simulation Modelling of Traffic Loading on Long Span Bridges*. PhD, University College Dublin.
- Hecht, E. 2002. *Optics*, Addison Wesley.
-

-
- Hidas, P. 2005. Modelling Vehicle Interactions in Microscopic Simulation of Merging and Weaving. *Transportation Research Part C*, **13**, 37-62.
- Hidas, P. & Wagner, P. Review of Data Collection Methods for Microscopic Traffic Simulation. *Proceedings of the World Conference on Transport Research*, 4-8 July 2004 Istanbul.
- Hoogendoorn, S. P. & Bovy, P. H. L. 2001. State-of-the-Art of Vehicular Traffic Modelling. *Proceedings of the Institution of Mechanical Engineers, Part I: Journal of Systems and Control Engineering*, **215**, 283-303.
- Hoogendoorn, S. P. & Hoogendoorn, R. 2010. Calibration of Microscopic Traffic-Flow Models Using Multiple Data Sources. *Philosophical Transactions of the Royal Society A*, **368**, 4497-4517.
- Hoogendoorn, S. P., van Zuylen, H. J., Schreuder, M., Gorte, B. & Vosselman, G. 2003. Microscopic Traffic Data Collection by Remote Sensing. *Transportation Research Record: Journal of the Transportation Research Board*, **1855**, 121-128.
- Institut für Algorithmen und Kognitive Systeme. 1995. *Image Sequence Server* [Online]. Universität Karlsruhe. Available: http://i21www.ira.uka.de/image_sequences/ [Accessed 28 February 2013].
- Ivy, R. J., Lin, T. Y., Mitchell, S., Raab, N. C., Richey, V. J. & Scheffey, C. F. 1954. Live Loading for Long-Span Highway Bridges. *American Society of Civil Engineers Transactions*, **119**, 981-1004.
- Jin, W.-L. 2010. Macroscopic Characteristic of Lane-Changing Traffic. *Transportation Research Record: Journal of the Transportation Research Board*, **2188**, 55-63.
- Kerner, B. S. & Rehborn, H. 1996. Experimental Features and Characteristic of Traffic Jams. *Physical Review E*, **53**, No. 2, R1297-R1300.
- Kesting, A. & Treiber, M. 2008. Calibrating Car-Following Models by Using Trajectory Data. *Transportation Research Record: Journal of the Transportation Research Board*, **2088**, 148-156.
- Kesting, A., Treiber, M. & Helbing, D. 2007. General Lane-Changing Model MOBIL for Car-Following Models. *Transportation Research Record: Journal of the Transportation Research Board*, **1999**, 86-94.
- Kesting, A., Treiber, M. & Helbing, D. 2010. Enhanced Intelligent Driver Model to Assess the Impact of Driving Strategies on Traffic Capacity. *Philosophical Transactions of the Royal Society A*, **368**, 4585-4605.
- Klein, L. A., Mills, M. K. & Gibson, D. R. P. 2006. *Traffic Detector Handbook. Third ed.* MacLean, VA: Federal Highway Administration.
-

-
- Knoop, V. L., Hoogendoorn, S. P. & Adams, K. 2009. Capacity Reductions at Incidents Sites on Motorways. *European Journal of Transportation and Infrastructure Research*, **9**, No. 4, 363-379.
- Knoop, V. L., Hoogendoorn, S. P., Shiomi, Y. & Buisson, C. 2012. Quantifying the Number of Lane Changes in Traffic: An Empirical Analysis. *Transportation Research Record: Journal of the Transportation Research Board*, **2278**, 31-41.
- Knoop, V. L., Hoogendoorn, S. P. & van Zuylen, H. J. 2008. Capacity Reduction at Incidents: Empirical Data Collected from a Helicopter. *Transportation Research Record: Journal of the Transportation Research Board*, **2071**, 19-25.
- Knoop, V. L., Wilson, R. E., Colé, J., Buisson, C. & van Arem, B. Quantifying the Number of Lane Changes in Traffic. *Summer meeting of the Traffic Flow Committee of the Transportation Research Board*, 7-9 July 2010 Annecy (France).
- Knospe, W., Santen, L., Schadschneider, A. & Schreckenberg, M. 2002. Single-Vehicle Data of Highway Traffic: Microscopic Description of Traffic Phases. *Physical Review E*, **65**, No. 5.
- Kopf, J. M., Nee, J., Ishimaru, J. M. & Hallenbeck, M. E. 2005. *Measurement of Recurring and Non-Recurring Congestion: Phase 2*. Seattle: Washington State Transportation Center.
- Kovvali, V. G., Alexiadis, V. & Zhang, L. P. E. Video-Based Vehicle Trajectory Data Collection. *Transportation Research Board 86th Annual Meeting*, 2007 Washington.
- Kurkjian, A., Gershwin, S. B., Houpt, P. K., Willsky, A. S., Chow, E. Y. & Greene, C. S. 1980. Estimation of Roadway Traffic Density on Freeways Using Presence Detector Data. *Transportation Science*, **14**, No. 3, 232-261.
- Kwon, J., Mauch, M. & Varaiya, P. 2006. Components of Congestion: Delay from Incidents, Special Events, Lane Closures, Weather, Potential Ramp Metering Gain, and Excess Demand. *Transportation Research Record: Journal of the Transportation Research Board*, **1959**, 84-91.
- Laval, J. A. & Daganzo, C. F. 2006. Lane-Changing in Traffic Streams. *Transportation Research Part B*, **40**, 251-264.
- Lee, J. & Park, B. B. 2012. Determining Lane Use Distributions Using Basic Freeway Segment Density Measures. *Journal of Transportation Engineering*, **138**, No. 2, 210-217.
- Lipari, A., Caprani, C. C. & O'Brien, E. J. Load Effect of Single-Lane Traffic Simulations on Long-Span Bridges. In: Nínualláin, N. A., Walsh, D., West, R., Cannon, E., Caprani, C. C. & McCabe, B., eds. *Joint Symposium on Bridge and Infrastructure Research in Ireland*, 2-3 September 2010 Cork. 231-238.
- Lutomirska, M. 2009. *Live Load Models for Long Span Bridges*. PhD, University of Nebraska.
-

-
- McDonald, M., Brackstone, M. A. & Jeffrey, D. 1994. Simulation of Lane Usage Characteristics on 3 Lane Motorways. *27th ISATA conference*. Aachen.
- Medina Soto, A. C. 2010. *Assessment of Non-Recurrent Congestion on Dutch Motorways*. MSc Civil Engineering, Delft University of Technology.
- Mirth, C. 2008. *Low-Level Features from Video for Traffic Jam Detection*, Saarbrücken, VDM Verlag Dr Mueller.
- Moridpour, S., Sarvi, M. & Rose, G. 2010. Modeling the Lane-Changing Execution of Multiclass Vehicles under Heavy Traffic Conditions. *Transportation Research Record: Journal of the Transportation Research Board*, **2161**, 11-19.
- Moses, F. 2001. *Calibration of Load Factors for LRFR Bridge Evaluation*. Washington: National Cooperative Highway Research Program.
- Nagel, K. & Schreckenberg, M. 1992. A Cellular Automaton Model for Freeway Traffic. *Journal de Physique I France*, **2**, No. 12, 2221-2229.
- Nahi, N. E. 1973. Freeway Data Processing. *IEEE Proceedings*, **61**, No. 5, 537-541.
- Naranjo, J. E., González, C., Reviejo, J., García, R. & de Pedro, T. 2003. Adaptive Fuzzy Control for Inter-Vehicle Gap Keeping. *IEEE Transactions on Intelligent Transportation System*, **4**, No. 3, 132-142.
- Ni, D. 2007. Determining Traffic-Flow Characteristics by Definition for Application in ITS. *IEEE Transactions on Intelligent Transportation System*, **8**, No. 2, 181-187.
- Nowak, A. S. 1995. Calibration of LRFD Bridge Code. *Journal of Structural Engineering*, **121**, No. 8, 1245-1251.
- Nowak, A. S., Lutomirska, M. & Sheikh Ibrahim, F. I. 2010. The Development of Live Load for Long Span Bridges. *Bridge Structures*, **6**, No. 1, 73-79.
- O'Connor, A. J., Jacob, B., O'Brien, E. J. & Prat, M. 2001. Report of Current Studies Performed on Normal Load Model of Ec1. *Revue française de génie civil*, **5**, No. 4, 411-433.
- O'Connor, A. J. & O'Brien, E. J. 2005. Traffic Load Modelling and Factors Influencing the Accuracy of Predicted Extremes. *Canadian Journal of Civil Engineering*, **32**, No. 1, 270-278.
- O'Brien, E. J. & Caprani, C. C. 2005. Headway Modelling for Traffic Load Assessment of Short to Medium Span Bridges. *The Structural Engineer*, **83**, 33-36.
- O'Brien, E. J., Caprani, C. C. & O'Connell, G. J. 2006. Bridge Assessment Loading: A Comparison of West and Central/East Europe. *Bridge Structures*, **2**, No. 1, 25-33.
- O'Brien, E. J. & Enright, B. 2011. Modeling Same-Direction Two-Lane Traffic for Bridge Loading. *Structural Safety*, **33**, 296-304.
-

-
- O'Brien, E. J., Hayrapetova, A. & Walsh, C. 2012. The Use of Micro-Simulation for Congested Traffic Load Modelling of Medium- and Long-Span Bridges. *Structure and Infrastructure Engineering*, **8**, No. 3, 269-276.
- O'Brien, E. J., Lipari, A. & Caprani, C. C. 2011. Estimation of Density and Gaps During Congestions. *Irish Transportation Research Network*. Cork.
- Orosz, G., Wilson, R. E. & Stépan, G. 2010. Traffic Jams: Dynamics and Control. *Philosophical Transactions of the Royal Society A*, **368**, 4455-4479.
- Pal, R., Latoski, S. P. & Sinha, K. C. 1998. Investigation of Freeway Incident Characteristics and Their Influence in Planning an Incident Management Program. *Transportation Research Record*, **1634**, 46-55.
- Pedrotti, F. L. & Pedrotti, L. S. 1993. *Introduction to Optics*, Upper Saddle River, Prentice Hall.
- Peeta, S., Zhang, P. & Zhou, W. 2005. Behavior-Based Analysis of Freeway Car-Truck Interactions and Related Mitigation Strategies. *Transportation Research Part B*, **39**, 417-451.
- Petrov, A. A., Lin, P.-W., Zou, N., Chang, G.-L. & Point-Du-Jour, J. Y. Evaluation of the Benefits of a Real-Time Incident Response System. *9th World Congress on Intelligent Transportation System*, 14-17 October 2002 Chicago.
- Portland Cement Association. *Thickness Design for Concrete Highway and Street Pavements*. Portland Cement Association, Skokie, 1984
- Potter, J., Tasnim, S., Tufte, K. & Bertini, R. L. Incorporating Incident Data into a Freeway Data Archive for Improved Performance Measurement. *86th Annual Meeting of the Transportation Research Board*, 2007 Washington.
- Prat, M. 2001. Traffic Load Models for Bridge Design: Recent Developments and Research. *Progress in Structural Engineering and Materials*, **3**, 326-334.
- Punzo, V. & Simonelli, F. 2005. Analysis and Comparison of Microscopic Traffic Flow Models with Real Traffic Microscopic Data. *Transportation Research Record: Journal of the Transportation Research Board*, **1934**, 53-63.
- Qiu, T. Z., Lu, X.-Y., Chow, A. H. F. & Shladover, S. E. 2010. Estimation on Freeway Traffic Density with Loop Detector and Probe Vehicle Data. *Transportation Research Record: Journal of the Transportation Research Board*, **2178**, 21-29.
- Rakha, H. & Zhang, W. 2005. Estimating Traffic Stream Space-Mean Speed and Reliability from Dual and Single Loop Detectors. *Transportation Research Record: Journal of the Transportation Research Board*, **1925**, 38-47.
- Ray, S. F. 2002. *Applied Photographic Optics*, Oxford, Focal Press.
-

-
- Ricketts, N. J. & Page, J. 1997. *Traffic Data for Highway Bridge Loading*. Crowthorne: Transport Research Laboratory.
- Roads and Maritime Services 2011. *Heavy Vehicle Driver Handbook*. Roads and Maritime Services.
- Roberts, N. P., Webb, S. A. & Coe, G. 1994. Incidents on Motorways. *Traffic Engineering + Control*, **35**, No. 10, 550-554.
- Rodgers, S., Wadsworth, B., Smith, S. D. & Forde, M. C. 2006. An Analysis of Road Traffic Incidents on the M25 Motorway, UK. *Proceedings of the ICE - Transport*, **159**, No. 1, 1-8.
- Sarasua, W. A., Davis, W. J., Clarke, D. B., Kottapally, J. & Mulukutla, P. 2004. Evaluation of Interstate Highway Capacity for Short-Term Work Zone Lane Closures. *Transportation Research Record: Journal of the Transportation Research Board*, **1877**, 85-94.
- Schönhof, M. & Helbing, D. 2007. Empirical Features of Congested Traffic States and Their Implications for Traffic Modelling. *Transportation Science*, **41**, No. 2, 135-166.
- Schulze, M. A. 1996. *Circular Hough Transform* [Online]. Available: <http://www.markschulze.net/java/hough/> [Accessed 28 November 2012].
- Skabardonis, A., Petty, K. F., Bertini, R. L., Varaiya, P. P., Noeimi, H. & Rydzewski, D. 1997. I-880 Field Experiment: Analysis of Incident Data. *Transportation Research Record*, **1603**, 72-79.
- Skabardonis, A., Petty, K. F. & Varaiya, P. P. 1999. Los Angeles I-10 Field Experiment: Incident Patterns. *Transportation Research Record*, **1683**, No. 22-30.
- Sonka, M., Hlavac, V. & Boyle, R. 2008. *Image Processing, Analysis, and Machine Vision, 3rd Edition*, Toronto, Thompson.
- Soriguera, F. & Robusté, F. 2011. Estimation of Traffic Stream Space Mean Speed from Time Aggregations of Double Loop Detector Data. *Transportation Research Part C*, **19**, 115-129.
- Sparmann, U. 1979. The Importance of Lane-Changing on Motorways. *Traffic Engineering & Control*, **20**, No. 6, 320-323.
- Tasnim, S., Monsere, C. M. & Bertini, R. L. Toward an Automated Incident Analysis Process Using Archived Data on the Portland Oregon Freeway System. *10th International Conference on Application of Advanced Technologies in Transportation*, 27-31 May 2008 Athens.
- The Council of the European Union. *Official Journal of the European Communities. Council Directive 96/53/EC of 25 July 1996 laying down for certain road vehicles circulating within the Community the maximum authorized dimensions in national and international traffic and the maximum authorized weights in international traffic*. 1996
-

-
- The European Parliament and the Council of the European Union. *Official Journal of the European Union. Directive 2004/54/EC of the European Parliament and of the Council of the European Union of 29 April 2004 on minimum safety requirements for tunnels in the Trans-European Road network.* 2004
- The Highways Agency. *Design Manual for Roads and Bridges. Volume 3, Section 4, Part 3: The Assessment of Highway Bridges and Structures.* The Stationery Office, London, 2001
- The Highways Agency. *Design Manual for Roads and Bridges. Volume 7, Section 2, Part 1: Traffic assessment.* The Stationery Office, London, 2006
- Thiemann, C., Treiber, M. & Kesting, A. 2008. Estimating Acceleration and Lane-Changing Dynamics Based on Ngsim Trajectory Data. *Transportation Research Record: Journal of the Transportation Research Board*, **2088**, 90-101.
- Transportation Research Board. *Highway Capacity Manual - Fourth Edition.* Transportation Research Board, 2000
- Transportation Research Board. *Highway Capacity Manual HCM 2010. Volume 2: Uninterrupted flow.* Transportation Research Board, Washington, 2010
- Treiber, M. 2011. *Microsimulation of Road Traffic Flow* [Online]. Available: <http://www.traffic-simulation.de/> [Accessed 30 May 2012].
- Treiber, M. & Helbing, D. Realistische Mikrosimulation von Straßenverkehr mit einem einfachen Modell. In: Tavangarian, D. & Grützner, R., eds. *16. Symposium Simulationstechnik ASIM*, 10-13 September 2002 Rostock. 514-520.
- Treiber, M., Hennecke, A. & Helbing, D. 2000. Congested Traffic States in Empirical Observations and Microscopic Simulations. *Physical Review E*, **62**, No. 2, 1805-1824.
- Treiber, M. & Kesting, A. 2010. An Open-Source Microscopic Traffic Simulator. *IEEE Intelligent Transportation Systems Magazine*, **2**, No. 3, 6-13.
- Treiber, M. & Kesting, A. 2012. Validation of Traffic Flow Models with Respect to the Spatiotemporal Evolution of Congested Traffic Patterns. *Transportation Research Part C*, **21**, No. 1, 31-41.
- Treiber, M. & Kesting, A. 2013. *Traffic Flow Dynamics: Data, Models and Simulation*, Springer.
- Treiterer, J. & Myers, J. A. The Hysteresis Phenomenon in Traffic Flow. In: Buckley, D. J., ed. *6th International Symposium on Transportation and Traffic Theory*, 26-28 August 1974 Sydney. Elsevier, 13-38.
- van Etten, W. C. 2005. *Introduction to Random Signals and Noise*, Chichester, John Wiley & Sons.
-

-
- Vass, G. & Perlaki, T. 2003. Applying and Removing Lens Distortion in Post Production. *2nd Hungarian Conference on Computer Graphics and Geometry*.
- Vrouwenvelder, A. C. W. M. & Waarts, P. H. 1993. Traffic Loads on Bridges. *Structural Engineering International*, **3/93**, 169-177.
- Wang, G., Xiao, D. & Gu, J. Review on Vehicle Detection Based on Video for Traffic Surveillance. *IEEE International Conference on Automation and Logistics*, September 2008 Qingdao. 2961-2966.
- Wardrop, J. G. 1952. Some Theoretical Aspects of Road Traffic Research. *Proceedings of the Institution of Civil Engineers: Engineering Divisions*, **1**, No. 3, 325-362.
- Wilson, R. E. 2011. From Inductance Loops to Vehicle Trajectories. In: Beal, G. J. (ed.) *75 Years of the Fundamental Diagram for Traffic Flow Theory*. Washington: Transportation Research Board.
- Wu, N. 2006. Equilibrium of Lane Flow Distribution on Motorways. *Transportation Research Record: Journal of the Transportation Research Board*, **1965**, 48-59.
- Yousif, S. & Hunt, J. 1995. Modelling Lane Utilisation on British Dual-Carriageway Roads: Effects on Lane-Changing. *Traffic engineering + control*, **36**, No. 12, 680-687.
- Zaurin, R. & Catbas, F. N. 2010. Integration of Computer Imaging and Sensor Data for Structural Health Monitoring of Bridges. *Smart Materials and Structures*, **19**.
- Zielke, B. A., Bertini, R. L. & Treiber, M. 2008. Empirical Measurement of Freeway Oscillation Characteristic. *Transportation Research Record: Journal of the Transportation Research Board*, **2088**, 57-67.